TRANSPORTATION RESEARCH

RECORD

No. 1448

Pavement Design, Management, and Performance

Strength and Deformation Characteristics of Pavement Sections

A peer-reviewed publication of the Transportation Research Board

TRANSPORTATION RESEARCH BOARD
NATIONAL RESEARCH COUNCIL

NATIONAL ACADEMY PRESS
WASHINGTON, D.C. 1994

Transportation Research Record 1448
ISSN 0361-1981
ISBN 0-309-06057-5
Price: $26.00

Subscriber Category
IIB pavement design, management, and performance

Printed in the United States of America

Sponsorship of Transportation Research Record 1448

GROUP 2—DESIGN AND CONSTRUCTION OF TRANSPORTATION FACILITIES
Chairman: Charles T. Edson, Greenman Pederson, Inc.

Pavement Management Section
Chairman: Joe P. Mahoney, University of Washington

Committee on Strength and Deformation Characteristics of Pavement Sections
Chairman: Albert J. Bush III, U.S. Army Engineer Waterways Experiment Station
Gilbert Y. Baladi, Richard D. Barksdale, Robert C. Briggs, Stephen F. Brown, George R. Cochran, Ronald J. Cominsky, Billy G. Connor, Mark P. Gardner, John P. Hallin, Dennis R. Hiltunen, Mario S. Hoffman, Lynne H. Irwin, Starr D. Kohn, Robert L. Lytton, Michael S. Mamlouk, Soheil Nazarian, Rasmus S. Nordal, Gonzalo R. Rada, J. Brent Rauhut, Byron E. Ruth, Larry Scofield, Tom Scullion, Stephen B. Seeds, R. N. Stubstad, Marshall R. Thompson, Per Ullidtz, Jacob Uzan, Thomas D. White, Haiping Zhou

Committee on Modelling Techniques in Geomechanics
Chairman: Deborah J. Goodings, University of Maryland
Sreenivas Alampalli, Sangchul Bang, Richard D. Barksdale, Richard J. Bathurst, Joseph A. Caliendo, Jack I. Clark, K. P. George, Mary E. Hynes, William M. Isenhower, Ilan Juran, Victor N. Kaliakin, Stephen Ketcham, Kenneth J. Larsson, Rita B. Leahy, Glen E. Miller, Victor A. Modeer, Jr., Reed L. Mosher, Yacoub M. Najjar, Clifford J. Roblee, Raymond L. Sterling, Harry E. Stewart, Tien H. Wu

Committee on Rigid Pavement Design
Chairman: Gary Wayne Sharpe, Kentucky Transportation Cabinet
Don R. Alexander, Mark W. Bintzer, Brian T. Bock, Larry J. Buttler, Judith B. Corley-Lay, Kathleen T. Hall, John E. Hunt, Anastasios M. Ioannides, Walter P. Kilareski, Starr D. Kohn, Roger M. Larson, Jo A. Lary, Brian R. McWaters, Theodore L. Neff, William Albert Nokes, Mauricio R. Poblete, Robert J. Risser, Jr., Mark B. Snyder, Shiraz D. Tayabji, Mang Tia, John P. Zaniewski, Dan G. Zollinger

Transportation Research Board Staff
Robert E. Spicher, Director, Technical Activities
Daniel W. Dearasaugh, Engineer of Design
G. P. Jayaprakash, Engineer of Soils, Geology, and Foundations
Nancy A. Ackerman, Director, Reports and Editorial Services
Naomi Kassabian, Editor

Sponsorship is indicated by a footnote at the end of each paper. The organizational units, officers, and members are as of December 31, 1993.

Transportation Research Record 1448

Contents

Foreword

This volume contains 13 papers, some of which were presented at the 1994 TRB Annual Meeting. Ten papers are sponsored by the Committee on Strength and Deformation Characteristics of Pavement Sections. Two more are sponsored by the Committee on Modelling Techniques in Geomechanics. The last one is sponsored by the Committee on Rigid Pavement Design.

Collop et al. describe a portable mat for measuring the dynamic tire forces of commercial vehicles and assessing the spatial repeatability of wheel loads. Siddharthan et al. discuss the use of a moving load model to compute pavement strains caused by vehicles transporting spent-fuel casks to a nuclear waste repository. Noureldin presents a small-scale investigation of the influence of stress levels and seasonal temperature and moisture variations on pavement layer modulus and other properties. Sousa and Solaimanian discuss their research on a quick and simple procedure to determine the permanent deformation characteristics of an asphalt concrete mix. Kirkner et al. present a methodology for analyzing flexible pavements by solving the problem of a moving load on an elastic-plastic half-space with the use of a three-dimensional, finite element model. Zaghloul et al. describe the development of an enhanced computerized procedure for permitting overloaded trucks on pavements and bridges in Indiana. Romero et al. correlate results of deflection measurements taken by a falling-weight deflectometer (FWD) and a Benkelman beam and examine factors that could affect results, such as speed of load application. Rohde proposes a procedure to determine a flexible pavement's structural number through the use of an FWD. Jooste and Fernando present an analysis of pavement response under multiple-axle, superheavy-load vehicles. Meier and Rix use artificial neural networks to speed up dramatically the backcalculation of pavement layer moduli from deflection basins generated by FWDs. De Beer et al. discuss the structural behavior and subsequent modeling of two cracked-and-seated semirigid pavements that had been overlaid with crushed stone and an asphalt surfacing. Mallela and George analyze rigid pavements subjected to dynamic loading through the use of a three-dimensional, finite element model. Uddin et al. also use a three-dimensional, finite element model in their investigation of the effects of pavement discontinuities and dynamic loads on surface deflection responses.

Investigation of Spatial Repeatability Using a Tire Force Measuring Mat

A. C. COLLOP, T. E. C. POTTER, D. CEBON, AND D. J. COLE

A portable mat for measuring the dynamic tire forces of commercial vehicles is described. The mat is 56 m long and 13 mm thick and has 141 capacitative strip sensors spaced at 0.4-m intervals. The accuracy of the mat for measuring dynamic tire forces generated by heavy commercial vehicles is assessed using an instrumented vehicle. The spatial repeatability of dynamic wheel loads generated by 14 uninstrumented articulated vehicles is investigated, and it is concluded that approximately half of the vehicles tested are likely to contribute to a repeatable pattern of road loading.

Dynamic tire forces are caused by vibration of a moving vehicle excited by road surface roughness. They are thought to be a significant cause of road damage, although the mechanisms are not well understood. Dynamic tire forces are influenced by vehicle speed, road roughness, and the design of the vehicle, particularly its suspension system.

There have been two main approaches to estimating the road-damaging effects of dynamic tire forces. Some researchers believe that the loading at each point along the road is essentially random, so that each point incurs forces statistically similar to each other point, and damage is uniformly distributed along the road. Studies in which such loading is assumed predict an increase in road damage of approximately 20 to 30 percent from dynamic loads (*1–3*). Other researchers believe that the peak forces applied by the heavy-vehicle fleet are concentrated at specific locations along the road (*4–6*), and thus some locations along the road may incur up to four times more damage than the average (*4*). This effect has been termed "spatial repeatability." The life of the road is then expected to be governed by damage at these heavily loaded areas.

Several studies indicate that a vehicle traveling over a road section at one speed generates a spatial distribution of dynamic loading that is repeated closely on subsequent test runs at the same speed (*4–9*). Hahn (*6*) suggests that because a large proportion of heavy vehicles tend to have similar geometry and dynamic characteristics and tend to travel at similar speeds, spatial repeatability of road loading may be expected in normal traffic flow. Vehicles in a particular class tend to have similar mass distributions and geometry because of the nature of vehicle construction and use regulations. There is, however, significant variation in suspension characteristics, although leaf-spring suspensions are fitted to the majority of heavy articulated vehicles (*10*).

Using a validated vehicle simulation, Cole and Cebon (*11,12*) examine the spatial repeatability of dynamic tire forces generated by a fleet of dynamically similar vehicles. They conclude that approximately two-thirds of the four-axle leaf-sprung articulated vehicles may contribute to a repeated pattern of road loading. Gyenes and Mitchell (*9*) sum the dynamic wheel loads generated by a variety of instrumented axles at particular locations on a test track in the United Kingdom. They observe that the sum of the wheel loads varied significantly more than would have been expected if the high loads had been distributed randomly over the track. Gyenes and Mitchell also performed a limited study of spatial repeatability using eight weigh-in-motion sensors mounted in a highway at 2.7-m spacings. Their preliminary results indicate some evidence of load concentration effects.

Substantial reductions in road damage could be achieved through regulating dynamic tire forces, if they are repeatable for normal traffic conditions. Research is therefore needed to establish whether loading patterns are random or repeatable for normal variations in the dynamic characteristics of heavy commercial vehicles.

MAT TESTS

Mat Installation

The research described in this paper was performed with a load measuring mat, developed by the authors in conjunction with Golden River Traffic Limited, for measuring the dynamic tire forces generated by heavy commercial vehicles (*13*). The mat contains capacitative strip sensors encapsulated in polyurethane tiles as shown schematically in Figure 1. The tiles are 1.2 m by 1.2 m by 13 mm thick, and each one contains three sensors (1.2-m long) laid transverse to the wheel path, 0.4 m apart.

Tests described in this paper were performed on the Transport Research Laboratory (TRL) test track during the winter months of 1991 and 1992. The mat was installed by TRL personnel on a long, straight section of the track. Each mat tile was attached to the brushed concrete surface by an adhesive sheet and six screws. There were 47 tiles in total, together containing 141 sensors, for an overall instrumented length of 56.4 m. Sheets of plywood were used to provide a ramp up to the mat and a run-off section, both

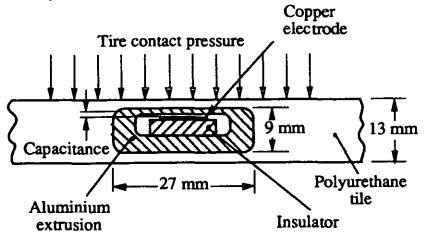

FIGURE 1 Cross section of capacitive strip sensor cast into polyurethane tile.

Engineering Department, Cambridge University, Cambridge CB2 1P2, England.

15 m long. The mat system was used in an earlier study for the Strategic Highway Research Program (SHRP) (*14,15*). The mat used in the present study incorporated the 32 tiles manufactured for the earlier U.S. SHRP study, as well as 15 new tiles.

Outputs of the sensors were logged and processed by nine Golden River Marksman M600 data-loggers. The data stored by each logger were transferred to a personal computer by a serial communications line. Figure 2 shows a vehicle with its nearside wheels on the mat. The data-logging boxes can be seen beneath the crash barrier.

Vehicle Tests

The accuracy of the mat's measurement of dynamic tire forces was assessed using a vehicle that was instrumented to measure dynamic tire forces. The vehicle was a two-axle rigid truck with single tires on the steering axle and dual tires on the drive axle. Steel spring suspensions were fitted to both axles, and the gross mass of the vehicle was 17 tons. Instrumentation fitted to the end of each axle consisted of strain gauges to measure axle bending and an accelerometer to correct for the inertia (linear and angular) of the mass outboard of the gauges (*1*). Data were logged by a digital data-logger on board the vehicle.

On-board measurements were synchronized with the mat sensor measurements by means of an infrared transmitter and detector mounted on the vehicle. The detector sensed reflective markers placed alongside the mat. Five markers were used along the length of the mat. The instrumented vehicle was driven over the mat 35 times at speeds varying from 2 m/sec to 27 m/sec (7 to 97 km/hr).

Following the instrumented vehicle tests, 14 uninstrumented articulated vehicles were tested on the mat. All the vehicles belonged to TRL and each included one of three tractor units and one of five trailers. Each vehicle was fully laden and driven over the mat about 50 times at speeds between 2 m/sec and 27 m/sec (between 7 and 97 km/hr). Table 1 describes the tractors (designated by numbers 1 to 3) and trailers (designated by letters A through E). The tractor-trailer combinations are designated by a number and a letter throughout the remainder of this paper (e.g., Vehicle 2C refers to Tractor 2 with Trailer C).

FIGURE 2 Load-measuring mat on TRL test track.

TABLE 1 Descriptions of Vehicles Tested on Load-Measuring Mat

		No. Axles	Suspension Description
Tractor 1	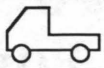	2	Steel (Multileaf) + Dampers
Tractor 2	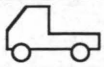	2	Air + Dampers
Tractor 3	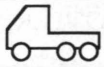	3	Steel (Multileaf)
Trailer A	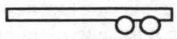	2	Wide-spread Steel Tandem (Monoleaf)
Trailer B	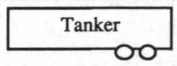	2	Wide-spread Steel Tandem (Monoleaf)
Trailer C	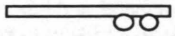	2	Rubber Tandem + Dampers
Trailer D	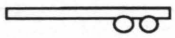	2	Air Tandem + Dampers
Trailer E	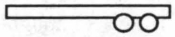	3	Steel Tri-Axle (Multileaf)

Calibration

Steering axles of articulated vehicles usually have relatively low dynamic force variation, and at low speeds the forces applied to the road surface are close to the static weights. Consequently, the mat sensors initially were calibrated using the measured static weights of the steering axles of three of the test vehicles. The static axle weights were measured by portable weigh pads.

Using this initial set of calibration factors, all of the low-speed axle force time histories measured with the mat were examined to determine which axles showed the least dynamic force variation. Five axles (two steer, one drive, and two trailer axles) were observed to have low dynamic loads. The results from a total of 23 low-speed tests for these axles were then used to determine a final set of calibration factors for the sensors in the mat.

Of the 141 sensors in the mat, three were found not to work, and seven were found to be noisy (most likely they were damaged in transit). The seven noisy sensors were included in the following accuracy calculations, but were ignored for subsequent analyses of the wheel forces.

Figure 3 shows the distribution of the root-mean-square (RMS) static error between the mat sensor measurements and the static weights (measured using weigh pads) for the final calibration runs,

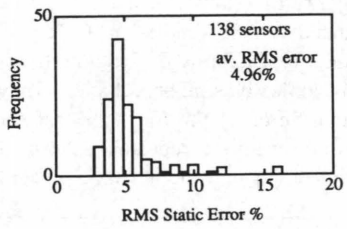

FIGURE 3 RMS error for 23 static calibration runs.

where the static error (percentage) is defined as

$$\text{static error} = 100\left(\frac{\text{static force} - \text{mat force}}{\text{mat force}}\right)\text{percent} \quad (1)$$

The average RMS error of all the sensors was 5 percent. This value can be considered the baseline accuracy of the system and compares closely with the 4 percent observed previously for a similar mat tested by Cebon and Winkler (*14*). The main difference is related to the seven noisy sensors. It is also apparent that there is a spread of sensor performance, with individual sensors showing errors as low as 2.5 percent RMS.

Instrumented Vehicle Tests

Figure 4 presents a comparison of the steering axle tire force measured by the mat and that measured on the instrumented vehicle for a speed of 25 m/sec. It is apparent from Figure 4 that the sensor measurements closely follow the on-board measurements.

Figure 5 indicates the distribution of the RMS dynamic error between all of the instrumented vehicle measurements and the mat. Here the dynamic error (in percent) is defined as

$$\text{dynamic error} = 100\left(\frac{\text{vehicle force} - \text{mat force}}{\text{mat force}}\right)\text{percent} \quad (2)$$

In this series of runs, four sensors were found not to work. Figure 5 therefore shows results from 137 sensors (including six noisy ones). The average RMS dynamic error is 6.7 percent. This error originates from several sources:

- Mat sensor error: The previous section showed that the mat sensors had an average baseline error of 5 percent RMS.
- Vehicle speed variation along the mat leading to a lack of synchronization between the markers: The relative speed variation (0.2 m/sec along the mat) was much higher at low speeds.
- Vehicle instrumentation error: An analysis of the vehicle instrumentation for straight line motion on a relatively smooth road surface suggests a contribution to the dynamic error of approximately 1.5 percent RMS (*11*). However, it is thought to be an underestimate of the source of error for the mat tests, as explained in the following.

Le Blanc et al. (*16*) examined the performance of various methods for measuring dynamic tire forces using instrumented axles. They found that the type of instrumentation system used in these measurements can generate large errors in the presence of roll or side-slip motion because of side forces and variation of the lateral position of the tire contact area. Analysis of the instrumented vehicle measurements showed that the roll component of tire force was a significant proportion of the total. Consequently, the dynamic error is likely to be greater than 1.5 percent RMS.

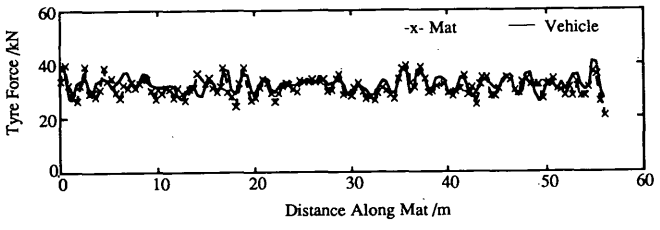

FIGURE 4 Comparison of wheel forces measured by mat and steer axle of instrumented vehicle traveling at 25 m/sec.

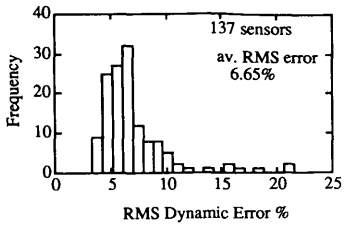

FIGURE 5 RMS error for 34 validation runs.

MEASURES OF SPATIAL REPEATABILITY

The analytical framework needed to assess the spatial repeatability of tire forces generated by heavy vehicles was presented by Cole and Cebon (*12*) and will be summarized briefly here.

Aggregate Force

The simplest measure of road loading that can be related to road damage is the "aggregate tire force" (*4,12*), which is simply the sum of the dynamic forces applied to each mat sensor by all of the axles of a vehicle. It is given mathematically by

$$A_k = \sum_{j=1}^{N_a} P_{jk} \qquad k = 1, 2, 3, \ldots, N_s \quad (3)$$

where

A_k = aggregate force at Sensor k along the mat,
P_{jk} = force applied by Tire j to Sensor k,
N_a = number of axles on the vehicle, and
N_s = number of sensors along the mat.

Aggregate force was calculated at each sensor along the mat. In order to minimize the effect of the 5 percent random sensor measurement errors, tire force histories from repeated tests of the same vehicle at the same speed were averaged together before the aggregate forces were calculated.

Aggregate Fourth-Power Force

The main disadvantage to using the aggregate force as a measure of road loading is that it does not reflect the mechanisms of road damage or the sensitivity of road materials to stress and strain levels. This disadvantage can be overcome by raising individual tire forces to a fourth power before summing their contribution at each mat sensor. This gives the aggregate fourth-power force (*12*):

$$A_k^4 = \sum_{j=1}^{N_a} P_{jk}^4 \qquad k = 1, 2, 3, \ldots, N_s \quad (4)$$

where A_k^4 is the aggregate fourth-power force at Sensor k along the mat and the exponent 4 represents the sensitivity of asphalt fatigue damage to cyclic strain level.

Spatial Repeatability Index (SRI)

To quantify spatial repeatability, aggregate tire force histories generated by each vehicle were compared with those generated by a reference vehicle. A suitable measure of spatial repeatability should indicate high repeatability when the peaks of the two force histories occur close together along the road. Low repeatability should be indicated when the peaks of one history occur near the troughs of the second history. A statistic that has this property is the correlation coefficient ρ, defined by (*17*)

$$\rho = \frac{E\{[u(t) - m_u][v(t) - m_v]\}}{\sigma_u \sigma_v} \tag{5}$$

where m_u, m_v, and σ_u, σ_v are the means and standard deviations of two signals $u(t)$ and $v(t)$, and $E\{\ \}$ is the expectation operator.

The value of ρ can be between +1 and −1. The properties of ρ may be examined by considering two sine waves of frequency ω and phase difference ϕ:

$$u(t) = \sin(\omega t) \qquad v(t) = \sin(\omega t + \phi) \tag{6}$$

In this case, Equations 5 and 6 give

$$\rho = \cos \phi \tag{7}$$

When ϕ = 0 degrees and ρ = +1, the two waves are in phase and the peaks (and troughs) of each wave occur at the same locations. When ϕ = 180 degrees and ρ = −1, the two waves are in antiphase and the peaks of one wave coincide with the troughs of the other wave.

Cole and Cebon (*12*) note that a reasonable threshold of repeatability is one-eighth of a cycle phase difference, or ϕ = 45 degrees, corresponding to a correlation coefficient of 0.707. For a speed of 22 m/sec and a frequency of 15 Hz, this threshold corresponds to a distance along the road of 0.18 m, about the length of a tire contact patch or a small pothole. For a frequency of 3 Hz, the threshold distance is 0.92 m.

SRI is defined as the correlation coefficient for an aggregate tire force history compared with a reference aggregate force history, both measured with the mat.

EXPERIMENTAL RESULTS

Effect of Speed

The effect of vehicle speed on spatial repeatability was investigated initially by calculating the SRI between the aggregate force of a reference vehicle (Vehicle 1A) traveling at a reference speed of 22 m/sec (80 km/hr) and aggregate forces for Vehicle 1A traveling at test speeds greater than and less than the reference speed. The results are presented in Figure 6, which shows that the SRI is 1.0 when the test speed is the same as the reference speed (as expected) and less than 1.0 when the test speed is different from the reference speed (22 m/sec).

Also shown in Figure 6 are the results of a simulation of the aggregate force SRI for the same Vehicle 1A from Cole and Cebon (*12*). The two results show striking similarity; however, the experimental SRI is generally less than the theoretical result by approximately 0.1, except at the reference speed. This difference is thought to be caused by the 5 percent random mat sensor error in the measurements. Note that at the reference speed, the noise is perfectly correlated with itself and therefore gives an SRI of 1.0.

Effect of Sensor Noise

Reduction in the SRI related to sensor errors may be investigated by considering the correlation between two dynamic tire forces g_1 and g_2 moving along the mat with speed V. The forces consist of sine waves of frequency ω, with added random noise:

$$g_1(x) = f_1(x) + \epsilon_1(x)$$
$$g_2(x) = f_2(x) + \epsilon_2(x) \tag{8}$$

where

$$f_1(x) = \bar{f}_1 + F_1 \sin\left(\frac{\omega x}{V}\right)$$
$$f_2(x) = \bar{f}_2 + F_2 \sin\left(\frac{\omega x}{V} + \phi\right)$$

x = distance along the mat,
$\bar{f}_1$, $\bar{f}_2$ = mean levels of $f_1(x)$ and $f_2(x)$,
F_1, F_2 = amplitudes of $f_1(x)$ and $f_2(x)$, and
ϵ_1, ϵ_2 = independent random errors with standard deviations σ_{ϵ_1} and σ_{ϵ_2}.

From Equations 5 and 8, the SRI for the modified sine waves becomes

$$SRI = \frac{\dfrac{\omega}{2\pi V}\displaystyle\int_0^{2\pi V/\omega} [g_1(x) - \bar{f}_1][g_2(x) - \bar{f}_2]dx}{\sigma_{g_1}\sigma_{g_2}} \tag{9}$$

In general, ϵ_1 and ϵ_2 are different functions of distance (although they are likely to have the same statistics), and they are both

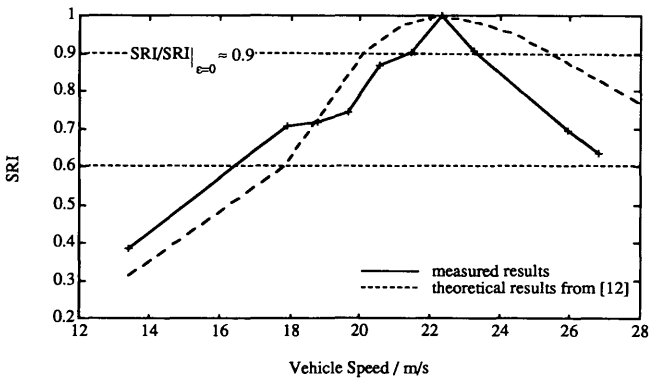

FIGURE 6 Measured and predicted SRI values for Vehicle 1A.

uncorrelated with $\sin(\omega x/V)$. Equation 9 then reduces to

$$SRI = \frac{\sigma_{f_1}\sigma_{f_2}\cos\phi}{\sqrt{(\sigma_{f_1}^2 + \sigma_{\epsilon_1}^2)(\sigma_{f_2}^2 + \sigma_{\epsilon_2}^2)}} \quad (10)$$

where σ_{f_1} and σ_{f_2} are the RMS values of $f_1(x)$ and $f_2(x)$.

Now consider the value of the SRI for two tests of the same vehicle at speeds near the reference speed (i.e., near 22 m/sec in Figure 6). Assuming the RMS dynamic loads for the two runs are approximately equal, $\sigma_{f_1} \approx \sigma_{f_2} = \sigma_f$, and that the amount of noise on the two measurements is similar, $\sigma_{\epsilon_1} \approx \sigma_{\epsilon_2} = \sigma_\epsilon$, Equation 10 can be rewritten as

$$\frac{SRI}{SRI|_{\epsilon=0}} = \frac{1}{[1 + (\sigma_\epsilon/\sigma_f)^2]} \quad (11)$$

where $SRI|_{\epsilon=0}$ is the SRI for the signals with no noise (from Equation 10) and σ_ϵ/σ_f is the ratio of RMS noise to RMS dynamic wheel load.

It can be seen from Equation 11 that for a given dynamic tire force level (σ_f), increasing the noise level decreases the maximum possible correlation between the two signals. If there is no noise ($\sigma_\epsilon/\sigma_f = 0$), the maximum possible SRI is 1.0. However, if the RMS noise level is equal to the RMS of the dynamic load (i.e., $\sigma_\epsilon/\sigma_f = 1$), the maximum possible SRI for the two signals is 0.5. Note that if a noisy signal is correlated with itself, $\epsilon_1(x) = \epsilon_2(x)$, and the SRI will be 1.0, irrespective of the fact that the signal contains some noise.

In order to estimate the maximum possible SRI from Equation 11, the standard deviations of the dynamic load and noise are both required. The standard deviation of the sensor error previously was found to be 5 percent of the average static load. The standard deviation of three averaged measurements (from the three test runs at 22 m/sec) is therefore $\sigma_\epsilon = 5/\sqrt{3} = 2.9$ percent. Knowing the standard deviation of the dynamic load plus noise (measured with the mat) and the standard deviation of the noise alone, it is possible to calculate the standard deviation of the dynamic load alone, σ_f for each axle. For the drive axle of Vehicle 1A, σ_f is approximately 8.7 percent of the static load. Substituting these values into Equation 11 gives a maximum possible SRI of approximately 0.9.

If the aggregate force history is used, as opposed to a single force history, this value of 0.9 can be shown to be a lower bound; the true value will be slightly higher. The value of 0.9 is marked on Figure 6 and can be seen to be a reasonable lower-bound estimate of the maximum SRI at the reference speed.

Because of the reduction in SRI related to noise, the threshold value of SRI in this study is 0.6 instead of 0.7 (see previous section). Figure 6 shows that the SRI is above this threshold value for speeds approximately 6 m/sec, on either side of the reference speed.

Effects of Vehicle Configuration

Figure 7 shows results for Vehicles 1A, 1B, 1C, 1D, and 1E at various speeds, correlated with the reference vehicle (Vehicle 1A) traveling at the reference speed of 22 m/sec. These vehicles all have the same tractor, with six different trailers (see Table 1). All the vehicles show a peak in SRI near the reference speed. The maximum SRI values range from 0.85 for Vehicle 1C to 0.58 for Vehicle 1D.

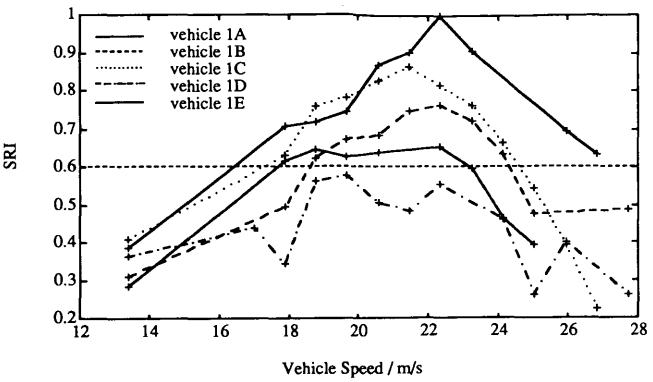

FIGURE 7 SRI for Vehicles 1A, 1B, 1C, 1D, and 1E; Vehicle 1A is reference vehicle.

In their theoretical study, Cole and Cebon [*12*] considered the dominant wavelength of the aggregate force history to be the main factor in determining the correlation between vehicles. (The dominant wavelength was calculated by dividing the speed by the dominant frequency component in the aggregate force spectral density.) Vehicle 1D includes a steel-sprung tractor and an air-sprung trailer. It is likely that the aggregate force history of this vehicle is not dominated by a single wavelength (*12*), and therefore the correlation with the reference vehicle is low. All the other vehicles (steel-sprung trailers and a rubber-sprung trailer) have trailer suspensions with similar stiffnesses to that of the reference vehicle and are likely to have similar dominant wavelengths. They therefore have maximum SRIs above the threshold of 0.6.

Figure 8 shows the corresponding graph for Vehicles 2A, 2B, 2C, 2D, and 2E, using Vehicle 2A at 22 m/sec as the reference (see Table 1). The SRIs vary less with speed than for Vehicles 1A through 1E (Figure 7). The reason for this is not yet known but may relate to the combination of dissimilar suspensions on the tractor and trailer, leading to the absence of a single dominant wavelength in the aggregate forces.

Figure 9 shows the results for Vehicles 3A, 3B, 3D, and 3E, using Vehicle 3A at 22 m/sec as the reference (see Table 1). All the vehicle combinations presented in Figure 9 (apart from the reference) display low repeatability. The tractor used in all these

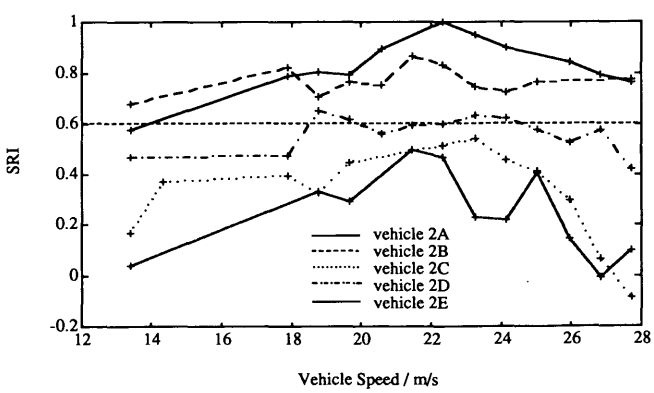

FIGURE 8 SRI for Vehicles 2A, 2B, 2C, 2D, and 2E; Vehicle 2A is reference vehicle.

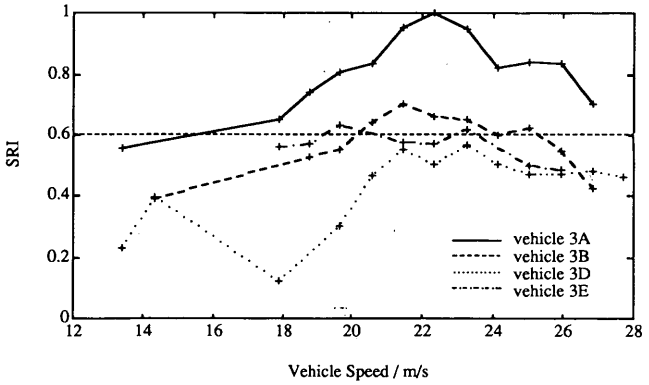

FIGURE 9 SRI for Vehicles 3A, 3B, 3D, and 3E; Vehicle 3A is reference vehicle.

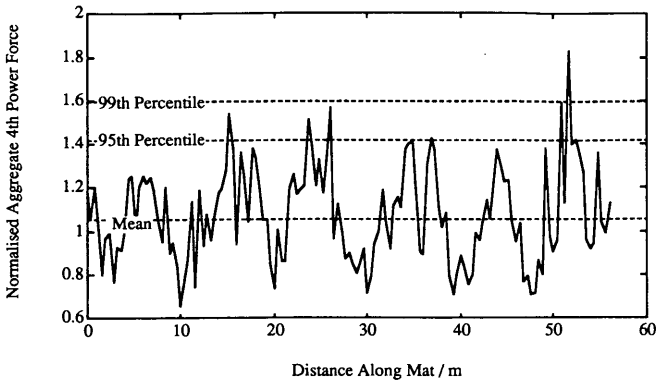

FIGURE 11 Normalized aggregate fourth-power forces for 140 vehicle runs.

vehicle combinations (Tractor 3) had a stiff tandem drive axle suspension with lightly damped axle pitch and body bounce modes of vibration. Possible causes of the low repeatability are (*a*) poor correlation because of the high-frequency tandem pitching mode, and (*b*) an increase in sensitivity to changes in the trailer suspension group caused by the stiff tractor suspension. These causes are the subject of current investigations.

Figure 10 indicates SRIs for the 14 vehicles traveling at 18 m/sec correlated with Vehicle 1A also traveling at 18 m/sec. The vehicles are ordered along the horizontal axis in descending order of correlation at this speed. The graph also shows the corresponding results for the speeds of 22 and 26 m/sec. In these cases the reference vehicle is Vehicle 1A, traveling at 22 and 26 m/sec, respectively.

For all three speeds, the SRI decreases as the vehicle becomes less similar to the reference vehicle. Most of the vehicles with the reference tractor (Tractor 1) have relatively high SRIs, and the vehicles most different from the reference vehicle tend to have low SRIs. This is particularly evident for Tractor 3, with its stiff tandem leaf-spring suspension, and Trailer D, which has an air suspension. Approximately half of the data points in Figure 10 have SRIs above 0.6, indicating that approximately half of the vehicles in this general class are likely to contribute to a repeatable pattern of road loading. However, it should be noted that the vehicles tested were of very diverse configurations and not representative of the highway fleet.

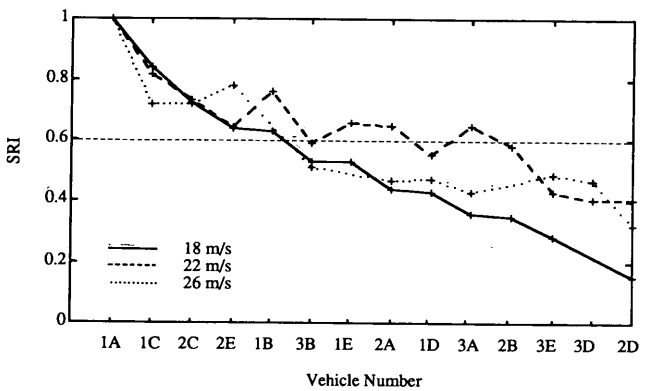

FIGURE 10 Ordered SRI for all vehicles for different reference speeds.

Aggregate Fourth-Power Force

Figure 11 shows the accumulated damage caused by 140 aggregate fourth-power force histories (Equation 4) for the 14 different vehicles. The results have been normalized by the damage from the static tire forces alone (i.e., a value of 1 corresponds to the damage caused by the static axle loads of the 140 vehicle passes). Despite the wide range of vehicles and speeds used in this study, there is a dominant wavelength of approximately 8 m in the aggregate fourth-power force history. This wavelength probably is associated with the sprung mass modes of vibration of the vehicles. It agrees reasonably well with the 7 m predicted by Cole and Cebon (*12*). The peak damage is approximately 1.8 times that caused by the static loads alone.

The horizontal lines on Figure 11 show upper-percentile levels of A_k^4. The 95th-percentile level of damage is 1.4 times the static damage (from the static loads alone). If it was assumed that there was no spatial repeatability (dynamic forces randomly distributed along the road), the damage would be uniformly distributed along the road at the mean level, which is 1.05 times the static damage. Spatial repeatability therefore causes a significant increase in the damage caused at some locations along the road surface by dynamic loads, even for the relatively smooth surface of the TRL test track.

CONCLUSIONS

1. The wheel load measuring mat is sufficiently accurate for measuring the dynamic tire forces of heavy vehicles. The sensors have an average baseline accuracy of 5 percent RMS, which compares closely with the 4 percent measured in a previous study. Some sensors were found to have much better performance than average, with baseline errors as low as 2.5 percent RMS.
2. The correlation between the aggregate force distributions generated by different vehicles depends strongly on the speed as well as the combination of tractor-trailer suspensions.
3. Approximately half of the articulated vehicles tested were found to contribute to a spatially repeatable pattern of road loading.

4. For a fleet of vehicles consisting of all the vehicles tested in the study, the fatigue damage incurred by 5 percent of the road surface would be approximately 1.4 times the fatigue damage from the static loads alone. This value would be expected to increase significantly for rougher roads.

5. The experimental results of this study largely confirm earlier theoretical predictions.

6. The implication of conclusions (3) and (4) is that fatigue failure of roads is likely to be governed by peak dynamic forces. Consequently, any measure of vehicle dynamic loading performance should consider these peak forces rather than average dynamic forces.

ACKNOWLEDGMENTS

The authors are very grateful to the Science and Engineering Research Council for funding the research described in this paper; to the director of the Transport Research Laboratory and members of the Vehicle and Environment Division for providing the test track, vehicles, and technical support and for installing the mat; and to Golden River Traffic Ltd., and the University of Michigan Transportation Research Institute for their assistance with the provision of the load-measuring mat.

REFERENCES

1. Mitchell, C. G. B. and L. Gyenes. Dynamic Pavement Loads Measured for a Variety of Truck Suspensions. *Proc., 2nd International Conference on Heavy Vehicle Weights and Dimensions*, Kelowna, British Columbia, Canada, 1989.
2. Monismith, C. L., J. Sousa, and J. Lysmer. Modern Pavement Design Technology Including Dynamic Load Conditions. *Proc., SAE Conference on Vehicle/Pavement Interaction*, SP765, Society of Automotive Engineers, Warrendale, Pa., 1988.
3. O'Connell, S., E. Abbo, and K. Hedrick. Analyses of Moving Dynamic Loads on Highway Pavements; Part I. Vehicle Response. *Proc., International Symposium on Heavy Vehicle Weights and Dimensions*, Kelowna, British Columbia, Canada, 1986.
4. Cebon, D. *An Investigation of the Dynamic Interaction Between Wheeled Vehicles and Road Surfaces*. Ph.D. thesis. University of Cambridge, Cambridge, England, 1985.
5. Ervin, R. D., et al. *Influence of Truck Size and Weight Variables on the Stability and Control Properties of Heavy Trucks*. Transportation Research Institute, University of Michigan, Ann Arbor, 1983.
6. Hahn, W. D., *Effects of Commercial Vehicle Design on Road Stress: Vehicle Research Results*. Institut für Kruftfahrwesen, Universität Hannover, Germany, 1985.
7. Addis, R. R., A. R. Halliday, and C. G. B. Mitchell. Dynamic Loading of Road Pavements by Heavy Goods Vehicles. *Proc., Congress on Engineering Design, Seminar 4A-03*, Institution of Mechanical Engineers, Birmingham, England, 1986.
8. Woodrooffe, J. H. F., P. A. LeBlanc, and A. T. Papagiannakis. Suspension Dynamics: Experimental Findings and Regulatory Implications. *Proc., SAE Conference on Vehicle and Pavement Interaction*, SP765, Society of Automotive Engineers, Warrendale, Pa., 1988.
9. Gyenes, L. and C. G. B. Mitchell. The Spatial Repeatability of Dynamic Pavement Loads Caused by Heavy Goods Vehicles. *Proc., Third International Symposium on Heavy Vehicle Weights and Dimensions*, Cambridge, England, Thomas Telford, London, England, 1992.
10. Cebon, D. Vehicle-generated road damage: A Review. *Vehicle System Dynamics*, Vol. 18 (1–3), 1989, pp. 107–150.
11. Cole, D. J. *Measurement and Analysis of Dynamic Tyre Forces Generated by Lorries*. Ph.D. thesis. Cambridge University, Cambridge, England, 1990.
12. Cole, D. J. and D. Cebon. Spatial Repeatability of Dynamic Tyre Forces Generated by Heavy Vehicles. *Proceedings of the Institution of Mechanical Engineers, Part I. Journal of Automobile Engineering*, Vol. 206, 1992, pp. 17–27.
13. Cole, D. J. and D. Cebon. A Capacitative Strip Sensor for Measuring Dynamic Tyre Forces. *Proc., 2nd Int. Conf. on Road Traffic Monitoring*, Institute of Electrical Engineers, London, England, 1989.
14. Cebon, D. and C. B. Winkler. *A Study of Road Damage Due to Dynamic Wheel Loads Using a Load Measuring Mat*. Strategic Highway Research Program, Final Report, UMTRI-90-13, Vol. 1, National Research Council, Washington, D.C., 1990.
15. Cebon, D. and C. B. Winkler. Multiple-Sensor Weigh-In-Motion: Theory and Experiments. In *Transportation Research Record 1311*, TRB, National Research Council, Washington, D.C., 1991, pp. 70–78.
16. Le Blanc, P. A., J. H. Woodrooffe, and A. T. Papagiannakis. A Comparison of Two Types of Instrumentation for Measuring Vertical Wheel Load. *Proc., Third International Symposium on Heavy Vehicle Weights and Dimensions*, Cambridge, England, Thomas Telford, London, England, 1992.
17. Newland, D. E. *Random Vibrations and Spectral Analysis*, 2nd edition. Longman, 1985.

Publication of this paper sponsored by Committee on Strength and Deformation Characteristics of Pavement Sections.

Pavement Strains Induced by Spent-Fuel Transportation Trucks

RAJ SIDDHARTHAN, PETER E. SEBAALY, AND ZIA ZAFIR

Four types of vehicles are being considered for the transportation of spent-fuel casks to the high-level nuclear waste repository that is to be located in Yucca Mountain, Nevada. The use of a finite-layer moving-load model to compute the pavement strains is described. Pavement strains are required to compare the relative pavement damage caused by each of the spent-fuel trucks and to estimate the increased cost associated with the increase in maintenance and rehabilitation on pavements caused by the spent-fuel trucks. The strain response induced by the spent-fuel trucks for a site near Reno, Nevada, is reported. The asphalt concrete layer and the unbound materials are assumed viscoelastic and elastic, respectively. Pavement material propeties were deduced from falling-weight deflectometer testing. The study reveals that the strain response is affected strongly by the axle configuration and by the speed of the vehicle. Increased vehicle speed reduces the pavement strains substantially; longitudinal strains in the asphalt concrete layer decrease by as much as 33 percent when the speed of the vehicle increases from 30 to 60 km/hr. A substantial compressive strain component is also present when tandem and tridem axle loading are considered. The difference in contribution to pavement distress between the two legal-weight trucks and between the two overweight trucks is minimal. Laboratory fatigue and cyclic triaxial tests are being evaluated to compare the effects of legal-weight and overweight axle loading.

The Yucca Mountain area, located in the state of Nevada, is the only site being considered for storage of high-level nuclear spent fuel. Numerous studies are under way to assess the suitability of the site to store high-level nuclear spent fuel permanently. If the studies reveal no serious concerns, the repository is scheduled to receive spent-fuel elements from nuclear power plants early in the next century. A number of transportation modes are being appraised for transporting spent fuel from nuclear power plants to the site (*1*). One mode would be to use existing highways and specially designed trucks. Some of these trucks are overweight (heavier than the legal weight).

Both construction of the repository and transportation of spent fuel to the repository are expected to contribute to the deterioration of the existing highway pavements in Nevada. One objective of a study now under way at the University of Nevada, Reno, is to estimate the cost of maintaining pavements that might be affected by repository-related traffic to Yucca Mountain. In an attempt to quantify the cost, it is necessary to estimate the contribution of the repository-related traffic to the increase in maintenance and rehabilitation required to keep the pavement serviceable above some critical level.

Repository-related traffic's contribution to pavement distress or deterioration may be predicted using either empirical or mechanistic analyses (*2–4*). Empirical methods are based on AASHO road tests carried out in the 1960s. Mechanistic methods are based on pavement performance models that require traffic-induced pavement response (mainly strains) to predict pavement distress. The mechanistic approach, which uses fundamental pavement material properties, is considered a more rational approach and therefore has been adopted for the University of Nevada, Reno, study. Major modes of pavement distress are fatigue cracking, rutting, low-temperature cracking, roughness, and debonding. Widely used pavement distress models relate fatigue cracking to the horizontal tensile strain at the bottom of the asphalt concrete (AC) layer and the rutting to the vertical compressive strains at the top of the subgrade (*3–5*).

The distress or performance indicators just identified are often computed using static loading conditions, assuming either linear or nonlinear material characterization. Recently, Zafir (*6–8*) outlined an efficient finite-layer moving-load model that can predict pavement strains. The model accounts for the important dynamic effects of the moving load, such as inertia, damping (material and radiation), and wave reflection, and also presents the rate-dependent (viscoelastic material) properties. The AC layer is treated as viscoelastic, whereas the base and the subgrade are treated as linear elastic.

This paper describes the application of the aforementioned moving-load model to compute pavement strains caused by four types of trucks that are to be used in spent-fuel transportation. One approach to deducing viscoelastic material (required for the model) from falling-weight deflectometer (FWD) data is also presented.

EXISTING METHODS FOR PAVEMENT STRAINS

Moving traffic wheel loads exert dynamic forces on pavement; therefore, effects such as inertia, damping (material and radiation), and resonance become important. The response of deposits to moving surface pressure loading has been studied by a number of researchers. Excellent summaries of the description and applicability of the methods have been presented by Werkle and Waas (*9*) and Siddharthan et al. (*10*).

Widely used pavement response computer models such as ELSYM5 and BISAR are based on layered-elastic theory. These models assume static loading conditions and single or multiple circular loaded areas that are fixed in location. This means that moving-load (dynamic) effects and the rate-dependent material properties have been neglected.

Pavement engineers have known the importance of the dynamic loading caused by the moving load for some time (*3,4*). A recent extensive field testing program sponsored by FHWA at the Pennsylvania State University test track has clearly indicated the influ-

R. Siddharthan and P. Sebaaly, Department of Civil Engineering, University of Nevada, Reno, Nev. 89557. Z. Zafir, Geospectra, 3095 Richmond Parkway, Suite 213, Richmond, Calif. 94806.

ence of the dynamic nature of the wheel loading (*11,12*). In these studies two new pavement sections, representing a thin (0.15 m of AC over 0.2 m of crushed aggregate) and a thick (0.25 m of AC over 0.25 m of crushed aggregate) section were subjected to moving traffic loads.

The experimental program measured a wide range of pavement response histories, such as vertical deflection and longitudinal strain at the bottom of the AC layer under moving truck loads (Figure 1). Testing revealed that pavement responses are influenced strongly by the speed of a vehicle and by its wheel load acting on the pavement. There was a reduction of as much as 70 percent in the maximum tensile strain in the AC layer when the speed of the vehicle increased from 32 to 80 km/hr. Furthermore, the study clearly demonstrated that the strain history response is a result of the complex dynamic interaction between adjacent wheel loadings (in the case of tandem configuration), resulting in a substantial compressive strain (as much as 57 percent of the maximum tensile strain) component in the AC layer. Widely used computer models, such as ELSYM5 and BISAR, cannot predict the observed responses. A dynamic moving-load model that accounts for the rate-dependent material properties is required for this purpose.

The most recent study to predict the entire strain history response is based on the three-dimensional finite-element model (*13*). Sousa and his colleagues at the University of California, Berkeley, are also working on the development of a moving-load model that is also based on the finite-element method (J. B. Sousa, personal communication, 1993). The rate-dependent material properties can be accounted for in these models. To obtain accurate results, the finite-element techniques require a relatively fine finite-element mesh to accommodate large strain gradients, and the discretization should include a substantial lateral extent to model the moving load. There is no doubt that the computational effort associated with such an undertaking will be substantial.

Sousa et al. reported on an analytical model for computing pavement strains subjected to stationary circular loaded plates (*14,3*). They developed a computer model, SAPSI, to compute the response of a viscoelastic or elastic-layered system in the frequency domain. The input of the layer properties are Young's modulus, Poisson's ratio, and damping ratio as a function of the excitation frequency. The load-time history on the loaded areas varies as a function of the velocity of the moving vehicle. Their approach is identical to one proposed by Sebaaly and Mamlouk (*15*).

However, these methods suffer from a major limitation in that they do not account for the true nature of the moving load. The assumption that a uniform pressure is present on the entire stationary loaded areas, even when the tire occupies only a part of the loaded area, is questionable. The assumption becomes more important, especially in the case of pavements, because the size of the loaded area and thickness of the AC layer are on the same order of magnitude.

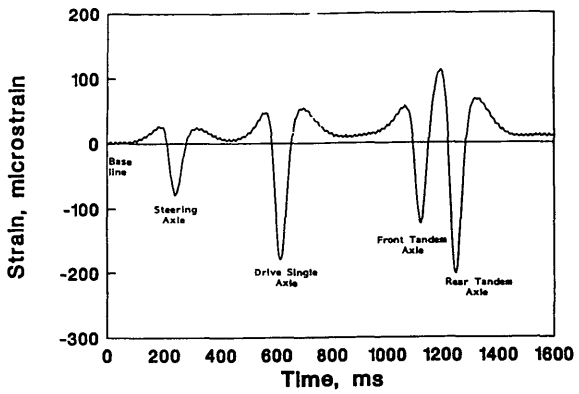

FIGURE 1 Measured longitudinal strain history in AC under moving semitrailer (*11,12*).

BRIEF OUTLINE OF MOVING-LOAD MODEL

Zafir and Siddharthan (*6*) and Zafir et al. (*8*) reported on the formulation of a continuum-based, "finite layer" model to evaluate dynamic pavement strains subject to moving traffic load. Complex surface loadings, such as multiple loads and nonuniform tire-pavement interaction pressures, can be handled relatively easily because the method uses Fourier transform technique. The pavement layer system may be characterized as consisting of a number of viscoelastic or elastic horizontal layers (as many as necessary) with each layer characterized using a set of uniform properties. For viscoelastic materials, the Young's modulus, the Poisson's ratio, and the material damping vary as a function of excitation frequency. Laboratory tests to produce such relationships are available (*3,14*). Currently, the three-dimensional effects of the wheel loading are taken into account by the use of two special viscous boundaries (front and back) connected to the two-dimensional strip model shown in Figure 2. More details on the formulation of the model have been presented elsewhere (*6,8*).

GOVERNING EQUATIONS AND SOLUTION SCHEME

Figure 2 shows a horizontally layered pavement subjected to a moving traffic load at the surface. It depicts a modified plane strain model proposed by Lysmer and his coworkers (*16,17*). Forces acting on an element in the x direction are also shown. The element has a width B in the y direction equal to the width of the loading. The equations of motion at any point in the x and z directions can be written as follows:

$$\frac{\partial \sigma_x}{\partial x} + \frac{\partial \tau_{xz}}{\partial z} + \frac{2\rho V_s}{B}\frac{\partial u}{\partial t} = -\rho \frac{\partial^2 u}{\partial t^2} \quad (1)$$

$$\frac{\partial \sigma_z}{\partial z} + \frac{\partial \tau xz}{\partial z} + \frac{2\rho V_s}{B}\frac{\partial w}{\partial t} = -\rho \frac{\partial^2 w}{\partial t^2} \quad (2)$$

where

σ_x, σ_z = normal stresses (compressive) in the x and z directions, respectively;
τ_{xz} = shear stress;
ρ = mass density;
u, w = displacements in the x and z directions, respectively; and
V_s = shear wave velocity.

Because the surface load moves at a constant speed c and the pavement layer properties do not vary in the horizontal direction,

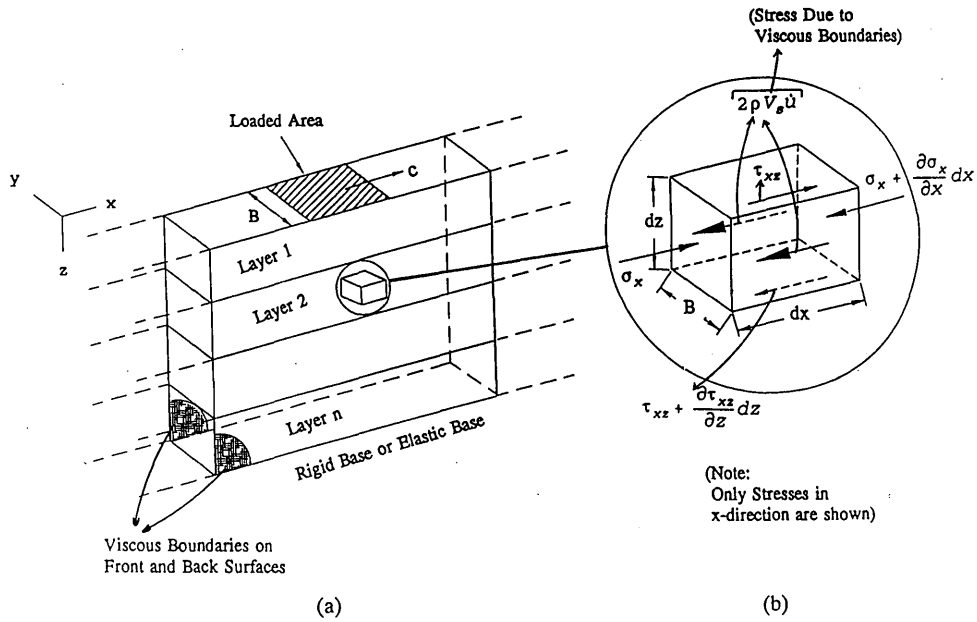

FIGURE 2 (*a*) **Rectangular load moving over layered medium;** (*b*) **stresses in an element.**

any response, say, for example, the displacement u using Fourier transform, can be written as

$$u = u(x - ct) = \text{Re} \sum_{n=0}^{N} U_n \exp[i\lambda_n(x - ct)] \tag{3}$$

where

U_n = variation in u with only z for the nth harmonic,
λ_n = wave number,
N = number of harmonics considered, and
$i = \sqrt{-1}$.

When responses are written in the form indicated in Equation 3, the derivatives with respect to x and t are simply

$$\frac{\partial u}{\partial x} = i\lambda_n u \qquad \frac{\partial u}{\partial t} = -i\lambda_n c u \tag{4}$$

After expansion of the stresses σ_x, σ_z, and τ_{xz} in terms of the displacements u and w, and subsequent use of the simplification presented in Equation 4, it is possible to derive the following equation for U_n from Equations 1 and 2:

$$\frac{d^4U_n}{dz^4} + \left[-2\lambda_n^2 + \frac{\bar{\rho}c^2\lambda_n^2(3 - 4\nu)}{2(1 - \nu)G}\right]\frac{d^2U_n}{dz^2} + \left[\lambda_n^4 - \frac{\bar{\rho}c^2\lambda_n^4(3 - 4\nu)}{2(1 - \nu)G} + \frac{\bar{\rho}^2\lambda_n^4c^4(1 - 2\nu)}{2(1 - \nu)G^2}\right]U_n = 0 \tag{5}$$

where G is the shear modulus, ν is the Poisson's ratio, and $\bar{\rho}$ is given by

$$\bar{\rho} = \rho + \frac{2i\sqrt{G\rho}}{\lambda_n cB} \tag{6}$$

The solution to the fourth-order ordinary differential equation above can be obtained using the method of characteristics.

The boundary conditions are as follows: First, at the surface, σ_z equals the applied traffic load, and τ_{xz} equals zero. Second, at the bottom boundary, the displacements u and w are zero. At the interfaces between the layers, continuity relations in terms of displacement u, w, σ_z, and τ_{xz} need to be satisfied. Finally, the responses from all of the harmonics are algebraically added to get the complete response.

A computer code DYNPAVE has been developed incorporating the steps above. This program can handle any number of layers with any type of load distribution at the surface. The higher the number of layers, the larger the computational effort. At present, the code is capable of incorporating frequency-dependent properties for the AC layer at the same time that the base and subgrade are treated as linear-elastic layers. There is no practical limit to the number of horizontal layers that can be considered by the program. The material characterization used for the AC layer in the proposed study is presented subsequently. It was not necessary to consider all of the harmonics, because the contribution of the harmonics with large wave numbers (λ_n) is quite small. The computational effort associated with the proposed analysis can be reduced substantially by specifying a cutoff wave number above which the computation of the response is not required.

PAVEMENT STRAINS FOR SPENT-FUEL TRUCKS

Configuration of Spent-Fuel Trucks

Spent-fuel elements currently are stored near nuclear power plants, but they will need to be transported to the Yucca Mountain repository. Plans are to enclose the fuel elements in a cask and mount the cask on a flatbed truck. A proposed cask-trailer system is presented in Figure 3. A detailed study has identified several types of trucks, both typical and atypical, that might possibly be

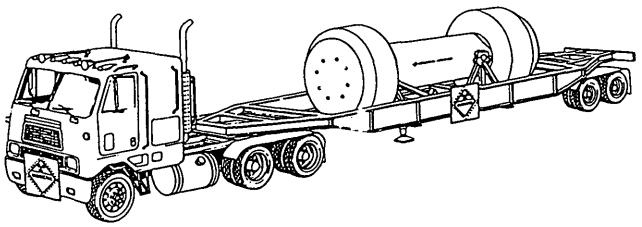

FIGURE 3 Typical spent-fuel truck and cask.

used in the spent-fuel transportation to the repository (*18*). The four types of vehicles under consideration are

- Existing legal-weight truck (LWT1),
- Future legal-weight truck (LWT2),
- Existing overweight truck (OWT1), and
- Future overweight truck (OWT2).

Table 1 shows the payload, gross vehicle weight, axle configuration, and axle load distribution for each vehicle. The overweight trucks use a tridem axle, whereas the legal-weight trucks use a tandem axle. It may be noted that if overweight trucks are used, there will be fewer trips to the repository site. On the other hand, overweight trucks' speed on state routes and through mountainous terrain will be slower.

Site and Material Characterization

The University of Nevada, Reno, and the Nevada Department of Transportation collected extensive FWD data for at least 4 years and during all four seasons on a variety of pavements located within the state. The data base consists of FWD measurements taken at 27 sites at 15.2-m intervals covering each test section, 305 m long. FWD testing using the Dynatest FWD model 8000 was carried out at four load levels, varying from 27 kN to as much as 90 kN (*19*).

Deflection basins obtained in the FWD tests were used with the MODULUS program to backcalculate layer moduli (*20*). Note that when using the MODULUS program the thickness of the subgrade layer is not required because the variable is treated as an additional unknown along with layer modulus values. The program is much more efficient than other backcalculation programs and yields reasonable results. Results from the program have been used to construct a resilient-modulus data base for all sites and all four seasons (*19,21*).

From this extensive data base, only the results corresponding to Site 24, which is located near Reno, Nevada, have been selected for the site-specific study reported in this paper. Pavement layer thicknesses obtained from coring and the average pavement layer resilient modulus values for summer were extracted from the data base and are shown in Figure 4 (*19,21*).

It may be noted that the proposed dynamic pavement response model is capable of handling viscoelastic characterization for the layers. Because only the AC layer exhibits strong frequency-dependent behavior, the viscoelastic layer characterization is used for the AC layer, and the base and the subgrade layers are assumed to be elastic. For the AC layer, the frequency-dependent resilient modulus must be deduced from the resilient moduli (elastic) backcalculated from FWD tests. A procedure adopted to achieve this is presented below.

Figure 5 indicates the load pulses applied during FWD testing. Two pulses are presented that have been normalized so that the shapes of the pulses can be seen clearly. The normalized Fourier transforms obtained for these pulses are represented in Figure 6. It is clear from Figures 5 and 6 that the dominant frequency range associated with the pulses is quite wide (up to 30 Hz). In other words, the backcalculated AC resilient modulus from FWD testing is, in fact, a representative value for this wide range of dominant frequencies.

Sousa and Monismith (*22*) studied the effects of different parameters on the resilient modulus of AC. The AC samples were tested under three different temperatures, 11, 25, and 40°C, and

TABLE 1 Cask and Vehicle Types and Weight Distribution

Vehicle Type	Loaded Cask Weight, kN	Gross Vehicle Weight (GVW), kN	Axle Configuration and Loads, kN
LWT1: Legal Weight	200.0	331.4	Single-Tandem-Tandem 44.5 - 144.6 - 142.3
LWT2: Future Legal Weight	224.6	351.4	Single-Tandem-Tandem 48.9 - 151.2 - 151.2
OWT1: Current overweight	349.6	493.7	Single-Tridem-Tridem 53.4 - 209.1 - 231.3
OWT2: Future Overweight	355.8	516.0	Single-Tridem-Tridem 48.9 - 226.8 - 240.2

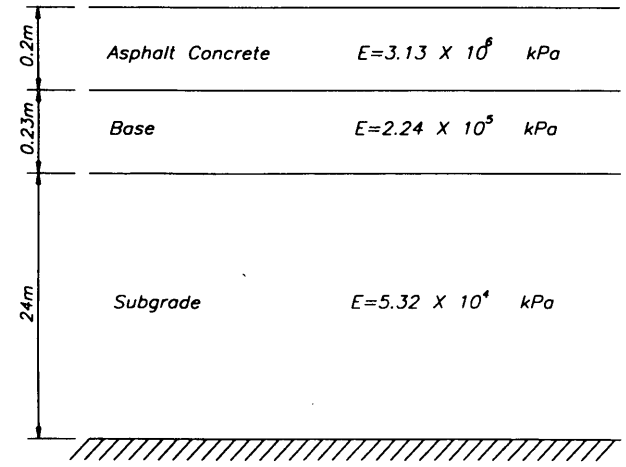

FIGURE 4 Pavement layer configuration at Site 24.

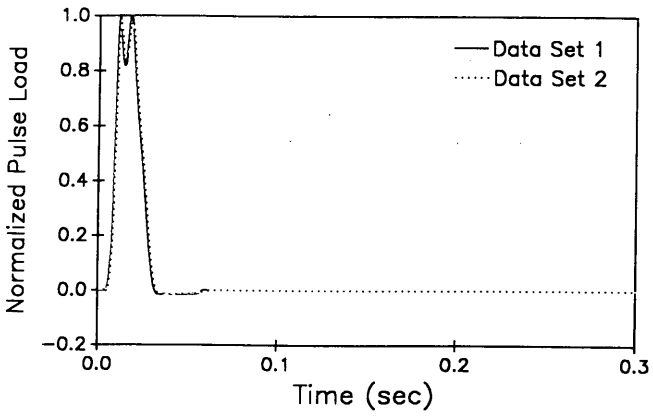

FIGURE 5 Normalized FWD pulses.

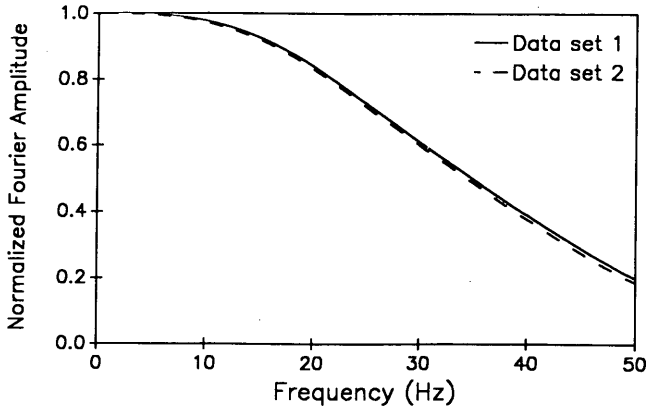

FIGURE 6 Normalized Fourier amplitude of FWD pulses.

were subjected to sinusoidal cyclic axial and torsional loading with varying frequencies. They found that for AC the amplitude of the dynamic complex Young's modulus $|E^*|$ is a function of temperature and frequency of the loading (Figure 7). Figure 7 illustrates that the dynamic Young's modulus for AC increases with an increase in frequency and decreases with an increase in temperature.

The steps employed to arrive at the frequency-dependent AC modulus can be summarized as follows:

1. Assume that the curves, $|E^*|$ versus frequency (f), given in Figure 7 are master curves. This means that the variation in $\log|E^*|$ in summer (T = 25°C) at Site 24 will vary linearly with $\log(f)$ as shown in Figure 8. Therefore, if E_o^*, which is the value of $|E^*|$ at f = 1 Hz, is known, the entire variation of E^* with frequency can be defined. Then an equation for $|E_n^*|$ at 25°C and at a frequency f_n (Figure 7) is given by the following:

$$\log|E_n^*| = \log(E_o^*) + 0.165 \log(f_n) \quad (7)$$

2. Assume a value for E_o^*, and compute the axial strain ϵ_f as

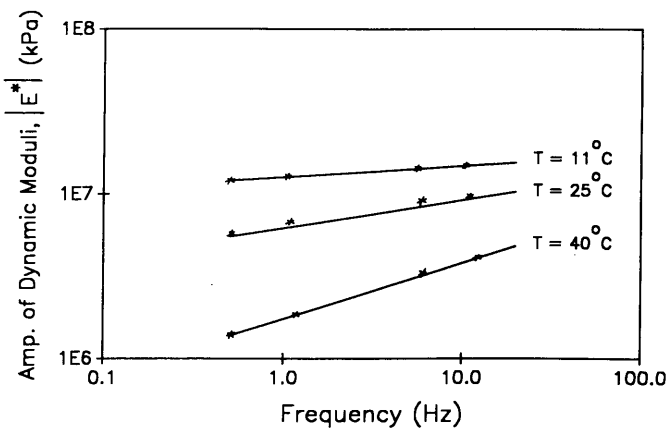

FIGURE 7 Variation of AC resilient modulus with frequency (23).

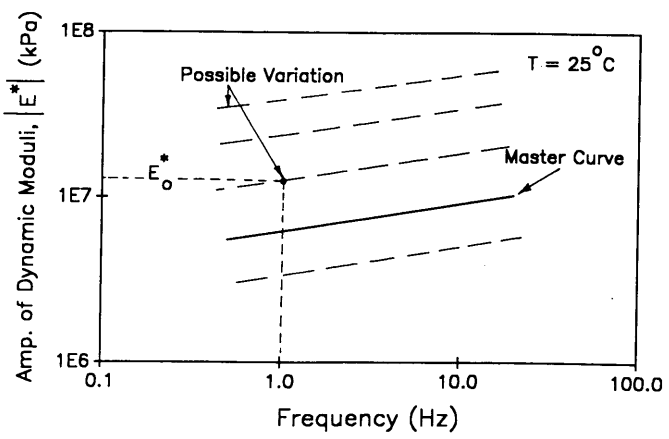

FIGURE 8 Curve fitting to obtain $|E^*|$ variation.

$$\epsilon_f = \sum_{n=0}^{N} \frac{P(t)}{|E_n^*|} = \sum_{n=0}^{N} \frac{p_n}{|E_n^*|} \tag{8}$$

where $P(t)$ and p_n are the pulse loading (Figure 5) and the corresponding Fourier amplitude.

3. Compute the axial strain ϵ_{fwd} that corresponds to the resilient modulus derived from FWD analysis as

$$\epsilon_{fwd} = \frac{1}{E_{AC}} \tag{9}$$

where E_{AC} is the resilient modulus given for AC by the FWD backcalculation. Note that unit pressure was used in the computations of ϵ_f and ϵ_{fwd}.

4. If the difference between ϵ_{fwd} and ϵ_f is not within an acceptable limit (say, 5μ), repeat Steps 2 through 4 with a new E_o^* until convergence is achieved.

5. Once the convergence has been reached, the value of E_o^* substituted into Equation 7 gives the variation of $|E^*|$ with the frequency for the AC layer at any site.

Convergence was reached for Site 24 (during summer) for $E_o^* = 8.3 \times 10^5$ kPa. Other material properties, such as a dynamic Poisson's ratio and the material damping, are assumed to be those reported by Sousa and Monismith (*22*).

Results of Pavement Strains

In pavement design, the contact area is determined by dividing the load on each tire by the contact pressure. In the literature the tire-pavement contact area often has been approximated by a rectangle ($0.4\,L \times 0.6\,L$) and two semicircles with a radius of $0.3L$ as shown in Figure 9(a), in which L is the total length of the loaded area. L can be obtained following Yoder and Witczak (*2*) or Huang (*3*) as follows:

$$L = \sqrt{\frac{A_c}{0.5227}} \tag{10}$$

where A_c is the contact area. Because the proposed approach can handle only a rectangular loaded area, one must arrive at an equivalent rectangular loaded area. The proposed equivalent rectangular area is indicated by dotted lines in Figure 9(a). The equivalent loaded area was obtained by selecting the length of the rectangle, such that the area of the rectangle equals A_c. Dual tires may be modeled by combining the two rectangular loaded areas as indicated in Figure 9(b). The tire pressure in all of the results reported here was assumed to be 861 kPa.

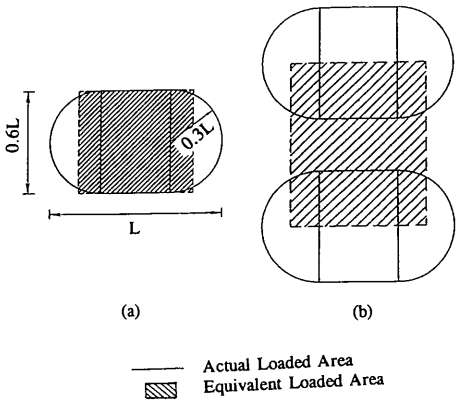

FIGURE 9 Approximate loaded areas for single and dual tires.

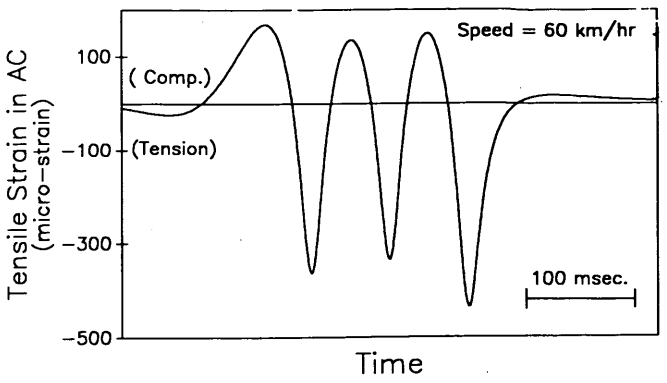

FIGURE 10 Computed tensile strain history induced in AC by tridem axle.

Although the program DYNPAVE can compute strain, stress, displacement, and acceleration at any point, only longitudinal strain response at the bottom of the AC layer is reported in this paper. A typical computed time history response of longitudinal strain for a tridem axle traveling at a speed of 60 km/hr is shown in Figure 10. Each tire in the axle was assumed to carry 19.3 kN, giving a total of 232 kN for the axle. There are three tensile axial strain peaks representing the three loaded axles. The maximum tensile and compressive strains are 435 and 168μ. Two observations similar to those made by Sebaaly et al. (*11,12*) in the field can be made: (a) the strain response has both tensile and a substantial compressive strain, and (b) the strain response is a result of complex interaction between adjacent wheels.

Figure 11 shows the maximum tensile and compressive AC strain and the vertical compressive subgrade strain induced by all four vehicles traveling at 60 km/hr. The tensile AC strains vary between 434 and 439μ, whereas the compressive AC strains vary between 168 and 175μ. The small variation in AC strains induced

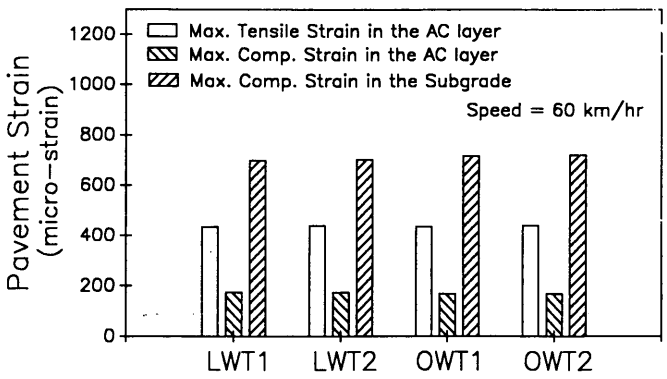

FIGURE 11 Dynamic pavement strains induced by spent-fuel trucks.

by the vehicles can be attributed to similar maximum load and tire values for the vehicles (see Table 1). The maximum compressive strain in the AC is as much as 40 percent of the maximum tensile strain. Note that, even though the maximum AC strains (tensile and compressive) may not be substantially different between tridem and tandem axle configurations, three and two strain pulses are caused by these configurations, respectively. The influence of the difference in the number of pulses on pavement damage can be quite important, and it can be evaluated readily in the laboratory using fatigue beam tests.

Vertical compressive strain in the subgrade varies between 698 and 720μ for all the vehicles. Higher strains are induced by overweight trucks. Unlike the AC strains, the axle configuration has a somewhat higher influence on the magnitude of the subgrade strain. However, because of the limited number of spent-fuel casks to be transported, the increase in the magnitude of the subgrade strain associated with the overweight trucks is not considered critical. However, given the different characteristics of the pulses generated by the tandem and tridem vehicles, their effect on the permanent deformation of the subgrade may be dissimilar.

The effect of vehicle speed on maximum tensile strain induced in the AC layer is illustrated in Figure 12. Reduction in strain is quite substantial in all cases (i.e., a decrease from 538 to 361μ —a reduction of 33 percent—when the speed of the LWT1 vehicle increased from 30 to 90 km/hr).

On the basis of the results of the DYNPAVE analyses presented in Figures 11 and 12, it can be concluded that axle configuration and vehicle speed are the most critical factors. Various vehicles considered here apply strain pulses with similar maximum amplitude yet different characteristics. Vehicle speed, however, is highly significant in determining the level of strain induced on the pavement. Therefore, in order to clearly identify the effects of various types of trucks on pavement performance, the influence of these factors must be considered.

It is evident from the results presented that the difference in contribution to pavement damage by the two legal-weight trucks, LWT1 and LWT2, is insignificant. This is also true for the overweight trucks, OWT1 and OWT2. It was pointed out earlier that the overweight trucks with heavier loads and tridem axle configuration will be traveling more slowly than the legal-weight trucks. Furthermore, it is customary for state departments of transportation to assign a speed limit to overweight trucks. On the other hand, the overweight trucks will carry heavier loads, which will reduce the number of trips they must make to the repository. Therefore, comparison of the effects of the overweight and legal-weight trucks is basically a choice between lower speed, more pulses, and fewer trips and higher speed, fewer pulses, and more trips. An effort to quantify these differences is under way at the University of Nevada, Reno.

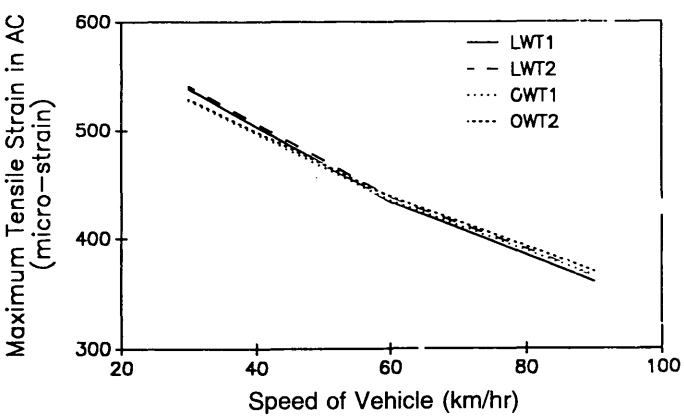

FIGURE 12 Variation of maximum tensile strain in AC with speed of vehicle.

SUMMARY AND CONCLUSIONS

Four types of vehicles were identified as vehicles that may be used to transport spent-fuel casks to Yucca Mountain in Nevada. The increase in traffic from spent-fuel trucks traveling to the repository will accelerate pavement deterioration in the state. One of the major goals of a study under way at the University of Nevada, Reno, is an estimation of the cost associated with the additional maintenance and rehabilitation of roads serving repository traffic.

To use mechanistic methods to evaluate pavement distress, strains induced on the pavement must be measured. This paper describes the use of a newly developed "finite-layer" moving-load model to compute pavement strains. In the model, a pavement layer system may be characterized as viscoelastic or as having elastic layers. The related computer program, DYNPAVE, can handle any number of layers with any type of load distribution at the surface.

A site near Reno, Nevada, was tested, and the response of the longitudinal strain in the AC layer and the vertical compressive strain in the subgrade caused by all four types of spent-fuel trucks were reported. The frequency-dependent material properties (viscoelastic) of the AC layer were deduced from the Fourier transform of the FWD load pulse, based on the assumption that the amplitude of the resilient modulus varies linearly with the logarithm of the frequency. Dynamic tests on triaxial samples support this assumption. The base and the subgrade were considered elastic, and their resilient modulus values were deduced from the data base of backcalculated moduli derived from FWD measurements.

The AC strain history results are similar to those reported by Sebaaly et al. (*11,12*), who measured AC strains under a moving semitrailer. The results reported in this paper indicate that (*a*) the strain response is a result of a complex interaction between adjacent wheel loads, (*b*) a substantial compressive strain component is present (as much as 40 percent of the tensile strain), and (*c*) the strain response is affected strongly by the speed of the vehicle.

The maximum tensile strain in the AC layer induced by the four trucks traveling at 60 km/hr varies between 434 and 439μ. The study reveals that the magnitudes of two important pavement strains (tensile strain in the AC and compressive strain in the subgrade) are similar for legal-weight vehicles considered in the study. Therefore, similar pavement deterioration may be expected from legal-weight trucks. Overweight trucks indicated the identical result. On the other hand, the characteristics of the strain pulses generated by the overweight trucks will be quite different from those generated by the legal-weight trucks because different axle configurations are used in the vehicles. Laboratory fatigue tests on AC beams and cyclic tests on subgrade soils are being considered to quantify the deterioration associated with the strain histories generated by tridem and tandem axle loading.

An increase in vehicle speed reduced the longitudinal strain in the AC layer by as much as 33 percent when the speed increased

from 30 to 60 km/hr. This result has serious implications. Legal-weight trucks may travel faster, and thus induce smaller strains. However, they would need to make more trips to the repository to deliver the same number of spent-fuel tanks. Research to quantify these factors and to evaluate trucks different effects on pavement deterioration is under way.

REFERENCES

1. Office of Civilian Radioactive Waste Management. *Department of Energy Section 175 Report.* Report DOE/RW-0205. U.S. Department of Energy, Dec. 1988.
2. Yoder, E. J. and M. W. Witczak. *Principles of Pavement Design*, 2nd ed., John Wiley and Sons, Inc., New York, 1975.
3. Monismith, C. L. Analytically Based Asphalt Pavement Design and Rehabilitation: Theory to Practice, 1962–1992. In *Transportation Research Record 1354*, TRB, National Research Council, Washington, D.C., 1992, pp. 5–26.
4. Huang, Y. H. *Pavement Analysis and Design.* Prentice Hall, Englewood Cliffs, N.J., 1993.
5. *Thickness Design: Asphalt Pavements for Highways and Streets.* Manual Series No. 1 (MS-1). Asphalt Institute, College Park, Md., Feb. 1991.
6. Zafir, Z. and R. Siddharthan. Dynamic Response of Elastic Layered Medium to Moving Loads, *Proc., 33rd AIAA/ASME Conference on Structures, Structural Dynamics, and Materials*, Dallas, Tex. Vol. 3, April 1992, pp. 1549–1557.
7. Zafir, Z. *Response of Layered Media to Moving Loads.* Ph.D. dissertation. Civil Engineering Department, University of Nevada, Reno, 1993.
8. Zafir, Z., R. Siddharthan, and P. Sebaaly. Dynamic Pavement Strain Histories from Moving Traffic Load. *Journal of Transportation Engineering*, ASCE, Oct. 1993.
9. Werkle, H. and G. Waas. Analysis of Ground Motion Caused by Propagating Air Pressure Waves. *Journal of Soil Dynamics and Earthquake Engineering*, Vol. 6, 1987, pp. 196–202.
10. Siddharthan, R., Z. Zafir, and G. M. Norris. Moving Load Response of Layered Soil I: Formulation. *Journal of Engineering Mechanics*, ASCE, Vol. 119, No. 10, Oct. 1993, pp. 2052–2071.
11. Sebaaly, P. E., N. Tabatabaee, B. T. Kulakowski, and T. Scullion. *Instrumentation for Flexible Pavements; Field Performance of Selected Sensors*, Final Report Vol. I and II. Report FHWA-RD-91-094. FHWA, U.S. Department of Transportation, Sept. 1991.
12. Sebaaly, P. E., and N. Tabatabaee. Influence of Vehicle Speed on Dynamic Loads and Pavement Response. In *Transportation Research Record 1410*, TRB, National Research Council, Washington, D.C., 1993, pp. 107–114.
13. Huhtala, M., and J. Pihlajamäki. New Concepts on Load Equivalency Measurements. *Proc., 7th International Conference on Asphalt Pavements*, Nottingham, England, 1992, pp. 194–208.
14. Sousa, J. B., J. Lysmer, S. S. Chen, and C. L. Monismith. Effects of Dynamic Loads on Performance of Asphalt Concrete Pavements. In *Transportation Research Record 1207*, TRB, National Research Council, Washington, D.C., 1988, pp. 145–168.
15. Sebaaly, P. E., and M. S. Mamlouk. Prediction of Pavement Response to Actual Traffic Loading. Presented at 66th Annual Meeting of the Transportation Research Board, Washington, D.C., Jan. 1989.
16. Hwang, R. N., J. Lysmer, and E. Berger. A Simplified Three-Dimensional Soil-Structure Interaction Study. *Proc., 2nd Specialty Conference on Structural Design of Nuclear Plant Facilities*, New Orleans, La., Vol. I-A, Dec. 1975, pp. 786–808.
17. Lysmer, J., T. Udaka, C. F. Tsai, and H. B. Seed. FLUSH: *A Computer Program for Approximate 3-D Analysis of Soil-Structure Interaction Problems.* Report EERC 75-30. University of California, Berkeley, Nov. 1975.
18. *Overweight Truck Shipments to Nuclear Waste Repositories: Legal, Political, Administrative and Operational Considerations.* Technical Report BMI/OTSP-01. Battelle Memorial Institute, Columbus, Ohio, March 1986.
19. Sebaaly, P. E., R. Siddharthan, M. Javaregowda, and S. Srikantiah. *Mechanistic Overlay Design Procedure for the State of Nevada.* Report 410-4. Nevada Department of Transportation, Carson City, June 1992.
20. Lytton, R. L., F. P. Germann, Y. J. Chou, and S. M. Stoffels. *NCHRP Report 327: Determining Asphaltic Concrete Pavement Structural Properties by Nondestructive Testing.* TRB, National Research Council, Washington, D.C., June 1990, 105 pp.
21. Siddharthan, R., P. E. Sebaaly, and M. Javaregowda. Influence of Statistical Variation in Falling Weight Deflectometers on Pavement Analysis. In *Transportation Research Record 1377*, TRB, National Research Council, Washington, D.C., 1992, pp. 57–66.
22. Sousa, J. B. and C. L. Monismith. Dynamic Response of Paving Materials. In *Transportation Research Record 1136*, TRB, National Research Council, Washington, D.C., 1987, pp. 57–68.

Publication of this paper sponsored by Committee on Strength and Deformation Characteristics of Pavement Sections.

Influence of Stress Levels and Seasonal Variations on In Situ Pavement Layer Properties

A. SAMY NOURELDIN

Presented is a small-scale investigation of how stress levels and seasonal variations affect pavement layer characteristics. Monitoring such effects is basic to the effort conducted under the Strategic Highway Research Program (SHRP) Long-Term Pavement Performance (LTPP) studies currently under the FHWA jurisdiction. Illustrated are the influences of stress levels, seasonal temperature variations, seasonal moisture variations, and accumulated equivalent single axle loads (ESALs) on (*a*) center deflection (D_o) measured by the falling-weight deflectometer; (*b*) in situ asphalt concrete modulus (E_{AC}); (*c*) in situ granular layer modulus (E_g); (*d*) in situ subgrade resilient modulus (*MR*); (*e*) in situ AASHTO effective structural number (SN_{eff}); and (*f*) variability within a section for each of the structural factors above. Analysis of results suggests that *MR* is the parameter most affected by a change in stress level, followed by E_g, E_{AC}, and SN_{eff}. On the other hand, E_{AC} is the parameter most affected by the change in temperature, followed by D_o, SN_{eff}, E_g and *MR*. Variations in *MR* and E_g with temperature are believed to be associated indirectly with variations in E_{AC} and temperature. Changes in E_{AC} and temperature result in changes in stress levels imposed on the underlying pavement layers that cause variations in *MR* and E_g. Accumulation of ESALs under dry conditions affect E_{AC}, followed by D_o, E_g, SN_{eff}, and *MR*, in order of diminishing effect. In addition, seasonal moisture variations affect D_o and *MR*, followed by E_g, E_{AC} and SN_{eff}. And variability within a section for each of the structural factors increases with an increase in temperature, moisture level, or accumulated ESALs. Among the structural factors, SN_{eff} has the lowest within-section variability, whereas E_g has the greater within-section variability.

Nondestructive deflection testing using the falling-weight deflectometer (FWD) is part of an ongoing monitoring effort planned by the Strategic Highway Research Program (SHRP) for the Long-Term Pavement Performance (LTPP) studies (*1*). Nondestructive deflection testing provides data necessary for in situ material characterization for the various pavement layers as well as information on material variability that became an explicit independent variable in the 1986 (AASHTO) design equations (*2*). Backcalculated moduli from deflection measurements at a number of locations within pavement test sections can be used to establish the mean, minimum, maximum, and standard deviation of moduli for each layer (*1*). Use of different load levels by the FWD at a single location also can provide information regarding variations of layer moduli with stress sensitivity. The effect of seasonal temperature variations on layer moduli may be investigated through successive testing with the FWD at different air temperatures, similar moisture conditions, and within a short time span. Similarly, the effect of seasonal moisture variations may be investigated through successive testing with the FWD at different moisture levels, similar air temperatures, and again, within a short time span. Finally, the effect of accumulated equivalent single axle loads (ESALs) on layer moduli can be investigated through testing at similar air temperatures, similar moisture levels, and during a long time period.

UNDP Experts Team, Materials and Research Department, Ministry of Communications, Riyadh 11178, Saudi Arabia.

The effects of stress levels and seasonal variations on pavement material properties are simulated in the laboratory; such tests have been reported in many research studies. Hicks, for example, reported the effect of stress level and moisture conditions on the laboratory-determined resilient characteristics of granular materials (*3*). Thompson et al. documented the effect of stress level and degree of saturation on resilient characteristics of subgrade soils (*4,5*). Witczak reported the effect of temperature on the dynamic modulus of asphalt concrete as determined in the laboratory (*6*).

A need still exists to verify that the influence of stress levels and seasonal variations on pavement material characteristics obtained in the laboratory under simulated field conditions is actually, or closely related to, those in situ characteristics. It is hoped that results of the SHRP LTPP studies will help to satisfy this need.

This paper presents a small-scale study that investigates the influence of stress levels, seasonal variations, and accumulated ESALs on in situ pavement layer characteristics.

EXPERIMENTAL DESIGN

The experimental part of this study is designed statistically to provide as many reliable inferences on such effects as possible. Three designs are used.

Design 1

The first design is set to investigate the effects of two main factors: stress levels and seasonal temperature variations.

Stress Levels

The stress-level factor consists of three levels, each of which is the stress induced by a specific load applied by the FWD. The FWD used for this study has seven geophones and a loading plate radius of 15 cm. Load levels selected are 9,000, 14,000 and 18,000 lb (40, 62, and 80 kN). Testing is conducted for pavement sections on the outer wheel path of the truck lane (approximately 90 cm from the shoulder edge).

Seasonal Temperature Variations

Seasonal temperature variation consists of three levels (hot, cool, and medium), and each level relates to a specific month: August (hot), November (cool), and April (medium). Note that most seasonal variations within Saudi Arabia can be represented by temperature variations; there is neither a frost period nor a spring thaw period to affect pavement. Changes in the moisture level within paving layers are less likely to occur as compared with changes in temperature. The effect of moisture variation is described later (Design 3).

Site conditions, including air temperature, pavement surface temperature, pavement temperature at the mid-point of the asphalt bound layer, temperature at the bottom of the asphalt bound layers, and moisture density characteristics of nonbound paving layers, are obtained at each of the three temperature levels.

Test Locations

Using test section lengths of 1 km, deflection testing is conducted at 50-m intervals (21 points per section) on the outer wheel path of the truck lane. Test locations are marked to ensure that subsequent seasonal testing is conducted at identical locations.

Response Variables

Main response variables measured (or computed) per load level (40, 62, or 80 kN) per seasonal temperature (August, November, or April) for each of 21 locations are

- Center deflection, D_o;
- Overall one-layer modulus, E_o, computed using the load level, the center deflection, and assuming a one-layer system;
- Backcalculated subgrade modulus, MR;
- Backcalculated modulus for the asphalt bound layer, E_{AC};
- Backcalculated modulus for the nonbound granular layer, E_g; and
- AASHTO effective structural number, SN_{eff}.

Backcalculated layer moduli and SN_{eff} are obtained for a three-layer system employing a simple modification of the two-layer process developed by the author (*7*). This process was tested thoroughly, and its accuracy and consistency were verified.

Replicate Segments

Design 1 is repeated for 12 pavement segments representing different regions in Saudi Arabia in order to investigate the variability between sections for the main factors included in the design.

Time Span Between Seasons

Note that the time span between seasons is set to allow as wide a range of temperature variation as possible. However, the time span factor also is adjusted to minimize the effect of moisture and traffic repetition on the response variables during this time span.

Design 2

The second design is prepared to investigate the effect of time in terms of accumulated traffic (fixed season and fixed stress level) on the same response variables described under Design 1. Two levels of this factor are considered, "time zero" and "time four." "Time zero" is November 1988, and "time four" is November 1992. Stress and season levels are fixed in order to make the time factor represent the effect of traffic in terms of loads ESALs as much as feasible. Aging effects would confound the ESAL effect in this case.

Design 3

The third design is set to investigate the effects of seasonal moisture variations on the same response variables described for Design 1. Because large changes in moisture levels within pavement layers are less likely to occur in Saudi Arabia, it was decided to conduct deflection testing on test segments directly after a period of rainfall. Two levels of the seasonal moisture variation factor were obtained, dry (November 1992) and wet (February 1993).

ANALYSIS OF RESULTS

Effect of Stress Levels and Seasonal Temperature Variations

Center Deflection, D_o

Figure 1 illustrates the influence of load level on the center deflections measured for Site 1 during November 1988. Note that the general shape of the center deflection profile is similar for the three load levels (9,000, 14,000, and 18,000 lb). Detailed conditions for Site 1 are given in Table 1.

Figure 2 shows the influence of season (August versus November) on the center deflection measured at a load level of 9,000 lb

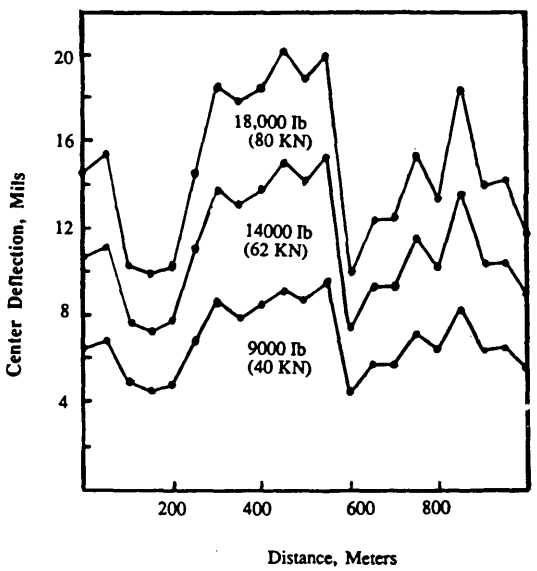

FIGURE 1 Influence of load level on FWD center deflection during November.

TABLE 1 Conditions of Site 1 During FWD Testing (Design 1)

Site Condition	August 1988	November 1988	April 1989	Cross Section
Temperature				
Air	44°C	24.5°C	34.2°C	7.0 Inch Asphalt Concrete
Surface	55°C	30.6°C	42.8°C	10.0 Inch Granular Subbase
Midpoint of AC Layer	49.5°C	27.5°C	38.5°C	
Bottom of AC Layer	44°C	24.5°C	34.2°C	
Subbase Layer				
Classification	A-2-4	A-2-4	A-2-4	
Moisture Content	5.6%	5.7%	5.8%	
Dry Density, t/m³	1.796	1.794	1.792	
Subgrade Layer				
Classification	A-2-6	A-2-6	A-2-6	
Moisture Content	7.6%	7.8%	8.2%	
Dry Density, t/m³	1.728	1.725	1.719	

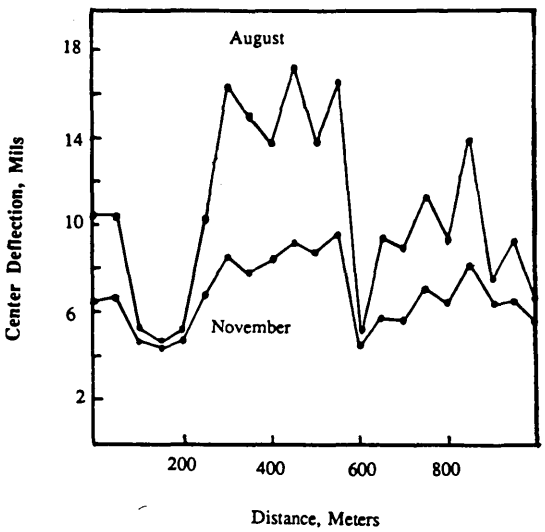

FIGURE 2 Influence of season (temperature level) on FWD center deflection at load level of 9,000 lb.

(40 kN). The seasonal effect is a temperature-related effect because moisture conditions are practically identical, as indicated in Table 1. Points with relatively low deflection values are not as sensitive to temperature as those with relatively high deflection values (Figure 2).

Table 2 presents statistics—means and coefficients of variation (c.o.v.)—of the FWD center deflection during various seasons and load levels for Site 1. Note that the within-section deflection variability represented by the coefficient of variation remains practically the same at various load levels. However, the variability increases with an increase in temperature during testing. Also, the mean center deflection obtained at a load level of 18,000 lb, for example, can be duplicated by simply multiplying the mean center deflection obtained at a load level of 9,000 lb by 2, with a marginal error. The possibility of using a higher load level when testing in cool weather conditions to simulate measurements in hot weather conditions is apparent as one compares the mean center deflection of a 14,000-lb load during the month of November (cool) with the mean center deflection of a 9,000-lb load during the month of August (hot).

TABLE 2 Statistics of FWD Center Deflections in Mils During Various Seasons at Three Load Levels

			Season		
		Statistics	August 1988	November 1988	April 1989
Load Level	9000 Pounds	Mean	10.47	6.78	7.90
		c.o.v.	39.5%	23.3%	28%
	14000 Pounds	Mean	16.29	10.98	13.32
		c.o.v.	39.5%	23.5%	27.6%
	18000 Pounds	Mean	21.34	14.75	17.77
		c.o.v.	37.30%	23.6%	26.9%

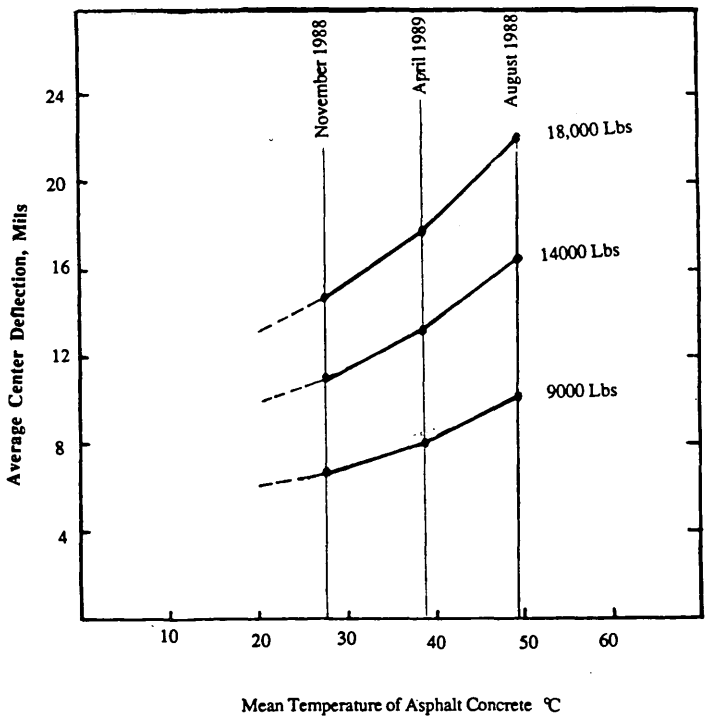

FIGURE 3 Center deflection and temperature relationship at various FWD load levels.

Figure 3 graphically represents data given in Table 2; the horizontal axis represents the mean temperature of asphalt concrete (measured at the mid-depth of the asphalt bound layer), and the vertical axis represents the average center deflection for Site 1. It is suggested that there is no effect of temperature and load level interaction on the center deflection, as indicated by the parallel lines.

Overall One-Layer Modulus, E_o

The overall one-layer modulus is computed using the load level, the center deflection, and by assuming that the pavement is a one-layer system.

Table 3 presents the statistics of E_o during the various seasons (August, November, and April) at load levels of 9,000, 14,000 and 18,000 lb for Site 1. It can be noted that the E_o value at a load level of 18,000 lb is 93 percent (on average) of its value at a load level of 9,000 pounds. On the other hand, the E_o value in August—when the average temperature of asphalt concrete is 49.5°C, (Table 1)—is (on average) 67 percent of its value in November, when the average temperature of asphalt concrete is 24.5°C (Table 1).

Asphalt Concrete Modulus, E_{AC}

Figure 4 (*top*) shows the influence of load level on the backcalculated asphalt concrete modulus. A slight but consistent (and statistically significant) effect is present. Moduli obtained at a load level of 18,000 lb (80 kN) are lower than those obtained at a load level of 9,000 lb (40 kN), indicating a slight, consistent, stress-softening pattern. In fact, the roadway from which the test site was selected does show signs of rutting and is currently scheduled for repair.

Figure 5 (*top*) illustrates the influence of season (August versus November) on the backcalculated asphalt concrete modulus. The reduction in moduli with temperature is apparent when the modulus profile in November (when the mean asphalt concrete temperature is 24.5°C) is compared with the modulus profile in August (when its average temperature is 49.5°C).

Table 4 presents statistics for the backcalculated asphalt concrete modulus during various seasons and load levels. Variability in terms of the coefficients of variation increases slightly with load level; it increases considerably with temperature.

TABLE 3 Statistics of Overall One-Layer Modulus, E_o, in Pounds per Square Inch During Various Seasons at Three Load Levels

			Season		
		Statistics	August 1988	November 1988	April 1989
Load Level	9000 Pounds	Mean	69,500	107,300	92,100
		c.o.v.	39.5%	23.3%	28%
	14000 Pounds	Mean	69,500	103,100	85,000
		c.o.v.	39.5%	23.5%	27.6%
	18000 Pounds	Mean	68,200	98,700	81,900
		c.o.v.	37.3%	23.6%	26.9%

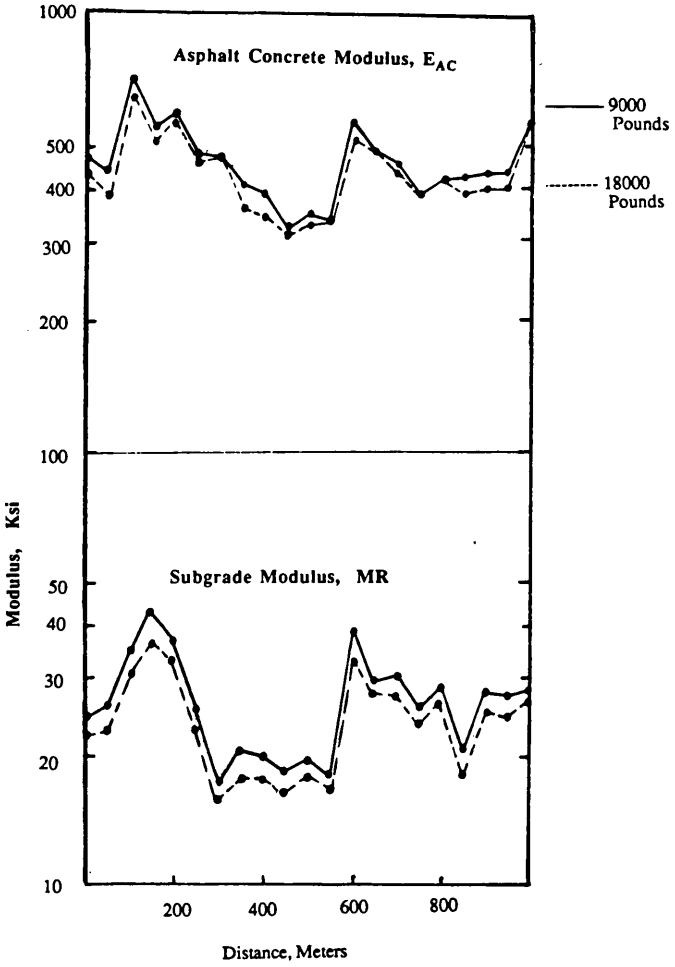

FIGURE 4 Influence of load level on backcalculated subgrade and asphalt concrete moduli during November 1988.

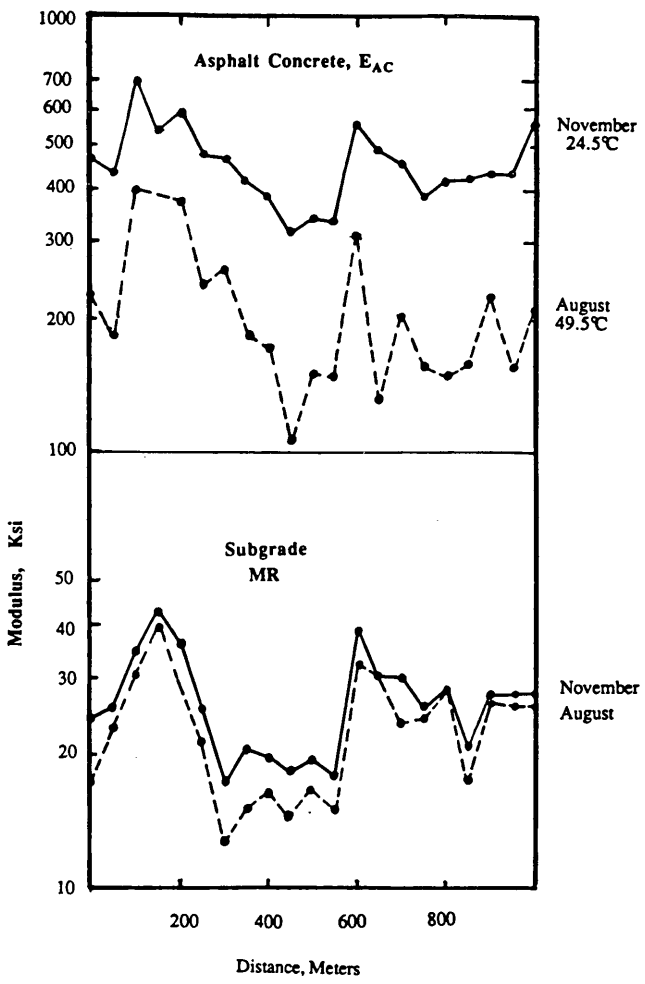

FIGURE 5 Influence of season (temperature level) on backcalculated subgrade and asphalt concrete moduli at load level of 9,000 lb.

TABLE 4 Statistics of Backcalculated Asphalt Concrete Modulus, E_{AC}, in Pounds per Square Inch During Various Seasons at Three Load Levels

			Season		
		Statistics	August 1988	November 1988	April 1989
Load Level	9000 Pounds	Mean c.o.v.	207,500 37.6%	461,000 20.5%	401,400 31.5%
	14000 Pounds	Mean c.o.v.	207,600 37.7%	449,300 20.1%	381,700 32.1%
	18000 Pounds	Mean c.o.v.	205,100 41.8%	448,600 22.4%	361,800 29.3%

TABLE 5 Statistics of Backcalculated Subgrade Modulus, *MR*, in Pounds per Square Inch During Various Seasons at Three Load Levels

			Season		
		Statistics	August 1988	November 1988	April 1989
Load Level	9000 Pounds	Mean c.o.v.	23,000 31.4%	26,700 27%	25,100 25.1%
	14000 Pounds	Mean c.o.v.	23,000 31.4%	25,300 26.3%	22,600 25.6%
	18000 Pounds	Mean c.o.v.	21,900 31.1%	23,900 25.9%	21,500 25.8%

Subgrade Modulus, MR

Figure 4 (*bottom*) shows the influence of load level on the backcalculated subgrade modulus. Moduli obtained at a load level of 18,000 lb (80 kN) are lower than those obtained at a load level of 9,000 lb (40 kN), indicating a consistent stress-softening pattern. The subgrade soil classification is A-2-6, as indicated in Table 1.

Figure 5 (*bottom*) illustrates the influence of the season (August versus November) on the backcalculated subgrade modulus. The reduction in subgrade moduli with temperature is also apparent when one compares the modulus profile in November with that in August (refer to Table 1 for site conditions). The sensitivity of subgrade modulus to temperature seems to be an indirect sensitivity to stress level. Reduction in asphalt concrete modulus, with higher temperature, results in an increased stress level on top of the subgrade that might have caused the reduction in the subgrade modulus.

Table 5 presents statistics of the backcalculated subgrade modulus during the various seasons at the three load levels. The largest variability in terms of the coefficient of variation is detected during August (i.e., it is associated with high temperature levels). Stress levels represented by load levels seem to have no effect on the within-section variability of the subgrade modulus (under dry conditions).

TABLE 6 Variations in Granular Subbase Modulus, E_g, in Pounds per Square Inch for Various Seasons at Three FWD Load Levels

Distance, meters	August 1988			November 1988			April 1989		
	9000	14000	18000	9000	14000	18000	9000	14000	18000
0	31,500	31,500	31,000	48,200	45,700	43,600	43,400	39,600	38,800
50	33,400	33,400	32,100	46,300	44,100	41,400	40,400	37,100	35,800
100	81,600	81,600	72,200	63,800	63,000	60,900	65,800	60,200	57,700
150	77,900	77,800	73,200	74,400	70,300	66,500	67,700	62,200	59,700
200	67,200	67,100	63,600	66,700	64,500	62,100	60,800	56,600	54,700
250	32,100	32,100	31,800	46,100	44,600	43,000	35,200	32,400	31,500
300	18,200	18,200	18,100	35,100	33,800	32,400	30,500	27,400	26,100
350	21.300	21,300	20,700	40,000	37,300	34,900	31,000	28,400	27,100
400	23,900	23,900	23,600	37,100	35,500	33,900	31,100	28,700	27,800
450	20,400	20,400	20,400	34,400	32,600	31,000	28,600	26,100	25,200
500	24,900	24,900	25,100	36,400	34,600	33,400	31,100	29,000	28,300
550	19,800	19,800	20,200	32,400	31,400	30,700	26,400	24,600	24,100
600	72,400	72,300	66,300	73,800	69,600	65,800	70,300	65,600	61,800
650	44,800	44,800	43,800	55,200	52,800	51,100	44,800	41,700	40,300
700	39,900	39,800	38,500	56,400	54,100	51,800	52,000	47,000	44,600
750	31,600	31,600	31,700	45,100	43,500	38,800	38,900	36,400	35,600
800	43,000	43,000	42,400	50,900	49,400	48,200	40,800	37,500	36,700
850	23,900	23,900	23,700	37,700	35,600	33,600	32,400	29,200	27,900
900	45,800	45,900	44,300	51,200	48,400	46,000	44,800	40,800	38,900
950	42,000	42,000	40,800	49,500	47,300	45,100	43,100	38,600	36,800
1000	58,000	58,000	54,500	56,600	54,400	53,000	54,700	48,200	46,000
Mean	40,600	40,600	39,000	49,400	47,300	45,100	43,500	39,900	38,400
c.o.v.	49.0%	49.0%	45.5%	25.5%	25.6%	25.8%	31.2%	31.4%	30.8%

NOTE: Three FWD load levels of 9,000, 14,000, and 18,000 lb were used.

TABLE 7 Statistics of Effective Structural Number, SN_{eff}, During Various Seasons at Three Load Levels

			Season		
		Statistics	August 1988	November 1988	April 1989
Load Level	9000 Pounds	Mean c.o.v.	3.33 12.1%	4.06 7.0%	3.85 9.4%
	14000 Pounds	Mean c.o.v.	3.33 12.1%	4.02 7.2%	3.77 9.3%
	18000 Pounds	Mean c.o.v.	3.30 11.8%	3.99 7.3%	3.72 8.7%

Granular Subbase Modulus, E_g

Table 6 presents the complete set of data obtained for the granular subbase modulus. Mean values suggest a general stress-softening pattern indicated by a slight reduction in the moduli with the increase in load level or the increase in temperature (refer to Table 1 for site conditions). However, occasional stress hardening and stress insensitivity patterns are also present. The subbase soil classification is A-2-4, as indicated in Table 1. The within-section variability increases with temperature, as indicated by the coefficient of variation in August compared with that in November. On the other hand, the within-section variability of E_g is the greatest when compared with the within-section variability of D_o, E_{AC}, and *MR*.

Effective Structural Number, SN_{eff}

Table 7 presents statistics of the AASHTO SN_{eff} computed in accordance with the process developed by the author (*7*). Results presented in Table 7 suggest a marginal reduction in SN_{eff} with the increase in load level and a considerable reduction with increasing temperature. Figure 6 presents a graphic representation of the relationship between SN_{eff} and temperature. The within-section variability of SN_{eff}, represented by the coefficient of variation, is obviously much lower than the within-section variability of other response variables (D_o, E_{AC}, *MR*, and E_g).

Adjustment Factors

Table 8 presents the stress-level adjustment factors for the pavement characteristics based on an adjustment factor of 1 at a load level of 9,000 lb. Values presented suggest a general reduction in stiffness associated with the increase in load level. The greatest stress sensitivity is associated with *MR*, followed by E_g, E_o, E_{AC}, and SN_{eff}. However, stress sensitivity for all response variables is generally low, assuming that all adjustment factors are greater than or equal to 0.9.

Table 9 provides temperature adjustment factors for pavement characteristics based on an adjustment factor of 1 at a mean asphalt concrete temperature of 20°C. As expected, the greatest temperature sensitivity is associated with E_{AC}, D_o, and E_o. However, the response variables SN_{eff}, E_g, and *MR* also show signs (probably indirect) of temperature sensitivity.

Effect of Accumulated ESALs

The effect of accumulated ESALs on pavement layer characteristics (D_o, E_{AC}, E_g, *MR*, and SN_{eff}) was investigated by conducting FWD testing in November 1988 and November 1992. A load level of 14,000 lb (62 kN) was employed. Testing during the same month eliminated the effect of temperature and moisture, although similarity of site conditions with respect to moisture and temper-

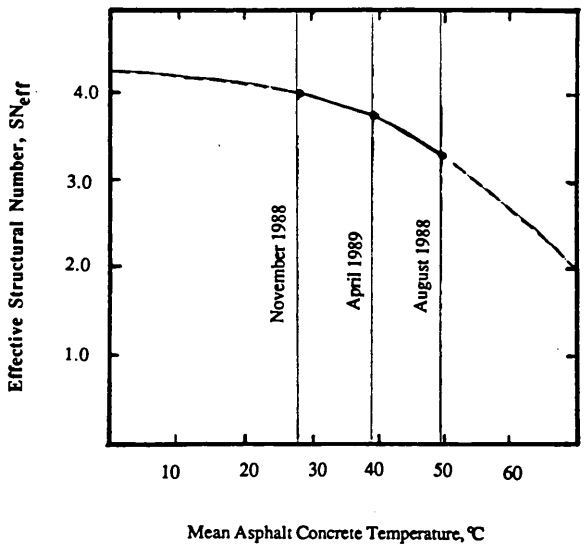

FIGURE 6 Influence of asphalt concrete temperature on effective structural number, SN_{eff}.

TABLE 8 Stress Level Adjustment Factors for In Situ Pavement Layer Properties

Characteristics	FWD Load Level		
	9000 Pounds	14000 Pounds	18000 Pounds
Overall One Layer Modulus, E_o	1.0	0.96	0.92
Asphalt Concrete Modulus, E_{AC}	1.0	0.97	0.95
Granular Subbase Modulus, E_g	1.0	0.96	0.92
Subgrade Resilient Modulus, MR	1.0	0.95	0.90
Effective Structural Number, SN_{eff}	1.0	0.99	0.98

ature levels for November 1988 and November 1992 (Table 10) may not always be that easy to obtain. On the other hand, both aging and the cyclical seasonal-variation effects statistically confound the effect of accumulated ESALs.

Accumulated ESALs during the 4-year period were $4 * 10^6$. ESALs were estimated on the basis of information obtained from the weigh and vehicle-classification stations located on the roadway.

Results provided in Table 10 suggest that accumulated ESALs result in a slight reduction in *MR* and E_g and a considerable reduction in E_{AC}. These reductions in pavement moduli also were associated with a general drop in the structural capacity of the pavement, as represented by values of D_o and SN_{eff}.

Also, the general reduction in pavement stiffness was associated with an increase in the within-section variability indicated by coefficients of variation.

Effect of Seasonal Moisture Variations

The effect of seasonal moisture variations on pavement layer properties (D_o, E_{AC}, E_g, *MR*, and SN_{eff}) was investigated by comparing the FWD test results of November 1992 with the results of February 1993. A load level of 14,000 lb (62 kN) was employed. A short time span (4 months) makes the side effect of accumulated ESALs during this time period relatively marginal. Testing in February 1993 was conducted on a sunny day following a week of unprecedented rain. Air temperatures between February and November do not vary much in Saudi Arabia. The authors were able to obtain conditions of similar temperature but different moisture levels, and within a short time span.

Table 10 (bottom) presents site conditions for November 1992 and February 1993. The heavy rain resulted in an increase in moisture content of the subbase and subgrade layers. Moisture content of the subbase increased from 5 to 9 percent, whereas the moisture content of the subgrade increased from 6.8 to 13 percent. Reductions in the field dry density of the subbase and the subgrade layers were 3.5 percent and 6.3 percent, respectively. Associated reductions in the subbase and subgrade layer moduli were 22.4 percent and 35 percent, respectively. Mean center deflection increased by 28.8 percent. Reductions in SN_{eff} and E_{AC} were relatively marginal (5.4 percent and 10 percent, respectively).

TABLE 9 Temperature Adjustment Factors for In Situ Pavement Layer Properties

Characteristics	Average Asphalt Concrete Temperature			
	20°C	27.5°C	38.5°C	49.5°C
Center Deflection, D_o	1.0	1.16	1.39	1.71
Overall One Layer Modulus, E_o	1.0	0.90	0.76	0.60
Asphalt Concrete Modulus, E_{AC}	1.0	0.90	0.76	0.41
Granular Subbase Modulus, E_g	1.0	0.91	0.78	0.77
Subgrade Resilient Modulus, MR	1.0	0.94	0.86	0.84
Effective Structural Number, SN_{eff}	1.0	0.96	0.90	0.79

TABLE 10 Site Conditions and FWD Test Results and Analysis for Designs 1 and 2

Characteristics	Statistics	November 1988	November 1992	February 1993
Center Deflection, D_o, mils	Mean c.o.v.	10.98 23.5%	13.35 29.7%	17.2 38.2%
Asphalt Concrete Modulus, E_{AC}, psi	Mean c.o.v.	449,300 20.1%	295,000 35%	265,500 37.2%
Granular Subbase Modulus, E_g, psi	Mean c.o.v.	47,300 25.6%	43,400 40%	33,700 44.7%
Subgrade Modulus, MR, psi	Mean c.o.v.	25,300 26.5%	23,700 30.5%	15,400 31.7%
Structural Number, SN_{eff}	Mean c.o.v.	4.02 12.%	3.68 10.0%	3.48 12.0%
Subbase Field Moisture Content Field Dry Density		 5.71% 1.794	 5.0% 1.774	 9.0% 1.712
Subgrade Field Moisture Content Field Dry Density, t/m³		 7.8% 1.725	 6.8% 1.711	 13.0% 1.603
Temperature Air Surface Midpoint of Asphalt Concrete Bottom of Asphalt Concrete		 24.5°C 30.6°C 27.5°C 24.5°C	 23°C 29°C 26°C 23°C	 22°C 27°C 24°C 20°C

FWD load level used was 14000 pounds (62 kN)

SUMMARY

Understanding the effects of stress levels and seasonal variations on pavement layer properties is important to SHRP's monitoring effort and its LTPP studies.

This paper presents a small-scale study that evaluates the effects of stress levels, seasonal temperature variations, seasonal moisture variations, and the accumulation of ESALs on in situ pavement layer properties. Pavement responses considered were the FWD center deflection D_o, the asphalt concrete modulus (E_{AC}), the granular layer modulus (E_g), the subgrade modulus (MR), and the effective structural number (SN_{eff}), determined through backanalysis of deflection data. The within-section variability of pavement responses that is expected to be an important, independent variable in future pavement performance models was investigated.

The author's analysis of results suggests that MR is the parameter most affected by a change in stress level, followed by E_g, E_{AC}, and SN_{eff}. However, the stress sensitivity of all pavement responses investigated generally was marginal. On the other hand, E_{AC} is the parameter most affected by temperature, followed by D_o, SN_{eff}, E_g, and MR. The temperature sensitivity of MR and E_g is believed to be an indirect stress sensitivity associated with the reduction in E_{AC} with temperature. Accumulation of ESALs under dry conditions affects E_{AC}, as well as D_o, E_g, SN_{eff}, and MR in descending order. An increase in moisture level affects MR, as well as E_g, D_o, E_{AC}, and SN_{eff}. The within-section variability of pavement responses increases with an increase in temperature, in moisture level, or accumulated ESALs. Among pavement responses, SN_{eff} has the lowest within section variability, whereas E_g has the largest.

REFERENCES

1. Richter, C. A., and J. B. Rauhut. *SHRP Plans for Nondestructive Deflection Testing in the Development of Pavement Performance Prediction Models.* Special Technical Publication 1026 (A. J. Bush III and G. Y. Baladi, eds.). ASTM, Philadelphia, Pa., 1989.
2. *AASHTO Guide for the Design of Pavement Structures.* AASHTO, Washington, D.C., 1986.
3. Hicks, R. G. *Factors Influencing the Resilient Properties of Granular Materials.* Ph.D. dissertation. University of California, Berkeley, 1970.
4. Thompson, M. R., and Q. L. Robnett. Resilient Properties of Subgrade Soils. *Transportation Engineering Journal,* ASCE, Vol. 105, Jan. 1979.
5. Thompson, M. R., et al. *Final Report; Subgrade Stability.* Report FHWA-IL-UI-169, FHWA, U.S. Department of Transportation, 1985.
6. Witczak, M. W. Design of Full Depth Asphalt Airfield Pavements. *Proc., 3rd International Conference on the Structural Design of Asphalt Pavements.* London, England, 1972.
7. Noureldin, A. S. New Scenario for Backcalculation of Layer Moduli of Flexible Pavement. In *Transportation Research Record No. 1384,* TRB, National Research Council, Washington, D.C., 1993, pp. 23–28.

Publication of this paper sponsored by Committee on Strength and Deformation Characteristics of Pavement Sections.

Abridged Procedure To Determine Permanent Deformation of Asphalt Concrete Pavements

JORGE B. SOUSA AND MANSOUR SOLAIMANIAN

Research was undertaken to find a quick and simple procedure for determining the permanent deformation characteristics of asphalt concrete mixes. Data on pavement structure, rutting, traffic level, and temperature were available for a number of test sections of the Strategic Highway Research Program's General Pavement Studies (GPS) and from Colorado sites. During a previous study, finite-element computations had indicated a strong linear relationship between rut depth and maximum shear strain developed in the field. Availability of field cores and data from GPS sites, along with the finite-element results, prompted a laboratory study to find a quick procedure to estimate permanent deformation of asphalt concrete pavements. Repeated simple shear tests at constant height were performed on specimens 6 in. (15 cm) in diameter by 2 in. (5 cm) high obtained from these cores. The shear stress was haversine in shape, with a peak magnitude of 10 psi (70 kPa), and was applied for 5,000 cycles at the mean highest average 7-day maximum pavement temperature and at a depth of 2 in. (5 cm). Maximum shear strain for each site was determined from the reported rut depth on the basis of the linear relationship between the two parameters. Then the number of laboratory cycles to yield this value of shear strain was determined. The number of laboratory cycles determined in this way was correlated with the traffic level (equivalent single axle loads) that had resulted in the reported rut depth. The correlation was encouraging, especially regarding pavements less than 10 years old with an R^2-value of about 0.68. For all pavements that did not exhibit excessive aging, this relationship was obtained with R^2 = 0.80. On the basis of this relationship, a simple procedure to evaluate the mix potential for permanent deformation is proposed.

A procedure that could be used for rapid evaluation and screening of asphalt aggregate mixes is presented. The procedure could also be adopted to evaluate the rutting propensity of a mix, taking into consideration traffic level—in terms of equivalent single axle loads (ESALs)—and the pavement location.

The underlying assumption in this approach is the fact that permanent deformation is primarily a plastic shear flow phenomenon at constant volume, occurring near the pavement surface and caused by shear stresses appearing below the edge of truck tires (*1*).

Intrinsic to this procedure is the assumption that most permanent deformation occurs during the hottest days and as a result of the heaviest trucks. That assumption stems from laboratory observations that asphalt concrete mixes exhibit strong plastic behavior, described by a plasticity function that exhibits kinematic hardening. This hardening seems to be associated with a mix's capability to develop better particle-to-particle contact as it develops shear strains, and with the capability of the aggregate skeleton to develop dilatancy forces that are in turn capable of developing stabilizing, confining stresses.

The phenomenon seems to be best captured by the repetitive simple shear test at constant height (RSST-CH) executed at the mean highest average 7-day maximum pavement temperature at a depth of 2 in. (5 cm). The test is executed using two actuators. One controls the magnitude of the applied shear stresses, whereas the other ensures that the specimen is tested under a strain-control boundary condition by maintaining the height of the specimen constant (within an acceptable margin of error).

The major drawback to the procedure is its inability to incorporate directly the effects of tire pressure and load magnitude. These effects can be brought into the analysis only indirectly, through computation of ESALs. However, equivalency factors could be accurately computed using the permanent deformation model and the finite-element methodology proposed by Sousa et al. (*2*).

BASIS FOR DEVELOPMENT OF PROCEDURE

Model Analysis

A series of finite-element analyses of the permanent deformation response of a pavement section was conducted using the model proposed (*2*). The model is intended to capture the macrobehavior of mixes, including (*a*) the shear dilatancy observed when the mix is subjected to shear strains, (*b*) the increase of effective shear modulus under increased confining pressure, (*c*) the significant variation of behavior with changes in temperature and rates of loading, and (*d*) the residual accumulation of permanent deformation under repetitive loading. Material properties were obtained from a series of volumetric, uniaxial shear and frequency sweep tests. In those analyses, only the nonlinear elastic and viscous properties of the mix were incorporated into the constitutive relationship. The purpose was to investigate the relationship among tire pressure, rut depth, and permanent shear and axial strains.

Two stress levels for the tire loading, 200 psi (1400 kPa) and 5 psi (3500 kPa), were used and were applied as a pulse loading with a duration of 0.3 sec and a 0.4-sec time interval between pulses. Conditions of high tire pressure and relatively long loading time were selected so that large ruts and the associated large permanent strains could be obtained within relatively few loading cycles. The magnified deformed finite-element mesh is represented (Figure 1) for the end of the second load cycle for the 500 psi (3500-kPa) tire loading condition. Note that a considerable

J. B. Sousa, SHRP Equipment Corporation, Richmond Field Station, 1301 South 46th Street, Richmond, Calif. 94804. M. Solaimanian, Center for Transportation Research, University of Texas at Austin, 3208 Red River Street, Suite 200, Austin, Tex. 78705.

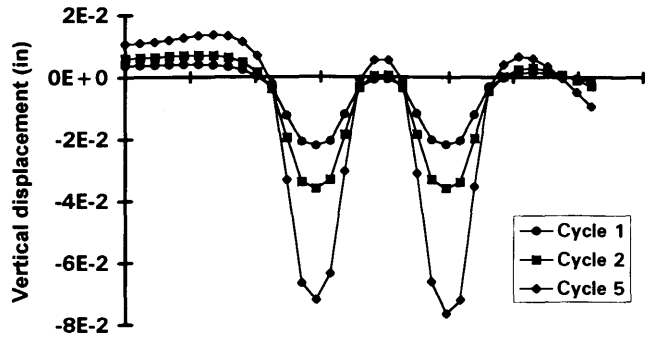

FIGURE 1 Variation of pavement profile with number of load applications; stress level, 3500 kPa; loading time, 0.3 sec; rest period, 0.4 sec.

upheaval of the pavement surface occurs between the tires. For 200 psi (1400 kPa) this upheaval is less pronounced (and even less so when nonlinear terms are ignored). Dilation exhibits a nonlinear dependence on the magnitude of the shear strain (*2*); essentially a nonlinear increase in the dilation is observed with an increase in shear strain. Figure 2 suggests that there may be a linear relationship between rut depth and maximum permanent shear strain.

After analysis, the authors decided to incorporate a plastic component into the permanent deformation model (*3*). With initial material characteristics for mixes containing eight Strategic Highway Research Program (SHRP) asphalts and two SHRP aggregate with air void contents varying between 3 and 8 percent, a series of analyses were performed for a pavement structure with a shoulder. In this case, a 10 psi (70-kPa) tire pressure and a load duration of 0.01 sec and a time interval between load applications of 0.06 sec were used. The computer runs, which included material properties obtained for the 16 mixes, yielded a relationship that best fits all the cases, especially for rut depths above 0.02 in. (0.05 cm). It is given by

$$\text{Rut depth (in.) } (rdp) = 11 * \text{maximum permanent shear strain } (mpss) \quad (1)$$

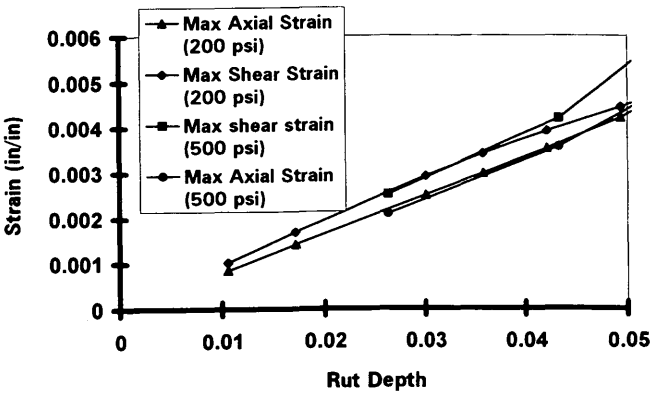

FIGURE 2 Comparison of relationships between rut depth and strain for 1400 kPa (200 psi) and 3500 kPa (500 psi) stress levels.

The relationship seems to hold true regardless of

- Pavement temperature (based on simulations using different material properties);
- Time of loading (based on simulations using 0.3 sec on and 0.4 sec off, 0.1 sec on and 0.6 sec off, and 0.01 on and 0.06 off);
- Material properties (changing nonlinear elastic, viscous, and plastic properties); and
- Tire pressure and load magnitude [100, 200, and 500 psi (700, 1400, and 3500 kPa) were used for a given tire size].

However Equation 1 should be validated for different pavement types and thicknesses, and for nonuniform variation of material properties. The relationship should be dependent on pavement geometry and loading geometry. Loading geometry (i.e., the relationship between tire dimensions and pavement dimension) is basically the same for most pavements. Pavement geometry, on the other hand, varies considerably. Most of the rutting develops near the pavement surface. It is expected that pavement thickness will only play a role up to some value beyond which the relationship will hold. However, these two considerations should be investigated further.

Field Data

Field data from SHRP's General Pavement Studies (GPS) were obtained from the SHRP A-005 project. Data consisted of the site number, date section was opened to traffic, rut depth measurement, date of rut depth measurement, and equivalent single axle loads (ESALs) (up to the time of the rut depth measurement) for each GPS site. Table 1 contains a summary of relevant data. Figure 3 shows a scatter plot of rut depth versus ESALs. The rut depth was measured using Pasco equipment, a Dynatest dipstick, or a 72-in. (1.2-m) straightedge.

Temperature Analysis

SHRP binder and mix specifications are developed on the basis of maximum and minimum pavement temperatures. Maximum pavement temperature is defined as the average maximum temperature for 7 consecutive days. It is believed that rutting correlates better with this temperature than with either the mean monthly maximum or the average yearly maximum pavement temperature.

Determination of Mean Highest 7-Day Maximum Air Temperature

GPS sites represent diverse environmental conditions; maximum pavement temperature for these sites varies widely. In order to calculate the maximum pavement temperature for the GPS sites, two or three weather stations close to each site were selected; the weather stations with more than 20 years of records were included. For each year the average 7-day maximum temperature was calculated. First, the maximum temperature for each day of the year was determined; then the maximum daily temperatures for 7 consecutive days were added together and the result divided by 7 to obtain an average 7-day maximum temperature. All the

TABLE 1 Summary of Test Conditions and Results

GPS SITES	Spec. name	ST	Max Pav Temp (C)	Voids Cont. (%)	AGE Years	ESAL YEARS	Rut Depth (mm)	Shear Strain	Number Cycles RSST-CH	REG. CRITERIA
21001	GX21-1	AK	32.2	6.1	7	399844	4.6	0.0164	87	
21004	GX1-1	AK	32.2	3.9	13	1791505	8.4	0.0300	3419	
41007	GX41-1	AZ	58.9	2.8	11	21365008	10.4	0.0373	576	out
41021	GX-19	AZ	57.2	1.0	11	11549655	13.2	0.0473	26876	void
					12	12633956	13.5	0.0482	28553	void
41025	GX22-1			0.0	13	13651008	4.1	0.0145	286	void
41036	GX8-1	AZ	58.9	6.6	6	4322385	3.6	0.0127	11523	
					7	4769968	3.6	0.0127	11523	
53071	GX64-1	AR	51.7	3.9	1	637500	3.6	0.0127	6872	
					2	1275000	4.1	0.0145	9694	
					3	1657500	4.1	0.0145	10585	
68153	GX51-1	CA	48.9	3.4	12	614903	4.1	0.0145	376	
68156	GX26-1	CA	48.9	6.3	15	820162	3.6	0.0127	30063	
82008	GX10-1	CO	51.7	1.5	17	1225650	10.7	0.0382	19963	
					18	1283072	11.7	0.0418	28155	
131031	GX33-1	GA	53.3		9	227047	7.1	0.0255	4763	
					10	256209	7.1	0.0255	4763	
161020	GX61-1	ID	48.9	6.0	3	142749	3.6	0.0127	44	
					4	178200	3.8	0.0136	52	
171003	GX32-1	IL	51.7	3.5	3	139986	3.0	0.0109	185	
					4	179982	4.3	0.0155	395	
					5	216645	3.8	0.0136	299	
201009	GX29-1	KS	54.4	7.9	4	284935	5.1	0.0182	451	
					5	404268	5.8	0.0209	582	
211014	GX14-1	KY	48.9	4.1	5	1418454	4.6	0.0164	3089	
					6	2051845	4.8	0.0173	3827	
231012	GX44-1	ME	43.3	2.1	4	980000	5.8	0.0209	756	
					5	1190000	6.4	0.0227	931	
261012	GX3-1	MI	46.1	6.5	9	714861	5.8	0.0209	803	
					10	802748	6.6	0.0236	1031	
271019	GX11-1	MN	46.1	9.0	9	435438	5.6	0.0200	83390	void
					10	472975	5.8	0.0209	9324	void
341030	GX23-1	NJ	48.9	0.5	18	1115000	14.2	0.0509	14355	void
					19	1160000	17.3	0.0618	23103	void
341031	GX31-1	NJ	48.9	1.0	16	5075000	9.4	0.0336	486	void
					17	5325000	9.7	0.0345	512	void
351022	GX62-1	NM	48.9	5.2	6	724306	3.8	0.0136	1304	
401015	GX43-1	OK	54.4	2.1	13	955031	5.8	0.0209	2016	
					14	1040193	6.1	0.0218	2692	
404164	GX35-1	OK	54.4	4.0	14	633750	3.8	0.0136	19076	
					15	686250	3.6	0.0127	15860	

(*continued on next page*)

average 7-day maximum temperatures during the hot days are determined, and the largest number obtained this way is recorded as the highest average 7-day maximum temperature for that particular year. The procedure is repeated for all years for which records are available. For example, if 30 years of data are available for one station, 30 numbers will be obtained in this way. The average value of these 30 numbers will be recorded as the mean highest average 7-day maximum temperature. This number was the value used in the calculations.

Determination of Pavement Temperature

Pavement surface temperature was calculated using the following formula, which was developed on the basis of energy balance at the surface (*4*) (it needs to be solved interatively):

$$422\alpha\tau_{\alpha}^{1/\cos z}\cos z + 0.7\sigma T_a^4 - h_c(T_s - T_a) - 90k - \epsilon\sigma Ts^4 = 0 \qquad (2)$$

where

z = zenith angle (approximately z = latitude-20 for May through August),
τ_α = sunshine factor (0.81 for perfectly sunny conditions),
α = solar absorptivity (default: 0.9),
σ = Stefan-Boltzman constant [0.1714 E-8 Btu/(hr·ft^2·R^4)],
h_c = surface coefficient of heat transfer [default = 3.5 Btu/(hr·ft^2·F)],

TABLE 1 (*continued*)

GPS SITES	Specimen name	ST	Max Pav Temp (C)	Voids Content (%)	AGE Years	ESAL	Rut Depth (mm)	Shear Strain	Number Cycles CHRSST	REG. CRITERIA
479025	**GX30-1**	**TN**	51.7	8.1	9	233159	3.6	0.0127	19804	void
					11	288553	4.6	0.0164	37120	void
481039	**GX71-1**	**TX**	54.4	3.9	7	1637481	4.1	0.0145	1105	
					8	1993484	5.8	0.0209	2170	
481047	**GX18-1**	**TX**	54.4	2.5	18	5500000	5.1	0.0182	1625	out
481048	**GX42-1**	**TX**	54.4	1.1	15	786000	5.1	0.0182	251336	void
					17	856600	4.1	0.0145	131878	void
481069	**GX81-1**	**TX**	54.4	2.3	13	2573568	8.6	0.0309	8205	
					14	2751168	8.1	0.0291	7185	
481077	**GX15-1**	**TX**	54.4	1.8	7	1394648	9.7	0.0345	3039	
811805	**GX65-1**	**CAN**	43.3	4.3	9	1190182	6.4	0.0227	133	out
851801	**GX4-1**	**CAN**	32.2	4.1	5	1183357	5.3	0.0191	2668	
892011	**GX63-1**	**CAN**	46.1	4.8	10	853376	4.3	0.0155	813	
					11	933380	5.1	0.0182	1258	

COLORADO SITES	Specimen name	ST	Max Pav Temp	Voids Content (%)	AGE Years	ESAL	Rut Depth (mm)	Shear Strain	Number Cycles CHRSST	REG. CRITERIA
14	**14 H**	**CO**	51.1	4.6	23	3282000	20.3	0.0727	166839	
29	**29 I**	**CO**	48.9	7.1	9	5002000	7.6	0.0273	4442	
30	**30 H**	**CO**	48.9	6.6	9	4622000	15.2	0.0545	3122	
13	**13 A**	**CO**	51.1	7.5	6	1257000	2.5	0.0091	1030	
13	**13 B**	**CO**	51.1	7.1	6	1257000	2.5	0.0091	675	

k = thermal conductivity [default: 0.8 Btu/(hr·ft²·F)/ft],
ϵ = surface emissivity (default: 0.9),
T_a = maximum air temperature (Rankine), and
T_s = maximum pavement surface temperature (Rankine).

Once the maximum pavement temperature at the surface is found using the preceding iterative procedure, the maximum pavement temperature for any depth of less than 8 in. (20 cm) is found through the following empirical formula (*4*):

$$T_d = T_s(1 - 0.063d + 0.007d^2 - 0.0004d^3) \quad (3)$$

where

d = depth in inches,
T_s = maximum pavement temperature (°F) at surface, and
T_d = maximum pavement temperature (°F) at depth d.

It seems that most permanent deformation from shear stresses developing near the edge of the tires takes place at depths up to 4 in. (10 cm). Maximum shear stress computed from nonlinear visco-elastic analysis took place at about 2 in. (5 cm). For this reason, and also because at this depth the ranges of temperatures computed for the GPS sections fell within reasonable testing ranges, the maximum pavement temperature at a depth of 2 in. (5 cm) was selected as the testing temperature for each of the GPS sections.

Laboratory Tests

Test Selection

Rutting (permanent deformation) in an asphalt concrete layer is caused by a combination of densification (volume change) and shear deformations, each resulting from repetitive application of traffic loads. For properly compacted pavements, shear deformations, caused primarily by large shear stresses in the upper portions of the asphalt-aggregate layer, are dominant. Repetitive loading in shear is required in order to accurately measure the influence of mix composition on resistance to permanent deformation in the laboratory. Because the rate at which permanent deformation accumulates increases rapidly with higher temperatures, laboratory testing must be conducted at temperatures simulating the highest levels expected in the paving mix in service.

To predict permanent deformation, laboratory tests must be able to measure properties under states of stress that are encountered

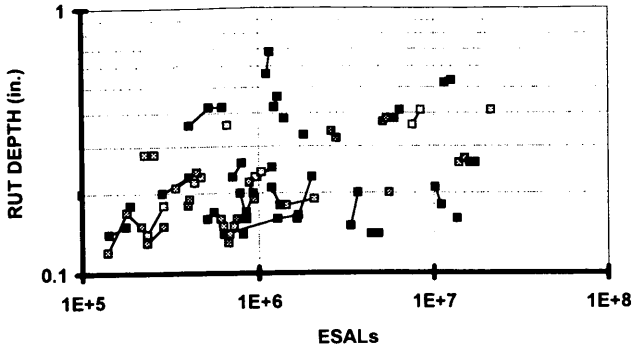

FIGURE 3 Variation of rut depth with ESALs for GPS sections.

within the entire rutting zone, particularly near the pavement surface. Because there are an infinite number of states of stress, it is impossible to simulate them all with a single test, given the nonlinear and viscous behavior of the material. For this reason, several tests have been proposed to determine a constitutive law for asphalt concrete (*2*). However, if a single test is to be performed to rapidly screen and evaluate the resistance of various mixes to permanent deformation, that test should be sensitive to the most important aspects of mix behavior and executed under conditions that most significantly affect that behavior (*3*).

The repetitive simple shear test at constant height on cylindrical specimens 6 in. (15 cm) in diameter by 2 in. (5 cm) high is proposed as an effective test to evaluate the rutting propensity of a mix.

Test Procedure

Execution of a repetitive simple shear test at constant height required the design and fabrication of totally new equipment. Taking into consideration that this test would be executed on a routine basis, efforts were made to ensure the easiest possible interface for the user.

The testing system fabricated by Cox and Sons, Inc. of Colfax, California, was presented by Sousa et al. (*5*). The system consists of two orthogonal tables that are mounted on bearings. The tables are connected to two hydraulic actuators that are controlled using servovalves under feedback, closed-loop digital algorithms. To ensure that shear and axial forces are transmitted to the specimen, aluminum caps are glued to the parallel faces of the specimen. A gluing device was developed by Cox and Sons, Inc. so that the parallel faces of the caps could be glued. Hydraulic clamps made the equipment easy to use by eliminating the need to use tools to fasten the specimens to the moving tables.

The equipment can accommodate several specimen sizes, but for permanent-deformation evaluation, the recommended specimen size for shear testing is a cylinder 6 in. (15 cm) in diameter and 2 in. (5 cm) high. If large stone mixes are to be tested, the recommended specimen size is 8 in. (20 cm) in diameter by 3 in. (7.5 cm) high.

In executing a repetitive simple shear test at constant height, the vertical actuator maintains the height of the specimen constant by using as feedback the output of a linear variable differential transformer (LVDT) measuring the relative displacement between the specimen caps. The horizontal actuator under the control of the shear load cell applies haversine loads corresponding to a 10-psi (70-kPa) shear stress magnitude with a 0.1-sec loading time and a 0.6-sec rest period. Experience with a wide range of mixes tested at different temperatures and stress levels demonstrates that the 10-psi (70-kPa) shear stress magnitude is a reasonable level at which good mixes exhibit some permanent deformation whereas poor mixes do not fail much too quickly. Finite-element computations indicate that critical shear stress levels in the field might be between 20 psi (140 kPa) to 25 psi (75 kPa). Associated with these shear stresses, confining pressures of about 30 psi (210 kPa) and axial stresses of about 80 psi (560 kPa) were also found. However, no lateral confinement is applied during the laboratory test.

Tests were executed until 5 percent shear strain was reached or there had been up to 5,000 cycles. Before testing, specimens were conditioned with 100 cycles of 1 psi (7-kPa) haversine loading with a 0.1-sec loading and 0.6-sec rest period. The preconditioning was done for the instrumentation setup. Tests can be executed at any temperature. For this study, the test temperature varied according to the geographic location of the pavement site.

Specimen Preparation

Cores were obtained from a total of 40 GPS sites to cover a wide range of environmental conditions. Specimens 2 in. thick were cut out of selected field cores with a double-blade saw. Efforts were made to cut specimens from an area 1 to 3 in. below the surface. Specific gravities of the specimens were determined using parafilm. Specimens were allowed to dry before being glued to the caps, and a DEVCON 5-min plastic steel putty was used to glue them, which was allowed to cure several hours before testing.

Each specimen was placed in an oven having the same temperature as the mean highest 7-day maximum pavement temperature [at a depth of 2 in. (5 cm)] for at least 2 hr (but no more than 4 hr) before being tested.

Given that the specimens had slightly different diameters, the shear load required to yield a 10 psi (70-kPa) shear stress level for each specimen was calculated on the basis of the area of the specimen.

Test Results

An RSST-CH was performed on one specimen from each GPS site. Each test was performed at 10 psi (70-kPa) stress amplitude (with a 0.1-sec loading time and a 0.6-sec rest period) and at 7-day maximum pavement temperature encountered at the 2-in. (5-cm) depth. Figure 4 exhibits a typical graph of the permanent shear strain versus number of cycles obtained from the tests. It is apparent that some mixes deform faster than others; not only do they have different slopes but different intercepts also.

Analysis

Based on Equation 1, the maximum shear strain corresponding to the measured rut depth for each of the GPS sites was computed. Typical results from repetitive shear tests on GPS specimens (Figure 4) were used to determine the number of shear cycles required to reach the level of maximum shear strain calculated using Equa-

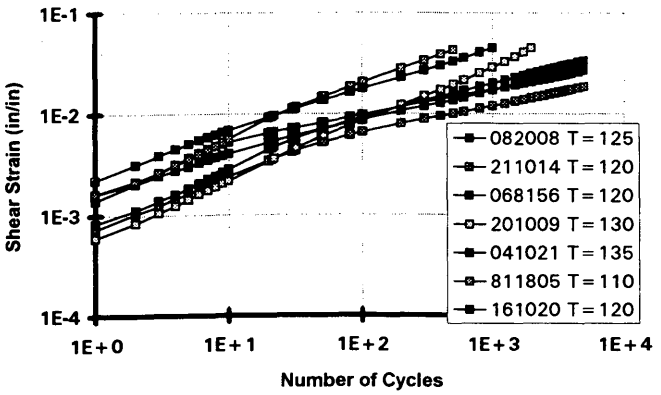

FIGURE 4 Variation of permanent shear strain in RSST-CH, with number of load repetitions for some GPS sites; temperatures in degrees Fahrenheit.

tion 1. The process relates the number of cycles in the RSST-CH to reach the same magnitude of permanent shear strain as is caused by the ESALs in the field. Table 1 contains the results from all the tests. The last column contains information about the rejection criteria used for the data (in some cases, specimens would have been rejected on the basis of other factors, such as a test executed at the wrong temperature or LVDTs that got loose during testing). Results from specimens with air voids less than 1.5 percent and more than 8.0 percent also were eliminated. Specimens with voids less than 1.5 percent are overcompacted and not representative of the conditions prevailing during most of the life of the pavement. Specimens with void content above 8 percent are likely to densify before entering into the plastic shear flow stage. Out of all the data, three points were removed as outliers.

The scatter plot of number of cycles in the test versus ESALs for all the data (without the outliers) is presented in Figure 5. In recognition of the possibility of two populations (Line A and Line B), a closer investigation of the age of the pavements was made. Table 2 contains two sets of data represented in Figure 5. Note that two trends can be observed in the data: one obtained from specimens tested after being aged in the field for an average of 16 years and another obtained from specimens aged in the field for an average of only 8 years. Sites in Line B have a maximum pavement temperature at 2 in. (5 cm) depth higher (on average) than those from Line A. The average air void content is similar for both populations.

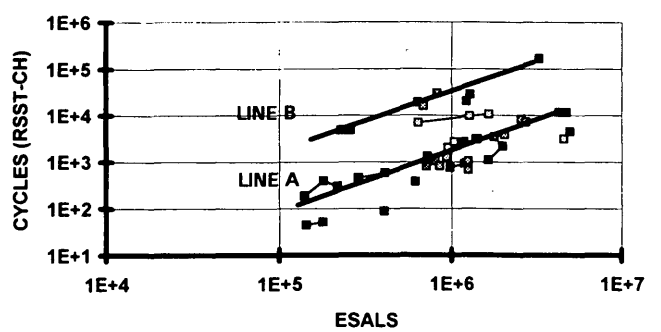

FIGURE 5 Relationship between number of cycles in RSST-CH and ESALs to reach the same shear strain level; Lines A and B indicate two possible populations.

Specimens with aged asphalt perform relatively better in the RSST-CH. Results were obtained from specimens taken from out-of-the-wheel-path field cores that had been subjected to aging and to limited traffic. However, because the specimens were obtained at a 2 in. (5 cm) depth, the magnitude of aging is less than what would occur at the surface.

Most variability in the data came from specimens taken from sites aged 10 or more years. This is to be expected, because ESAL prediction, aging, and traffic are all factors that can cause data variability. An investigation of the relationship between cycles in RSST-CH and ESALs was made for pavements that were less than 10 years old. The following relationship was obtained with an R^2 = 0.68:

$$\log (\text{cycles}) = -4.09 + 1.204 \log (\text{ESAL}) \quad (4)$$

One expects that mixes with high air voids from older pavements exposed to higher temperatures have probably aged more. Therefore, the product (age × voids × temperature/10) represents a variable, and a high value indicates the greater likelihood of having a more aged mix than if the value were low. The last two columns of Table 2 contain product values. The last column presents the values for sites more than 10 years old.

Observe that the average product (age × voids × temperature/10) for Line A is almost half that of the average product for Line B (for all sites). The average product for pavements more than 10 years old in Line A (517) is lower than the corresponding average product in Line B (891) and is close to the average for all points in Line A (427). That observation provides a rationale to justify that specimens in Line A more than 10 years old are not really as aged as the specimens belonging in Line B.

Using all the data except those points from Line A and discarding points from site 53071 as outliers, it can be observed that a very clear trend with very little data variability exists (see Figure 6). The equation of the best fit is given by

$$\log (\text{cycles}) = -4.36 + 1.240 \log (\text{ESAL}) \quad (5)$$

This relationship was obtained with an R^2 = 0.80.

The best-fit lines obtained from the two criteria are presented in Figure 7. On the basis of these results, Equation 5 might be used to develop an abridged procedure to evaluate permanent deformation for asphalt concrete pavements. The product value is indicative of a very good correlation, especially if the following is considered:

- The rut might also be related to densification, subgrade effect, or pavement surface irregularities in some cases;
- The RSST-CH was executed with specimens that, although not in the wheel path, already had been subjected to traffic to various degrees and whose behavior might be different from specimens obtained from newly compacted mixes;
- The calculation of the maximum pavement temperature at a depth of 0.05 m is just an estimate of the real temperature;
- The testing rate is a 0.1-sec loading and 0.6-sec unloading, whereas in the pavement, the rate is closer to a 0.02-sec loading and almost random spacing; and
- The ESALs were not actually measured but were extrapolated from U.S. Department of Transportation data.

TABLE 2 Summary of Test Conditions and Results for Lines A and B

LINE A SITES	Specimen name	ST	Max Pav Temp (F)	Voids Content (%)	AGE YEARS	Temp * Voids* Age	
21001	GX21-1	AK	90	6.10	7	384	
21004	GX1-1	AK	90	3.90	13	456	456
41036	GX8-1	AZ	138	6.60	7	638	
53071	GX64-1	AR	125	3.90	3	146	
68153	GX51-1	CA	120	3.40	12	490	490
161020	GX61-1	ID	120	6.00	4	288	
171003	GX32-1	IL	125	3.50	5	219	
201009	GX29-1	KS	130	7.90	5	514	
211014	GX14-1	KY	120	4.10	6	295	
231012	GX44-1	ME	110	2.10	5	116	
261012	GX3-1	MI	115	6.50	10	748	748
351022	GX62-1	NM	120	5.20	6	374	
401015	GX43-1	OK	130	2.10	14	382	382
481039	GX71-1	TX	130	3.90	8	406	
481069	GX81-1	TX	130	2.30	14	419	419
481077	GX15-1	TX	130	1.80	7	164	
851801	GX4-1	CAN	90	4.10	5	185	
892011	GX63-1	CAN	115	4.80	11	607	607
29	29 I	CO	120	7.10	9	767	
30	30 H	CO	120	6.60	9	713	
13	13 A	CO	124	7.50	6	558	
13	13 B	CO	124	7.10	6	528	
	LINE A	AVERAGE	119	4.84	8	427	517

LINE B SITES	Specimen name	ST	Max Pav Temp	Voids Content (%)	AGE YEARS	Temp * Voids* Age	
131031	GX33-1	GA	128		10		
404164	GX35-1	OK	130	4.00	15	780	780
68156	GX26-1	CA	120	6.30	15	1134	1134
82008	GX10-1	CO	125	1.50	18	338	338
14	14 H	CO	124	4.60	23	1312	1312
	LINE B	AVERAGE	125	4.10	16	891	891

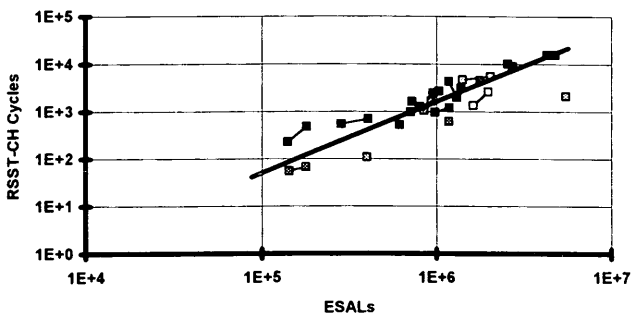

FIGURE 6 Variation of number of cycles to field shear strain in RSST-CH with ESALs for sections that did not exhibit significant aging.

Overall the relationship between the proposed test procedure and the rutting behavior in the field is a strong one.

ABRIDGED PROCEDURE

On the basis of test results, an abridged procedure to determine the rutting propensity of a mix can be developed by following these steps:

1. Determine the number of ESALs for design life. (Corrections should be made to account for reliability factors in the procedure and in the tests.)
2. Select maximum allowable rut depth (*mrd*).

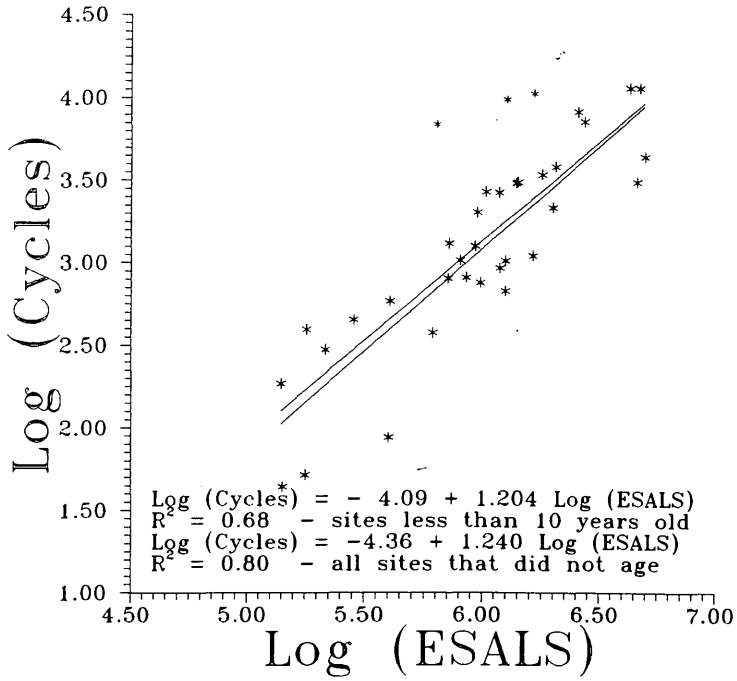

FIGURE 7 Variation of number of cycles to field shear strain in RSST-CH with ESALs for sections that did not exhibit significant aging and those less than 10 years old.

3. Determine 7-Day maximum pavement temperature at a site at a depth of 0.05 m.
4. Execute the RSST-CH at 70 kPa at that temperature.
5. Using Equation 1, relate the rut depth to the maximum permanent shear strain in a pavement section and determine the maximum allowable permanent shear strain (*mpss*).
6. Using the results obtained from the RSST-CH, determine the number of cycles needed to reach the maximum allowable permanent shear strain.
7. Determine the number of ESALs that can be carried by that mix in the pavement before the maximum allowable rut depth is reached by using the relationship between ESALs and number of cycles in RSST-CH. The relationship derived from Equation 5 is as follows:

$$ESAL_{mrd} = 10 \text{ ^ } [(4.36 + \log (N_{mpss})]/1.24) \quad (6)$$

where $ESAL_{mrd}$ equals the number of equivalent single axle loads to develop maximum allowable rut depth (*mrd*), and N_{mpss} is the number of cycles in RSST-CH to reach the maximum permanent shear strain (*mpss*) correspondent to the maximum allowable rut depth (*mrd*). (Testing conditions included 70 kPa, a 7-day maximum pavement temperature, 0.1 sec on, and 0.6 sec off.)

OTHER CONSIDERATIONS

To implement this procedure, a few factors should be considered (*6*):

- Evaluation of tire pressure effects on the rate of accumulation of permanent deformation can be done only by computing ESALs for the axles with different tire pressures. This could be achieved using, for instance, a permanent deformation model as presented by Sousa et al. (*2*).
- Aging and water sensitivity should both be addressed and incorporated into the procedure. The mix should be subjected to short-term aging that is representative of the field mixing and placement process and to water sensitivity conditioning before being subjected to the RSST-CH. Such treatment would represent the most severe conditions encountered in the field. Executing the water conditioning procedure might weaken the asphalt-aggregate interface and reduce the resistance to shear deformation. Long-term aging should not be carried out; it would stiffen the asphalt binder and therefore provide improved performance. Furthermore, the correlation presented was obtained for pavements less than 10 years old.
- The assumption of uniformly distributed ESALs (inherent in the procedure) during the year and during the day could be improved. This might be achieved also by taking advantage of a comprehensive finite-element model for permanent deformation, which could also take into account the relative contribution to permanent deformation of the ESALs applied at different temperatures. It is likely that most permanent deformation occurs from traffic passing when the pavement temperature is within 5°C of the maximum pavement temperature at a 2-in. (5-cm) depth.

The procedure could be improved if the test were executed at the mean highest 7-day maximum pavement temperature, corrected to compensate for the rate of loading effect. Normal traffic, traveling at 90 km/hr, applies pulse loads with a duration of about 0.015 sec at 2-in. (5-cm) depth. Laboratory tests are executed with a 0.1-sec loading pulse. Taking advantage of time-temperature superposition, decreasing the temperature simulates the faster rate

of loading encountered in the field. That might provide a more accurate balance between permanent deformation from the viscous behavior of a binder and the plastic component because of changes in the magnitude of the shear strains. The exact amount of temperature shift could be given by temperature shift factors obtained by the shear frequency sweep results executed at different temperatures. The testing temperature would be adjusted further to account for the field rate of loading (mixes placed in up-hill pavement sections with slower traffic could be tested at higher temperatures than mixes placed in level sections).

In addition, when an RSST-CH is done, a specimen hardly changes volume. Therefore, tests should be executed on a mix with air void contents representative of those that predominate during the life of a pavement (*6*).

To implement the procedure on the basis of these findings, it must be recognized that Equation 1 might not be valid in all cases. However, the assumption can be demonstrated and validated by executing analyses the authors presented earlier for a series of pavement configurations. It is likely that a family of curves could be developed for different pavement thicknesses. Also, there is inherent variability in any test procedure; therefore, reliability considerations should be incorporated into the procedure (*7*).

SUMMARY

Foundations for the development of an abridged procedure to determine the permanent deformation potential of an asphalt aggregate mix have been presented. Asphalt aggregate mixes exhibit nonlinear, elastic, viscous, and plastic behavior. Nonlinear behavior, such as dilation or stress hardening, is mostly influenced by the aggregate skeleton. A finite-element model that takes these aspects of mix behavior into account was used to establish a relationship between rut depth and maximum permanent shear strain in pavement sections. The relationship seems to be independent of a wide range of input variables and material properties; however, it is probably dependent upon pavement structure for thin pavement sections.

RSST-CH was used as the accelerated laboratory test for evaluating rutting propensity of a mix. The test was executed at the critical pavement temperature at a depth of 2 in. (5 cm). For this analysis, critical pavement temperature was defined as the 7-day maximum pavement temperature at a 2-in. (5-cm) depth. This depth was selected because computations have shown that maximum shear stresses, those causing the permanent deformation in the pavements, are encountered 2 in. (5 cm) beneath the surface near the edge of the tire tracks. The procedure was derived from data obtained from 40 GPS sections around the North American continent. The procedure is mainly based on the execution of the RSST-CH at the mean highest 7-day maximum pavement temperature encountered at a 2-in. (5-cm) depth. The fundamental link between the laboratory tests and the field performance was derived from the relationship between the number of cycles in the RSST-CH to reach a given permanent shear strain and the number of ESALs to cause the same permanent shear strain in the pavement section. For pavements that did not exhibit significant aging, that relationship was obtained with an R^2 of 0.80. Specimens should be compacted in the laboratory to air voids contents expected in the field with a compaction procedure that simulates the aggregate structure caused by traffic. It is suggested that the RSST-CH be performed on specimens compacted in the laboratory to about 3 to 4 percent voids content. If this procedure is to be used in a mix design framework, efforts should be made to age and moisture condition laboratory-prepared specimens to be representative of the conditions expected in the field. As more rut-depth measurements from sites become available, and predictions are made on the basis of the proposed procedure, results can be compared, and the existing relationship can be either verified or improved.

ACKNOWLEDGMENTS

The work reported was conducted as part of SHRP Project A-003A. The project, Performance Related Testing and Measuring of Asphalt Aggregate Interactions and Mixes, is being conducted by the Institute of Transportation Studies, University of California, Berkeley. Carl L. Monismith is principal investigator and Jorge B. Sousa, assistant research engineer. Carl Monismith's unwavering challenges to this procedure are especially appreciated as they strengthen the foundations where it rests. The authors express their appreciation for the collaboration and support of John Deacon in the conceptual development of some aspects of the abridged procedure and to Shmuel Weissman of Symplectic Engineering Inc. for the development of the modeling capabilities that permitted the determination of the relationship between rut depth and maximum shear strain. Michell Jamjim ran the finite-element program and John Harvey coordinated some aspects of the specimen preparation. Timothy Aschenbrener from the Colorado Department of Transportation provided the data and cores for the Colorado Sites. His efforts in testing those cores are appreciated.

REFERENCES

1. Sousa, J. B., J. Craus, and C. L. Monismith. *Summary Report on Permanent Deformation in Asphalt Concrete*. Strategic Highway Research Program, Report No. SHRP-A/IR-91-104, National Research Council, Washington, D.C., 1991.
2. Sousa, J. B., S. L. Weissman, L. J. Sackman, and C. L. Monismith. A Nonlinear Elastic Viscous with Damage Model To Predict Permanent Deformation of Asphalt Concrete Mixes. In *Transportation Research Record 1384*, TRB, National Research Council, Washington, D.C., 1993, pp. 80–93.
3. Sousa, J. B. and S. L. Weissman. Modeling Permanent Deformation of Asphalt-Aggregate Mixes. *Proc., Association of Asphalt Paving Technologists*, Vol. 62, 1994.
4. Solaimanian, M. and T. Kennedy. Predicting Maximum Pavement Surface Temperature Using Maximum Air Temperature and Hourly Solar Radiation. In *Transportation Research Record No. 1417*, TRB, National Research Council, Washington, D.C., 1993, pp. 1–11.
5. Sousa, J. B., A. Tayebali, J. Harvey, P. Hendricks, and C. Monismith. Sensitivity of Strategic Highway Research Program A-003A Testing Equipment to Mix Design Parameters for Permanent Deformation and Fatigue. In *Transportation Research Record 1384*, TRB, National Research Council, Washington, D.C., 1993, pp. 69–79.
6. Sousa, J. B. Asphalt-Aggregate Mix Design using the Simple Shear Test (Constant Height). *Proc., Association of Asphalt Paving Technologists*, Vol. 62, 1994.
7. Sousa, J. B., J. Harvey, M. G. Bouldin, and A. Azevedo. Application of SHRP Mix Performance Based Specifications. Presented at the 73rd Annual Meeting of the Transportation Research Board, Washington, D.C., 1994.

Three-Dimensional, Finite-Element Simulation of Permanent Deformations in Flexible Pavement Systems

DAVID J. KIRKNER, PETER N. CAULFIELD, AND DENNIS M. MCCANN

A methodology for obtaining a three-dimensional finite-element solution to the problem of a moving load on an elastic-plastic half-space is presented. The problem is particularly suited to an analysis of flexible pavement systems. The basis of the model is the following set of assumptions: (*a*) the material is homogeneous and infinite in extent in every horizontal plane, (*b*) the load is moving at a constant velocity, (*c*) the system is at steady state, (*d*) inertial effects are neglected. A model problem was examined that consisted of a homogeneous half-space of an isotropic material obeying the von Mises yield criterion and the associated flow rule. The magnitude of the permanent deformations is calculated versus the value of the applied surface pressure. The residual stress field remaining after the passing of the load is also obtained. More general problems are solvable with the current version of the code. Extensions are discussed.

The ability to predict the amount and growth of permanent deformation in pavement systems is an important aspect of pavement design. A method for calculating the permanent deformation in three-dimensional, layered, elastic-plastic half spaces is described. This method is particularly suitable for the analysis of flexible pavement systems, for which the permanent deformation may result in large measure from a failure of the granular base material.

Development of a mechanical model to predict permanent deformations in a pavement system is a difficult task because of many complicating factors that attend the problem. Such a physical system is inherently three dimensional; the load is moving and the constitutive laws for the materials are nonlinear and history dependent. Currently models do not exist that incorporate all pertinent aspects of the problem.

Good reviews of state-of-the-art prediction of permanent deformations in pavement systems are given by Sousa et al. (*1*) and by Zaniewski (*2*). Methods for predicting permanent deformations may be grouped in the following broad categories: mechanical models, combined mechanical-empirical models, and empirical models. A mechanical model is defined to be a set of equations containing a set of physical parameters that must be specified in advance, the solution of which is capable of predicting the behavior of the physical system of interest. The required physical parameters are obtained from laboratory experiments and are usually constitutive parameters (i.e., coefficients in the stress-strain law). The set of equations normally is determined from the basic axioms of continuum mechanics. A combined mechanical-empirical model uses the results of a mechanical model as input to a set of experiments meant to simulate the physical phenomena. Thus, final predictions are made on the basis of physical simulations. Empirical models are laboratory or field-scale experiments the results of which are meant to simulate the actual phenomena of interest. Most engineering design strives to develop efficient and reliable mechanical models on which to base design, because these require only a sufficient data base of experimental results and therefore are the simplest to implement on a regular basis.

It seems reasonable that the ability to predict accurately the permanent deformation occurring after one pass of a moving load should be a prerequisite to predicting the accumulated permanent deformation resulting from potentially thousands of passes. Some of the combined mechanical-empirical models attempt to predict the accumulated permanent deformation, but they require an estimate of the state of stress in the pavement when it is subjected to a single pass of a moving load. The so-called "layer strain methodology" is such an approach (*3*). However, the analysis typically used to compute the stress does not usually include such features of the problem as the inelasticity and nonlinearity of the response nor the effect of the moving load. This information must come from a suitable mechanical model.

A perusal of the current literature [see work by Sousa et al. (*1*) and Majidzadeh et al. (*4*) for reviews] reveals that complete mechanical models have not yet been developed for predicting permanent deformation of pavement systems. Important facets of the problem that cannot be ignored are (*a*) the load moving on the pavement system and (*b*) the inelastic and nonlinear response. Structural analysis of systems subjected to moving loads is a subject by itself. An excellent treatise on the subject is given by Fryba (*5*), which covers beams, plates, as well as continua. However, Fryba deals only with analytical solutions and only with systems possessing linear constitutive laws. No current models are available that include both of these aspects of the problem. There are models that allow for a moving load [Battiato et al. (*6*), Elliot and Moavenzadeh, (7)]. However, these models are based on linear viscoelastic constitutive laws using the Maxwell fluid concept. This type of constitutive law allows permanent deformation but does not include any plastic strains and is inapplicable for modeling permanent deformations in granular base materials, an important feature in flexible pavement systems.

In this paper a method is described for performing three-dimensional, nonlinear analysis of layered, elastic, and elastic-plastic systems, including the effects of a moving load. Thus it is particularly applicable to flexible pavement systems. The model is based on a steady-state solution to the problem of a moving load on a layered system and presumes the layered system to be homogeneous in the horizontal direction and infinite in extent. These assumptions greatly simplify the analysis of an extremely

D. Kirkner and P. Caulfield, Department of Civil Engineering and Geological Sciences, University of Notre Dame, Notre Dame, Ind. 46556. D. McCann, Lawson-Fisher Associates, P.C., 525 West Washington Avenue, South Bend, Ind. 46601.

complicated problem. It should be noted that three-dimensional finite-element analyses, including nonlinear behavior, of pavement systems have been performed [by Ioannides and Donnelly (*8*), Kokkins (*9*), and Forte et al. (*10*)] but have not included moving load effects, which is the principal focus of this work.

This paper is primarily expository; it is to explain the methodology and its application to a three-dimensional problem. To focus on the principal effects of the plasticity and the moving load, a simplified model problem is studied. This is a homogeneous layer overlaying a rigid subbase of an isotropic material subjected to a moving, uniform load distributed over a square area. The quasistatic solution is obtained. Inertial effects below the critical speed are easily accommodated, however. The methodology, and in fact the code employed, can also accommodate layering, more complicated material descriptions, and a nonuniform moving load distributed over an arbitrarily shaped region.

MODELING STRATEGY

A cross section through the problem to be studied is depicted schematically in Figure 1. This is the x_1-x_2 plane at $x_3 = 0$. The problem domain consists of a half-space defined by the region $x_2 < 0$. This region is subject to a uniform pressure of magnitude p distributed over a square $a \times a$ moving with a constant velocity c in the x_1 direction. This problem may be stated as a boundary value problem with the stresses σ_{ij}, strains ϵ_{ij}, and displacements u_i as unknowns. Note that the load moves with constant velocity c, and that steady-state conditions are assumed; that is, the load began an infinite time in the past. Because of the steady-state assumption and the assumption that the domain is homogeneous in the x_1 direction, a moving coordinate system can be used to advantage. Let

$$y_1 = x_1 - ct \qquad y_2 = x_2 \qquad y_3 = x_3 \tag{1}$$

Using the moving coordinate system (y_1, y_2, y_3) rather than the fixed reference frame (x_1, x_2, x_3) allows time to be removed as an explicit variable in the problem. Integration in time is thus replaced by integration in y_1. Further details of the mathematical development are given by Kirkner (*11*).

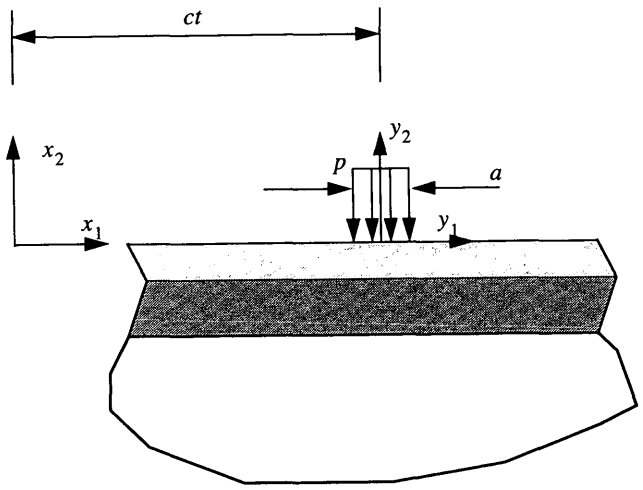

FIGURE 1 Schematic of model three-dimensional moving load problem.

For the work considered here, the constitutive equations will take the form of rate-independent plasticity. For simplicity of presentation, the von Mises yield criterion and the associated flow rule will be used, and the problem domain is assumed to be homogeneous. Thus,

$$\sigma_{ij} = C_{ijkl}\epsilon^e_{ij} \tag{2}$$

where

σ_{ij} = stress tensor;
C_{ijkl} = elasticity tensor, corresponding here to an isotropic material; and
ϵ^e_{ij} = elastic strain tensor.

The additive decomposition of strains is assumed; that is,

$$\epsilon_{ij} = \epsilon^e_{ij} + \epsilon^p_{ij} \tag{3}$$

where ϵ_{ij} is the total strain tensor and ϵ^p_{ij} is the plastic strain tensor. The von Mises yield criterion is

$$f(\sigma_{ij}) = \sigma_e - \sigma_y = 0 \tag{4}$$

where σ_e, the effective stress, is given by

$$\sigma_e = \left[\frac{1}{2}(\sigma_{22} - \sigma_{33})^2 + \frac{1}{2}(\sigma_{33} - \sigma_{11})^2 + \frac{1}{2}(\sigma_{11} - \sigma_{22})^2 + 3\sigma^2_{23} + 3\sigma^2_{31} + 3\sigma^2_{12}\right]^{\frac{1}{2}} \tag{5}$$

and σ_y is the yield stress. The associated Prandtl-Reuss flow rule is

$$\dot{\epsilon}^p_{ij} = \dot{\lambda}\frac{\partial f}{\partial \sigma_{ij}} \tag{6}$$

With the introduction of the moving coordinate system, the time derivatives appearing in Equation 6 become derivatives with respect to y_1.

Note that the coordinate y_1 may be given different physical interpretations. If time is considered as fixed at an instant, the solution to the problem in terms of y_1, y_2, y_3 may be thought of as a "snapshot" of the physical domain (in terms of x_1, x_2, x_3) at an instant. Alternatively, if x_1 is to be held fixed, a graph of any quantity (stress, strain, displacement) expressed as a function of y_1 is actually a time history of that particular quantity. Both of these views are useful in understanding the following.

In order to evaluate the constitutive relation for an elastic-plastic material, the evolution equation for the plastic strain must be evaluated. This requires tracking the response history at each point. However, as explained above, if y_1 is thought of as a time-like variable for fixed x_1, an integration of the response history in time is equivalent—in the moving reference frame—to an integration over y_1. This integration forms the basis of a numerical solution strategy described here.

The finite-element technique employed here is based on the weak form (virtual work) of the problem (*12*) using the moving

coordinate frame (y_1, y_2, y_3). Complete details of the development may be found in a paper by Kirkner (*11*).

An iterative strategy based on the initial stress method has been found to work well for this problem. Following the development by Kirkner (*11*), global finite-element equations result:

$$\mathbf{K}\,\Delta\mathbf{d} = \mathbf{p}^m \tag{7}$$

where

$\mathbf{K}$ = elastic stiffness matrix,
$\Delta\mathbf{d}$ = vector containing the difference in the nodal displacements between the previous iteration (mth iteration) and the new solution [$(m + 1)^{st}$ iteration], and
$\mathbf{p}^m$ = solution-dependent load vector (the superscript indicates that the load vector is evaluated at the previous solution)

An iteration scheme using a consistent tangent modular matrix has also been used, but the method above works very well and is the easiest to implement.

The stress tensor at each Gauss point must be evaluated, and each iteration given the state at the last iteration. This, in essence, requires that the flow rule (Equation 6) be integrated. However, because integration in time has been replaced by integration over y_1, this simply means tracing the history over the space coordinate, y_1. The algorithm operates on the elements in a preferred order. Starting at the right side of the mesh, that is, large y_1, where it may be presumed that the response is purely elastic, the stresses are calculated for succeeding elements proceeding right to left (for a load traveling left to right). In order to evaluate the stress at a particular Gauss point, only the stress and strain at the Gauss point to the right need to be known. A backward Euler method is used to integrate the flow rule; a thorough discussion of this and other schemes for integrating the flow rule has been presented elsewhere (*13*).

Note that although a moving load problem seems inherently more difficult than a corresponding stationary load problem, the algorithm employed here requires only negligible storage compared with the stationary load problem, for which the stress and strain tensors at all Gauss points that have yielded must be stored from iteration to iteration.

RESULTS

A model problem will be analyzed in this section to demonstrate the implementation of the methodology. For simplicity, a homogeneous domain is considered with an isotropic material obeying the von Mises yield criterion without hardening. The results are most useful when expressed in terms of dimensionless variables. Table 1 gives the dimensionless variables in terms of the primary variables of the problem. All the figures following give results in terms of the dimensionless variables. The truncated domain used for analysis is presented in Figure 2. Note that symmetry about the y_1-y_2 plane is represented. Once inelastic effects are present, symmetry about the y_2-y_3 plane no longer exists. The size of the truncated domain in the horizontal directions was determined experimentally. That is, domains larger than that shown give essentially identical results. The depth to the bottom boundary was chosen arbitrarily and was assumed to be a reasonable distance to a stiffer subgrade. Roller-type boundary conditions are used on all external faces except the top surface. Other conditions such as complete fixity on the bottom boundary can easily be accommodated. This problem has been solved for several values of the pressure load p. A uniform mesh consisting of standard eight-node hexahedral isoparametric elements was employed. The results following were obtained using a uniform mesh consisting of 40 elements in the y_1 direction, 12 elements in the y_2 direction, and 16 elements in the y_3 direction. This corresponds to 25,511 unknown displacement degrees of freedom.

TABLE 1 Variable Definitions

Variable Name	Primary Variable	Dimensionless Variable
Distance	y	y/a
Stress	σ	σ/σ_y
Applied Pressure	p	p/σ_y
Yield Stress	σ_y	1
Displacement	u	$(uE)/(\sigma_y a)$
Modulus of Elasticity	E	1
Poisson's Ratio	υ	$\upsilon = 0.3$

Figure 3 shows displacement profiles corresponding to several different values of the applied pressure. These are plots of the displacement of the points on the y_1 axis—in essence, the pavement centerline. It is useful to keep in mind the dual interpretation of the moving coordinate y_1. The profiles may be viewed as "snapshots" capturing one instant or as a displacement time history that every point on the original x_1 axis will follow. Thus, values of the displacement at large positive values of y_1 occur long before the load arrives, and values of the displacement at large negative values of y_1 occur long after the load has passed. At an applied pressure of 1.43, note that the profile is symmetric and that no permanent displacement is left after the load has passed. For pressures of 1.7 and 2.0, permanent displacements are left and the profile is no longer symmetric because of the fact that once yielding occurs, energy is dissipated and the applied load must now perform work. This phenomenon is discussed further by Kirkner (*11*). Figure 4 shows the peak values of the displacement that occurs under the load and the peak value of the permanent displacement versus pressure. No permanent displacement occurs until the pressure is approximately 1.57, which is approx-

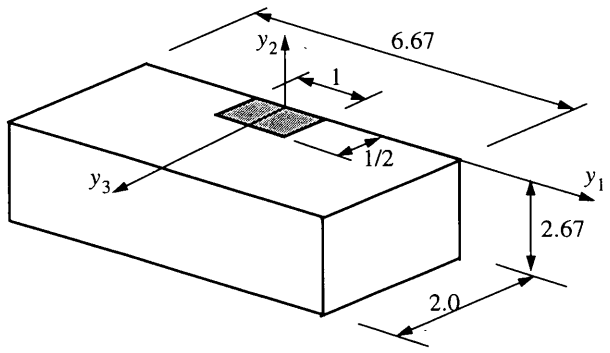

FIGURE 2 Model problem showing truncated domain in dimensionless units.

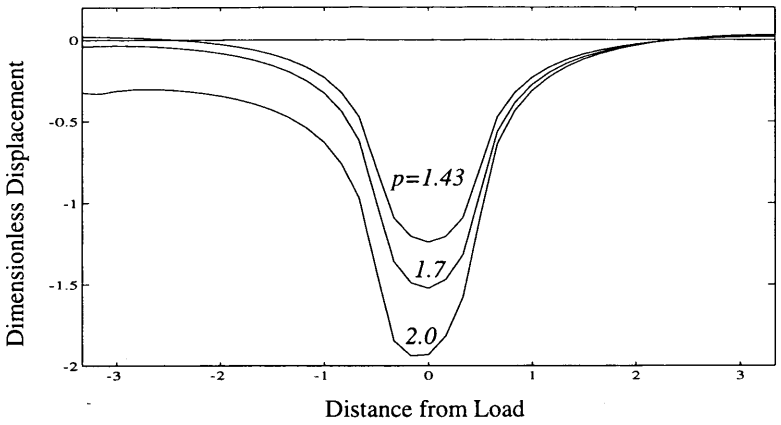

FIGURE 3 Displacement profiles.

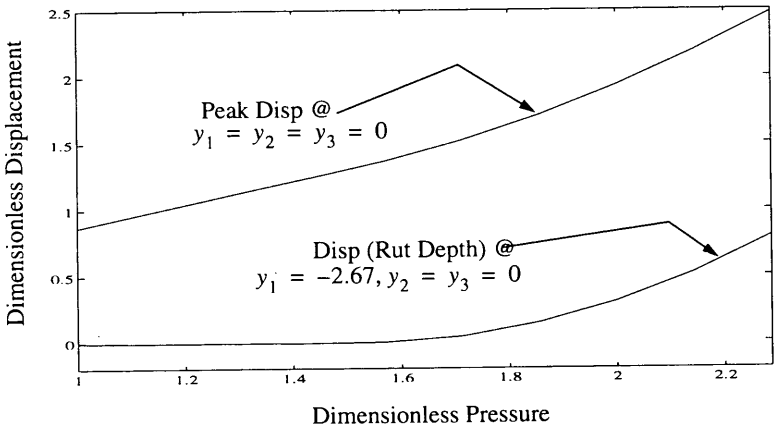

FIGURE 4 Peak displacement and rut depth versus pressure.

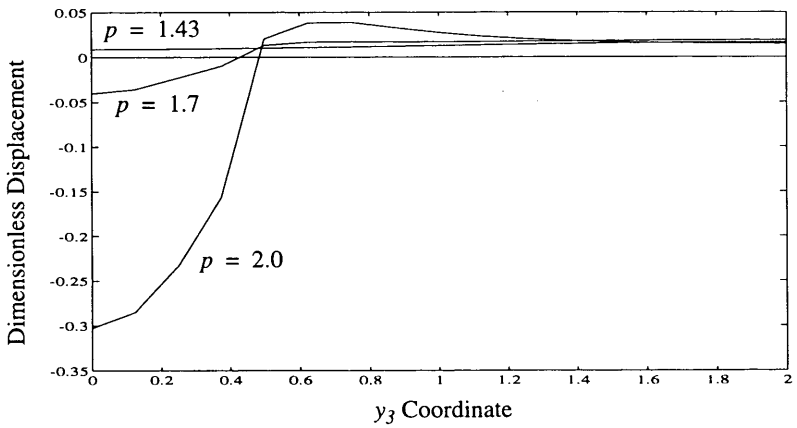

FIGURE 5 Rut profiles at $y_1 = -2.67$.

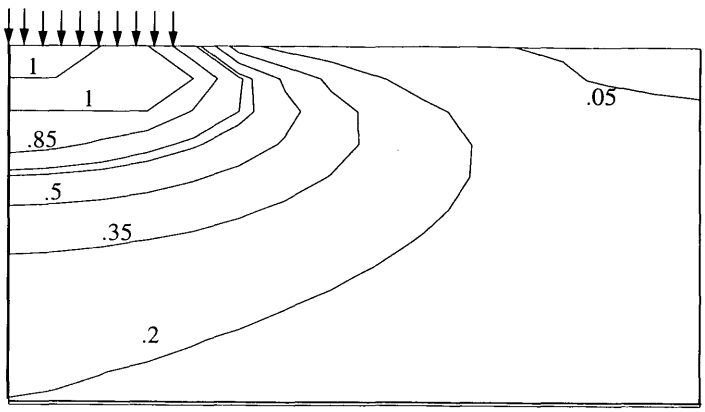

FIGURE 6 Equivalent stress contours on $y_1 = 0$ for $p = 2$.

imately the load to cause first yield. However, the magnitude of the permanent displacement or rut depth then grows rapidly with increasing pressure. That is, as the pressure increases beyond the pressure to cause yield, a smaller percentage of the maximum displacement is recovered through elastic rebound.

It is also instructive to examine surface profiles of points on the surface on lines parallel to the y_3 axis. In essence, such plots show the rut profile. Figure 5 shows rut profiles for several values of the applied pressure viewed from the negative side.

Once the moving load causes the material to yield, the system is left not only with permanent displacements but with residual stresses. Stress contours provide a convenient method to examine the stress state in the system. Contours will be shown for planes parallel to the y_2-y_3 plane as viewed from the negative side. Figure 6 shows stress contours on the plane $y_1 = 0$ corresponding to an applied pressure of 2.0. Again these contours may be thought of as those every cross section is subjected to when the load is directly passing over. The contours are of the equivalent stress since this quantity directly determines whether a material point yields according to the von Mises criterion. Note that there is a zone below the surface that has yielded. The depth of this zone below the surface is greatly affected by the depth to the bottom boundary. Figure 7 shows a similar plot for the plane $y_1 = -2.67$, which is far enough behind the load that it is essentially in a steady state. That is, this stress state remains in every plane long after the load has passed and is the stress state that would be used in the elements on the right boundary as initial stresses in a reanalysis to perform a second pass.

CONCLUSION

A methodology has been presented for the analysis of three-dimensional pavement systems subjected to moving loads and containing materials exhibiting elastic-plastic behavior. The model is capable of predicting permanent deformations. Key to understanding the model are the following assumptions: (*a*) the material is homogeneous and infinite in extent on every horizontal plane; (*b*) the load is moving at a constant velocity; (*c*) the system is at steady state; (*d*) inertial effects are neglected. Potential application of this model to pavement systems was demonstrated by the analysis of a model three-dimensional system. The permanent deformation, rut profiles, and development of residual stresses were studied. The following features can be included within this format with only minor changes in the coding: inertia effects, viscous or rate-dependent material behavior (important for asphaltic materials), more realistic constitutive behavior applicable to granular

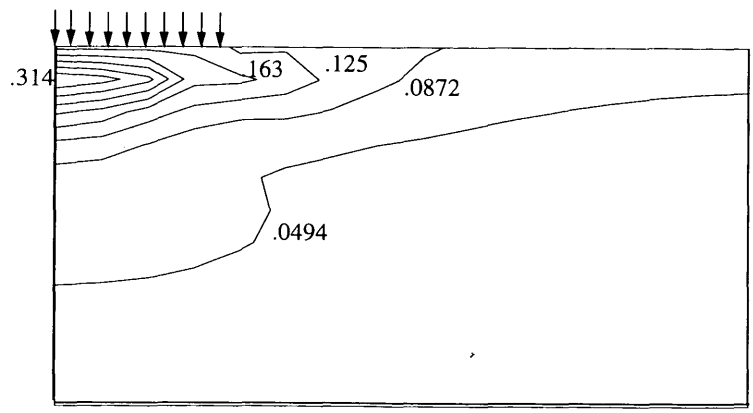

FIGURE 7 Equivalent stress contours on $y_1 = -2.67$ for $p = 2$.

materials [see work by Desai (*14*), for example]. Studies are currently under way that investigate these features of the problem.

ACKNOWLEDGMENT

This work was partially supported by a Jesse H. Jones Faculty Research Grant at the University of Notre Dame. The support is gratefully acknowledged by the authors.

REFERENCES

1. Sousa, J. B., J. Craus, and C. L. Monismith. *Summary of Report on Permanent Deformation in Asphalt Concrete*. Strategic Highway Research Program, SHRP-A/IR-91-104, National Research Council, Washington, D.C., 1991.
2. Zaniewski, J. State of the Art of Airport Pavement Analysis and Design. In *Proc., Unified Airport Pavement Design and Analysis Concepts Workshop*, DOT/FAA/RD-92/17, FAA, U.S. Department of Transportation, 1992.
3. Brown, S. F. and C. F. Bell. The Validity of Design Procedures for the Permanent Deformation of Asphalt Pavements. *Proc., 4th International Conference on the Structural Design of Asphalt Pavements*, Vol. 1, Ann Arbor, Mich., 1977.
4. Majidzadeh, K., C. L. Saraf, S. Mesarovic, and G. J. Ives. State of the Art Review of Rutting and Cracking in Pavements. *Proc., Unified Airport Pavement Design and Analysis Concepts Workshop*, DOT/FAA/RD-92/17, FAA, U.S. Department of Transportation, 1992.
5. Fryba, L. *Vibration of Solids and Structures Under Moving Loads*. Noordhoff International Publishing, Gronigen, Netherlands, 1972.
6. Battiato, G., F. Ronco, and A. Verga. Moving Loads on a Viscoelastic Double Layer: Prediction of Recoverable and Permanent Deformations. *Proc., 4th International Conference on the Structural Design of Asphalt Pavements*, Vol. 1, Ann Arbor, Mich., 1977.
7. Elliot, J. F. and F. Moavenzadeh. Analysis of Stresses and Displacements in Three-Layer Viscoelastic Systems. In *Highway Research Record 345*, HRB, National Research Council, Washington, D.C., 1971, pp. 45–57.
8. Ioannides, A. M. and J. P. Donnelly. Development of User Guidelines for a Three-Dimensional Finite Element Pavement Model. *Proc., Unified Airport Pavement Design and Analysis Concepts Workshop*, DOT/FAA/RD-92/17, FAA, U.S. Department of Transportation, 1992.
9. Kokkins, S. J. FAA Unified Pavement Analysis 3-D Finite Element Method. *Proc., Unified Airport Pavement Design and Analysis Concepts Workshop*, DOT/FAA/RD-92/17, FAA, U.S. Department of Transportation, 1992.
10. Forte, T., K. Majizadeh, J. Kennedy, J. Hadden, and T. White. Federal Aviation Administration Pavement Modeling. *Proc., Unified Airport Pavement Design and Analysis Concepts Workshop*, DOT/FAA/RD-92/17, FAA, U.S. Department of Transportation, 1992.
11. Kirkner, D. J. Steady State Solutions to Moving Load Problems with Elastic-Plastic Foundation Models. *Journal of Engineering Mechanics*, in preparation.
12. Zienkiewicz, O. C. and R. L. Taylor. *The Finite Element Method*, Vol. 1. McGraw-Hill Book Co., London, England, 1989.
13. Crisfield, M. A. *Nonlinear Finite Element Analysis of Solids and Structures*. John Wiley and Sons, Inc., New York, 1991.
14. Desai, C. S. and H. J. Siriwardane. *Constitutive Laws for Engineering Materials with Emphasis on Geologic Materials*. Prentice-Hall, Inc., Englewood Cliffs, N.J., 1984.

Publication of this paper sponsored by Committee on Strength and Deformation Characteristics of Pavement Sections.

Computerized Overload Permitting Procedure for Indiana

SAMEH M. ZAGHLOUL, THOMAS D. WHITE, JULIO A. RAMIREZ, DONALD W. WHITE, AND NBR PRASAD

Truck weight regulations are used to control the rate of damage accumulation for pavements and bridges. Permitting heavier loads can increase the rate at which pavement damage and bridge deterioration accumulate and the costs of maintainance. Truck weight limits have always been controversial. Each state has legal truck weight limits. In many cases, trucks carrying weights higher than legal limits need to use the highway system and a special overload permit is required. A study conducted at Purdue University and funded by the Indiana Department of Transportation and FHWA developed an enhanced procedure for permitting overloaded trucks in Indiana. The procedure evaluates damage effects of overloaded trucks for pavements and bridges. Both pavement and bridge analyses use statistical models developed especially for this study. The pavement statistical models are based on a three-dimensional, nonlinear dynamic finite-element analysis of rigid, flexible, and composite pavements. Repeated axle loads moving at different speeds are considered, and realistic material models, such as viscoelastic and elastic-plastic models, are used for pavement materials and subgrades. The bridge statistical models are based on analysis using the AASHTO Bridge Analysis and Rating System and selected samples of bridges and overloaded trucks. User-friendly computer software was developed to implement this enhanced procedure, which allows the user to run damage analysis for overloaded trucks at the network level (e.g., route-independent analysis) as well as at the project level for specific pavement or bridge structures. Three options are available at both project levels: to check for pavements only, to check for bridges only, or to check for both, the default option. At the project level, the user is permitted to enter all cross-section and load parameters. Typical default values are provided for material properties.

Indiana's legal truck weight limits are described in the *Oversize-Overweight Vehicular Permit Handbook* (*1*). Trucks exceeding these limits—overloaded trucks—are required to have an overload permit before using the Indiana highway network. The permit is granted for a fee if the overloaded truck does not exceed the following limits (*1*):

- Maximum gross weight, 108,000 lb;
- Maximum single axle weight, 28,000 lb;
- Maximum tandem axle weight, 24,000 lb;
- Maximum axle group weight, 51,000 lb;
- Maximum wheel weight, 800 lb per linear inch of tire measured between the flanges of the rim.

S. Zaghloul, Roads Department, Dubai Municipality, P.O. Box 67, Dubai, United Arab Emirates. T. White, J. Ramirez, and D. White, School of Civil Engineering, 1284 Civil Engineering Building, Purdue University, West Lafayette, Ind. 47907-1284. NBR Prasad, Department of Theoretical and Applied Mechanics, 132 Talbot Lab, College of Engineering, University of Illinois at Urbana-Champaign, Urbana, Ill. 61801-2350.

Currently Indiana Department of Transportation (INDOT) regulations allow a truck exceeding the above limits to apply for an overload permit, which is evaluated for bridges and processed in two phases. In Phase 1, a simply supported beam and a two-equal-span, continuous beam are analyzed for the given permit vehicle for spans from 20 to 120 ft (6.1 to 36.8 m) in increments of 10 ft (3.05 m). The equivalent HS loading of the given overloaded truck is calculated by comparing the bending moments induced by the overloaded truck with those induced by the HS20 design truck in AASHTO's 1983 bridge maintenance standards. The overloaded truck will be permitted if its equivalent HS loading is less than HS30, (i.e., 1.5 times the HS20 design truck). When a truck matches a previously permitted truck, earlier results from Phase 1 are applied to make a quick evaluation. If the overloaded truck does not satisfy Phase 1 criteria, Phase 2, which involves a detailed load rating is implemented. The detailed load rating of Phase 2 requires specific information about the truck and bridges on the route for which the permit is requested. No evaluation for the damage effect of overloaded trucks on pavements currently is made.

PROBLEMS WITH CURRENT INDIANA TRUCK WEIGHT REGULATIONS

In Phase 1 of the current procedure, only beam-type bridges are considered. Hence, other types of bridges, such as trusses and arches, are not directly addressed. Girder cross-sectional properties are assumed uniform along the length of the span, and multi-span bridges are represented, along with only two-span bridges. It is observed that long, overloaded trucks with multiple axles are controlled by the negative moment at the central support of the two-equal-span, continuous beam. From past experience with this procedure, INDOT has found that allowable loads for these long trucks are conservative. Nevertheless, the approximate nature of the procedure demands that the limits on its use be very restrictive.

The current procedure ignores pavements. Although pavement failures are not as potentially catastrophic as bridge failures, the cost of repairing or reconstructing pavements that have failed from heavy loads is significant.

PAVEMENT ANALYSIS

A three-dimensional, dynamic finite-element program (3D-DFEM) (*2*) was used in this study to analyze flexible, rigid, and composite pavement. A composite pavement is an asphalt-overlaid concrete

pavement. The 3D-DFEM was verified for flexible and rigid pavement analysis. Two verification studies were conducted for each pavement type: static linear-elastic analysis and dynamic nonlinear analysis. Verification studies for both pavement types showed excellent agreement between field and predicted pavement response. Details of these analyses are reported by Zaghloul and White (*3,4*). No field measurements were available at the time of the study to conduct a similar verification study for composite pavements. However, considerable sensitivity studies were conducted to evaluate predicted composite pavement response.

Features of Finite-Element Model

Model Geometry

In this analysis, pavements were modeled as three-dimensional problems. For example, Figure 1 shows one of the three-dimensional finite-element meshes (FEMs) used to model flexible pavements. The FEM consists of two equally spaced meshes in the horizontal (xy) plane. A coarse mesh with 22.2-in. (56.39-cm) spacing was used in both the transverse (x) and longitudinal (y) directions. In the region of the load path, a finer mesh with 4.44-in. (11.28-cm) spacing was used in the x direction. Mesh dimensions in the vertical direction were selected to match the pavement layer thicknesses (i.e., surface, base, and subbase). The number of layers required to model the subgrade depends on the detail desired in predicting the vertical pavement response. In this example, the surface and base course were each modeled as a single layer, whereas the subgrade was modeled as a set of five layers. Adhesion between layers was considered a function of friction and normal pressure on the layers, according to the Mohr-Coulomb theory (*3*).

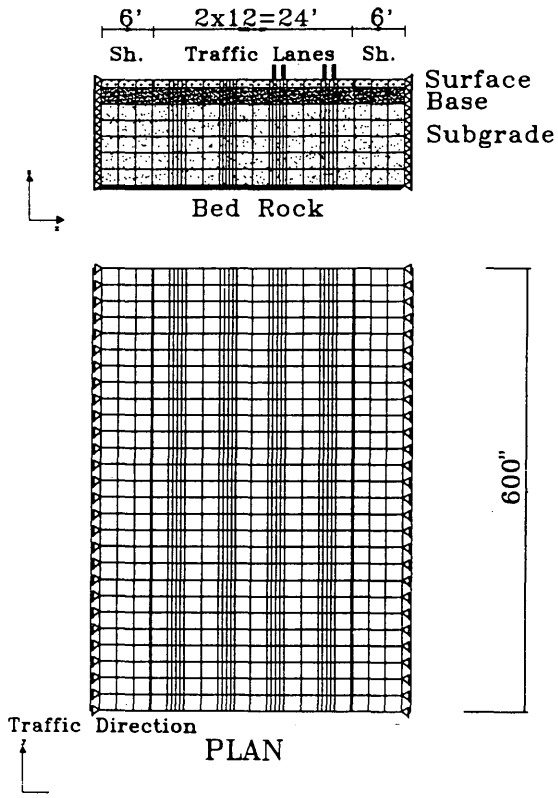

FIGURE 1 Example of the 3D-DFEM used in the analysis. (1 in. = 2.54 cm, 1 ft = 30.48 cm, and 1 kip = 453.7 kg).

Boundary Conditions

Boundary conditions for the finite-element model have significant influence on predicted response. Reasonable boundary conditions were assumed for edges parallel and perpendicular to the traffic direction, bottom of the mesh (deep foundation), and joints (such as lane and shoulder joints for flexible pavements and longitudinal and transverse joints for concrete pavements) (*3,4*).

Material Properties

Pavement materials were divided into four groups: asphalt concrete; portland cement concrete; unbound granular base, subbase, and subgrade soils; and cohesive subgrade soils. Actual material behavior under repeated loads was considered for each group. Details of these material models are reported by Zaghloul (*3,4*).

Asphalt concrete was modeled as a viscoelastic material. This type of material is time and temperature dependent (*5*). The time-dependent properties are represented by the instaneous and long-term shear moduli (*6*). The instantaneous shear modulus was selected at a loading time of 0.1 sec, which is equivalent to a speed of 40 mph. The long-term shear modulus was selected at a loading time of 1.0 sec, which is equivalent to a speed of 1.5 mph. The temperature effect was considered through the shear modulus values. Figure 2(a) shows the effect of loading time and temperature on asphalt mixture stiffness.

Granular materials, base, subbase, and subgrade, in some cases, were modeled using the Drucker-Prager model (*6,7*). This is an elastic-plastic model in which granular materials are assumed to behave elastically for low stress levels. When the stress level reaches a certain yield stress, the material will start to behave as an elastic-plastic material. Figure 2(b) shows a typical stress-strain curve for a granular material.

The Cam-Clay model (*6,8,9*) was used to model cohesive soils. This model uses a strain rate decomposition in which the rate of deformation of the clay is decomposed addictively into an elastic and a plastic part. Figure 2(c) shows the assumed soil response in pure compression.

Three stages of portland cement concrete (PCC) were modeled: elastic, plastic, and after-failure stages. Figure 2(d) shows the stress-strain curve used to model PCC. If the PCC slab is subjected to a stress level less than its yield stress, it will behave elastically. When the stress level exceeds the yield stress of PCC, the behavior is elastic-plastic until the failure stress. At that point, the after-failure stage will start (*6*).

Other material and layer characteristics required in the analysis include modulus of elasticity, Poisson's ratio, damping coefficient, and bulk density. Table 1 gives an example of the material properties used in the analysis.

Finite-Element Model Verification

Before general application, the 3D-DFEM was verified in a two-step process for asphalt and concrete pavements. The two steps

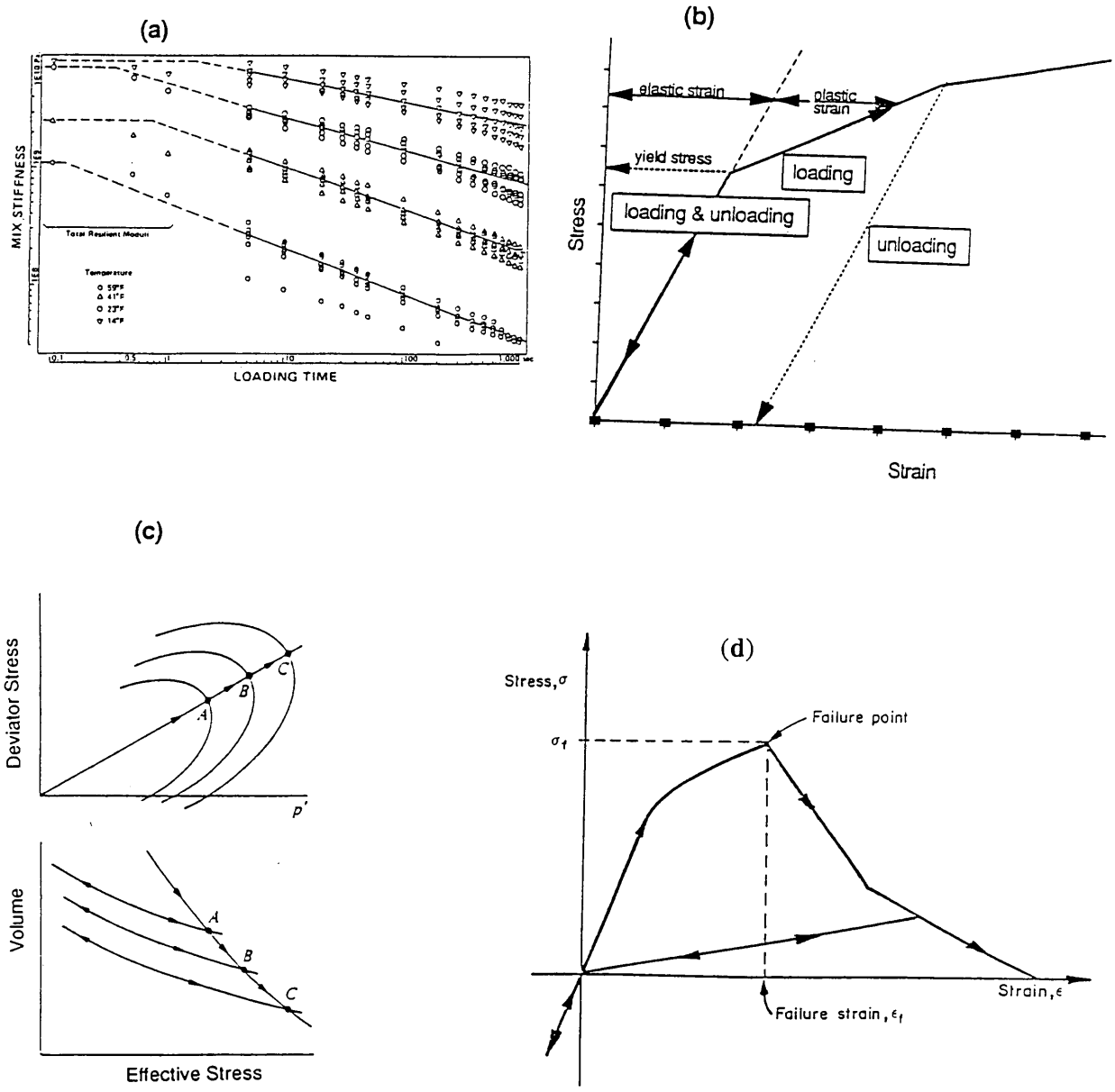

FIGURE 2 Material models used in the analysis; (a) asphalt mixtures, (b) granular materials, (c) clays, and (d) concrete. (1 in. = 2.54 cm, 1 ft = 30.48 cm, and 1 kip = 453.7 kg).

included evaluation of its capabilities to predict pavement response for both static and dynamic cases.

Static Analysis Verification

Design of experiments (DOEs) were developed for the elastic, static case. Subsequently, analyses of sections with factor combinations satisfying the design of experiment were conducted using a layered-elastic analysis for asphalt pavements and the Westergaard analysis for concrete pavements, and then compared with the 3D-DFEM analysis assuming elastic material properties for the various layers and static loading.

Three factors were included in the asphalt pavement DOE: surface layer thickness (T_s), base course thickness (T_b), and subgrade modulus of elasticity (E_{sg}). Two levels for each factor were included, low and high. Three factors were also included in the concrete pavement DOE: slab thickness (three levels), load position (three levels), and subgrade type (two levels). Linear correlation analyses were made between multilayer analysis predictions for asphalt pavements and Westergaard analysis predictions for concrete pavement as well as corresponding 3D-FEM predictions. High linear correlations were found for both asphalt and concrete pavements (R^2 = 96.4 percent and 97.8 percent, respectively).

Dynamic Analysis Verification

A study was also conducted to evaluate the time-dependent dynamic analysis feature of the 3D-DFEM. Because there is no stan-

TABLE 1 Material Properties Used in the Analysis

Material Name	Material Property	Typical Value
Concrete Slabs	Modulus of Elasticity - psi(GPa)	4,000,000 (27.62)
	Poisson's Ratio	0.15
	Initial Yield Stress - psi (MPa)	2670 (18.4)
	Failure Plastic Strain	1.3E-03
	Density - pcf (gm/cm^3)	150 (2.403)
	Damping Coefficient (%)	5
Granular Subbase	Modulus of Elasticity - psi (GPa)	40,000 (0.276)
	Poisson's Ratio	0.3
	Initial Yield Stress - psi (MPa)	19.29 (0.133)
	Initial Plastic Strain	0.0
	Angle of Friction - degree	33
	Density - pcf (gm/cm^3)	135 (2.1625)
	Damping Coefficient (%)	5
Lean Clay (CL) Subgrade	Shear Modulus - psi (MPa)	2750 (18.964)
	Poisson's Ratio	0.3
	Logarithmic Hardening Modulus	0.174
Lean Clay (CL) Subgrade	Initial Overconsolidation Parameter - psi (KPa)	8.455 (58.306)
	Permeability - ft/sec (cm/sec)	0.000021 (0.00064)
	Initial Void Ratio (%)	8
	Initial Stress psi (MPa)	weight of the pavement layers
	Density - pcf (gm/cm^3)	130 (2.0824)
	Damping Coefficient (%)	5

dard dynamic analysis method for the dynamic case, as there is for the static case, a decision was made to compare the predictions with measured response of pavements from moving loads. Figure 3 shows comparisons between field-measured and predicted pavement deflections of asphalt and concrete pavements. As can be seen, high linear correlations between the measured and predicted pavement deflections are found for both asphalt and concrete pavements, (R^2 = 99.9 percent and 99.6 percent, respectively). These high correlations imply that the 3D-DFEM can be used to predict the dynamic response of pavements subjected to moving loads (*3,4*).

Load Equivalency Factors

A sample of overload permit applications was reviewed to determine what truck configurations had been given permits. The sam-

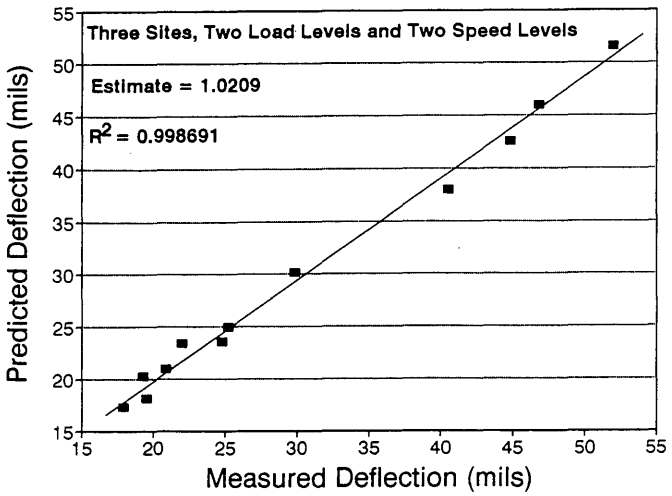

a) Asphalt Pavement

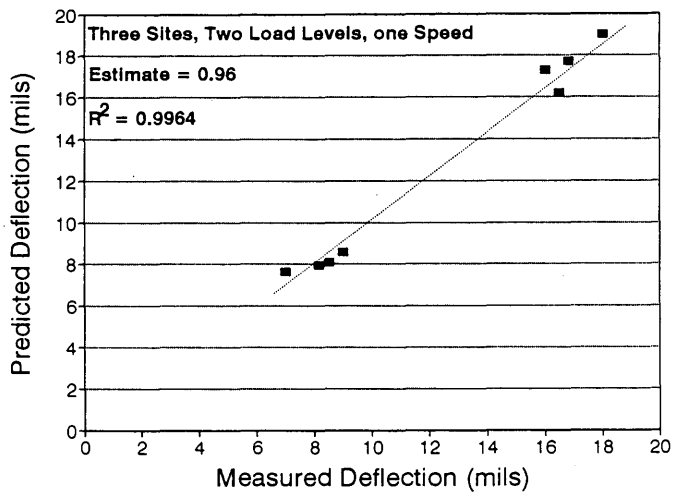

b) Concrete Pavement

FIGURE 3 Dynamic analysis verification. (1 in. = 2.54 cm, 1 ft = 30.48 cm, and 1 kip = 453.7 kg).

ple revealed that permits were requested for trucks with up to nine axles in one group as well as for trucks with single axle loads of 72 kips (32 666 kg). Load equivalency factors (LEFs) were required to account for the variation in truck configurations. There are two types of LEFs: analytical-based LEFs and empirical-based LEFs. Current pavement analysis methods used to develop the analytical-based LEFs incorporate unrealistic assumptions, such as static loads and linear-elastic material properties, whereas empirical LEFs, such as the AASHTO LEFs, are based on data that are limited to single and tandem axle configurations with maximum axle loads of 30 and 48 kips (13 611 and 21 778 kg), respectively.

Because of these limitations, the 3D-DFEM was used to develop LEFs for the overload permitting study. Three LEF sets were developed for flexible, rigid, and composite pavements. Permanent deformation at the pavement surface, which accumulates from different layers, was used as the equivalency criterion for flexible pavement LEFs, whereas total surface deformation, elastic and plastic, was used for rigid and composite pavement LEFs. The LEFs developed incorporated the effect of load repetitions. Figure 4 shows comparisons between Purdue LEFs for conditions similar to those of the AASHO road test and the appropriate AASHTO LEFs (*10–12*). Figure 5 shows the relationship between LEFs and maximum surface deformation. It was found that the rate of increase in the maximum surface deformation with LEFs increases significantly when the LEF exceeds 35. Therefore, a LEF of 35 is used in the permitting procedure as an upper limit for any axle group on an overloaded truck.

Typical Pavement Cross Sections for Indiana

On the basis of an Indiana Highway Inventory Annual Report (*13*), there are approximately 91,500 mi of roads within the state of Indiana. INDOT is responsible for approximately 11,300 mi, or about 28,203 lane-mi. Local government units are responsible for the rest. The road life data base (*14,15*) has detailed information about the cross sections and subgrades for 14,766 lane-mi (more than 50 percent of the total lane miles). From the data available in the road life data base, the pavement structure distribution was obtained for different highway classes: Interstate U.S., and state roads. Typical pavement cross sections shown in Figure 6 were selected to represent different highway classes. These typical cross sections are used for evaluating the damage effect of overloaded trucks at the network level. Table 1 indicates typical values of the material properties used in the analysis.

BRIDGE ANALYSIS

Sampling of Bridges and Overloaded Trucks

Preliminary information was obtained from INDOT for about 3,700 Indiana highway bridges classified into 19 different groups on the basis of structural form, material type, and type of construction. Within each group, the bridges are divided further into subgroups on the basis of the number of spans and overall length. Using a proportionate, stratified random sampling procedure, 148 bridges were selected.

On the basis of 550 permit requests received by INDOT during 1990 and 1991, 80 representative loading patterns were identified. Various significant truck parameters were identified: the number of axles (N), the distance between the front and the last axle, the wheel base (L), the number of equivalent axles (N_{cq}), the distance of the resulting load from the first axle ($\bar{x}$), and the standard deviation of the vehicle load distribution (x_σ). N_{cq} for any given truck is obtained by counting closely spaced axles [i.e., within 9 ft (2.74 m)] as a single equivalent axle.

One objective of this study is to formulate a procedure for a route-independent evaluation of overload permit requests. Such a procedure can contain only truck parameters as input variables. Lack of proper representation of truck parameters in the truck sample could lead to serious restrictions on the scope of the results. Hence, it was important to obtain a truck sample that would uniformly cover the range of chief truck characteristics. A uniform sample of 22 trucks was selected. In addition to these trucks, an HS20 design vehicle with variable spacing and two recommended

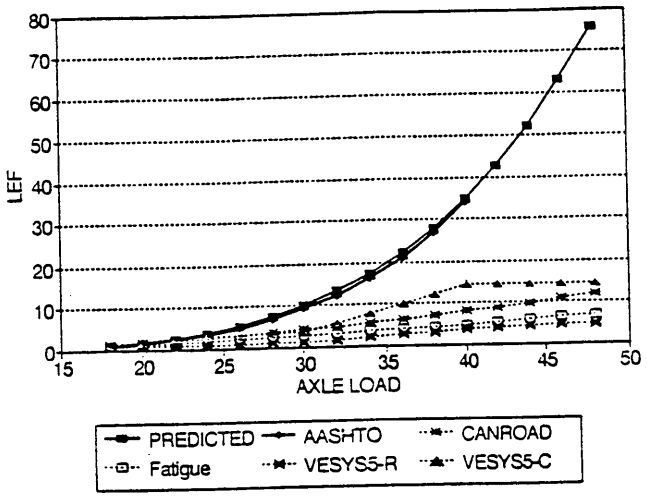

a) Asphalt Pavement (Single Axle Configuration)

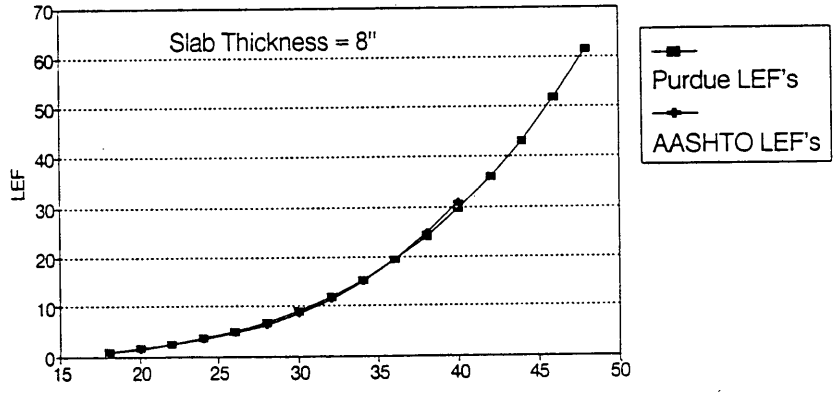

b) Concrete Pavement (Single Axle Configuration)

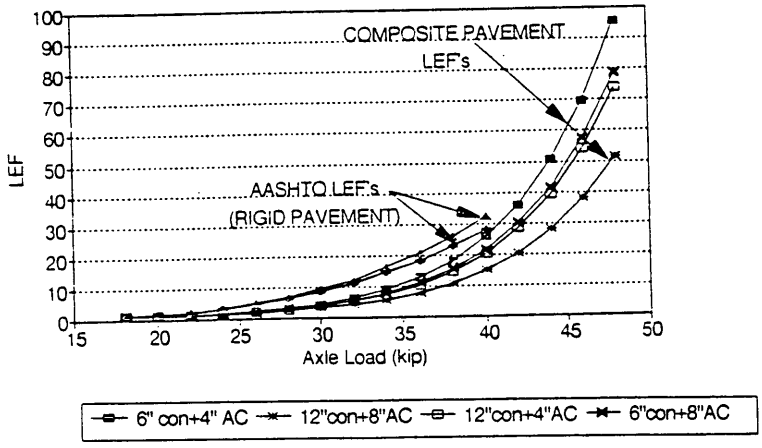

c) Composite Pavement (Single Axle Configuration)

FIGURE 4 Comparison between Purdue and AASHTO LEFs. (1 in. = 2.54 cm, 1 ft = 30.48 cm, and 1 kip = 453.7 kg).

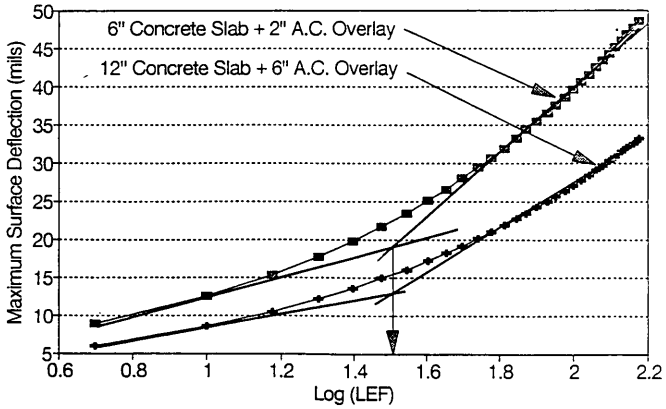

FIGURE 5 Effect of LEFs on maximum surface deflection. (1 in. = 2.54 cm, 1 ft = 30.48 cm, and 1 kip = 453.7 kg).

Indiana toll road loadings—to be used as alternative bridge loadings for bridge design in the future—were included in the sample.

Bridge Analysis and Rating

Detailed information for the 148 bridges selected was obtained from INDOT. The AASHTO Bridge Analysis and Rating System (BARS) was used in the analysis of bridge samples for the 25 selected trucks. The procedures in this program are based on elastic line girders and truss analysis. The rating of various structural components (i.e., girders, floor beams, stringers, and truss members) is performed using the working stress method at the operating stress levels defined in the 1983 AASHTO standard specifications for highway bridges. The operating stress level is 1.36 times the inventory stress level or design stress level, which corresponds to normal traffic. Stringers and girders lie parallel to the direction of traffic, whereas floor beams lie perpendicular to the traffic. Only flexural analysis is performed in this evaluation. The BARS program redistributes 10 percent of the negative moment over the supports to the positive moment area for compact section members of structural steel and composite steel and concrete. No redistribution of negative moments is used for either prestressed concrete or reinforced concrete bridges. The load distribution factors for a two-lane loading and the impact factor specified by the 1983 AASHTO bridge maintenance standards are used in the bridge analysis. The distribution factors are used in distributing the wheel load to the structural components (i.e., girders, stringers, and floor beams).

Data Base

Bridge components considered include stringers, girders, floor beams, and trusses. The BARS program gives the maximum allowable truck load for each of these bridge elements for a given truck. The information is recorded for all the elements. In this study the most critical of these values is used in the subsequent analysis as the maximum allowable load at the operating stress level for a given vehicle and bridge.

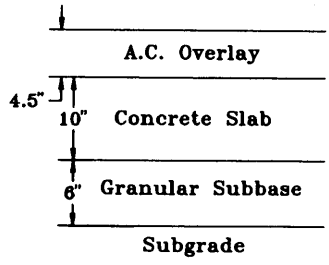

Typical JRCP Cross Section for Interstate Highways

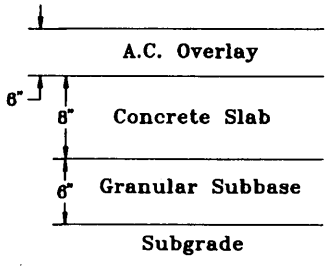

Typical JRCP Cross Section for U.S. Highways

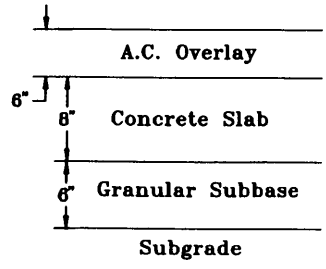

Typical JRCP Cross Section for State Roads

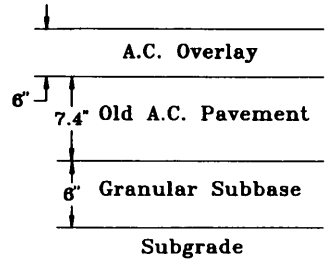

Typical JRCP Cross Section for State Roads

FIGURE 6 Typical jointed reinforced concrete pavement (JRCP) cross sections for Indiana.

Five different material types are also identified among the bridges. They are structural steel, reinforced concrete, composite steel and concrete, prestressed concrete, and composite prestressed concrete.

Statistical Procedure

In general, the allowable load may depend on a number of bridge and truck parameters. The purpose of this study was to identify the primary bridge and truck parameters that explain the variation in the dependent variable (i.e., the allowable load). On the basis of these parameters, different confidence limits were calculated.

A linear regression analysis was performed on various models that relates allowable load as the dependent variable to the bridge and truck parameters. It was assumed that the dependent variable is distributed normally. This assumption was verified at a later stage in the study. The correlation coefficient, r, was used in assessing the importance of each model. The regression models and values for constants at various reliability levels developed for the bridge analysis are shown below.

Route-Independent Model

$$\sqrt{W} = c_1 L + c_2 \tag{1}$$

where

W = maximum allowable load (tons),
L = wheel base (ft), and
c_1, c_2 = regression coefficients.

Route-Dependent Model

$$\sqrt{W} = c_1 (HS_{\text{truckcapacity}})L + c_2 \tag{2}$$

where the variables are those defined previously.

OVERLOAD PERMITTING PROCEDURE

Figures 7–10 show the flow chart of the overload permitting procedure. A user-friendly computer software was developed to implement this procedure. The procedure follows these steps:

1. Data entry, which includes

- Permit type (overweight, oversize, or mobile home);
- Vehicle information (overall length, width, and height; number of axles; gross load; axle loads and spacing; company name; and license; and
- Trip information (origin, destination, and route, if any).

The user is permitted to enter, review, and change the data.

2. Load parameters for bridge and pavement analyses are extracted from the vehicle information. Bridge analysis load parameters include wheel base, gross load, and number of equivalent axles. An equivalent axle is any group of axles that are placed within a distance of 9 ft (2.74 m). Pavement analysis load parameters include grouping the trucks into sets based on the distance between axles if less than 5 ft. (1.52 m) and calculating the axle group load, spacing, number of wheels, and number of axles for each axle group.

3. Selection of the level of analysis:

TABLE 2 Route-Independent Model

Factor	Reliability Level	Value
σ for individual predictions		1.031
Coefficient of Correlation (r)		0.830
c_1 / c_2	50%	0.0484 / 6.891
c_1 / c_2	85%	0.0484 / 5.822
c_1 / c_2	90%	0.0484 / 5.570
c_1 / c_2	95%	0.0484 / 5.195
c_1 / c_2	99%	0.0484 / 4.493

TABLE 3 Route-Dependent Model

Factor	Reliability Level	Value
σ for individual predictions		0.686
Coefficient of Correlation (r)		0.93
c_1 / c_2	50%	7.495E-4 / 6.795
c_1 / c_2	85%	7.495E-4 / 6.084
c_1 / c_2	90%	7.495E-4 / 5.916
c_1 / c_2	95%	7.495E-4 / 5.667
c_1 / c_2	99%	7.495E-4 / 5.2

- In network-level (default) analysis, typical pavement cross sections are used representing different highway classes. A route-independent formula is used for bridge analysis.
- In project-level: analysis, the user has to enter the pavement cross-section parameters and material properties. Default values are provided as a guide to the user. A route-dependent formula is used for bridge analysis.

4. Selection of type of analysis:

- Bridge analysis only,
- Pavement analysis only, or
- Bridge and pavement analysis (default).

If the user selects bridge and pavement analyses (the default), the bridge analysis is made first. The pavement analysis will be run

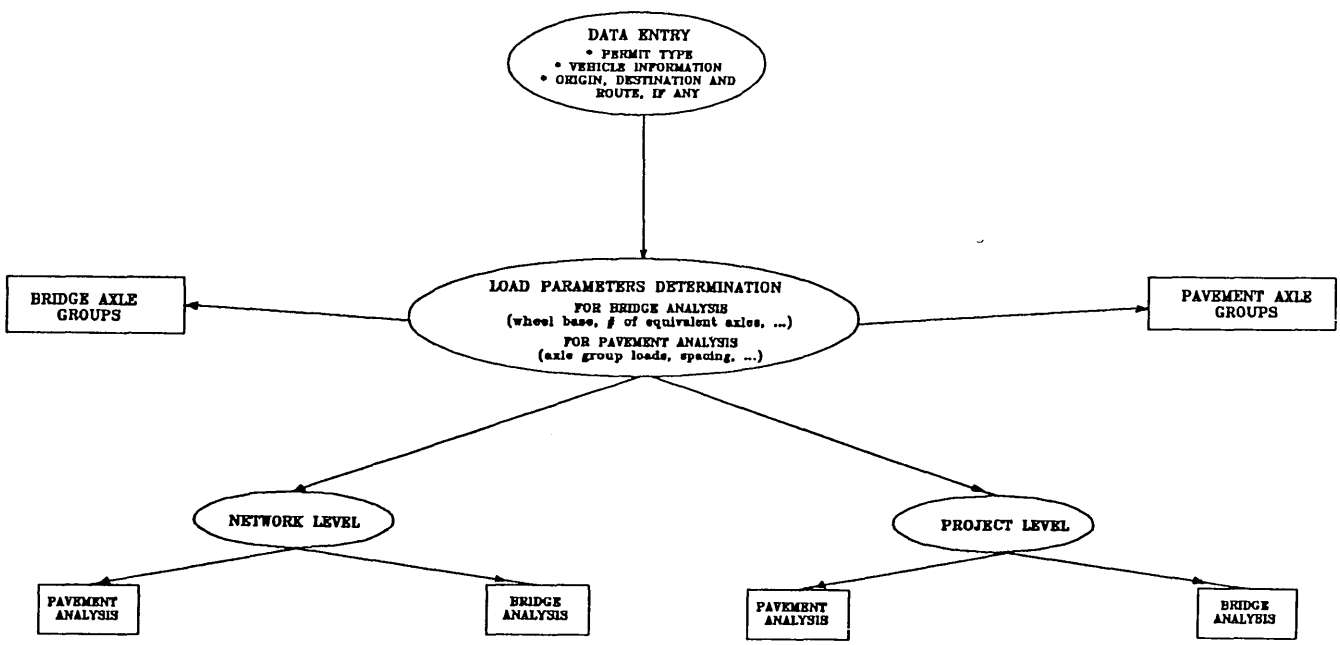

FIGURE 7 Flow chart of the overload permit procedure, Part 1.

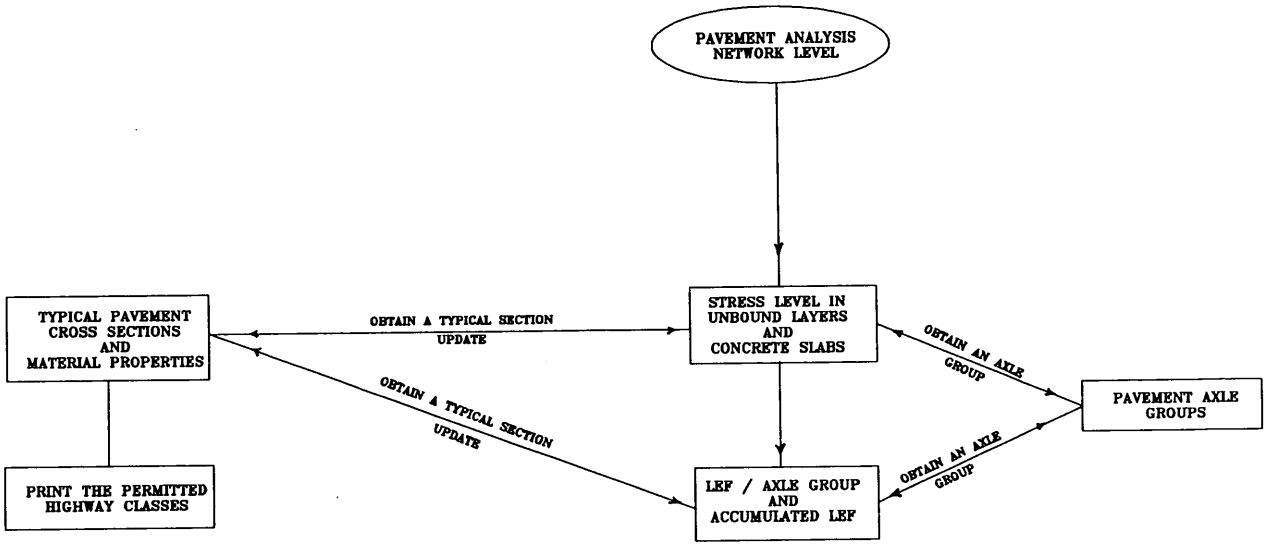

FIGURE 8 Flow chart of the overload permit procedure, Part 2.

regardless of the results of the bridge analysis. If the truck is not permitted, the reason why the truck is not permitted, bridge, pavement or both, will be shown in the permit.

Truck-damage effects on bridges and pavements are evaluated based on the user selections, as described in the next sections.

Network-Level Analysis

Bridge Analysis

The truck must have a minimum of six equivalent axles if the wheel base is more than 70 ft (21.34 m), or a minimum of three equivalent axles if the wheel base is more than 25 ft (7.62 m). The number of equivalent axles for any given truck is obtained by counting closely spaced axles [those within 9 ft (2.74 m)] as a single equivalent axle. Furthermore, the wheel base has to be in the range of 10 to 120 ft (3.05 to 36.6 m). If the truck satisfies the foregoing conditions, the route-independent model mentioned earlier (Equation 1) is used to evaluate the bridge damage. The results of this analysis are a function of truck parameters only.

Pavement Analysis

Typical pavement cross sections are used in this analysis to represent different highway classes (Interstate, U.S., and state roads). Trucks are represented as a set of axle groups. A sample of overload permit applications was reviewed, and it was found that the break point in axle spacing is 5 ft (1.52 m). Therefore, any two

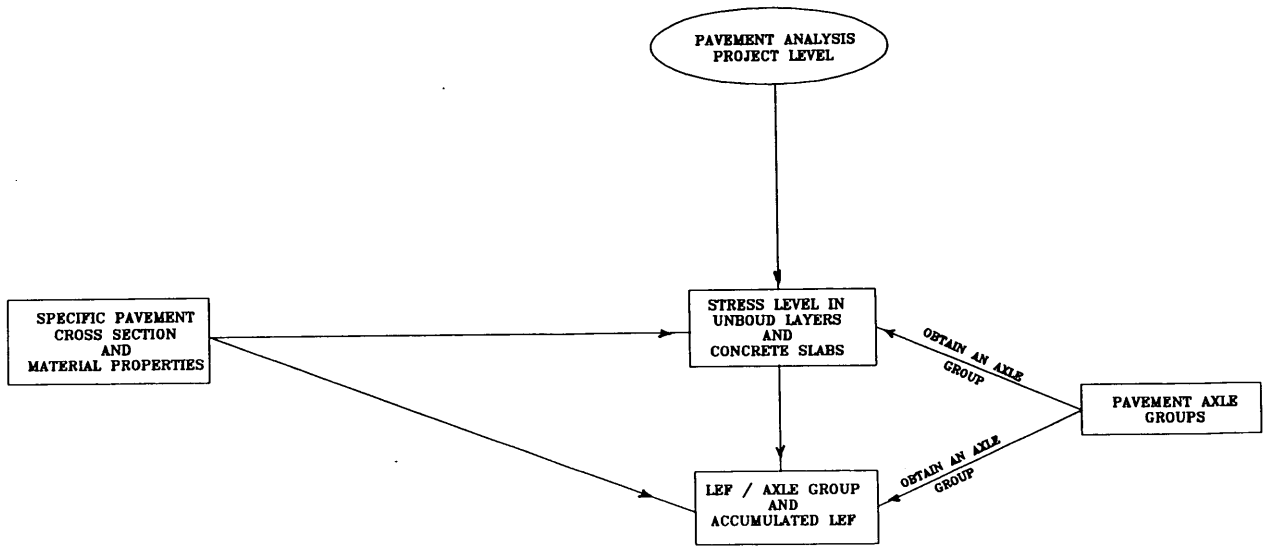

FIGURE 9 Flow chart of the overload permit procedure, Part 3.

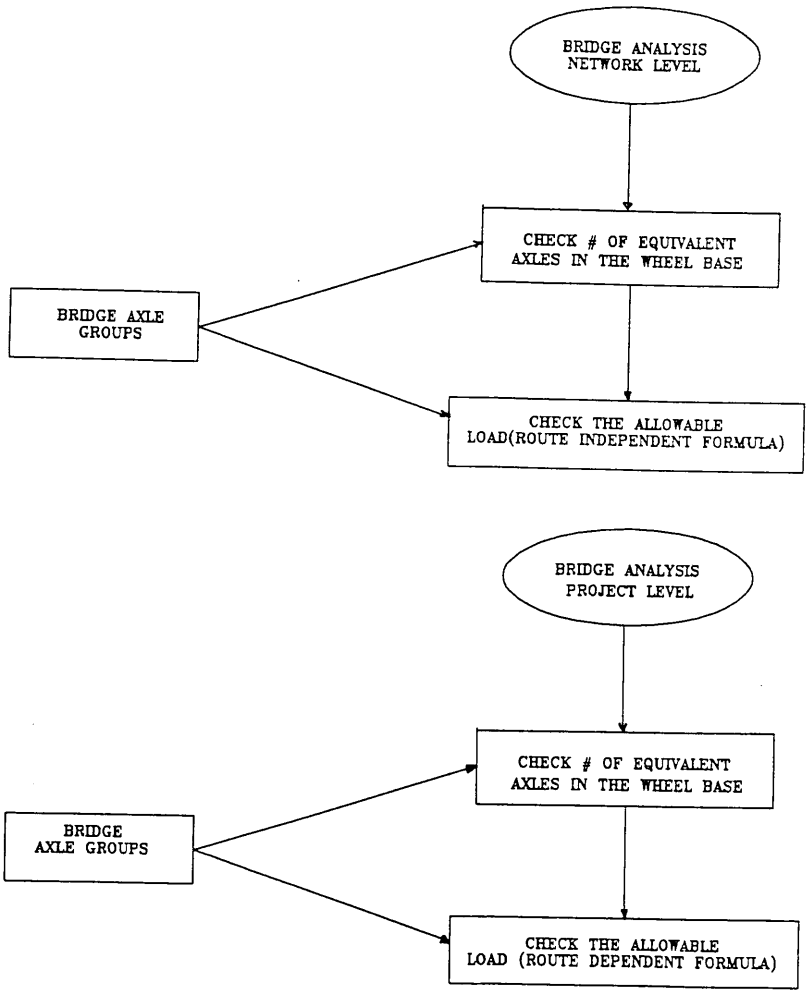

FIGURE 10 Flow chart of the overload permit procedure, Part 4.

successive axles with spacing equal to or less than 5 ft (1.52 m) are considered to be in one group. The pavement analysis involves (*a*) evaluating stress levels, and (*b*) determining LEFs.

Evaluation of Stress Levels When a pavement is subjected to a heavy load, some permanent deformation could develop in one or more of the pavement layers. Figure 11 shows the effect of heavy loads on asphalt and concrete pavements. As can be seen, when the pavements were subjected to an 18-kip (8 167-kg) single axle load (SAL), no permanent deformation developed in any of the unbound layers of the asphalt or the concrete pavements. When a heavy load was applied [a 58-kip (26 315-kg) SAL on the asphalt pavement and a 60-kip (27 222-kg) SAL on the concrete pavement], some permanent deformation developed in the unbound layers of both types of pavement. These permanent deformations developed because the unbound layers were subjected to stress levels higher than their yield stresses. Therefore, if stress levels in the unbound layers are kept below their yield stresses, no permanent deformation is expected and the pavement damage is minimal (*3,4*). Regarding concrete slabs, if the ratio of the stress to the modulus of rupture exceeds 0.5 (*5*), some fatigue damage develops.

The purpose of this evaluation is to estimate stress levels developed by the overloaded truck axle groups in the unbound layers and concrete slabs of the typical pavement sections. These stresses are compared with the corresponding yield stress of the unbound layers and the modulus of rupture of the concrete, respectively. Statistical models were developed to estimate stress levels in the unbound layers and the concrete slabs of the typical sections as a function of truck parameters. Previous analysis (*3,4*) determined that the effect of static loads is more severe for pavements than that of moving loads; therefore, static loads were used in the development of the statistical models. For each of the typical cross sections, if the yield stress in any of the unbound layers, including the subgrade, is exceeded or the concrete stress ratio (stress/modulus of rupture of the concrete) exceeds 0.5, the overloaded truck is not permitted to use this highway class. Further analysis will be made only for the typical cross sections that pass this check (satisfactory cross sections).

Determination of LEFs For each satisfactory cross section, the LEF of each axle group is determined using Purdue LEF sets (*10–12*). If the axle group LEF exceeds a certain limit (35 ESALs), the truck is not allowed to use this highway class. The

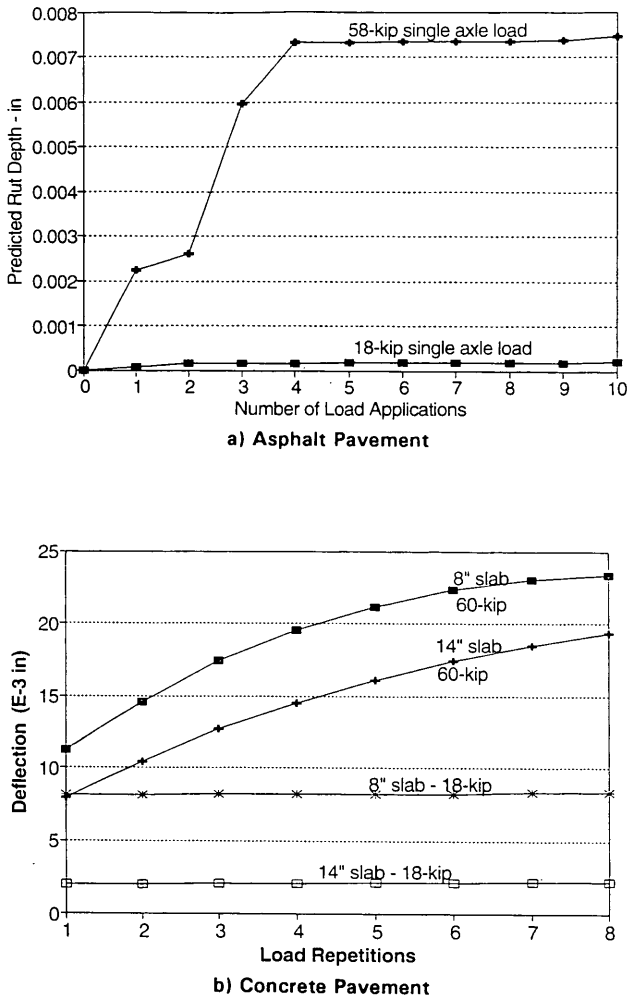

FIGURE 11 Effect of heavy loads on pavements (1 in. = 2.54 cm, 1 ft = 30.48 cm, and 1 kip = 453.7 kg).

35-ESAL limit is based on Figure 5. Also, the accumulated LEF for the truck is calculated by summing the LEFs of all axle groups. If the accumulated LEF exceeds a certain percentage of the average daily truck traffic of a certain highway class, the truck will not be permitted to use this highway class.

The truck is permitted to use highway classes that pass the previous checks. These highway classes are shown on the permit.

Project-Level Analysis

Bridge Analysis

In the bridge analysis, the allowable load at the operating stress level depends on both bridge and truck parameters. The bridge parameter is referred to as the HS truck capacity, which is defined as the maximum gross vehicle load that the bridge can carry within the operating stress level for a vehicle with the same configuration in terms of axles and axle-load distribution as the standard HS20 truck with variable axle spacing. In addition the truck has to satisfy both the minimum number of axles per wheel base and length of wheel base (*16*). The route-dependent model mentioned earlier (Equation 2) is used in this analysis.

Pavement Analysis

For the pavement analysis, the user has to provide information about the pavement cross section and material properties, including

- Pavement type (asphalt, concrete, or composite
- Layer thicknesses, and
- Material properties of each type of layer as follows:

–Asphalt surface layer—Modulus of elasticity, Poisson's ratio, damping coefficient, bulk density and G-ratio, expressed as

$$\left(1 - \frac{\text{long-term shear modulus}}{\text{instantaneous shear modulus}}\right)$$

–Granular layers—Modulus of elasticity, Poisson's ratio, initial yield stress, yield function, cohesion, angle of internal friction, damping coefficient, and bulk density.

–Cohesive layers—Modulus of elasticity, Poisson's ratio, initial yield surface, yield function, water content, cohesion, angle of internal friction, damping coefficient, and bulk density.

Typical default values for these properties are provided to the user. As for the network-level analysis, the overloaded truck has to pass the stress level and LEF checks in order to obtain a permit.

SUMMARY AND CONCLUSIONS

This study, conducted at Purdue University, was funded by INDOT and FHWA to develop an enhanced procedure for permitting overloaded trucks. In the procedure, damage effects of overloaded trucks are evaluated for pavements and bridges. The bridge analysis includes two steps:

1. The truck must satisfy a minimum of six equivalent axles if the wheel base is more than 70 ft (21.34 m), or a minimum of three equivalent axles if the wheel base is more than 25 ft (7.62 m). The number of equivalent axles for any given truck is obtained by counting closely spaced axles, those within 9 ft (2.74 m) as a single equivalent axle. Second, the wheel base has to be in the range of 10 to 120 ft (3.05 to 36.6 m).
2. The overloaded truck weight is checked versus the allowable weight calculated from statistical models based on analysis using BARS and selected samples of bridges and overloaded trucks.

A three-dimensional, nonlinear dynamic analysis of rigid, flexible, and composite pavements was used to develop statistical models to correlate pavement damage with load and cross-section parameters. Repeated axle loads moving at different speeds were considered, and realistic material models, such as viscoelastic and elastic-plastic models, were used for the pavement materials and subgrade. The pavement analysis can be conducted in two steps:

1. Check whether the stress level developed by the overloaded truck axle groups in the unbound layers of the pavement structure, including the subgrade, exceeds the layers' yield stresses, and whether the ratio of stress to modulus of rupture for the concrete

exceeds 0.5. The stress level in this step is estimated on the basis of static loads.

2. Calculate the LEF of each axle group of the overloaded truck using Purdue LEF sets and check whether this LEF exceeds a certain limit. Also, check that the accumulated LEF for the truck, which is the sum of the LEFs of the truck axle groups, exceeds a certain limit. This analysis is based on moving loads.

A user-friendly computer software was developed to implement the permitting procedure, one that allows a user to run a route-independent damage analysis for overloaded trucks at the network level, as well as at the project level, for specific pavements and bridges. At both levels, three options are available: (*a*) to check for pavements only, (*b*) to check for bridges only, or (*c*) to check for both (the default). At the project level, a user is allowed to enter all of the cross-section and load parameters. Also, typical values for material properties are available as default values.

REFERENCES

1. *Oversize-Overweight Vehicular Permit Handbook.* Indiana Department of Highways, Indianapolis, 1988.
2. *ABAQUS, Finite Element Computer Program Version 4.9.* Hibbitt, Karlsson and Sorensen, Inc., 1989.
3. Zaghloul, S. M., and T. D. White. Use of a Three-Dimensional, Dynamic Finite Element Program for Analysis of Flexible Pavement. In *Transportation Research Record 1388*, TRB, National Research Council, Washington, D.C., 1993, pp. 60–69.
4. Zaghloul, S. M., and T. D. White. Non-Linear Dynamic Analysis of Concrete Pavements. *Proc., 5th International Conference on Concrete Pavement Design and Rehabilitation* Vol. 1, Purdue University, West Lafayette, Ind., 1993, pp. 277–292.
5. Yoder, E. J., and M. W. Witczak. *Principles of Pavement Design*, 2nd edition. John Wiley and Sons, Inc., New York, 1975.
6. *ABAQUS, Finite Element Computer Program Version 4.9: Theory Manual.* Hibbitt, Karlsson and Sorensen, Inc., 1989.
7. Drucker, D. C., and W. Prager. Soil Mechanics and Plastic Analysis or Limit Design. *Quarterly Journal of Applied Mathematics*, Vol. 10, 1952, pp. 157–165.
8. Schofield, A. and C. P. Worth. *Critical State Soil Mechanics.* McGraw Hill, New York, 1968.
9. *Stress-Strain Behavior of Soils.* (R. H. Parry, ed.), G. T. Foulis and Company, Henley, England, 1972.
10. Zaghloul, S. M., and T. D. White. Load Equivalency Factors for Flexible Pavements. Presented at the 1994 Annual Meeting of the Association of Asphalt Paving Technologists, St. Louis, Mo., Feb. 1994.
11. Zaghloul, S. M., and T. D. White. Evaluation of Heavy Load Damage Effect on Concrete Pavements Using a Three-Dimensional, Non-Linear Dynamic Analysis. Presented at the 73rd Annual Meeting of the Transportation Research Board, Washington, D.C., 1994.
12. Zaghloul, S. M. and T. D. White. Use of a Three-Dimensional, Dynamic, Non-Linear Analysis to Develop Load Equivalency Factors for Composite Pavements. Presented at the 73rd Annual Meeting of the Transportation Research Board, Washington, D.C., 1994.
13. *How Many Miles: Highway Inventory and Systems Unit Annual Report.* Indiana Department of Highways, Indianapolis, 1989.
14. Lindly, J., and T. D. White. *Development of an Overlay Design Procedure for Flexible Pavements in Indiana.* Joint Highway Research Project, FHWA/IN/JHRP-87/9, FHWA, U.S. Department of Transportation, 1987.
15. Pumphrey, N., and T. D. White. *Development of Asphaltic Concrete Overlay Design Procedure for Rigid Pavements in Indiana.* Joint Highway Research Project, FHWA/IN/JHRP-89/14, FHWA, U.S. Department of Transportion, 1989.
16. Prasad, NBR, D. White, J. Ramirez, and T. Kuczek. *Statistical Analysis of Overload Vehicle Effects on Indiana Highway Bridges.* Joint Highway Research Project, FHWA/IN/JHRP-93/1, FHWA, U.S. Department of Transportation, 1993.
17. Roque, R., M. Tia, and B. E. Ruth. Asphalt Rheology to Define the Properties of Asphalt Concrete Mixtures and the Performance of Pavements. In *Asphalt Rheology: Relationship to Mixture*, Special Technical Publication 941 (O. E. Briscoe, ed.), ASTM, Philadelphia, Pa. 1987, pp. 3–27.
18. Wood, D. *Soil Behavior and Critical State Soil Mechanics.* Cambridge University Press, New York, 1990.

Publication of this paper sponsored by Committee on Strength and Deformation Characteristics of Pavement Sections.

Variation of Deflection with Measuring Equipment and Load Speed on Test Track

RECAREDO ROMERO, AURELIO RUIZ, RAMÓN RODIL, AND MIGUEL ANGEL LECHUGA

Deflection is used on the full-scale test track to establish moduli for pavement layers and to provide useful information for strengthening studies and performance models. Results from falling-weight deflectometer and Benkelman beam correlation studies are set out, including an examination of possible factors that could affect the results, such as speed at which the load is applied and pavement deformation. Flexible and semirigid pavements are included.

The Centro de Estudios y Experimentación de Obras Públicas (CEDEX) full-scale pavement test track has novel features compared with other test tracks. Its oval shape provides two straight sections totaling 150 m of testing facilities as opposed to the 10 to 12 m that is the norm for other linear tracks (*1*,*2*). Simultaneous comparison between different types of pavement constructed with conventional road equipment is possible given the track's length.

The principal objective of tests carried out on the track is to compare the service life of different pavement sections in a controlled and accelerated manner. Service life is defined on the basis of surface cracking and evenness.

Other parameters also are measured on test tracks to establish the characteristics of pavements tested and to monitor their evolution. One of these is deflection, which is used to establish moduli for pavement layers and to provide useful information for strengthening studies and performance models.

The Benkelman beam (BB) is used in Spain as a standard reference for deflection. On the test track, deflection is measured with a falling-weight deflectometer (FWD) in order to carry out subsequent back calculation for the pavements. It is therefore necessary to carry out studies on the correlation between both types of equipment in order to relate deflection measured with the FWD to standard deflection. Results from such correlation studies are set out in this paper and include an examination of factors that could affect the results (the speed at which the load is applied and pavement deformation). The study also includes a comparison with the Lacroix deflectograph, which is the equipment used most widely in Spain for measuring deflection. Deflection measurements made with the different types of equipment were compared with those from sensors contained within the pavements.

The novel contribution of this work compared with other similar studies is that by carrying it out on test track pavements, it was possible to control the different variables with a high degree of precision.

Centro de Estudios de Carreteras, CEDEX MOPT, Autovia de Colmenar, Room 18200, El Goloso 28049, Madrid, Spain.

DESCRIPTION OF TEST TRACK

The CEDEX test track is oval with two straight sections joined by two curved sections (see Figure 1). Each straight section is approximately 75 m long, and the track has a total circumference of 304 m (*1*,*2*). Leaving out the transition areas between the curved and straight sections, 67 m is available on each straight section to carry out pavement testing. Because the minimum length for each test is 20 m, a total of six sections can be tested at the same time. The curved sections are not used for pavement testing but are reserved for studying surface materials, such as paints and wearing courses.

Although the curved sections are laid directly on the natural subgrade, on the straight portions there is a reinforced concrete casing inside which the pavement sections are constructed. This system enables the test sections to be completely isolated from the surrounding ground. It also makes it possible to flood the embankment to simulate different water levels. The concrete casings are 2.60 m deep, enabling embankments of at least 1.25 m to be constructed. They are 8 m wide; therefore, conventional road construction equipment can be used.

A concrete rail has been constructed along the inside perimeter of the track to serve as a guide for the traffic simulation vehicle and to provide control over the trajectory of the load. On the straight sections, the concrete rail rests over accessible underground galleries that are used to house connections for sensor cables installed in the pavement and the permanent data-gathering system. A structure has been built that enables sections of the track to be covered over if desired or water sprinklers to be in-

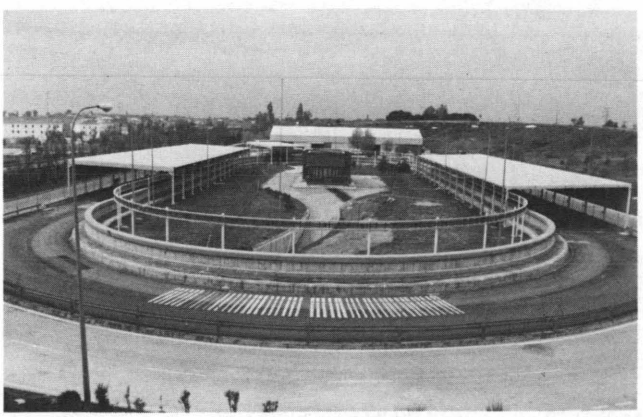

FIGURE 1 CEDEX test track.

stalled to simulate rainfall, along with other equipment to control climatic conditions.

The traffic simulation vehicle is made up of two parts, the guiding section and the load assembly (see Figure 2). The latter exerts the load by gravity. The total weight (vehicle and ballast) is 6.5 ton, equivalent to a 13-ton half-shaft, which is the maximum permitted limit for simple axles in Spain. It is fitted with twin wheels with conventional tires inflated to a pressure of 8.5 kg/cm^2. The load assembly contains the driving gear and provides the motive power for the assembly as a whole. An electric motor is used that draws power from a roller path located on the guide rail. When in continuous use, the vehicle has a maximum circulation speed of 50 km/hr, with an average speed of 40 km/hr. The vehicle can move in a sideways direction because of a hydraulic jack within it. The maximum sideways movement is ± 400 mm; taking into account the width of the tires, that produces a rolling strip with a maximum width of 1.3 m. Vehicle passes are distributed following a normal curve that corresponds with actual distributions measured on roads. Another two vehicles are under construction.

An automatic system has been installed in the control center in the middle of the track to control the vehicle's movements, and instructions are passed to the vehicle by radio. The automatic system for gathering data from the instruments has a maximum capacity of 300 sensors per test, with data gathered in real time and stored in a data base (*3*).

It should be emphasized that the installation as a whole, and the vehicle and its control system in particular, are purpose-built prototypes.

PAVEMENTS TESTED

The tests included in this paper were sponsored by Spain's Directorate General for Roads, Ministry of Public Works, Transport and the Environment. The essential purpose of the tests was to compare asphalt pavements with different types of road base and to also study the effects of different types of subgrade.

For this purpose three sections were chosen from directive 6.1 and 2-IC (the Spanish standard pavement catalogue), corresponding to a T2 traffic level (up to 800 trucks daily per lane) resting on subgrades of type E2 [10 < California bearing ratio (CBR) < 20] and E3 (CBR > 20). The sections studied are shown in Figure 3.

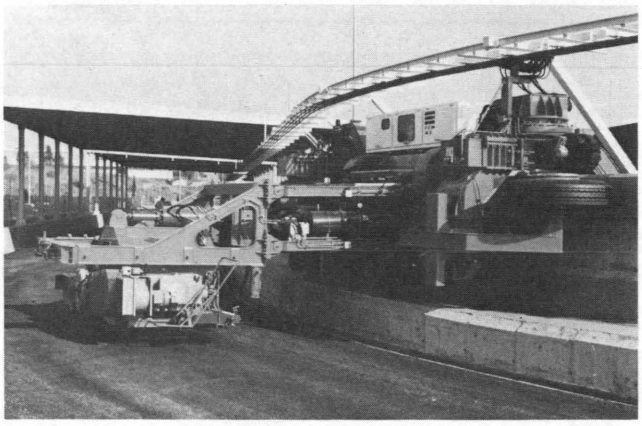

FIGURE 2 Traffic simulation vehicle.

The cement-stabilized soil included 5 percent cement, giving an average simple compressive strength at 7 days of 2.9 MPa. The cement content of the cement-bound granular material was 4 percent with an average simple compressive strength at 7 days of 6.6 MPa. Regarding the asphalt, the bitumen used was B60/70, with an aggregate that had an average binder content of 4.8 percent; the average dynamic modulus at 20°C and 10 Hz was 5300 MPa.

As a result of the tests, it is expected that the relative service life of asphalt pavement sections resting on graded aggregate, cement-stabilized soil, and cement-bound granular material will be determined. In addition, the procedure adopted in the catalog for reducing the thickness of pavements when moving from an E2-type subgrade to an E3-type will be analyzed.

Initial deflection of pavements and their evolution during the first 600,000 load cycles are represented in Figure 4. The deflection is corrected for temperature by calibration carried out on the test track pavements themselves.

EQUIPMENT USED

A KUAB double mass FWD was used, with a 30-cm-diameter, segmented, flexible-type circular plate. Deflection was measured at the center of the plate and at different distances, although only data obtained from the seismometer located in the center of the plate are included in this study. For each measuring operation, three loads were applied of 2500, 6500, and 6500 kg (in Spain the maximum legal simple axle limit is 13 ton), with the deflection results from the latter two loads averaged out.

The Benkelman beam follows the standing rebound procedure. The truck used has a simple back axle with twin wheels and an axle load of 13 000 kg.

The sensors located in the pavement consist of a rod embedded in the concrete slab at a depth of approximately 2 m and a sensor joined to the pavement, with strain gauges. There are eight sensors of this type (two in Sections 3 and 4 and one in the other sections).

The Lacroix deflectograph has a short chassis and 13 tons per axle with a distance between measurements of approximately 5 m. It works at a measuring rate of 2 to 3 km/hr. It provides measurements 1.9 m apart along two rolling lines corresponding to the back wheels. The sensors are of the linear variable differential transformer (LVDT) type.

All the equipment was calibrated using micrometers before the measurements were carried out.

COMPARISON BETWEEN FWD AND BB

A comparison between FWD and BB was made, after 50,000 loads had been applied to the pavements, and then again after 600,000 loads had been applied. The first measurements were made for two semirigid pavements (Sections 1 and 3) and one flexible pavement (Section 2). The second measurements were taken only for Sections 1 and 2. In each pavement three points were selected that had a deflection close to the average deflection for the pavement. Measurements were made at each point, first with the BB, then with the FWD, and finally with the BB. An average was taken of the two measurements made with the latter equipment. The operation was repeated three times at each point.

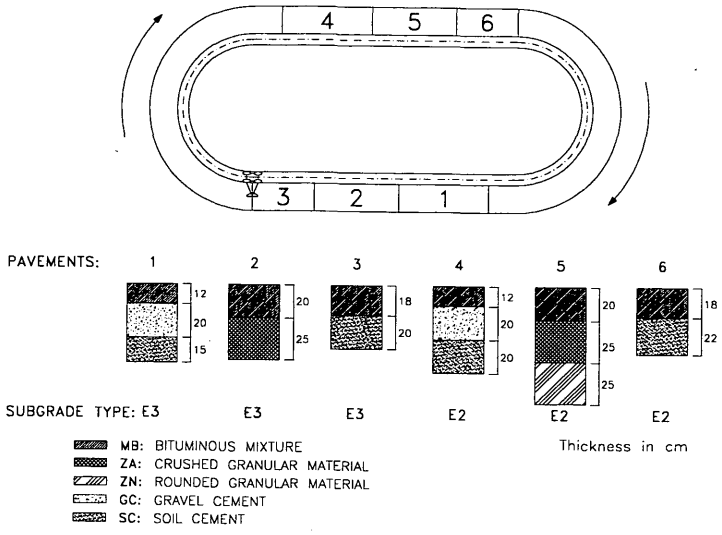

FIGURE 3 Pavements tested.

As a result, coefficient α was defined as the ratio between the deflection with the BB and that with the FWD. The results are presented in Table 1.

The results varied widely, mostly because of the dispersion of measurements obtained with the BB. If each set of results were represented by their average, it could be said that the ratio between the FWD and the BB depends on pavement type, with higher ratios in the case of flexible pavements as compared with semirigid pavements. The same trend appears in the results from the second series of measurements.

During an earlier investigation (*4*) on different flexible pavements, it was ascertained that the ratio between deflection measured with the two types of equipment also depended on temperature and thickness of the different layers (α increases both with temperature and with thickness of the asphalt layer) and that the coefficient became gradually less throughout the service life. Furthermore, in the case of flexible pavements with a different composition but with the same deflection, different values were obtained for coefficient α. Specific values for coefficient α as a whole varied between 0.7 and 2 in the tests carried out.

As a result, it is difficult to establish correlation coefficients between the two sets of equipment. If a conversion needs to be made, the most suitable procedure is to make a comparison on the section to be evaluated, as carried out on the test track. In addition, the lack of consistency obtained in measurements with the BB cast doubt on using it as standard measuring equipment.

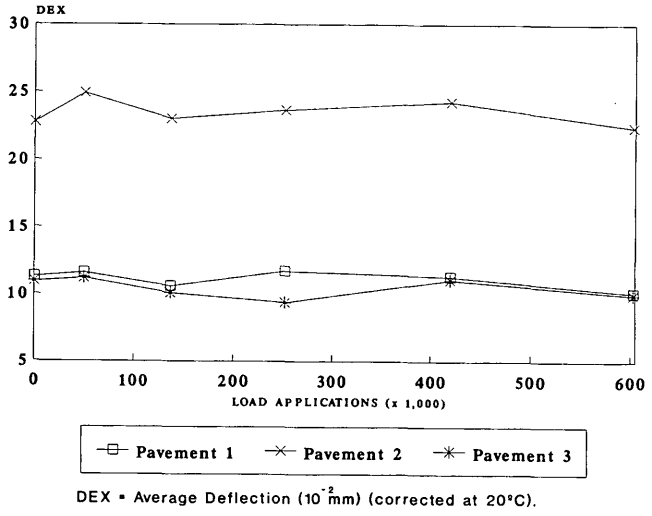

FIGURE 4 Deflections along the test track.

COMPARISON BETWEEN FWD AND LACROIX

Owing to the characteristics of the Lacroix deflectograph, which takes measurements in motion every 5 m, a comparison between the two pieces of equipment could not be carried out point by point. The operation was carried out by repeatedly passing the Lacroix deflectograph over the test sections and staggering the starting point in an attempt to obtain equidistant measurements at 1-m intervals. Maximum positioning errors of $\pm$ 30 cm were measured.

Measurements were carried out after 50,000 loads had been applied to the pavements. As a result of the measurements, coefficient Σ was defined as the result of dividing the average deflection results from the Lacroix deflectograph by the average deflection obtained using the FWD (Table 2). As a comparative example, the specific deflections obtained from both pieces of equipment on Section 1 are shown in Figure 5.

A comparison of the measurements made it clear that although average deflection values were comparable, the specific measurements obtained using the Lacroix deflectograph showed a higher dispersion around the mean than did those gathered by the FWD. On the other hand, and unlike the case of the FWD-BB comparison, coefficient Σ is not related to the pavement type and does not show higher values for flexible pavements as compared with semirigid types. Results obtained on the two rolling lines of the Lacroix deflectograph are presented in Figure 6, and it can be seen that the deflections follow the same trend on both lines. For that

TABLE 1 α Values

LOADS APPLIED	50,000			600,000	
DATE	MAY 1992			APRIL 1993	
PAVEMENT TEMPERATURE	14 - 15			9 - 10	
PAVEMENT Nº	1	2	3	1	2
DEX	10.2	20.8	9.0	8.7	17.9
[α]	0.82 - 1.54	1.35 - 1.71	0.92 - 1.65	0.72 - 1.29	1.22 - 1.65
α	1.03	1.51	1.19	0.92	1.44

DEX = AVERAGE DEFLECTION (FWD) (10^{-2} mm)
[α] = INTERVAL
α = α AVERAGE

$$\alpha = \frac{BB\ DEFLECTION\ (6,5t)}{FWD\ \ DEFLECTION\ (6,5t)}$$

reason, the difference between these results and those obtained with the FWD is not attributable to the differences in the measuring points because of errors in positioning the equipment. Possible causes of the differences that were considered included the effect of the position of the beam tip between the twin wheels and the effect of the dynamic load applied by the vehicle.

The average deflection value measured with the Lacroix deflectograph shows the difference between low and high deflection, but it could give rise to significant deviation from FWD results if specific values or characteristics are used, particularly with deflections of less than 20.10^{-2} mm.

The FWD clearly seemed to be a more reliable and consistent piece of equipment, with better characteristics for precision work such as that on test tracks or for working with specific values such as those used with back calculation models. The deflectograph appears to be suitable for large-scale work because of the large quantity of information it supplies, provided that average values are used because specific values show a considerable dispersion.

COMPARISON BETWEEN FWD OR BB AND SENSORS

The comparison between the FWD and the sensors was carried out by placing the circular FWD plate in such a way that the central seismometer point rested on the sensor embedded in the pavement. Three loads were then applied (2.5, 6.5, and 6.5 ton), and in each case deflection measured by the embedded sensor was recorded. One of the deflection curves obtained is presented in Figure 7, in which deflection can be seen as a result of the first blow and those blows caused by subsequent bounces. The shape of the wave sequence is similar for all measurements that were made.

Values for deflection measured by the FWD and the sensors are presented in Table 3, along with coefficient β, obtained by dividing the first by the second and multiplying the result by 100. The deflections measured correspond with a difference of about 5 percent, which is within the range of calibration error for both pieces

TABLE 2 FWD Versus Lacroix Deflectometer Results

	INTERVAL (10^{-2} mm)		AVERAGE (10^{-2} mm)		σ		
PAVEMENT	DI	DL	DI	DL	DI	DL	Σ
1	9-13	4-18	10.2	10.4	1.1	4.1	1.02
2	19-24	15-36	21.1	24.2	1.2	6.5	1.14
3	8-10	5-20	9.1	11.5	0.5	4.7	1.27

σ = Standard Deviation
DI = FWD Deflection
DL = Lacroix Deflection

$$\Sigma = \frac{(DL)}{(DI)}$$

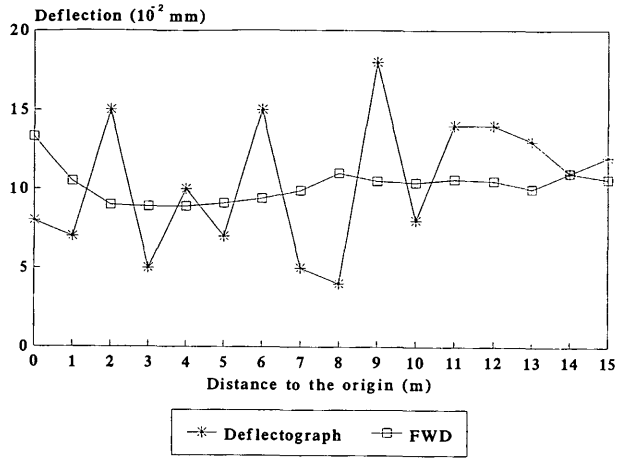

FIGURE 5 Lacroix deflectograph versus FWD deflections (Pavement 1; 50,000 load applications).

of equipment. All sections, regardless of their type, showed similar values for β.

A comparison of the BB and the sensors was then made. The twin wheels of the truck were positioned in such a way that the sensor was between them, and the beam tip of the BB rested directly over the sensor.

In Table 4, the results obtained from all sections are indicated along with coefficient λ, which was obtained by dividing the two deflections (BB and sensor). The value of this coefficient is 92 and 96 in the case of flexible sections and varies between 64 and 80 in the case of semirigid pavements. In the latter case, error brought in by the Benkelman beam therefore could be considerable.

The difference between the two measurements must be based on the fact that the BB's support is partly within the deformation bowl produced by the load. The effect of the deformation factor is much greater for semirigid sections than for flexible sections.

The half-length of the deformation bowl obtained in the test with the load simulation vehicle moving at 1 to 2 km/hr is 500 cm in Section 1 (semirigid) and 350 cm in Section 2 (flexible).

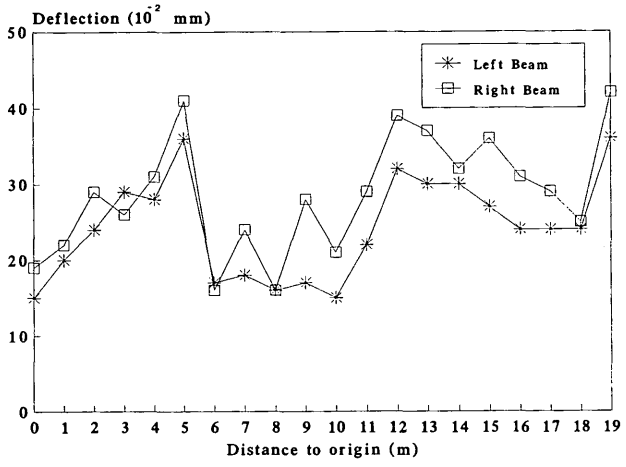

FIGURE 6 Deflections measured with Lacroix deflectometer (Pavement 2).

Because the BB's support is 240 cm from the beam tip, the latter is located in the middle of the half-length of the deformation bowl on the semirigid sections and 1 m from their beginning on flexible sections.

INFLUENCE OF SECOND SET OF REAR WHEELS

Whereas the FWD applies only to a single load, deflection measured with the BB is produced by the whole set of wheels on the track used in the test. If the effect of the front axle is ignored, since it is of minor importance to the total deflection, the main effect comes from the second assembly of the rear axle wheels.

According to multilayer simulation, these rear wheels contribute 44 to 55 percent of the deflections in the semirigid sections and 24 to 34 percent in the flexible sections. From the deflection curves measured with the vehicle moving at 2 km/hr, these figures have an average of 33 and 20 percent, respectively. The values with the vehicle stopped would be a little bit higher than those, but other measures not being available, these values were used.

On the basis of these results, BB/FWD deflection ratios can be calculated, eliminating the effects of the deformation bowl and the second set of wheels. The results are indicated in Table 5 for Sections 1 (semirigid) and 2 (flexible) in the form of variable ω. In making this calculation, the average of values obtained for semirigid sections was applied to Section 1 and the average for flexible sections to Section 2. Taking average values at 15°C, the deflection produced by BB is greater than the deflection produced by the FWD by 50 percent (on semirigid pavements) and 70 percent (on flexible pavements).

VARIATION IN DEFLECTION WITH LOAD SPEED

In order to carry out this study, deflections from sensors embedded in the pavements were measured as the load simulation vehicle passed over them at different speeds. The data shown here relate to the position of the vehicle with the sensor midway between the two wheels. Values for the resulting deflections are indicated in Table 6. Figure 8 shows an example of the results and their adjustment using logarithmic equations.

The deformation bowl half-length (the distance from the start to the point of maximum value) is between 350 and 400 cm on the flexible sections (Sections 2 and 5) at speeds of 1 to 2 km/hr and decreases as the speed increases to values of 230 to 260 cm. On semirigid pavements, the variation is 400 to 500 cm at low speeds and 300 to 350 cm at higher speeds. Deflections decrease as speed increases. Contrary to what might be expected, the decrease is always greater on semirigid sections than on flexible sections. In the former, the variation is high, up to 15 to 20 km/hr, but then decreases more slowly. In the case of flexible pavements, the greater decrease occurs at up to 10 km/hr (Figure 9).

On flexible and semirigid pavements, the vehicle speed that produces a deflection similar to that of the BB is between 1 and 2 km/hr, whereas in the case of the FWD there is a considerable difference in the equivalent speed for the two types of pavement. On flexible pavements the speed is around 25 km/hr; on semirigid pavement it is between 1 and 2 km/hr. These speed values are obtained by calculating the vehicle speed that produces a deflection on pavements similar to that of the FWD, which gives a ratio

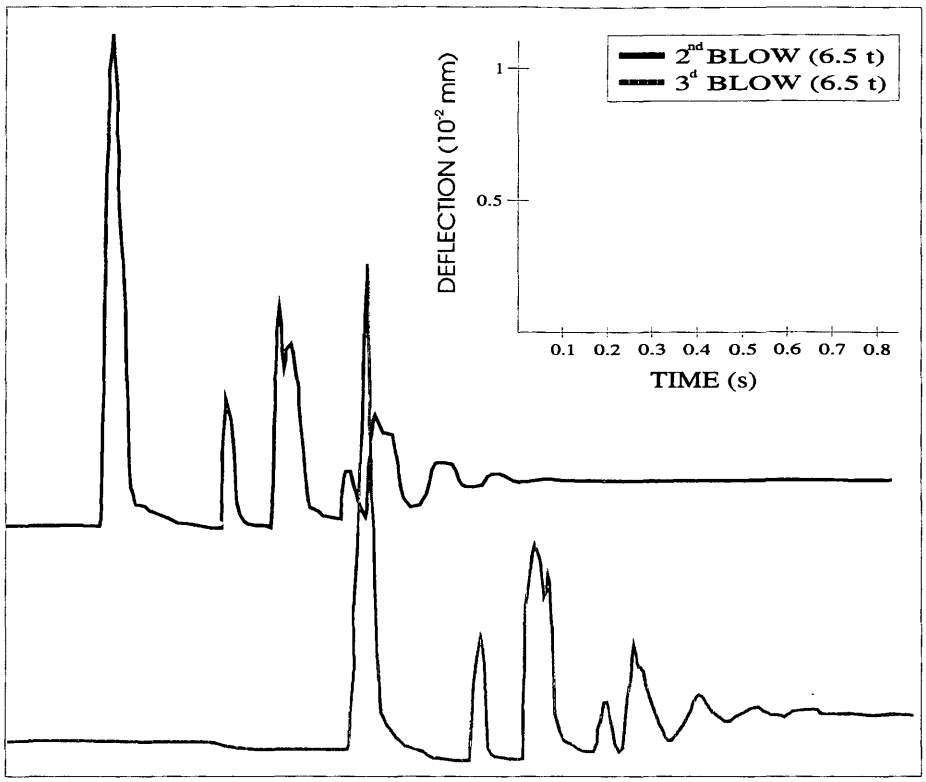

FIGURE 7 FWD deflection-time curve measured by the sensor.

TABLE 3 β Values

GENERAL DATA	
DATE	MARCH 1993
LOADS APPLIED	600,000
PAVEMENT TEMPERATURE	7 - 9°C

	2nd BLOW (6,5t)			3nd BLOW (6,5t)		
PAVEMENT	DI	SE	β	DI	SE	β
1	8.3	8.1	102	8.2	8.0	102
2	19.7	18.9	104	19.1	18.6	103
3	8.2	7.6	108	8.2	7.7	106
4	6.6	5.9	111	6.5	5.9	110
5	26.7	25.9	103	26.0	25.0	104
6	7.6	7.5	101	8.0	7.6	105
AVERAGE			105			105

DI = FWD Deflection (10^{-2} mm)
SE = Sensor Deflection (10^{-2} mm)
β = (DI/SE) x 100

TABLE 4 γ Results

GENERAL DATA	
DATE	FEBRUARY 1993
LOADS APLIED	550,000
PAVEMENT TEMPERATURE	6 - 8°C

PAVEMENT	BB	SE	γ
1	8	10.0	80
2	30	31.3	96
3	9	11.6	78
4	6	8.3	73
5	36	39.3	92
6	8	12.5	64
AVERAGE 1,3,4,6	7.8	10.6	74
AVERAGE 2,5	33	35.5	94

BB = BB Deflection (10^{-2} mm)
SE = Sensor Maximum Deflection (10^{-2} mm)
γ = (BB/SE) x 100

TABLE 5 α Versus ω

	TEMPERATURE * ≃ 15°C		TEMPERATURE * ≃ 10°C	
PAVEMENT	α	ω	α	ω
1	1.03	0.98	0.92	0.87
2	1.51	1.34	1.44	1.28

* = Pavement average temperature

$$\alpha = \frac{\text{BB Deflection (6,5t)}}{\text{FWD Deflection (6,5t)}}$$

$$\omega = \frac{\text{BB Deflection (6,5t)}}{\text{FWD Deflection (6,5t)}}$$

between the speed assigned to the FWD and the BB speed of 1 on semirigid pavements and 15 to 20 on flexible pavements.

Response times to the load, measured with the sensors located in the pavements and made with the BB, are approximately 15 sec for flexible pavements and 25 sec for semirigid types. In the case of measurements made with the FWD, 0.12 sec for both types of pavements. The ratio between the deflection response times of the two pieces of equipment is therefore 125 for flexible pavements and 210 for semirigid types. A comparison of these values with earlier ones, even taking into account possible errors in measurement, indicates that a consideration of speed and deformation is not enough to explain the difference between deflections measured with the two types of equipment, particularly in the case of semirigid pavements.

CONCLUSIONS

- The ratio between deflections measured with the BB and the FWD depends on the pavement temperature, the thickness of the asphalt layer, the pavement type, and the point in the lifetime of the pavement at which the measurements are made.
- Higher ratios are obtained with flexible pavements than with semirigid pavements. The ratio increases with temperature and thickness of the asphalt and decreases over the lifetime of the pavement.

TABLE 6 Deflections at Different Speeds (Test Track Vehicle; 7°C; 550,000 Load Applications)

	SPEED (km/h) (*)							
PAVEMENT	1.5	1.8	5.2	10	15	20	30	38
1	10.7	10.4	7.9	7.4	7.9	7.0	7.0	7.0
2	30.0	30.0	26.7	24.8	25.4	24.3	23.1	21.2
3	11.1	9.6	8.4	7.4	7.7	7.3	6.6	6.1
4	8.3	8.0	7.1	6.4	6.7	5.9	5.6	5.2
5	40.7	39.3	30.8	30.8	32.2	30.4	30.1	27.4
6	11.9	11.0	9.1	8.4	8.8	8.1	--	--

(*) Deflection in 10^{-2} mm

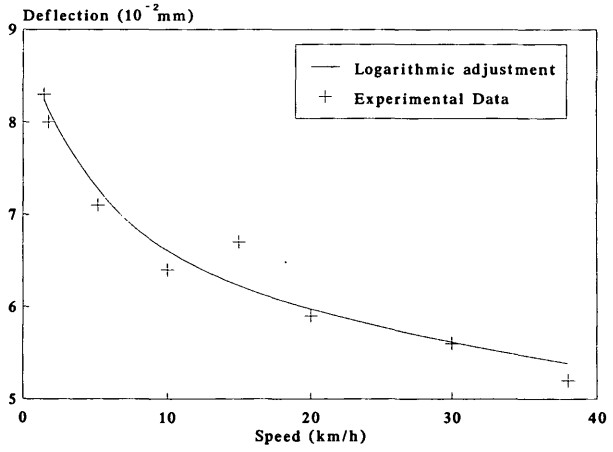

FIGURE 8 Deflection versus load speed (Pavement 4).

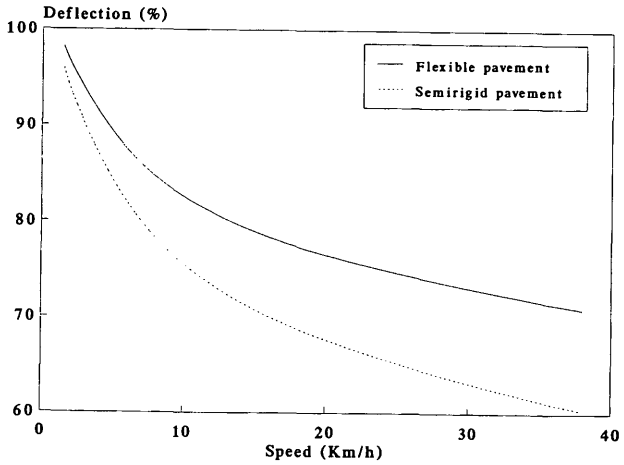

FIGURE 9 Deflection versus load speed in flexible and semirigid pavement (logarithmic adjustment).

- Compared with the deflectograph, the deflectometer is more reliable and consistent and more suitable for precision work such as that done on test tracks or for working with specific values such as those used in back calculation models.
- The deflectograph appears suitable for high-capacity work but could give rise to considerable error if specific values or characteristics are used, particularly with deflections of less than 20.10^{-2} mm.
- The FWD measures the same deflection as sensors embedded in the pavement. The BB, on the other hand, gives lower deflection measurements because its support legs are within the area of pavement deformation. The deviation is greater in the case of semirigid pavements (20 to 35 percent) than with flexible pavements (4 to 8 percent).
- Taking average values at a pavement temperature of 15°C, FWD deflection on sections tested should be increased by 50 percent (before corrections) or 35 percent (after corrections for deflection bowl and second set of wheels), in the case of flexible pavements, to obtain the deflection produced by the BB. Deflections produced by both instruments for semirigid pavements are practically the same.
- Decrease in deflection with an increase in speed of load application depends on the pavement type.
- On semirigid pavements tested between 1 and 40 km/hr, the deflection decreased between 35 and 45 percent. The rate of decrease was greater during the first 15 to 20 km/hr; it then became more gradual.
- For the flexible pavements tested, the decrease in deflection between 1 and 40 km/hr was around 30 percent, with the greatest decrease occurring up to 10 km/hr.
- Deformation bowl length decreased as load application speed increased. On the flexible pavements tested, deformation varied from 700 to 800 cm at 1 to 2 km/hr to 460 to 520 cm from 20 km/hr onward. On semirigid pavements, deformation values of 800 to 1,000 cm for low speeds and 600 to 700 cm at higher speeds were obtained.
- Different load application times between the FWD and the BB alone do not explain the differences obtained between the deflections produced by the two types of equipment, especially in semirigid pavements.

ACKNOWLEDGMENT

This study was financed by the Directorate General for Roads of the Spanish Ministry of Public Works, Transport and the Environment.

REFERENCES

1. Ruiz, A., and R. Romero. La Pista de Ensayo a Escala Real del Centro de Estudios de Carreteras del CEDEX. *Revista Carreteras*, Vol. 3, No. 29, May/June 1987.
2. Ruiz, A., and R. Romero. La Pista de Ensayo a Escala Real del Centro de Estudios de Carreteras, *Revista Ingeniería Civil*, No. 63, July/August 1987.
3. Aparicio, A., and R. Romero. La Base des Données du Manège de Fatigue du Centre d'Études des Routes, Colloque Route et Informatique, École Nationales des Ponts et Chaussées, Paris, France, March 13–15, 1990.
4. Ruiz, A., R. Romero, and A. Gonzalez. Analysis of Deflections on a Test Track. Presented at Symposium on Nondestructive Testing and Back Calculation for Pavements, Paper NDT-040, Nashville, Tenn. Aug. 1991.

Publication of this paper sponsored by Committee on Strength and Deformation Characteristics of Pavement Sections.

Determining Pavement Structural Number from FWD Testing

GUSTAV T. ROHDE

A structural number is used as an indicator of pavement strength in a number of pavement design and deterioration models. In determining the structural number of an existing pavement structure, traditional methods of laboratory testing have become expensive and are not always appropriate. The parameter preferably is obtained from nondestructive deflection testing. Currently two techniques to determine structural numbers from surface deflections have been suggested and documented by AASHTO. A powerful alternative procedure for determining a pavement's structural number from falling-weight deflectometer surface deflections is presented. The approach has been verified and compared with other available techniques on 62 in-service pavement sections. The method is rapid, does not need mechanistic analysis tools, and is highly suitable for characterizing pavement strength in pavement management systems.

Notwithstanding acceptance and widespread use of mechanistic principles in pavement analysis and design, several agencies worldwide are using empirically based design and performance models. The concept of structural number, first defined by the AASHO road test (*1*), is a convenient and an often used index of pavement strength. Although the adequacy of the index has been debated by a number of researchers (*2–4*), the index is currently embedded in design and deterioration modeling procedures of organizations such as AASHTO, the Transport and Road Research Laboratory (*5*), and the World Bank (*6*).

Traditionally the structural number of a pavement has been determined from its layer thicknesses and laboratory-determined material properties. The 1986 AASHTO guide design for pavement provides additional techniques to determine a pavement's structural number using nondestructive deflection testing. Both techniques proposed in the AASHTO guide cause problems in characterizing the structural strength for pavement management at the network level. In this paper an alternative approach is provided, developed, and discussed whereby a pavement's structural number can be determined from its total thickness and the shape of the measured surface deflection bowl. This approach, verified on 62 pavement structures, provides a powerful technique that does not require the process of backcalculation of layer moduli.

BACKGROUND

The concept of structural number was first defined in the AASHO road test (*1*):

$$SN = \sum_{i=1}^{n} a_i h_i \quad (1)$$

where

SN = structural number,
a_i = material and layer coefficient, and
h_i = layer thickness (in.).

In 1975 the Transport and Road Research Laboratory adopted the structural number as the index of pavement strength in the Kenya Road Transport Cost Study (*7*). However, in this study they included an additional variable, SN_{sg}, to account for variation in subgrade strength. The modified structural number, SNC, was defined as

$$SNC = \sum_{i=1}^{n} a_i h_i + SN_{sg} \quad (2)$$

where

SNC = modified structural number,
$SN_{sg} = 3.51 (\log CBR) - 0.85 (\log CBR)^2 - 1.43$, and
CBR = in situ California bearing ratio (percent).

The need for and rationale of modifying the structural number for subgrade effects was described by Hodges et al. (*7*):

> The most satisfactory way of taking into account the strength of the subgrade is to modify the measured structural number of the pavement so that it is equal to the structural number of a pavement of the same type which would behave in the same way but is built on a standard subgrade. To allow direct comparisons with the AASHO Road Test, the most convenient subgrade to use for this purpose is the subgrade of the AASHO road test itself.

The design charts of Road Note 31 were analyzed (*5*) to examine how the required structural number decreases as subgrade strength increases. The analysis resulted in the SN_{sg} term shown in Equation 2. In the Brazil/United Nations Development Program study (*8*), which followed the Kenya study, the structural number again was used as an index of pavement strength. During the study, an attempt was made to relate measured Benkelman beam deflections to the modified structural number as defined in Equation 2. It was found that the two parameters are not directly interchangeable, with a rather poor coefficient of determination (r^2 = 56 percent). Furthermore, it was established that the structural number was a better performance indicator than peak deflection. The structural number concept subsequently was adopted in the HDM-III pavement performance models (*9*). Because these models are promoted by the World Bank, they have been captured and used in several pavement management sytems in developing countries. The performance models use structural number as a

Van Wyk & Louw, Inc., P.O. Box 905, Pretoria, 0001, South Africa.

variable, so this parameter is required for an entire network consisting of various pavement types, layer thicknesses, and strengths, which is built on a wide variety of subgrades. The nature and speed of nondestructive deflection devices, such as the falling-weight deflectometer (FWD), ideally should be used to provide this parameter.

The 1986 AASHTO design guide documents two procedures for determining structural numbers from FWD deflections; the first technique involves the backcalculation of layer moduli, a field actively researched in recent years (*10*). Once the layer moduli are determined, they are related to layer coefficients using a procedure documented in Volume 2 of the AASHTO guide. Although the AASHTO procedure is the preferred approach, it requires exact knowledge of layer thicknesses, is time consuming, and relies heavily on backcalculation expertise. A second approach uses outer deflection sensors to determine subgrade stiffness and then applies the peak deflection, D_o, to determine the pavement's structural number. The formulation documented in the AASHTO guide was modified by Ioannides (*4*) in 1990. He suggested the following relationship:

$$D_o = \frac{1.5P}{\pi a}\left\{\frac{(0.0045h)^3}{SN^3}\left[1 - \frac{1}{(1 + (h/a)^2)^{1/2}}\right] + \frac{1}{E_s\left(1 + \frac{40000SN^2}{a^2E_s^{2/3}}\right)^{1/2}}\right\} \quad (3)$$

where

D_o = peak FWD deflection,
P = FWD load (lb),
h = pavement layer thickness (in.),
a = load radius,
E_s = subgrade modulus (psi), and
SN = structural number from Equation 1.

The problem with this approach in practice is that it is founded on Burmister's two-layer model in which the subgrade is assumed to be an infinitely thick linear-elastic material. Real pavements are founded on stress-sensitive subgrades that are often underlain by stiff layers or even bedrock. If Burmister's formulation is used, the subgrade stiffness is overpredicted, resulting in incorrect structural numbers.

DETERMINING *SN* FROM FWD DEFLECTIONS

The peak deflection measured below an FWD is a combination of deflection in the subgrade and the elastic compression of the pavement structure. In 1983 Irwin (*11*) suggested a general rule of thumb, the "two-thirds rule," which explains the stress distribution and origin of deflections found below an FWD. The rule is based on the fact that approximately 95 percent of the deflections measured on the surface of a pavement originate below a line deviating 34 degrees from horizontal (see Figure 1). With this simplification, it can be assumed that the surface deflection measured at an offset of 1.5 times the pavement thickness originates entirely in the subgrade. By comparing this deflection with the peak deflection, an index associated with the magnitude of deformation that occurs within the pavement structure can be defined:

$$SIP = D_o - D_{1.5Hp} \quad (4)$$

where

SIP = structural index of pavement (Figure 1),
D_o = peak deflection measured under a standard 40-kN (9,000-lb) FWD load,
$D_{1.5Hp}$ = surface deflection measured at offset of 1.5 times Hp under standard 40-kN (9,000-lb) FWD impulse load, and
Hp = total pavement thickness.

It is hypothesized that the index SIP should be strongly correlated with the stiffness of the pavement structure and subsequently with its structural number. To investigate this hypothesis and to develop a relationship between FWD-measured surface deflections and a pavement's structural number, a large number of pavements were analyzed using layered-elastic theory. A total of 7,776 pavement structures with a wide range of stiffness-thickness combinations was used. Properties of the analyzed pavements are presented in Table 1. For each of the pavement structures, the structural number was calculated using AASHTO guidelines:

$$SN = \sum_{i=1}^{n} h_i a_g \left(\frac{E_i}{E_g}\right)^{1/3} \quad (5)$$

where

a_g = layer coefficients of standard materials (AASHO road test),
E_g = resilient modulus of standard materials (AASHO road test),
h_i = layer thickness (in.), and
SN = structural number (units of h_i).

The best relationship was found after including the total pavement thickness in the analysis. A relationship of the following format was selected:

$$SN = k_1 SIP^{k2} Hp^{k3} \quad (6)$$

where

SN = structural number (in.), as used in HDM-III;
SIP = structural index of pavement (μm);
Hp = total pavement thickness (mm); and
$k1$, $k2$, $k3$ = coefficients as listed in Table 2.

Figure 2 illustrates the good correlation between the structural numbers determined by using Equation 6 on the data base of 7,776 pavement structures. However, it should be kept in mind that this relationship is purely theoretical and is founded on layer elastic theory. As described by Ullidtz (*12*):

> It is important to realize that layer elastic theory is only a rather poor approximation to the extremely complex conditions of real pavement structures. Most pavement materials will show viscous, visco-elastic and/or plastic deformations under stress, in addition to elastic deformations. Pavement materials are often inhomogeneous, anisotropic and have non-linear stress-strain (or stress-strain rate) relations. Many materials are even particulate, i.e., consisting of discrete particles.

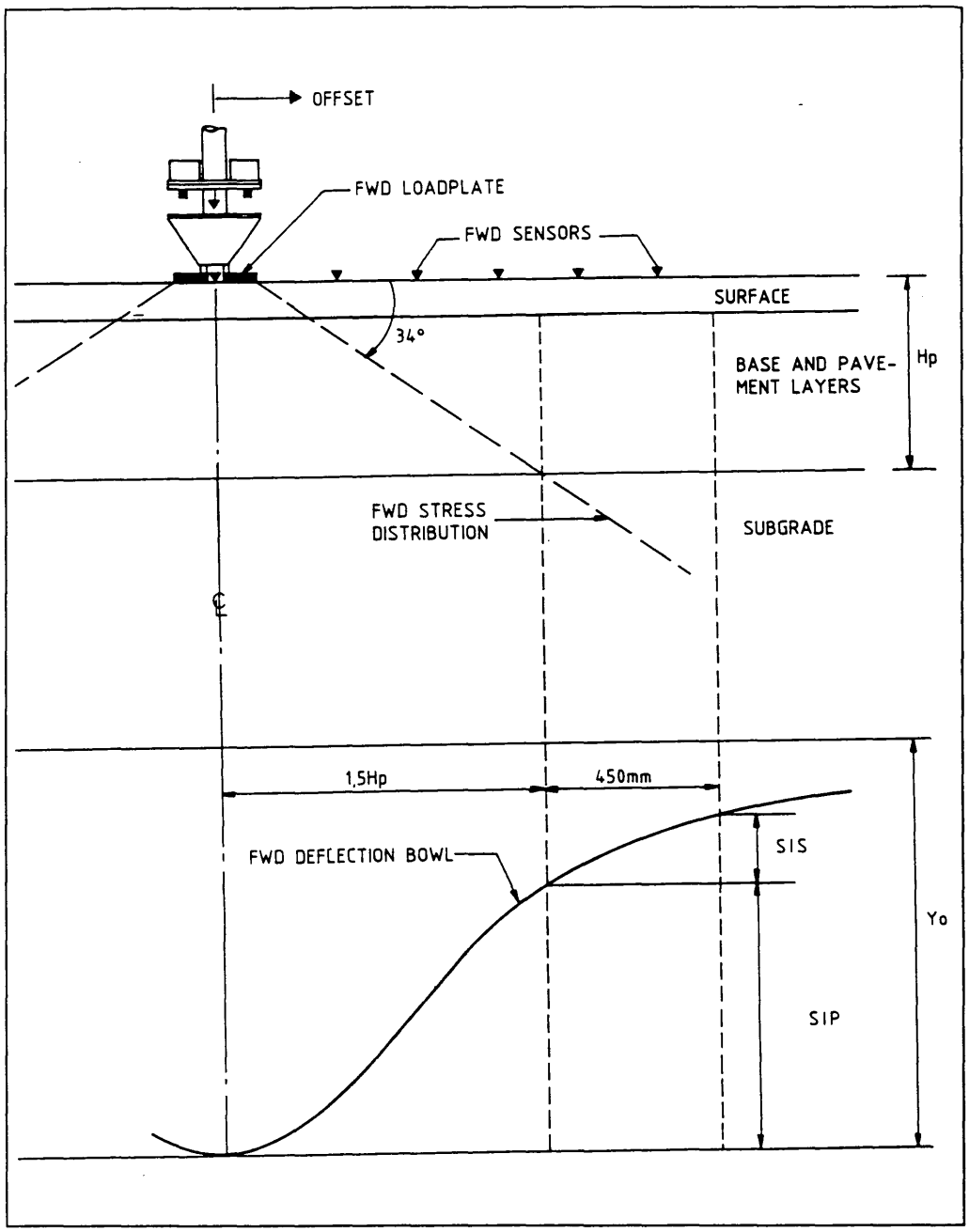

FIGURE 1 Stress distribution and measured deflection bowl beneath FWD load.

TABLE 1 Layer Moduli and Thicknesses Used To Develop *SN* Versus *SIP* Relationship

Layer	Moduli (MPa)	Thicknesses (mm)
Surface	1500, 3000, 5000	20, 50, 100, 200
Base	400, 700, 1000	150, 300
Subbase	150, 300, 500	0, 150, 300
Subgrade	50, 75, 100, 200	1500, 3000, 5000

Total Number of Combinations : 3x3x3x4x4x2x3x3 = 7776

TABLE 2 Coefficients for *SN* Versus *SIP* Relationships (Equation 6)

Surface Type	*k1*	*k2*	*k3*	r²*	n**
Surface Seals	0,1165	-0,3248	0,8241	0,984	1944
Asphalt Concrete	0,4728	-0,4810	0,7581	0,957	5832

* Coefficient of Determination
** Sample Size

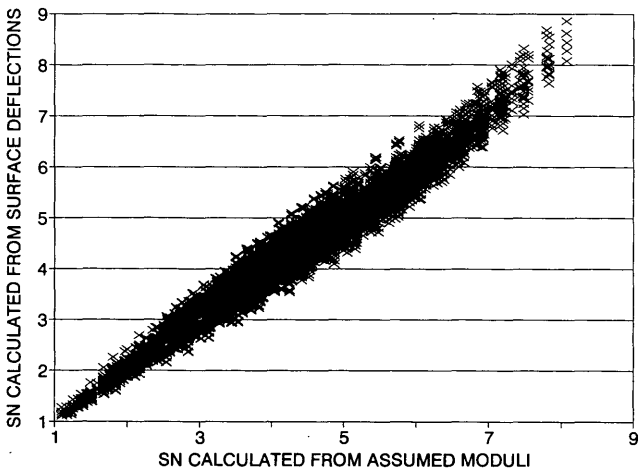

FIGURE 2 Correlation of structural numbers using Equation 6.

Discontinuities, like edges, joints or cracks, are often present, and the conditions at the interfaces (rough or smooth) are not well known.

To evaluate the effectiveness of the above theoretically based relationships on actual pavements, a detailed investigation was carried out on some 62 in-service pavements. The findings are described later in this paper.

The same rationale used to determine *SN* from surface deflections can be used to obtain the subgrade stiffness. It is argued that the weakest part of the subgrade, say the top 300 mm (1 ft), should be used for performance prediction purposes. Irwin's "two-thirds rule" (*11*) again can be used to define an index representing the subgrade strength. For this purpose a structural index for the subgrade (*SIS*) has been defined:

$$SIS = D_{1.5Hp} - D_s \tag{7}$$

where *SIS* equals the structural index of the subgrade (Figure 1) and D_s equals the surface deflection measured at an offset of ($1.5Hp$ + 450 mm).

SIS and total pavement thickness were subsequently related to the subgrade stiffness using the following relationship:

$$E_{sg} = 10^{k4} SIS^{k5} Hp^{k6} \tag{8}$$

where E_{sg} equals the subgrade stiffness in megapascals, and *k*4, *k*5, and *k*6 are coefficients as listed in Table 3.

The approach to determine the structural number of a pavement from surface deflections can be summarized in the following steps:

1. Normalize measured FWD deflections to standard 40-kN (9,000-lb) load deflections.
2. Determine the deflection at an offset of $1.5Hp$. This will require interpolation among deflections measured at the fixed sensor positions. For this purpose, the following relationship can easily be programmed:

$$D_X = \frac{(R_X - R_B)(R_X - R_C)}{(R_A - R_B)(R_A - R_C)} D_A + \frac{(R_X - R_A)(R_X - R_C)}{(R_B - R_A)(R_B - R_C)} D_B + \frac{(R_X - R_A)(R_X - R_B)}{(R_C - R_A)(R_C - R_B)} D_C \tag{9}$$

where

D_X = deflection at offset of R_X;
D_i = deflection at Sensor i;
R_i = offset of Sensor i;
i = A, B, C being three closest sensors to Point X; and
X = point for which deflection is determined.

3. Use Equations 4 and 6 to determine the pavement structural number. It should be noted that the calculated structural number is relevant for the prevailing temperature and moisture conditions at the time of deflection testing. To determine the structural number at a standard temperature, the peak deflection, Y_o, should be corrected to an equivalent peak deflection at the reference temperature. For this purpose, the correction factors proposed by AASHTO (Figure 3) should be used before Equation 4. For pavements with thin asphalt surfaces, no temperature correction is required.

TABLE 3 Coefficients for *E* Versus *SIS* Relationship (Equation 8)

Total Pavement Thickness	*k4*	*k5*	*k6*	r²	n
Hp ≤ 380mm	9,138	-1,236	-1,903	0,862	2592
380 mm < *Hp* ≤ 525mm	8,756	-1,213	-1,780	0,810	2592
525 mm < *Hp*	10,655	-1,254	-2,453	0,809	2592

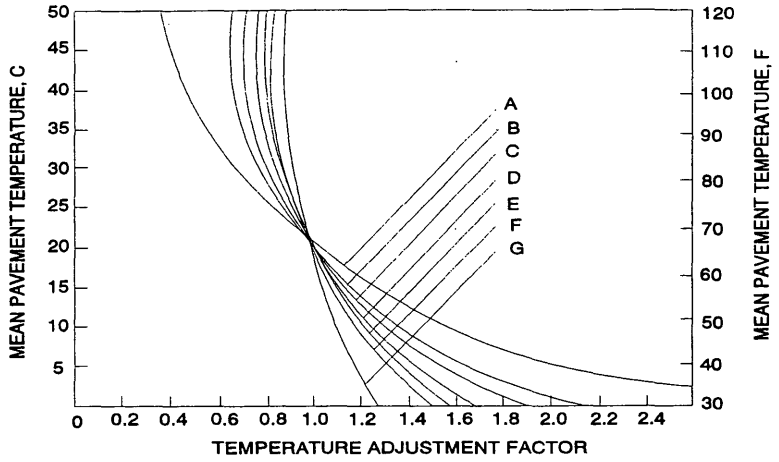

FIGURE 3 Temperature correction factors for peak measured deflections (AASHTO).

To determine the SN_{sg} for use in HDM-III model the following additional steps are required:

1. Determine D_s through interpolation (Equation 9),
2. Calculate *SIS* using Equation 7 and E_{sg} using Equation 8, and
3. Relate the subgrade modulus to equivalent CBR using a relationship such as that suggested by Emery (*13*):

$$E_{sg} = 30.79CBR^{0.44} \quad (10)$$

where E_{sg} equals the subgrade modulus in megapascals.

4. Calculate SN_{sg} and *SNC* using Equation 2.

VERIFICATIONS

To evaluate the developed relationships, a detailed study was carried out on 52 in-service pavement structures. The test sections were selected specifically to cover a wide range of pavements with various ages, present conditions, pavement compositions, and subgrade conditions. A detailed visual condition assessment and FWD deflection testing were done on each test section. The information was analyzed statistically to select one representative test position within each section. Dynamic cone penetration (DCP) testing was done at this position, after which a test hole was dug to measure the actual layer thicknesses. Four methods were used to calculate the structural number from the information for each of the test positions.

Model A (Backcalculated Moduli, AASHTO NDT Method 1)

Method A involves the mechanistic analysis of measured deflections using two backcalculation programs: MODULUS (*14*) and ELMOD (*12*). The layer moduli are translated to layer coefficients using Equation 5. The determined layer coefficients and recorded layer thicknesses are then used to determine the structural number.

Method B (DCP Analysis)

Method B involves the analysis of the DCP results. First, the penetration rate through each granular pavement layer is used to determine the layer's in situ CBR by using the following relationship (*15*):

$$CBR = 410 \log DN^{-1.27} \quad (DN>2 \text{ mm/blow})$$

$$CBR = 66.66DN^2 - 330DN + 563 \quad (DN \leq 2 \text{ mm/blow}) \quad (11)$$

where *CBR* is the in situ California bearing ratio (percent) and *DN* is the penetration rate of DCP (mm/blow).

CBRs were translated into layer coefficients using a relationship suggested by Patterson (*8*) and originally proposed by Chastain and Schwartz (*16*):

$$a_i = 29.14CBR - 0.1977CBR^2 + 0.00645CBR^3 \quad (12)$$

where a_i is the layer coefficient for use in Equation 1 or 2. For the surface layers, a coefficient was assumed based on the visual condition.

Method C (AASHTO NDT Method II)

Method C is the second approach suggested in the AASHTO pavement design guide and involves purely the surface deflections. Outer sensors are used to determine the subgrade stiffness, after which Equation 3 is used to determine the pavement's structural number.

Method D (from the Shape of the Deflection Bowl)

Method D involves the use of the surface deflections only and the total layer thickness described earlier. For each pavement section the parameter *SIP* is determined using Equation 4. Parameter *SIP* and the total layer thickness H_p are then used to determine the structural number (Equation 6).

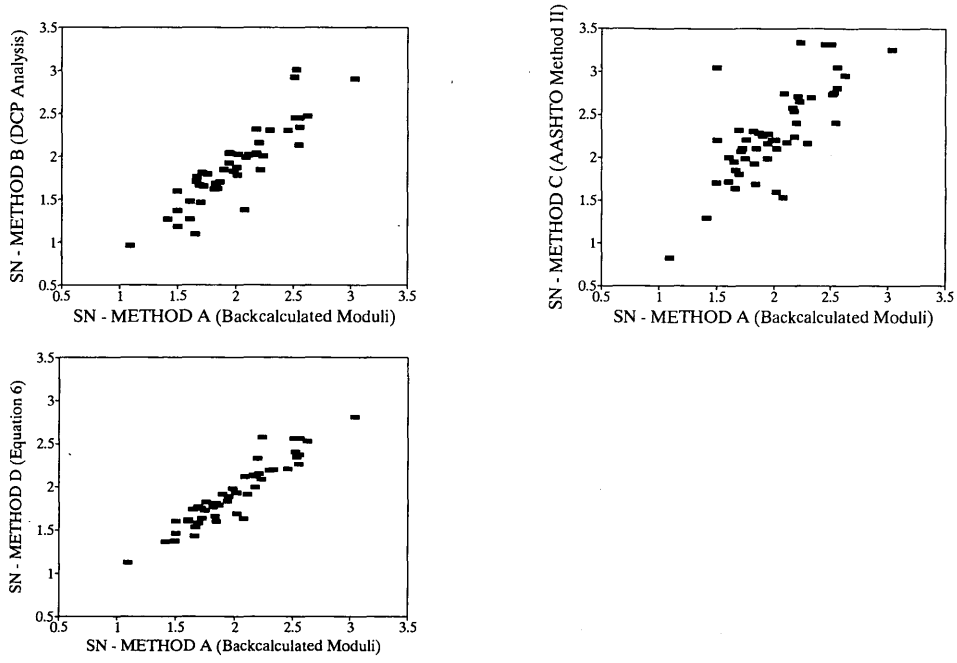

FIGURE 4 Comparison of results from four methods of analysis.

Results obtained from the four approaches are compared in Figure 4. The correlation coefficients calculated between the various methods on the 52 sections are given in Table 4. It is evident that the approach developed in this paper (Method D) leads to predicted structural numbers similar to those obtained when incorporating backcalculation techniques (Method A). As given in Table 4, a correlation of 0.928 was obtained between these two techniques.

The structural numbers obtained from the DCP analysis compare less favorably with the other techniques. The poor correlation is not surprising because the penetration test is a function of each layer's shear strength, whereas the measured deflection is a function of the elastic response of the entire layered system. The results from Method C, the second AASHTO method, correlate poorly with all the other techniques. This is probably because it takes no account of nonlinear elastic behavior of the subgrade or the presence of rigid layers below the subgrade. Both MODULUS (*14*) and ELMOD (*12*) do account for these factors. Through the inclusion of a rigid layer in the data base used to develop Equation 6, the presence of rigid layers below the subgrade has been accounted for also. Recent investigations (*17*) indicate that these factors should be accounted for in order to lead to realistic pavement modelling.

Although the procedure offers a rapid and effective method of determining structural numbers, issues such as seasonal variations should not be overlooked. Seasonal variations in the structural number can be obtained by measuring the deflections in various seasons and applying the above techniques. Pavement sections used in the verification process all consisted of relatively thin pavements with structural numbers of less than 3.5. The procedure was subsequently tested on a large data base of deflections collected on 10 in-service test pavement sections in Texas (Table 5).

On each pavement section, FWD deflections were measured monthly, in both the morning and the afternoon. For this study, deflections collected at two positions per test site were analyzed. Figure 5 compares structural numbers determined through backcalculation (Method A described above) and those obtained using Equation 6. The overall coefficient of determination for 436 tests

TABLE 4 Linear Correlations Between Parameters Calculated on 52 Pavement Sections

	Method A	Method B	Method C	Method D	*Do*	*SIP*	*Hp*
SN Method A	1.000	0.668	0.742	0.928	-0.320	-0.057	0.829
SN Method B	0.668	1.000	0.560	0.684	-0.355	-0.083	0.615
SN Method C	0.742	0.560	1.000	0.841	-0.374	-0.127	0.730
SN Method D	0.928	0.684	0.841	1.000	-0.383	-0.083	0.882
D_o	-0.320	-0.355	-0,374	-0,383	1.000	0.908	0.345
SIP	-0.057	-0.083	-0.127	-0.083	0.908	1.000	0.364
Hp	0.829	0.615	0.730	0.882	0.345	0.364	1.000

Method A - Through Backcalculation of Layer Moduli (AASHTO NDT Method I)
Method B - From DCP Results
Method C - AASHTO NDT Method II
Method D - Procedure developed in this paper

TABLE 5 Texas Test Sections Used in Evaluation of Method To Determine Structural Numbers of FWD Testing

Site	Position (Road, Milepost)		Surface (mm)	Thickness Base (mm)	Subgrade	Comparison between Methods A and D	
						r^{2*}	n^{**}
1	US 77	MP 4.1	165	150	Sand	0.94	50
2	SH 186	MP 33.2	25	223	Sand	0.91	50
4	FM 1425	MP 5	100	125	Clay	0.91	32
5	FM 1425	MP 3	150	150	Sand	0.93	46
6	FM 491	MP 6.1	30	200	Clay	0.58	30
7	IH 20	MP 293	250	280	Clay	0.96	32
8	IH 20	MP 273.6	200	330	Clay	0.96	44
9	FM 1235	MP 21	25	200	Clay	0.87	44
11	IH 20	MP 216	125	450	Sand	0.76	50
12	FM 1983	MP 1.0	25	200	Sand	0.81	580
All						0.98	4.36

* Coefficient of Determination
** Sample Size

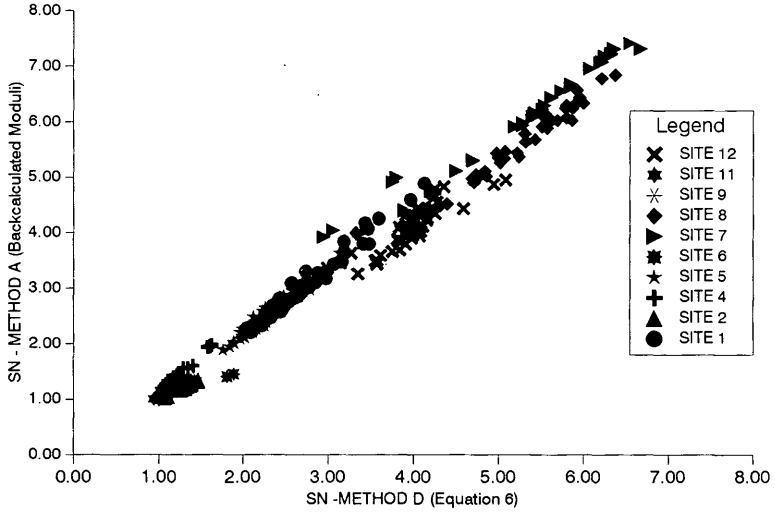

FIGURE 5 Comparison of structural numbers obtained by Method A and those obtained using Equation 6.

on the 10 sections is 98.6 percent. Results per test section are given in Table 5.

CONCLUSION

This paper describes the development of an effective method for calculating a pavement's structural number from FWD deflections. Through a detailed analysis of data collected on 52 in-service pavement structures in Africa and 10 sections in Texas, the authors determined that the developed procedure gives results similar to those obtained using backcalculation techniques, such as AASHTO NDT Method I. It also was shown that AASHTO NDT Method II provided disappointing results because it does not account for shallow rigid layers or stress-sensitive subgrades, a phenomenon commonly found in Sub-Saharan Africa.

REFERENCES

1. *Special Report 61E: The AASHO Road Test.* HRB, National Research Council, Washington, D.C., 1962.
2. Gomez, M., and M. R. Thompson. *Structural Coefficients and Thickness Equivalency Ratios.* Illinois Cooperative Highway Research Program Series 202. University of Illinois, Urbana, June 1983.
3. Coffman, B. S., G. Ilves, and W. Edwards. Theoretical Asphaltic Concrete Equivalences. In *Highway Research Record 239*, HRB, National Research Council, Washington, D.C., 1968, pp. 95–119.
4. Ioannides, A. M. Theoretical Implications of the AASHTO 1986 Nondestructive Testing Method 2 for Pavement Evaluation. In *Transpor-*

tation Research Record 1307, TRB, National Research Council, Washington, D.C., 1991, pp. 211–220.
5. *Guide to the Structural Design of Bitumen-Surfaced Road in Tropical and Sub-tropical Countries*. Road Note 31. U.K. Transport and Road Research Laboratory, Crowthorne, England, 1977.
6. Watanatada, T., C. G. Harral, W. D. O. Paterson, A. M. Dhareshwar, A. Bhandari, and K. Tsunokawa. *The Highway Design and Maintenance Standards Model* (Vols. 1 and 2). Highway Design and Maintenance Standards Series. Johns Hopkins University Press, Baltimore, Md., 1987.
7. Hodges, J. W., J. Rolt, and T. E. Jones. *The Kenya Road Transport Cost Study: Research on Road Deterioration*. TRRL Laboratory Report 673. U.K. Transport and Road Research Laboratory, Crowthorne, England, 1975.
8. Geipot. *Research on the Interrelationships between Costs of Highway Construction, Maintenance and Utilization (PICR)*. Final Report, 12 volumes. Empresa Brasileira de Planejamento de Transportes (GEIPOT), Ministry of Transport, Brasilia, Brazil, 1982.
9. Patterson, W. D. O. *The Highway Design and Maintenance Standards Model*, Vol. III (HDM-III). "Road Deterioration and Maintenance Effects: Models for Planning and Management." Transportation Department, World Bank, Washington, D.C., 1987.
10. Lytton, R. L. Backcalculation of Pavement Layer Properties. In *Nondestructive Testing of Pavements and Backcalculation of Moduli*, STP 1026, ASTM, Philadelphia, Pa., 1989, pp. 7–38.
11. Irwin, L. H. *User's Guide to MODCOMP2, Version 2.1*. Local Roads Program, Cornell University, Ithaca, N.Y., 1983.
12. Ullitdz, P. *Pavement Analysis*. Elsevier, New York, 1987.
13. Emery, S. J. *Prediction of Moisture Content for Use in Pavement Design*. Ph.D. dissertation. University of the Witwatersrand, Johannesburg, South Africa, 1985.
14. Rohde, G. T., and T. Scullion. *Improvements to the MODULUS Program*. Research Report 1123-3F. Texas Transportation Institute, College Station, 1990.
15. Kleyn, E. G., and P. F. Savage. The Application of the Pavement DCP to Determine the Bearing Properties and Performance of Road Pavements. *Proc., International Symposium on Bearing Capacity of Roads and Airfields*, Trondheim, Norway, 1982.
16. Chastain, W. E., and D. R. Schwartz. AASHO Road Test Equations Applied to the Design of Bituminous Pavements in Illinois. In *Highway Research Record 90*. HRB, National Research Council, Washington, D.C., 1965, pp. 3–25.
17. Rohde, G. T., R. E. Smith, and T. Scullion. Pavement Deflections on Sections Where the Subgrade Varies in Stiffness with Depth. *Proc., 7th International Conference on Asphalt Pavements*, Nottingham, England, 1992.

Publication of this paper sponsored by Committee on Strength and Deformation Characteristics of Pavement Sections.

Modeling of Pavement Response Under Superheavy Loads

F. J. JOOSTE AND E. G. FERNANDO

An analysis of pavement response under multiple-axle, superheavy-load vehicles is presented. Pavement displacements under superheavy loads were measured using multidepth deflectometers. A procedure for data acquisition and modeling of the pavement structure and multiple-axle wheel loads is described. Pavement response is calculated using multilayer elastic theory, and the measured and calculated results are compared. It was found that layered elastic theory can provide a fairly accurate estimate of pavement displacements under expected superheavy loads, provided that the wheel load magnitudes are known.

The Texas Department of Transportation (TxDOT) has been issuing permits for the movement of superheavy loads on an ever-increasing basis. TxDOT defines gross vehicle weights in excess of 1114 kN (250 kips) as superheavy loads. Superheavy loads in excess of 8909 kN (2,000 kips) have been moved. The effects of superheavy loads on pavements are not well established. To address that problem, TxDOT funded a research project to study the movement of superheavy loads over the state's highway system. The objective of the study was to develop a procedure to evaluate the potential for pavement damage on a proposed superheavy-load route and to determine the need for temporary strenthening measures to minimize or prevent pavement damage.

In this paper the methodology for pavement structural capacity evaluation and modeling of pavement response under superheavy loads is described. The methodology includes field data acquisition for evaluation of pavement structural capacity, as well as modeling of pavements and superheavy loads to analyze stresses and strains and determine the potential for pavement damage. The methodology described is meant to serve as a first-stage procedure only; it is likely to be improved upon as research progresses. Application of the methodology and the results obtained with it are illustrated with a case study.

DATA ACQUISITION AND PAVEMENT MODELING

One of the aims of the research project is to formulate a procedure for the routine evaluation of pavement structural capacity to be implemented on routes on which superheavy-load movements are planned. The modeling of the pavement response under a simulated load plays an important part in this process. The procedure that is being developed for the purposes of this study uses the most modern nondestructive testing methods available to TxDOT. This procedure is expected to have a tiered structure with varying levels of complexity depending on the magnitude of the superheavy load and the importance of the superheavy-load route. A proposed scheme for the route evaluation is presented in the following.

The nondestructive testing procedure is based on falling-weight deflectometer (FWD) measurements. For flexible pavements, FWD measurements are analyzed using backcalculation of pavement properties (*1,2*). The MODULUS backcalculation program (*3*) is used for routine backcalculation purposes. It is recognized that the nonlinear load response of unbound pavement materials has to be accounted for in any pavement model. Therefore, FWD measurements are taken at load levels that are comparable with the wheel loads expected to be applied by the superheavy-load vehicles.

Extensive use is made of ground-penetrating radar (GPR) to provide for the nondestructive determination of layer thicknesses and to identify weak or wet spots within a given route (*4,5*). A video log is taken of the roadway in conjunction with GPR measurements to assist in the interpretation of the radar data and to document roadway features such as curves and turns, as well as potential obstructions such as traffic signs and signals. GPR measurements are verified by taking cores as needed. Dynamic cone penetrometer (DCP) measurements are used to assist in the determination of pavement layer properties (*6*).

The frequency of GPR and FWD measurements is generally dictated by the length of the pavement being evaluated. Typically, GPR measurements are taken at 3-m (10-ft) intervals, whereas FWD measurements are taken at 800-m (0.5-mi) intervals. Pavement analysis consists of two phases. First, subsections having similar construction types and layer thicknesses are identified. The subsectioning is done using a computerized procedure that is based on the GPR predicted layer thicknesses (*7*). The second part of the analysis consists of modeling the pavement structure in order to calculate stresses and strains under the expected loading conditions. Backcalculated layer properties are verified as needed by further testing the cores as well as considering DCP measurements.

In addition to measurements for structural evaluation purposes, a condition survey is done using TxDOT's automatic road analyzer (ARAN) unit (*8*), which provides measurements of rut depth and present serviceability along the proposed superheavy-load route. Also, the presence of surface cracking is established by viewing the video of the pavement surface taken with the ARAN. The condition survey is done before and after the superheavy-load moves.

CASE STUDY

Two superheavy-load moves took place in Victoria, Texas, during December 1992 that were monitored by the Texas Transportation

Texas Transportation Institute, Texas A&M University, College Station, Tex. 77843.

Institute. Both loads were structural components of an offshore pipe layer. The heavier of the two loads, the "tower," was transported on a self-propelled multiple-axle trailer that consisted of three units, each having six lines. As used by superheavy-load haulers, a line denotes a row of two axles on the trailer unit, with each axle having two tires. The second, lighter load, the "base support," was transported by means of a tractor-trailer combination. Gross vehicle weights of the tower and the base support were 2380 kN (534.3 kips) and 1131 kN (254 kips), respectively.

The route along which the loads were moved consisted of three sections. The total length of the route was 19.8 km (12.4 mi). Figure 1 presents typical results of the GPR layer thickness predictions together with a comparison of measured core thicknesses. FWD measurements were taken at 800-m intervals. A number of cores were taken on each pavement section, and DCP measurements were taken inside selected core holes.

MODELING OF LOAD AND PAVEMENT RESPONSE

One of the most important instruments used for modeling pavement response under multiaxle loads is the multidepth deflectometer (MDD). The MDD uses linear variable differential transducers to measure in situ pavement displacements (*9,10*). An MDD was installed along one of the sections of the superheavy-load route. The site of the MDD installation was that which FWD and GPR measurements determined to be the weakest part of the route. MDD sensors were installed at three different depths, that is, 95, 340, and 635 mm (3.7, 13.3 and 25 in.). The arrangement allowed displacements to be measured in each of the three layers of the pavement system. Figure 2 presents a schematic representation of the MDD installation. MDD measurements allowed pavement response to be measured under various loads, including the two superheavy loads. The principal reason for using MDD measurements was to help establish a model for predicting pavement response. By comparing the measured displacements with the predicted displacements from theory, a verification of the pavement model could be made before an evaluation of stresses and strains for damage assessment was undertaken.

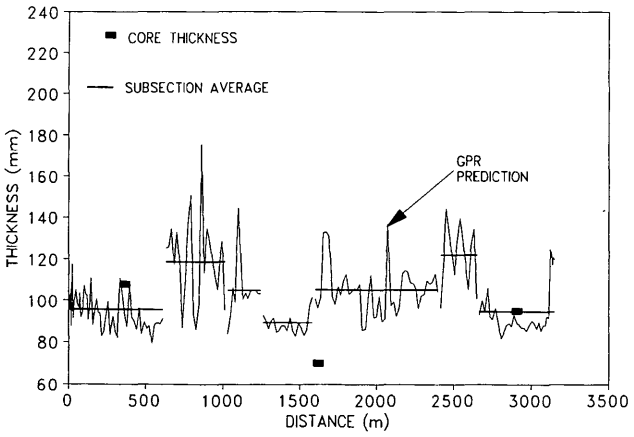

FIGURE 1 GPR measurements on FM 1432, Victoria, Texas (1 mm = 0.04 in., 1 m = 3.29 ft).

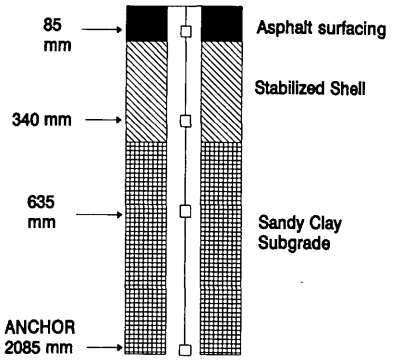

FIGURE 2 MDD installation on FM 1432, Victoria, Texas (1 in. = 25.4 mm).

During the superheavy load moves in Victoria, Texas, FWD measurements were taken at a 229-mm (9-in) offset from the MDD installation point, to allow for measurement of the MDD anchor movement. The movement of the rod was monitored by coupling the MDD anchor rod to the seventh sensor of the FWD. Backcalculations that were subsequently made using the FWD measurements provided estimates of the pavement layer stiffnesses in the area of the MDD installation. The backcalculated-pavement structure is summarized in Table 1. The pavement structure shown in Table 1 was used in all subsequent modeling of the pavement response under simulated loading conditions.

FWD measurements were made close to the time the superheavy load would move. In practice, there is a time window within which a route evaluation must be completed so that a permit will be issued within a reasonable time before the scheduled date of the superheavy-load move. Thus, differences in environmental conditions existing at the time of testing and the projected conditions at the time of the move must be considered in the evaluation.

MDD displacements measured under the FWD load are indicated in Figure 3. The applied FWD load was used as input in the WESLEA program (*11*) to simulate the pavement response under FWD loading. A comparison of the measured and calculated displacements is presented in Figure 4, showing an acceptable correlation between the measured and calculated displacements for the uppermost sensors. In the case of the third (lowest) sensor, however, calculated and measured displacements reflect poor agreement. Note that the low displacement measured on the bottom sensor is somewhat unusual. Typically, third sensor readings are much closer to the top and second sensor readings, as was seen earlier (*10*). There are two possible explanations for the present observation:

1. The third sensor may be founded on a stiff subgrade, whereas there may be a soft interlayer between the third sensor and the two sensors closer to the surface.
2. The low displacement may be the result of an electrical or mechanical problem, such as slipping.

The first of these possibilities was tested by trying to recalculate the layer moduli with the inclusion of a soft interlayer in the pavement system. However, no feasible solution could be obtained with this arrangement. This observation was supported by the

TABLE 1 Backcalculated Pavement Structure Used in Load and Pavement Modeling

Layer Description	Thickness (mm)	Backcalculated Moduli (MPa)
Asphalt Surfacing	107	2,645
Stab. Shell Base	305	69.0
Subgrade	1054	23.4
Stiff Layer	semi-infinite	69,000

(Note: 1 mm = 0.04 in, 1 MPa = 0.14 ksi)

DCP measurements, which indicated that the subgrade was soft, with no apparent sublayering. On the basis of these results, it was concluded that the third sensor was suspect and was subsequently not used in the modeling of pavement response.

The modeling of multiaxle superheavy-load vehicles consisted of two phases. First, a sensitivity analysis was conducted in order to establish how the multiple wheels of the superheavy-load vehicle should be modeled. Second, the actual modeling of the superheavy loads was done, and a comparison of the calculated and measured displacements was made. A sensitivity analysis was conducted through repeated runs of the BISAR linear-elastic layered computer program (*12*). As part of a sensitivity analysis, stresses, strains, and displacements were calculated at various offsets from the applied load, thereby establishing the zone of influence of the load for different pavement structures. Results of the sensitivity analysis are published elsewhere (*13*) and are not detailed here. The sensitivity analysis showed that only about 5 percent of the maximum displacement is calculated at distances greater than 2.74 m (9 ft) from the load. That would seem to indicate that, for the purposes of modeling multiple wheel loads, all loads falling within a radius of approximately 2.74 to 3.05 m (9 to 10 ft) from the point where stresses and strains are to be evaluated should be included in the analysis.

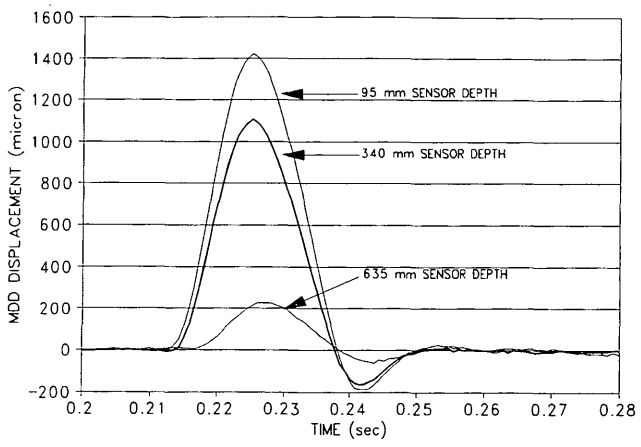

FIGURE 3 MDD response under FWD loading (1 μm = 0.04 mil).

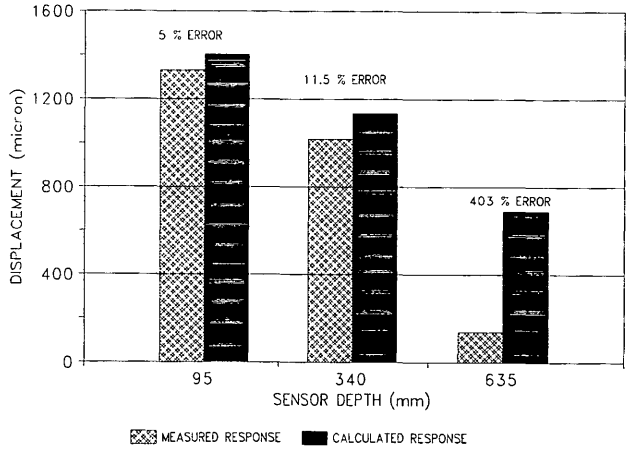

FIGURE 4 Measured versus calculated MDD response (1 μm = 0.04 mil).

MODELING OF PAVEMENT RESPONSE UNDER TOWER

The MDD response measured under the tower is illustrated in Figure 5. The positions of the peaks and troughs of the waveform represent the displacements measured under and between the axles, respectively. It should be noted that the movement of the anchor could not be measured under the superheavy load and was not taken into account in this figure. However, the error from this is expected to be relatively small, because the anchor movement measured under the dynamic FWD loading was only 6 percent of the peak MDD displacement (i.e., that of the MDD sensor).

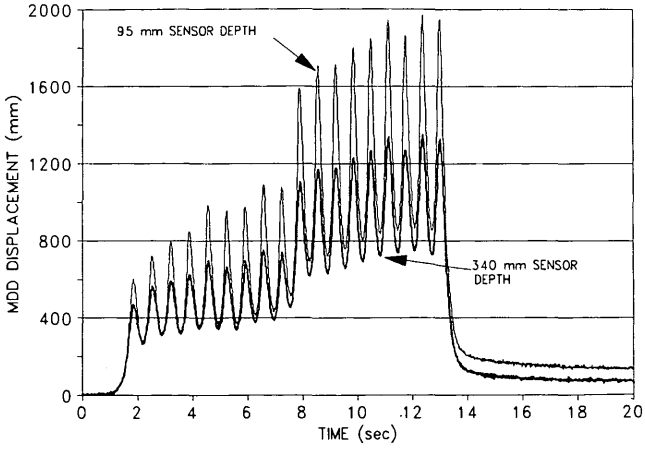

FIGURE 5 MDD response under tower (1 μm = 0.04 mil).

Figure 5 clearly indicates that there are two distinct phases in the pavement response. Displacements measured under the first nine lines are substantially lower than those measured under the last nine lines. A possible explanation for this observation may be an uneven distribution of the load. As a first attempt at modeling this load, the gross vehicle weight was divided by the total number of wheels to obtain the average load per wheel. The load model was set up to resemble the line and wheel spacing of the transport vehicle. By varying the position at which the pavement response was calculated, the effect of a moving load could be simulated. A video taken during the move showed that for the first five lines of the transport vehicle, the outer wheels were slightly offset from the MDD sensor. In modeling the load, this initial offset was simulated by calculating the displacements at a similar offset from the vehicle tires. Displacements that were calculated in this way are represented in Figure 6.

Several interesting observations follow from Figure 5. Differences between the displacements calculated for the top and middle sensors are similar to those of the measured responses. Also, the tendency of the measured top and middle displacements to fall together between the axles is reflected in the calculated response. Note that the calculated response (see Figure 6) falls approximately halfway between the higher and lower portions of the measured response (as in Figure 5). This last observation seems to support the suspicion that the load was not evenly distributed across all vehicle axles.

In order to test the hypothesis of an uneven load distribution, it was necessary to first establish whether an MDD response accurately reflects the magnitude of the load under which the displacements are being measured. It also had to be determined whether displacements calculated by means of the assumed mechanistic model can reflect accurately a change in the applied load. Verification involved considering the MDD response measured under a dump truck for which the exact axle weights were known.

Figure 7 shows the MDD response measured under the dump truck. Also reported is the calculated response. Clearly, there is good agreement between the measured and calculated responses. It is significant that the ratio of 0.48 between the lower and higher displacements is very close to the ratio of 0.41 between the front and rear axle weights. This indicates that for the pavement under consideration, pavement response closely resembles linear elastic behavior.

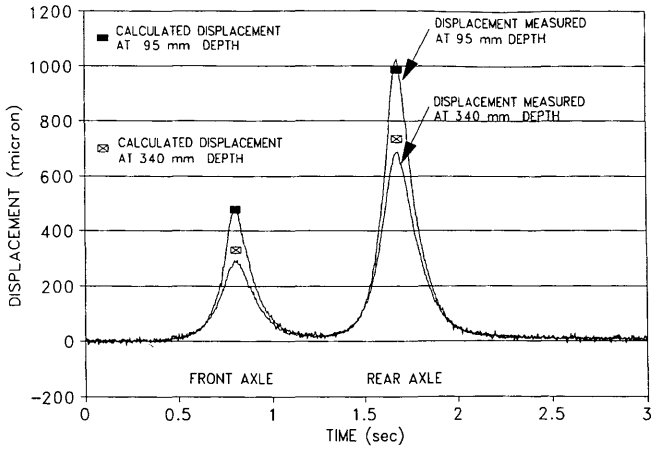

FIGURE 7 Measured and calculated responses under dump truck (1 μm = 0.04 mil).

The superheavy-load simulation was redone following this observation. However, the measured response was divided into two phases: the first consisted of displacements measured under the first nine lines, the second of measurements under the last nine lines. For each of the two phases, the average maximum displacement under each line was calculated. Gross vehicle weight was then distributed between the first and last nine lines according to the ratio of these averages to each other. The arrangement resulted in the modeling of the last nine lines with a load that was 30 percent higher than the theoretical average load per line. Conversely, the first nine lines were modeled with a load that was 30 percent lower than the theoretical average load.

Figures 8 and 9 plot the measured MDD response together with the calculated response for the first and second sensors. The measured response is represented only by sampled points (such as the peaks and troughs) of the total measured response indicated in Figure 5. It is clear that the redistribution of the load resulted in

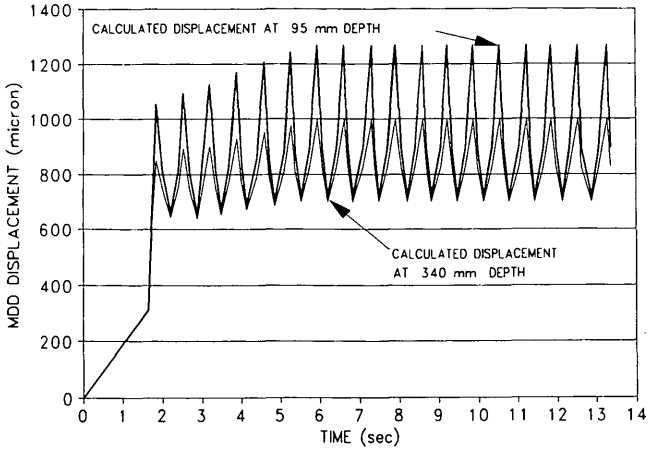

FIGURE 6 Calculated MDD response under tower (1 μm = 0.04 mil).

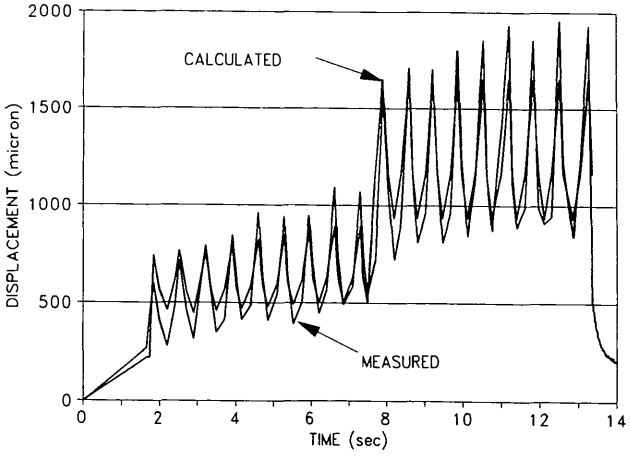

FIGURE 8 Measured and calculated responses under tower at 95-mm depth (1 mm = 0.04 in.).

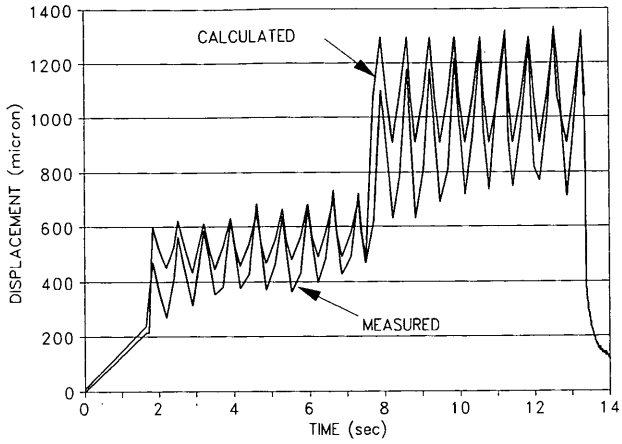

FIGURE 9 Measured and calculated responses under tower at 340-mm depth (1 mm = 0.04 in.).

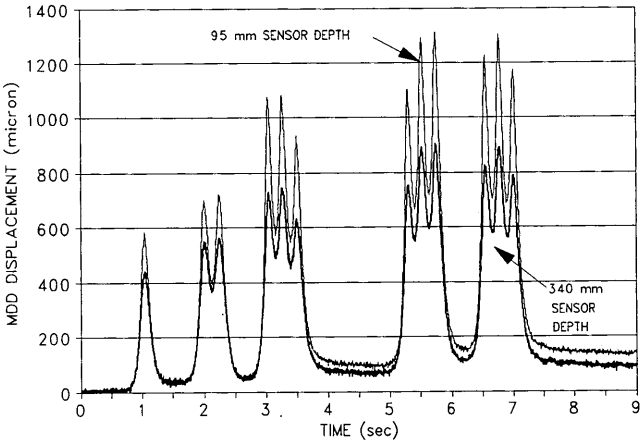

FIGURE 10 Measured and calculated responses under base support (1 mm = 0.04 in.).

a much-improved agreement between the measured and calculated responses.

Preferably, wheel loads could be measured before a superheavy-load move. However, this is difficult to do in practice because route assessment needs to be made and a permit issued well in advance of the superheavy-load move. The problem was addressed in the development and implementation of a route assessment procedure for this study.

MODELING OF PAVEMENT RESPONSE UNDER BASE SUPPORT

The MDD response measured under the 1131-kN (254-kip) load is shown in Figure 10. Peak-displacements under each of the load groups are clearly visible. In the modeling of this load, the gross vehicle weight was distributed between axle groups in a way similar to that described for the tower load. For each axle group, the average maximum measured displacement was calculated. The gross vehicle weight was then assigned to each axle group according to the average. Displacements were then calculated as before. Figures 11 and 12 show the measured and calculated responses. As was the case with the tower load, measured and calculated responses show good agreement.

APPLICATION OF LOAD AND PAVEMENT MODELING

The ultimate aim of load and pavement modeling is to predict the possibility of subgrade failure under expected loading conditions. Such a prediction can only be made after considering stresses and strains, together with an engineering estimate of the pavement's resistance to deformation or shear failure. For the load and pavement case discussed here, a detailed analysis of stresses and strains was undertaken and is published elsewhere (*13*).

In this analysis, the potential for immediate failure of the subgrade was evaluated by calculating the ratio of the octahedral shear stresses to the octahedral shear strength of the subgrade material under expected loading conditions. Damage assessment based on rutting of the subgrade or asphalt fatigue cracking was

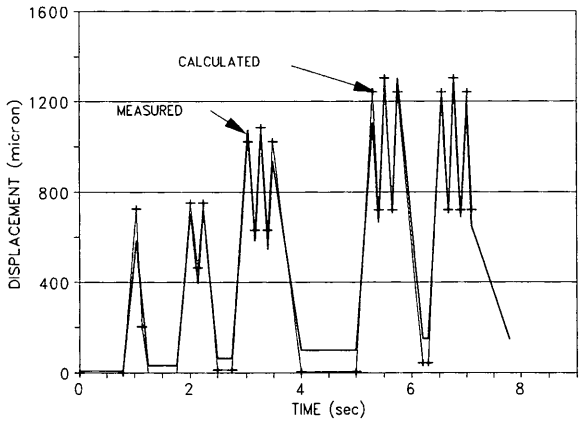

FIGURE 11 Measured and calculated responses under base support at 340-mm depth (1 mm = 0.04 in.).

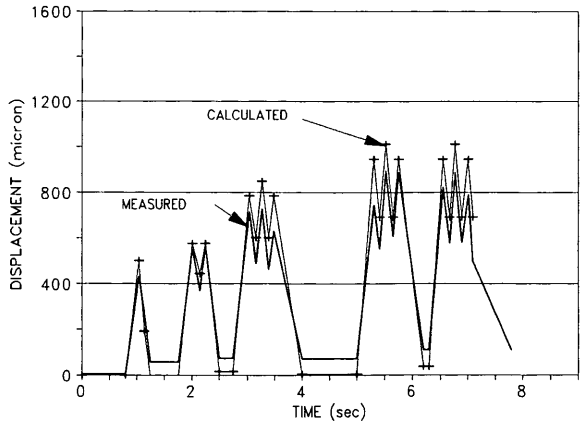

FIGURE 12 Measured and calculated responses under base support at 340-mm depth (1 mm = 0.04 in.).

also evaluated. Analysis methods described above are not necessarily the most accurate, and use of other types of failure criteria may be justified. However, once it has been established that the load and pavement model can simulate accurately the actual response of the pavement under the applied load, any further analysis of stresses and strains can be undertaken with relative ease simply by altering the positions where stresses and strains need to be calculated in order to suit that particular method of analysis.

SUMMARY AND CONCLUSIONS

A procedure for modeling pavement response under superheavy loads was presented. To date, results obtained with the procedure have led to the following conclusions and suggestions for further work:

1. Measured MDD data can be of considerable use in validating any assumption made in the modeling pavement structures and multiaxle wheel loads. Although the use of MDD data on a regular basis would not be feasible, its application in the development of load and pavement modeling procedures is recommended.
2. For the pavement section discussed in this paper, results obtained in simulating pavement response by using layered elastic theory are encouraging. The results reported indicate that layered elastic theory can provide a reasonable estimate of pavement response under multiaxle superheavy loads, as long as the wheel load magnitudes are known. A route assessment scheme using elastic layered theory can function as a Level 1 procedure within the multilevel framework established for evaluating proposed superheavy load routes.
3. The manner in which the load is distributed over the axles of the transport vehicle is of extreme importance. Movers and owners of superheavy loads should be made aware of the importance of achieving the projected wheel loads that they provide to the highway department in the process of requesting a permit. Some transport vehicles are equipped with gauges that measure the pressures inside the hydraulic lines of the vehicle axles. These gauges can be used to monitor vehicle loads. Consideration should be given to encouraging their use, and it is important to discuss the matter with the highway department and movers of superheavy loads.

ACKNOWLEDGMENT

The reported work is part of an on-going research study sponsored by TxDOT. The authors wish to thank Michael Murphy of TxDOT for his continued support and guidance.

REFERENCES

1. Ullidtz, P. *Pavement Analysis.* Elsevier, New York, 1987.
2. Lytton, R. L. Backcalculation of Pavement Layer Properties. In *Nondestructive Testing of Pavements and Backcalculation of Moduli.* Special Technical Publication 1026, ASTM, Philadelphia, Pa., 1989, pp. 7–38.
3. *MODULUS: Preliminary User's Manual-Version 4.0.* Texas Transportation Institute, Texas A&M University, College Station, Tex., 1990.
4. Scullion, T., C. L. Lau, and Y. Chen. *Implementation of the Texas Ground Penetrating Radar System.* Research Report 1233-1. Texas Transportation Institute, Texas A&M University, College Station, 1992.
5. Fernando, E. G. *Highway Speed Pavement Thickness Surveys Using Radar.* Texas Transportation Institute, Texas A&M University, College Station, 1992.
6. Klein, E. G., J. H. Maree, and P. F. Savage. The Application of a Portable Pavement Dynamic Cone Penetrometer to Determine In-Situ Bearing Properties of Road Pavement Layers and Subgrades in South Africa. *Proc. 2nd European Symposium on Penetration Testing,* Amsterdam, Neitherlands, May 1982, pp. 277–283.
7. Fernando, E. G., and T. Chua. *Development of a Procedure for Route Segmentation Using Predicted Layer Thicknesses from Radar Measurements.* Florida DOT State Project 99700-7550, Phase 2A Report. Texas Transportation Institute, Texas A&M University, College Station, 1993.
8. Lu, J., C. Bertrand, and W. R. Hudson. *Evaluation and Implementation of the Automated Road Analyzer (ARAN).* Research Report 1223-2F, Project 3-18-89/0-1223. Center for Transportation Research, University of Texas at Austin, July 1991.
9. Scullion, T., J. Uzan, I. Yazdani, and P. Chan. *Field Evaluation of the Multi-Depth Deflectometer.* Research Report 1123-2. Texas Transportation Institute, Texas A&M University, College Station, Sept. 1988.
10. Kim, Y. R., N. P. Khosla, S. Satish, and T. Scullion. Validation of Moduli Backcalculation Procedures Using Multidepth Deflectometers Installed in Various Flexible Pavement Structures. In *Transportation Research Record 1377,* TRB, National Research Council, Washington D.C., 1991, pp. 128–142.
11. Van Cauwelaert, F. J., D. R. Alexander, T. D. White, and W. R. Barker. Multilayer Elastic Program for Backcalculating Layer Moduli in Pavement Evaluation. In *Nondestructive Testing of Pavements and Backcalculation of Moduli,* Special Technical Publication 1026, ASTM, Philadelphia, 1989.
12. De Jong, D. L., M. G. F. Pentz, and A. R. Korswagen. *Computer Program Bisar.* Koninklijke/Shell Laboratorium, Rotterdam, Netherlands, 1973.
13. Jooste, F. J., and E. G. Fernando. *Movement of Superheavy Loads over the Highway System.* Research Report 1335-1. Texas Transportation Institute, Texas A&M University, College Station. 1993.

Publication of this paper sponsored by Committee on Strength and Deformation Characteristics of Pavement Sections.

Backcalculation of Flexible Pavement Moduli Using Artificial Neural Networks

ROGER W. MEIER AND GLENN J. RIX

Artificial neural networks provide a fundamentally new approach to backcalculation of pavement layer moduli from falling-weight deflectometer deflection basins. An artificial neural network is a highly interconnected collection of simple processing elements that can be trained to approximate a complex, nonlinear function through repeated exposure to examples of the function. In the context of backcalculation, a neural network can be trained to approximate the inverse function by repeatedly showing it forward problem solutions. The single most important advantage of using neural networks for backcalculation is speed. Neural networks trained in this study are more than three orders of magnitude faster than conventional gradient search algorithms. Such speed makes real-time backcalculation of moduli possible. Two backpropagation neural networks were trained to backcalculate pavement moduli for three-layer flexible pavement profiles. Synthetic deflection basins with a wide variety of layer moduli and thicknesses were used to train both networks. One network was trained using ideal deflection basins. Subsequent testing showed that the network could backcalculate pavement layer moduli accurately. A second network was trained using basins, with random noise added to simulate measurement errors. When tested using similarly noisy deflection basins, that network did a reasonably good job of predicting moduli, although it exhibited much more scatter in the results. That same network performed very well on experimental data from two pavement test sections of the Strategic Highway Research Program.

The falling-weight deflectometer (FWD) is used widely to nondestructively assess the structural properties of flexible pavements. Evaluation of FWD test results entails backcalculating in situ pavement layer moduli from measured deflections. It is usually accomplished by matching theoretical and experimental deflection basins. Theoretical deflection basins commonly are calculated using static, multilayer, linear-elastic analyses. In principle, it is also possible to use algorithms that account for dynamic effects and nonlinear material behavior, but they involve significantly greater computation times, which makes them unacceptable for production use.

Current basin-matching programs fall into two broad groups. Most programs employ gradient search techniques to adjust the pavement layer moduli iteratively until the theoretical and experimental deflection basins agree within a specified tolerance. The __DEF series of programs (*1*) is typical of the approach. Required inputs include experimental deflection measurements and pavement layer thicknesses. The iterative solution technique also requires an initial estimate of the solution (seed moduli) and a range of moduli to constrain the solution.

A second approach is to interpolate within a data base of theoretical basins. The MODULUS program (*2*) is an example of this approach. A data base of theoretical basins is generated for prescribed pavement layer thicknesses by parametrically varying the pavement layer moduli within expected ranges. Once the data base is complete, MODULUS uses the Hooke-Jeeves pattern-searching algorithm to choose the deflection basins in the data base that most closely match the experimental basin. MODULUS then calculates the layer moduli corresponding to the experimental basin using Lagrange interpolation. Besides deflection measurements, MODULUS requires a range of moduli for the surface layer and base course and an initial estimate of the subgrade modulus.

The authors of this paper present a fundamentally different approach to FWD backcalculation by using artificial neural networks. Artificial neural networks have been used to solve problems involving pattern recognition, classification, and mapping (*3*). The class of neural networks known as backpropagation networks is universal functional approximators (*4*) that can "learn" a functional mapping through repeated exposure to examples of that mapping. In the context of FWD analysis, a backpropagation neural network can be "trained" to map deflection basins onto their corresponding pavement layer moduli. The best way to train such a network is to use experimentally determined deflection basins along with independently measured pavement layer moduli. Lacking sufficient quantities of such data over a broad range of layer moduli and thicknesses, synthetic deflection basins can be obtained by solving the forward problem with many different combinations of pavement layer properties. A neural network can then be taught to map these synthetic deflection basins back onto their corresponding layer moduli. The latter approach is taken in this paper.

There are several advantages to using neural networks for FWD analysis. The mathematical simplicity of neural networks makes them computationally efficient. They make real-time backcalculation of moduli possible using personal computers. Unlike other backcalculation techniques, a neural network does not require seed moduli or moduli ranges. That eliminates the subjectivity associated with choosing seed moduli and allows the backcalculation procedure to be automated for use by less experienced operators. Furthermore, because a neural network does not explicitly match deflection basins, the pavement moduli determined by the neural network are independent of the error measures (e.g., mean-squared error, maximum absolute error) and the tolerance criteria used to determine convergence.

ARTIFICIAL NEURAL NETWORKS

Artificial neural networks are biologically inspired analogues of the human brain. They are composed of a great many operation-

R. Meier, U.S. Army Engineer Waterways Experiment Station, Geotechnical Laboratory, Mobility Systems Division, 3909 Halls Ferry Road, Vicksburg, Miss. 39180-6199. G. Rix, Georgia Institute of Technology, School of Civil Engineering, Atlanta, Ga. 30332-0355.

ally simple but highly interconnected processing units. The processing units themselves have certain functional similarities to biological neurons, and their organization bears at least superficial resemblance to the organization of neurons in the brain.

Artificial neural networks exhibit many characteristics of the human brain (*5*). For example, certain types of neural networks will "teach themselves," through repeated exposure to a set of data, to recognize common features within the data and to group the data accordingly. Other types of neural networks can be programmed to associate a set of input patterns with their respective output patterns. Artificial neural networks can also generalize an ideal mapping from imperfect examples and extract essential information from input containing both relevant and irrelevant data. Their ability to "see" through noise and distortion to the underlying pattern has been exploited successfully for solving many problems related to pattern recognition.

The most common network architecture used for mapping, classification, and forecasting problems is the multilayer, feed-forward network (*6*). Such networks consist of several layers of processing elements (Figure 1). The processing elements pass information in the form of signal patterns from the input layer of the network through a series of hidden layers to the output layer. Signals travel between processing elements along connections whose strengths can be adjusted to amplify or attenuate the signal as it propagates. Each processing element sums the impinging signals to determine a net level of excitation. A nonlinear activation function provides a graded response to that excitation. The element then passes on the response to each of the processing elements in the next layer (Figure 2). The distribution of connection strengths throughout the network uniquely determines the output signal pattern that results from a given input signal pattern. In that respect, the connection strengths store the "knowledge" contained in the network.

The excitation level of a processing element is modeled mathematically as a weighted sum of its inputs:

$$N_j = \sum_{i=1}^{n} w_{ji} x_i \tag{1}$$

where x_i is the signal coming from the ith processing element in the preceding layer, and w_{ij} is the weight assigned to that connection. The weights determine the degree of signal amplification or attenuation on the incoming connections.

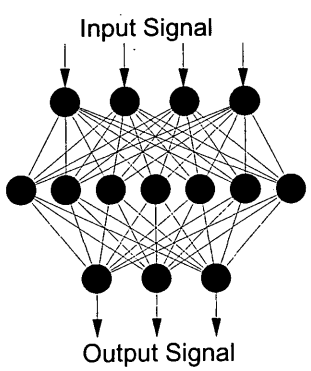

FIGURE 1 Artificial neural network architecture.

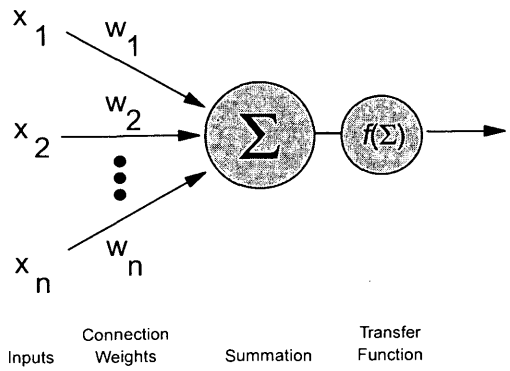

FIGURE 2 Basic processing element for multi-layer, feed-forward network.

The processing element's response to the net excitation N_j commonly is modeled by the sigmoidal logistic function:

$$a_j = f(N_j) = \frac{1}{1 + e^{-N_j}} \tag{2}$$

The function accepts input over the range $(-\infty, \infty)$ and uniquely maps it into the range [0,1]. That not only prevents the signals from growing unbounded as they are summed repeatedly and passed on, but it also introduces nonlinearity into the network. Without this nonlinearity, the network would simply output linear combinations of the input signals. That would severely limit the type of mapping it could perform.

A neural network gains its knowledge through training. A supervised learning method commonly is used to train feed-forward networks. In supervised learning, a set of training data (consisting of pairs of input-output patterns exemplifying the mapping to be learned) is presented to the network, one example at a time. For each example, the input pattern is propagated through the network, and the resulting output pattern is compared with the target output. A learning algorithm is employed to adjust incrementally the connection weights in order to reduce the difference between calculated and target output. The ability to self-adjust is an essential feature of neural computing. It would be impossible to establish manually the connection weights needed to perform any but the simplest of mappings.

Multilayer, feed-forward networks commonly are trained by a technique known as error backpropagation. After each training example is presented to the network, the differences between the calculated and target output patterns are computed and propagated backward through the network according to the existing network connection weights. Individual connection weights then are adjusted in the direction that reduces the error apportioned to them. If training is successful, connection weights attain values that globally minimize the output error (commonly expressed as either the root-mean-square or arithmetic mean) for all the inputs in the training set.

The most common learning algorithm used in backpropagation networks is the generalized delta rule (*7,8*). The generalized delta rule is essentially a gradient descent scheme that seeks a global minimum of the error surface that relates the output errors to the connection weights. In the simplest form of the generalized delta

rule, weight changes at each step in the gradient descent are calculated as follows:

$$\Delta w_{ij} = \alpha \nabla E(w_{ij}) \tag{3}$$

where $\nabla E(w_{ij})$ is the gradient of the error surface with respect to the weight in question, and α is the "learning rate." The learning rate regulates the step size of the gradient descent. A more advanced form uses an additional momentum term to help the gradient descent avoid shallow local minima:

$$\Delta w_{ij}(t) = \alpha \nabla E(w_{ij}) + \beta \Delta w_{ij}(t - 1) \tag{4}$$

where $\Delta w_{ij}(t - 1)$ and $\Delta w_{ij}(t)$ are the weight changes applied on successive steps, and β regulates the amount of momentum.

Invoking the chain rule of differentiation, the gradient of the error surface with respect to an individual connection weight, w_{ij}, instead can be expressed as

$$\nabla E(w_{ij}) = \frac{\partial E(w_{ij})}{\partial N_j} \frac{\partial N_j}{\partial w_{ij}} = \delta_j \frac{\partial N_j}{\partial w_{ij}} = \delta_j a_i \tag{5}$$

where the δ_j (from which the generalized delta rule takes its name) are the gradients of the error surface with respect to the net excitation level of each processing element, and the a_i are the individual inputs to each processing element. At the output units, the δ_j are computed as the product of the output error and the derivative of the activation function:

$$\delta_j = (t_j - a_j) \frac{df(N_j)}{dN_j} \tag{6}$$

where t_j is the target output. One of the reasons the sigmoidal logistic function is so popular as an activation function is that the derivative can be calculated easily:

$$\frac{df(N_j)}{dN_j} = a_j(1 - a_j) \tag{7}$$

At the processing elements in the other network layers, the target outputs are not known a priori. Instead, the errors attributed to those processing elements are estimated by assessing each element's relative contribution to the outputs and, thus, the errors of the elements in the succeeding layer:

$$\delta_j = \frac{df(N_j)}{dN_j} \sum_{k=1}^{n} \delta_k w_{jk} \tag{8}$$

By working backward from the output layer, errors can be apportioned successively to the processing elements in the remaining layers of the network.

Once trained, the network will provide an approximate functional mapping of any input pattern onto its corresponding output pattern. This process is extremely fast because the input pattern is propagated once through the network, a task that involves passing only weighted sums through the sigmoidal logistic function.

The authors implemented the algorithm described above in a FORTRAN computer program. The program logic is summarized in Figure 3. The implementation is relatively straightforward because a neural network gains its processing power from its highly interconnected architecture, not from mathematical complexity.

FWD BACKCALCULATION USING ARTIFICIAL NEURAL NETWORKS

Initial Network Training

Backpropagation neural networks are universal approximators; their training times increase rapidly with increasing problem complexity, which places some practical limit on the mappings that they can learn. Instead of trying to train a network to handle a variable number of pavement layers, the authors chose to train a neural network to backcalculate moduli for a three-layer profile consisting of an asphaltic concrete (AC) surface layer, an unstabilized base course, and a subgrade. Assumed ranges of the layer properties are indicated in Table 1. Thickness of the subgrade was arbitrarily assigned a value of 30.4 m (100 ft) to eliminate the influence of the rigid layer, resulting in an essentially infinite subgrade (*9*). The authors attempted to cover a broad range of realistic layer properties. If the anticipated layer properties were substan-

```
Read in the training parameters and network dimensions
Initialize the connection weights to small random numbers
For each training epoch:
    For each input/output pair in the training set:
        Propagate the input through the network (Eqs. 1,2)
        Compute the deltas for the output layer (Eqs. 6,7)
        Compute the deltas for the remaining layers (Eqs. 7,8)
        Compute the weight changes for all of the layers (Eqs. 4,5)
    For each input/output pair in the testing set:
        Propagate the input through the network (Eqs. 1,2)
        Compute output errors and update output error statistics
Report on the training progress
Close all input and output files
```

FIGURE 3 Computer implementation of backpropagation algorithm.

TABLE 1 Pavement Layer Properties Used To Train Neural Networks

Layer	Layer Modulus (MPa)[a]	Layer Thickness (cm)[b]	Poisson's Ratio
Asphalt	1725 - 20,685	5 - 30	0.325
Base	35 - 1035	15 - 75	0.35
Subgrade	35 - 345	3050	0.35

[a] 1 MPa = 0.145 ksi
[b] 1 cm = 0.394 in

tially different from those used here, another neural network would have to be trained.

A training set of 10,000 synthetic deflection basins was generated using the static, multilayer, linear-elastic program WESLEA (*10*). For each deflection basin, the thicknesses and moduli of the AC and base layers and the modulus of the subgrade were selected randomly from uniform distributions within the limits identified in Table 1. Pavement deflections were calculated for a dynamic load of 40 kN (9,000 lb) acting over an area with a radius of 15 cm (5.91 in.). The authors assumed a fixed sensor spacing to reduce further the complexity of the mapping to be learned. Initial experimentation revealed that the Strategic Highway Research Program (SHRP) sensor spacings of 0, 20, 30, 45, 60, 90, and 150 cm (0, 8, 12, 18, 24, 36, and 60 in.) provided the network with more information about the AC and base moduli than did a uniform 30-cm (12-in.) spacing and allowed the network to make better predictions. SHRP spacing therefore was used exclusively.

If conventional backpropagation networks are used, the network architecture must be established before the start of training. At a minimum, the network must have an input layer and an output layer. The number of neurons in those layers is easy to determine: they are equal to the number of input and output parameters, respectively. There are, however, no well-established procedures for choosing the number of hidden layers nor the number of neurons in each hidden layer (*11*). As a result, trial and error must be used to determine the optimum network architecture, which must strike a balance between insufficient knowledge capacity (too few connections) and excessive capacity. If the network has insufficient capacity, it will be incapable of accurately performing the required mapping. On the other hand, if the network has excessive capacity, it will in essence "memorize" the training examples. In that case, the network will be incapable of performing mappings for deflection basins that it has not memorized.

In principle, it is possible to approximate any functional mapping with a network consisting of one hidden layer (*4*). In practice, however, two hidden layers often allow the same functional mapping to be learned with fewer neurons. After experimenting with several different architectures, the authors chose the network architecture represented in Figure 4. The first hidden layer (closest to the input layer) contained 11 processing elements and the second contained eight processing elements. The input layer of that network contained nine processing elements (corresponding to the AC and base layer thicknesses and the seven deflections), and the output layer contained three processing elements (corresponding to the AC, base, and subgrade moduli).

Training proceeded by iteratively prsenting training examples to the network. Each pass through the set of 10,000 examples constituted a training epoch. During each epoch, the first 9,750

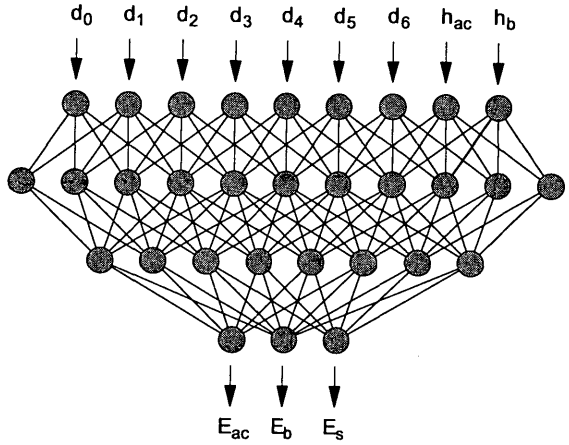

FIGURE 4 Neural network architecture used for backcalculating pavement layer moduli from synthetic deflection basins.

examples were used to train the network. The remaining 250 examples were used to test the network to monitor its training progress. (Neural networks should never be tested with the same data that are used to train them. It is important that the network be able to generalize beyond the training examples, instead of simply memorizing them.) At first, the mean squared error of the outputs drops rapidly as the training epochs are completed, as indicated in Figure 5(a). With further training, the output error asymptotically approaches some minimum level. Training of the network continued until it was clear that this level substantially had been reached.

Figure 5(b), (c), and (d) are scatter plots that compare the target and computed moduli of the asphalt, base, and subgrade layers, respectively, for the 250 test basins. The plots clearly show that the network successfully learned to backcalculate pavement layer moduli from synthetic deflection basins for the entire range of pavement layer properties included in the training set. In a broader context, these results are significant because they indicate that neural networks can be taught to solve complex, nonlinear inverse problems using training data generated by solving the forward problem.

Increasing Network Robustness

Accurate deflection basin measurements are essential if backcalculated layer moduli are to be correct. However, it is unrealistic to expect field measurements to be perfectly accurate. Two pri-

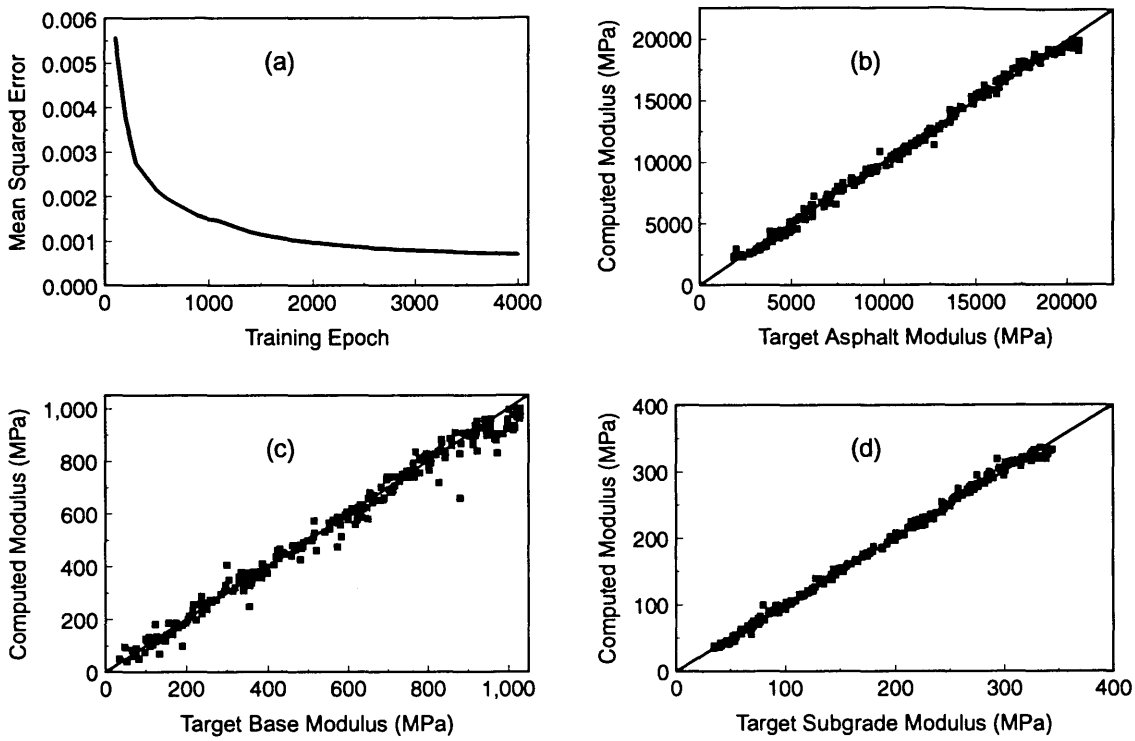

FIGURE 5 *(a)* **Training progress; moduli for network trained with synthetic data, including test results for** *(b)* **asphalt,** *(c)* **base, and** *(d)* **subgrade.**

mary sources of deflection measurement error exist: systematic errors and repeatability errors. Typical specifications for the FWD test (*12*) require a systematic error no greater than 2 percent of the measured deflection and a repeatability error no greater than 2 μm (0.08 mil). Periodic calibration of the velocity transducers can minimize the systematic error, but repeatability errors are random.

One approach to dealing with errors is to include random noise in the deflection basins that are used to train a network—a technique known as noise injection (*13*). Including random noise in the training data makes the network more robust because it learns to produce reasonably accurate moduli in the presence of noise. The authors trained a robust version of the network by adding random noise to each of the seven deflections in each training example just before presenting it to the network. In this way, even though the training basins were reused for each epoch, the added noise was different every time. The random variates were drawn from uniform distributions whose limits were equal to the larger of ± 2 percent of the ideal deflection or ± 2.5 μm (± 0.1 mil). The latter was made slightly larger than the test specification to permit some room for error. Because the task of learning to map noisy data is more difficult for the network, the authors arbitrarily increased the number of processing elements in both hidden layers to 15 before the start of training.

The training progress of the robust network is presented in Figure 6(a). Note that the final value of mean squared error is about 0.0055 for the robust network compared with 0.0007 for the network trained with noise-free data, as seen in Figure 5(a). A tradeoff between accuracy and robustness is to be expected. Also note that the network required about twice as many epochs of training (8,000 versus 4,000) to achieve a nearly constant mean squared error. That is also to be expected because the technique used to generate the random noise ensured that the network never saw the same basin twice, whereas the network trained using ideal deflection basins saw each of those basins 4,000 times.

To assess the robust network's backcalculation abilities, the 250 deflection basins used to test the original network were also modified by adding random noise to the deflection measurements. Tests to determine the repeatability of FWD measurements (*14*) have shown that individual transducers have a standard deviation of ± 1.95 μm. Because the error is random, it can be lessened by replicating the test and averaging the results. Irwin et al. (*14*) recommend that three to five replicates be conducted for each test. Therefore, the amount of noise added to each deflection is established by averaging five random variates drawn from a Gaussian distribution with a mean of zero and a standard deviation that is rounded off to ± 2 μm (0.08 mil). Because the random variates were drawn from a Gaussian distribution instead of the uniform distribution used to train the network, it is possible that some of the test basins contained more noise than was present in the training set.

Figures 6(b), 6(c), and 6(d) compare the target and computed moduli of the asphalt, base, and subgrade layers, respectively, for the 250 modified test basins. The fine dotted lines included in those figures indicate the 95 percent prediction interval associated with a linear regression of the calculated moduli on the target moduli. Those are the bounds within which 95 percent of all future predictions should lie. There is a very good linear correlation between the predicted and target moduli: the R^2 values for the linear regressions are 0.961, 0.918, and 0.995 for the asphalt, base,

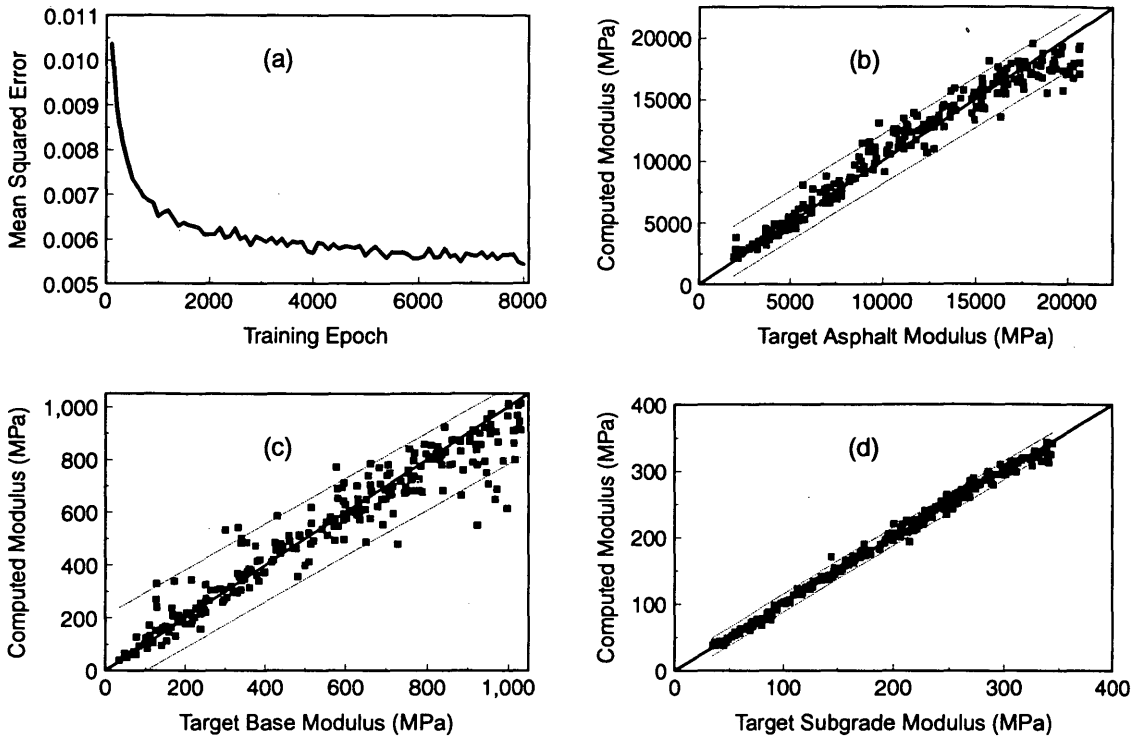

FIGURE 6 (*a*) **Training progress; moduli for network trained with noise injection, including test results for** (*b*) **asphalt,** (*c*) **base, and** (*d*) **subgrade.**

and subgrade, respectively. The precision of results is, however, much lower than it is for the ideal deflection basins. There are more elaborate training algorithms and more complex network architectures that researchers could employ in the future to achieve better precision in the presence of noise.

Backcalculation of Experimental Data

The neural network's performance on experimental deflection basins was evaluated using data from two SHRP pavement test sections described by Rada et al. (*15*). Pavement Sections A and B were selected because they were considered similar to the three-layer, flexible pavements used to train the neural network. Pavement profiles for Sections A and B are presented in Table 2. In Section A, the crushed limestone base and the soil aggregate subbase were combined to form a single base layer. In both sections, the subgrade was assumed to be semiinfinite because Rada et al. (*15*) report that no bedrock was encountered in either section within the top 6.5 m (20 ft).

Pavement deflections were normalized to a load of 40 kN (9,000 lb) and propagated through the robust network. The same deflections and layer thicknesses were used in MODULUS 4.0 (*2*) and WESDEF (*10*) and the results compared (Table 2). The asphalt and base moduli calculated by the neural network were similar to those computed by MODULUS 4.0. The WESDEF program predicted higher asphalt moduli and lower base moduli. All three programs predicted virtually identical subgrade moduli. Because the true moduli at the two test sections are not known, success can only be measured in comparison to the predictions produced by other programs. The similarity of the neural network moduli to those predicted by MODULUS 4.0 (which uses the data base approach) and WESDEF (which uses the gradient-search approach) is taken as an indication that the neural network performed well on these experimental data.

Comparison of Processing Times

An advantage of using artificial neural networks is the speed at which pavement moduli can be backcalculated. Table 3 shows the processing times required for the trained neural network to backcalculate moduli for the 250 synthetic testing basins, with and without the addition of random noise. Also included in Table 3 are the times required by WESDEF to analyze the same 250 basins. Convergence criteria in WESDEF were adjusted to yield predictions as accurate as those of the neural network (Figures 5 and 6). Timing comparisons were conducted on a 33-MHz 80486 personal computer.

For basins with no random noise added, the neural network backcalculated moduli for all 250 basins in 0.9 sec. WESDEF required 25 min to complete the task. With random noise (± 1.95 μm) added to the synthetic deflections, WESDEF required 37.5 min. The artificial neural network processed "noisy" data as quickly as noise-free data because deflection inputs were simply propagated through the network. WESDEF, on the other hand, had to seek iteratively a theoretical basin to match the noisy experimental basin. The authors know of no other backcalculation algorithm that has the neural network's ability to backcalculate pavement moduli in real time.

TABLE 2 Comparison of Backcalculated Moduli for SHRP Pavement Test Sections

Section	Layer	Layer Thickness (cm)[b]	Backcalculated Moduli (MPa)[a] Artificial Neural Network	MODULUS 4.0	WESDEF
A	Asphalt	12.6	8922	8619	11570
	Base[c]	64.5	290	283	221
	Subgrade	Semi-Infinite	221	207	228
B	Asphalt	10.7	5895	6350	10343
	Base	12.7	365	386	138
	Subgrade	Semi-Infinite	186	186	200

[a]1 MPa = 0.145 ksi
[b]1 cm = 0.394 in
[c]Combination of crushed limestone base and soil/aggregate subbase

Another advantage of a neural network is that the creation of the training data and the training of the network are completely separate from the use of the trained network. Thus, it is possible to train a network to account for dynamic effects and nonlinear material behavior without increasing its processing time. Although it will take significantly longer to create the training set, and slightly longer to train the network because of the increased complexity of the mapping, the trained network will backcalculate moduli as quickly as one trained using a static, multilayer, linear-elastic solution. That is in marked contrast to gradient-search programs that must repeatedly solve the more-complex dynamic and nonlinear forward problem to obtain an answer.

FUTURE CONSIDERATIONS

This research is a first step in the development of a real-time backcalculation procedure for the FWD test that accounts for nonlinear material behavior and the dynamic nature of the test. The applicability of the present neural network is limited by the range of pavement layer properties included in the training set. Networks capable of operating across a broader spectrum of field conditions than were addressed here are certainly feasible but will require a more diverse training set. For this feasibility study, a brute-force approach using a large number of randomly generated profiles was adopted. The authors anticipate that a comprehensive training set can be developed without increasing the number of training examples, by using more refined methods of parameter variation. They also anticipate that network training can be accelerated despite a broader scope by using second- and third-generation training algorithms.

SUMMARY AND CONCLUSIONS

Artificial neural networks provide a fundamentally different way to backcalculate pavement layer moduli from FWD deflection basins. Unlike conventional approaches that backcalculate moduli by trying to match theoretical and experimental deflection basins, a neural network simply maps deflection basins into their corresponding layer moduli. The network learns this functional mapping by adjusting the connection weights between its processing elements during repeated exposure to a set of examples (training data). In this study, the training data consisted of synthetic deflection basins generated for a wide range of pavement layer thicknesses and moduli using WESLEA.

Two backpropagation neural networks were successfully trained to backcalculate moduli for three-layer, flexible pavement systems. The first network was trained using synthetic basins with no random noise added. After training, the network was capable of backcalculating layer moduli with excellent accuracy. This initial result is important because it illustrates that a neural network can learn to solve an inverse problem by training it using forward problem solutions. A second network was trained using deflection basins with random noise added to simulate measurement errors. By using random noise in the training data, a final network should be most robust (i.e., it should provide reasonable estimates even for imperfect data). Although the calculated moduli contained

TABLE 3 Comparison of Processing Times To Backcalculate 250 Deflection Basins[a]

	Noise-Free Deflection Basins	Basins with ±1.95μm of Random Noise
Neural Network	0.9 sec	0.9 sec
WESDEF[b]	25 min	37.5 min

[a]Processing times measured on a 33-MHz 80486 personal computer
[b]Using sum of absolute percentage differences less than 3.5% as the convergence criterion and a 20-iteration limit

more scatter than the noise-free results, the estimates from the network trained and tested with noisy data were still reasonably accurate. The neural network trained with noise injections also backcalculated moduli that were similar to those predicted by MODULUS 4.0 for two SHRP pavement test sections.

Artificial neural networks offer several advantages for the backcalculation of moduli. The most important one is speed. Neural networks trained in this study are 1,500 to 2,200 times faster than a conventional gradient search technique. Such speed makes it possible to determine moduli in real-time on personal computers. Neural networks also eliminate the need for the user to specify seed moduli and moduli ranges. Without seed moduli and moduli ranges, backcalculations are less dependent on subjectivity introduced by the user.

The most promising aspect of neural networks is the ability to use more complex and realistic pavement and material models as the basis for a backcalculation. Solving the forward problem to create a training set is completely separate from use of the trained network for backcalculation. That means a neural network can be trained to account for dynamic and nonlinear material behavior and still be able to backcalculate moduli in real time.

ACKNOWLEDGMENTS

Unless otherwise noted, information presented here was obtained from research conducted by the U.S. Army Engineer Waterways Experiment Station. The views of the authors do not purport to reflect the position of the Department of the Army or the Department of Defense. The second author would like to acknowledge the financial support provided by the Waterways Experiment Station. Both authors are grateful to Albert J. Bush III and to Don R. Alexander of the Waterways Experiment Station for their advice and support.

REFERENCES

1. Bush, A. J., III. *Nondestructive Testing for Light Aircraft Pavements, Phase II: Development of the Nondestructive Testing Methodology.* Report FAA-RD-80-9-II, FAA, U.S. Department of Transportation, 1980.
2. Uzan, J., R. L. Lytton, and F. P. Germann. General Procedure for Backcalculating Layer Moduli. In *Nondestructive Testing of Pavements and Backcalculation of Moduli* (A. J. Bush III and G. Y. Baladi, eds.), ASTM 1026, ASTM, Philadelphia, Pa., 1989, pp. 217–228.
3. Dayhoff, J. *Neural Network Architectures: An Introduction.* Van Nostrand Reinhold, New York, 1990.
4. Hornik, K., M. Stinchcomebe, and H. White. Multilayer Feedforward Networks Are Universal Approximators. *Neural Networks,* Vol. 2, 1989, pp. 359–366.
5. Wasserman, P. D. *Neural Computing: Theory and Practice.* Van Nostrand Reinhold, New York, 1989.
6. Hecht-Nielsen, R. *Neurocomputing.* Addison-Wesley, Reading, Mass., 1990.
7. Werbos, P. J. *Beyond Regression: New Tools for Prediction and Analysis in the Behavioral Sciences,* Ph.D. dissertation. Harvard University, Cambridge, Mass., 1974.
8. Rumelhart, D. E., G. E. Hinton, and R. J. Williams. Learning Internal Representations by Error Propagation. In *Parallel Distributed Processing,* Vol. 1 (D. E. Rumelhart and J. L. McClelland, eds.), MIT Press, Cambridge, Mass., 1986, pp. 318–362.
9. Rohde, G. T. *The Mechanistic Analysis of Pavement Deflections on Subgrades Varying in Stiffness with Depth.* Ph.D. dissertation. Texas A&M University, College Station, 1990.
10. Van Cauwelaert, F. J., D. R. Alexander, T. D. White, and W. R. Barker. Multilayer Elastic Program for Backcalculating Layer Moduli in Pavement Evaluation. In *Nondestructive Testing of Pavements and Backcalculation of Moduli* (A. J. Bush III and G. Y. Baladi, eds.), ASTM 1026, ASTM, Philadelphia, Pa., 1989, pp. 171–188.
11. Hertz, J., A. Krogh, and R. G. Palmer. *Introduction to the Theory of Neural Computation.* Addison-Wesley, Reading, Mass., 1991.
12. American Society for Testing and Materials. Standard Test Method for Deflections with a Falling-Weight-Type Impulse Load Device, In *Annual Book of ASTM Standards,* Vol. 04.03, 1993, pp. 566–568.
13. Matsuoka, K. Noise Injection into Inputs in Back-Propagation Learning. *IEEE Transactions on Systems, Man, and Cybernetics,* Vol. 22, No. 3, 1992, pp. 436–440.
14. Irwin, L., W. Yang, and R. Stubstad. Deflection Reading Accuracy and Layer Thickness Accuracy in Backcalculation of Pavement Layer Moduli. In *Nondestructive Testing of Pavements and Backcalculation of Moduli* (A. J. Bush III and G. Y. Baladi, eds.), ASTM 1026, ASTM, Philadelphia, Pa., 1989, pp. 229–244.
14. Rada, G. R., C. A. Richter, and P. J. Stephanos. Layer Moduli from Deflection Measurements: Software Selection and Development of Strategic Highway Research Program's Procedure for Flexible Pavements. In *Transportation Research Record 1377,* TRB, National Research Council, Washington, D.C., 1992, pp. 77–87.

Publication of this paper sponsored by Committee on Strength and Deformation Characteristics of Pavement Sections.

Field Behavior and Modeling of Cracked-and-Seated Semirigid Pavement After Rehabilitation

MORRIS DE BEER, EDUARD G. KLEYN, AND HERMAN WOLFF

Discussed are the structural behavior and subsequent modeling of a typical rehabilitation pavement design of a pavement with stabilized layers (semirigid) in South Africa. The rehabilitation consists of a 150-mm, high-quality crushed stone on a pre-cracked-and-seated semirigid pavement. Its structural behavior was determined through full-scale accelerated testing with a heavy vehicle simulator and associated technology. The modeling was done with a nonlinear, multilayer finite element method. Typical results are given, together with detailed modeling of the pavement response. A manual method for backcalculation of nonlinear granular material properties based on multidepth deflection measurements was used successfully to fit the full deflection basins at different depths within the pavement structure.

Recent trends in South Africa regarding road infrastructure funding necessitate improved pavement rehabilitation design and evaluation methods. As most of southern Africa is relatively dry, the use of thick (> 150 mm) flexible asphalt bases in road pavements is limited. Semirigid pavements are more popular, especially in the former province of the Transvaal, where more than 80 percent of the pavements incorporate stabilized (cementitious) base or subbase layers with relatively thin (< 50 mm) asphalt surfacing or normal surface treatments, or both. Pavement research during the past 7 years has been aimed primarily at reducing the gap between theory and practice. Detailed studies of failure mechanisms and structural behavior have been conducted and suitable transfer functions for the designer developed with the aid of full-scale accelerated tests using a South African heavy vehicle simulator (HVS) belonging to the Roads Branch of the Transvaal Provincial Administration (TPA). Studies of existing pavements as well as of several rehabilitation strategies were made (*1–3*).

In this paper some behavioral and modeling aspects of a typical heavy rehabilitation of an original pavement with portland blast furnace cement–stabilized layers are discussed. The rehabilitation option involves a 150-mm high-quality crushed stone base on the pre-cracked-and-seated semirigid pavement structure. [Another rehabilitation option of 35-mm asphalt surfacing on the cracked-and-seated stabilized layers was also investigated during this project and was analyzed with the mechano-lattice method (*4*). This work, however, is reported elsewhere (*5*).] Aspects such as permanent deformation and resilient response are addressed, both during a so-called crack-and-seat operation and subsequent HVS testing.

The pavement response to traffic loading was modeled with nonlinear stress-dependent layer moduli using the finite element method for the crushed stone base layer section. The study determined that multidepth deflection measurements with the multidepth deflectometer (MDD) (*6,7*) are ideally suited for the backcalculation of granular and sublayer material properties to represent measured deflection basins on these pavements. Further, the study also indicates that plastic deformation measured by the MDD system can be used to aid in the prediction of potential cracking in thin asphalt surfacings. The latter, however, is discussed elsewhere (*5*).

Both the field quantification of structural behavior with the HVS and the subsequent modeling provided the designers as well as the road authority with adequate data, and models with a relatively high degree of confidence, to address effectively infrastructure needs of the next decade in southern Africa.

M. de Beer, Division of Roads and Transport Technology, CSIR, P.O. Box 395, Pretoria 0001, South Africa. E. Kleyn, Roads Branch, Transvaal Provincial Administration, Pretoria, South Africa. H. Wolff, Theron Prinsloo Grimshell & Pullen (Durban) Consulting Engineers, Durban, South Africa.

PREPARING REHABILITATION SECTIONS

Background

During studies using HVS technology on existing pavement and similar structures indicated in Figure 1, several important aspects regarding structural behavior mechanisms of these pavements were identified. The purpose of this paper, however, is not to describe these aspects in detail, although reference will be made occasionally to some of the more important mechanisms. The mechanisms are also summarized by De Beer elsewhere (*2,8*). They include effective fatigue life, (*Nef*), and crushing failure, (*Nc*) of lightly stabilized base or subbase layers with relatively thin asphalt surfacings. The specific structure in Figure 1 was classified as a relatively shallow pavement structure using the dynamic cone penetrometer (DCP) technology (*9,10*). Hence, fatigue failure of the base is most likely to be the dominant failure mechanism of this pavement. Another interesting fact about this pavement is that a relatively softer interlayer, by DCP definition, was found between the base and subbase.

The existence of this interlayer can be attributed to two factors: poor construction (mixing) of the stabilizer, and possible carbonation of the stabilized subbase layers (*11*). HVS tests indicated fatigue failure after 1 million standard (80-kN) axles (MISA), after which the rate of permanent deformation increased from approximately 2.27 mm/MISA to 10 mm/MISA. Cracking in the conventional double seal also started at this failure point. HVS tests at higher loads displayed relatively short fatigue lives for these pavements, indicating a relatively high load sensitivity for fatigue failure. From these basic structural performance data, and taking into account the risk of overloading in South Africa, it was decided to

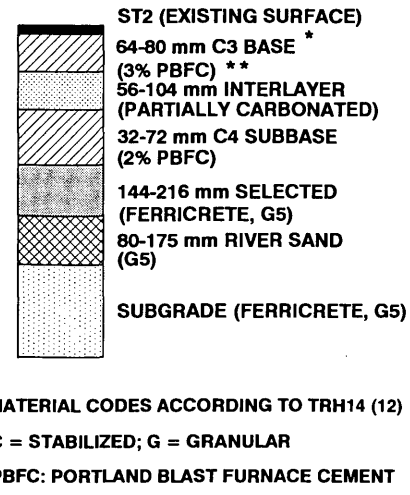

FIGURE 1 Existing pavement structure before crack-and-seat operation.

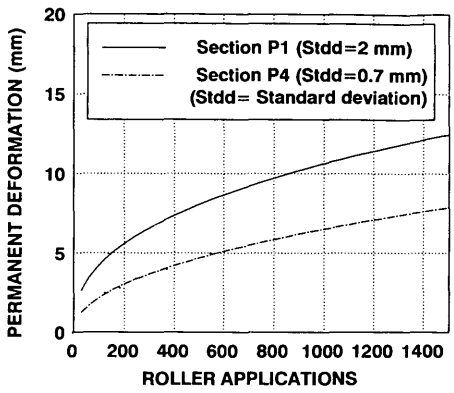

FIGURE 2 Permanent deformation during crack-and-seat operation.

study various rehabilitation options for this kind of pavement. The relatively small HVS test section (1 m by 8 m) was considered too small for a proper rehabilitation investigation. The authors decided to use a so-called crack-and-seat method to convert relatively large pavement areas (40 m by 3.5 m, Section P1; 80 m by 3.5 m, Section P4) of originally stabilized layers from the pre- to the post-cracked state (similar to that established with the HVS), using an 8-ton vibratory roller.

Crack-and-Seat Operation

Permanent deformation measured with the rod-and-level method and resilient surface deflections measured with a modified Benkelman beam were used for control measurements during the crack-and-seat operation (*1*). Figure 2 shows the permanent deformation during the crack-and-seat operation on these two sections, and Figure 3 shows the resilient standard 40-kN maximum deflections before and after the rolling. Not only did deflections increase, but so did variability because of the cracked state of the stabilized material. The stabilized material was broken down into blocks of varying sizes from 150-mm blocks to relatively large blocks of over 500 mm (as determined visually). Cracks were found to be often plane-like (oblique to horizontal) cracks rather than classical vertical fatigue cracks, similar to those that were found after HVS testing. After the crack-and-seat operation, the upper 20 to 30 mm was completely pulverized and manually removed with brooms before the 150-mm crushed stone dolomite base was constructed of G1-base material [Technical Recommendations for Highways 14 (*12*)], with a coarse (13-mm) single seal and sand slurry. Standard 80-kN axle road surface maximum deflections after the G1-base construction varied between 200 and 400 μm (see Figure 3).

HVS TESTING ON REHABILITATED SECTIONS

Permanent Deformation

Figure 4 shows measured permanent deformations at various stages of HVS testing on a crushed stone (G1-base) section (Section 339A4). During the dry state, relatively little plastic or permanent deformation (rut) was measured (approximately 2 mm). The initial rut of 2 to 3 mm existed primarily within the single seal, including the sand slurry (the slurry was used to provide a relatively smooth surface for rut measurements on the HVS test section). No difference occurred between the upper two curves, indicating no local failure around the MDD positions during testing in the dry state. After the artificial introduction of water onto the pavement at approximately 3.7 MISA, local failure around the MDD positions occurred. During the dry state (N < 3.7 MISA), the rate of deformation was approximately 0.54 mm/MISA and increased to 6.76 mm/MISA during the wet state on the basis of the average rut. At a wheel load of 70 kN the rate of deformation also increased in both the dry and wet conditions. The relative damage based on the well-known power law (*13*) was calculated and the average relative damage exponent, d, for this section is 2.31 for dry and 2.44 for wet conditions (see Equation 1). No cracks other than those around the MDDs and the DCP test positions appeared in this section; the majority of the deformation resulted from stone loss from the surfacing.

$$D_l = (P/40)^d \quad (1)$$

where

D_l = relative damage factor,
d = relative damage exponent, and
P = test wheel load in kilonewtons.

Nuclear density measured before and after the HVS test indicated that a slight increase (2.2 percent) in dry densities had occurred (or 87.7 to 89.9 percent of apparent density) as a result of HVS trafficking. During this period, the average moisture content also increased from approximately 1.8 percent to between 3 and 4 percent as a result of surface water ingress. Figure 5 shows permanent deformation measured at different depths with an MDD system within the pavement and indicates that approximately 50 percent of the deformation occurred within the base. However, upon inspection most of the rutting appeared to occur within the sand slurry seal. After water was introduced, permanent deformation increased dramatically, mainly as a result of failure around the MDD holes.

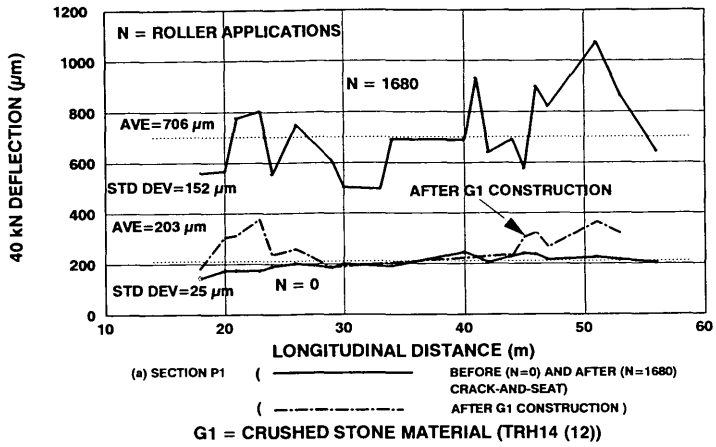

FIGURE 3 Increase in maximum road surface deflection as result of roller applications.

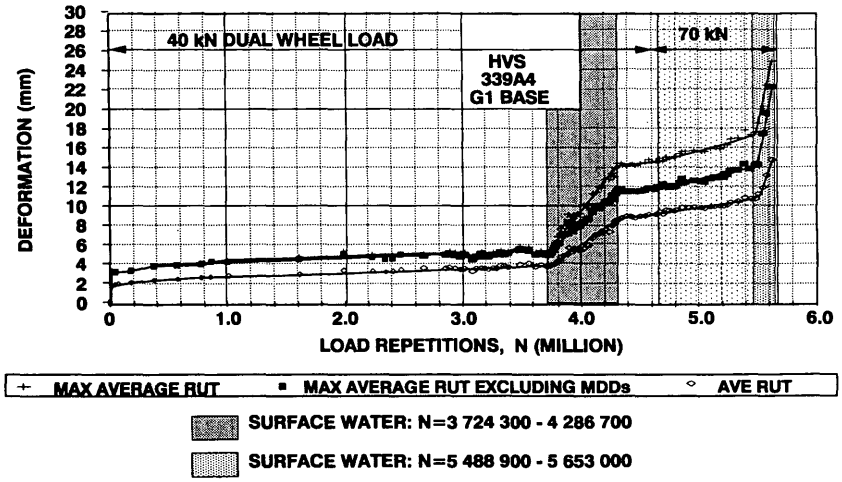

FIGURE 4 Permanent deformation on crushed stone base pavement section.

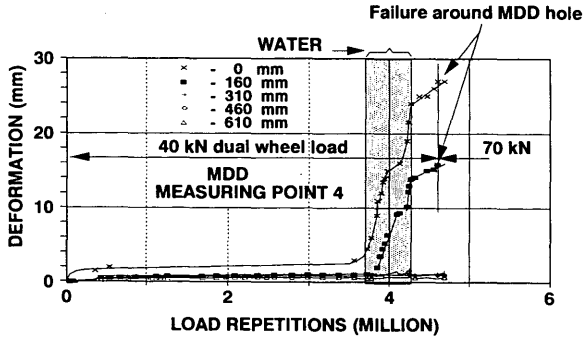

FIGURE 5 Permanent deformation at different depths in crushed stone pavement section.

Resilient Response

Figure 6 illustrates resilient deflection at various stages of trafficking on the G1-base section. The initial 40-kN maximum deflection was approximately 330 μm, and it increased to a steady level (upper limit) at around 500 μm. According to TPA practice, threshold and warning levels of maximum standard deflection are between 300 and 400 μm, respectively. An increase in deflection to approximately 640 μm occurred during the wet test. Figure 7 illustrates the standard 40-kN maximum depth deflections from the MDDs at the start of the test and after 3.67 MISA. Very few changes in depth deflections occurred during the test. The actual measured deflection basins at different depths are given in Tables 1 and 2. An increase in relative deflection within the crushed stone

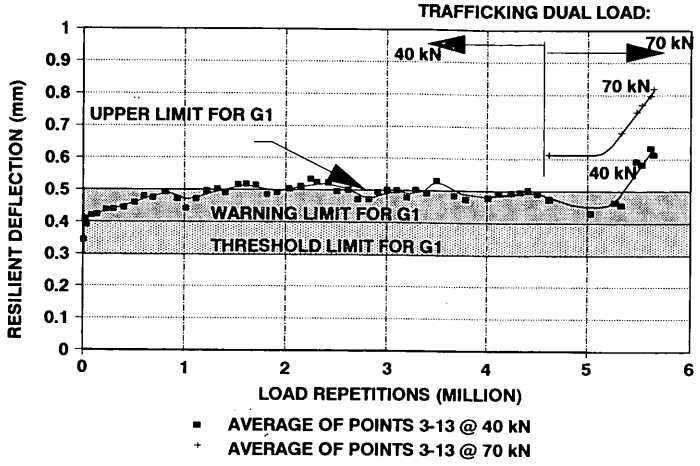

FIGURE 6 Average road surface deflection on crushed stone base pavement at various stages of HVS testing.

base was measured as well as an increase in subgrade deflection. Measurements on the MDD anchor showed that there was no movement under loading, and extrapolation of MDD deflections at depths of 460 and 610 mm was used to calculate the zero deflection level (ZDL), also referred to as depth to "apparent rigid layer" (*14*). Pavement modeling using the MDD depth deflection basin measurement as well as the maximum road surface deflection was applied to backcalculate layer and material properties, which are discussed later.

Modeling of Crushed Stone Pavement

Modeling of the crushed stone base pavement section was done primarily with the MICH-PAVE finite element code developed by Harichandran and Yeh (*15*). The crushed stone layer was modeled using the well-known stress dependent model:

$$Mr = K1\Theta^{K2} \tag{2}$$

where $\Theta = \sigma_1 + \sigma_2 + \sigma_3$ and $K1$, $K2$ are material constants.

The rest of the pavement was divided into three layers, with a rigid layer, represented by a relatively stiff layer ($E6$ = 35 000 MPa) at a depth (ZDL), calculated from MDD measurements (Figure 7). The backcalculated material and layer properties for the two stages of HVS trafficking are summarized in Figure 8. Figures 9 and 10 show the measured and calculated deflection basins. At the time of this study, the backcalculation was done manually, which was very time consuming. However, the method of a flexible boundary used within the MICH-PAVE code (*15*) was approximately 14 times faster than the manual ILLI-PAVE code

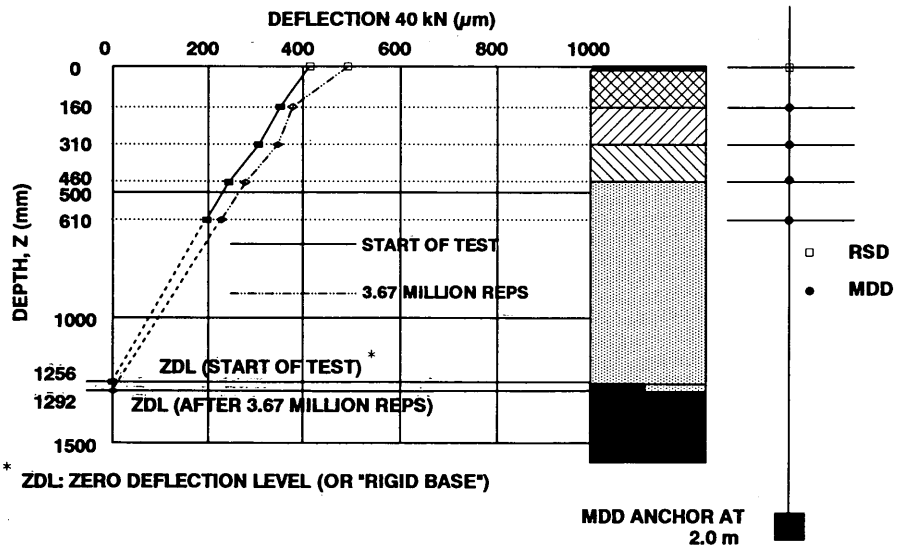

FIGURE 7 Multidepth deflectometer deflection at two stages of HVS trafficking on crushed stone pavement structure.

TABLE 1 Measured and Predicted Deflections (μm) at Start of HVS Testing on Crushed Stone Section

DEPTH (mm)													
0 Measured Deflection	413.03												
Predicted Deflection	413.00												
Horizontal Dist (mm)	0	29.25	58.5	87.75	117	175.5	234	292.5	380.25	468	585	731.25	906.75
160 Measured Deflection		349.45	341.81	333.71	323.26	299.89	276.14	251.14	203.11	163.76	118.19	80.49	45.03
Predicted Deflection		348.51	342.52	332.78	319.96	290.15	259.40	226.68	187.00	151.34	108.47	70.43	24.11
Error (%)		-0.27	0.21	-0.28	-1.02	-3.25	-6.06	-9.47	-7.93	-7.59	-8.22	-12.50	-16.47
ABS error (μm)		-0.94	0.71	-0.92	-3.30	-9.74	-16.74	-24.46	-16.11	-12.42	-9.72	-10.16	-20.92
RMSE (%)		0.16											
RMSE 1 (%)*		0.07											
310 Measured Deflection		303.89	299.31	293.21	287.74	269.09	252.49	233.79	198.04	160.29	117.31	82.24	48.39
Predicted Deflection		303.25	299.85	294.29	286.61	266.99	244.81	220.00	183.33	149.30	107.47	69.79	23.87
Error (%)		-0.21	0.18	0.37	-0.39	-0.78	-3.04	-5.90	-7.43	-6.86	-8.39	-15.14	-50.68
ABS error (μm)		-0.64	0.54	1.08	-1.13	-2.10	-17.68	-13.79	-14.71	-10.99	-9.84	-12.45	-24.52
RMSE (%)		0.17											
RMSE 1 (%)		0.06											
460 Measured Deflection		240.23	237.21	234.06	232.53	221.34	210.69	196.46	171.23	145.71	112.23	83.01	50.63
Predicted Deflection		242.65	240.80	237.76	233.32	221.52	207.31	192.08	163.67	136.23	99.22	64.44	21.73
Error (%)		1.01	1.51	1.58	0.34	0.08	-1.60	-2.23	-4.42	-6.51	-11.60	-23.11	-57.08
ABS error (μm)		2.42	3.59	3.70	0.79	0.18	-3.37	-4.38	-7.56	-9.48	-13.01	-19.37	-28.90
RMSE (%)		0.19											
RMSE 1 (%)		0.08											
610 Measured Deflection		195.90	195.35	193.82	191.01	186.32	177.88	169.33	151.20	134.00	103.4	79.73	50.11
Predicted Deflection		197.27	196.10	194.15	191.29	183.36	173.55	163.64	142.71	121.44	91.84	62.49	24.37
Error (%)		0.70	0.39	0.17	0.14	-1.59	-2.43	-3.36	-5.61	-9.37	-11.18	-21.63	-51.37
ABS error (μm)		1.37	0.75	0.33	0.28	-2.96	-4.33	-5.69	-8.49	-12.56	-11.56	-17.24	-25.74
RMSE (%)		0.18											
RMSE 1 (%)		0.08											

NOTE: Load 40 kN; tire pressure 520 kPa.

*RMSE 1 *excludes* data at horizontal distance 906.75 mm, RMSE includes data at horizontal distance 906.75 mm.

TABLE 2 Measured and Predicted Deflections (μm) After 3.67 Million Load Repetitions on Crushed Stone Section

DEPTH (mm)													
0 Measured Deflection	489.73												
Predicted Deflection	489.00												
Horizontal Dist(mm)	0	29.25	58.5	87.75	117	175.5	234	292.5	380.25	468	585	731.25	906.75
160 Measured Deflection		375.23	369.60	359.60	347.85	320.30	285.23	249.25	198.23	156.08	110.55	68.43	38.18
Predicted Deflection		376.60	370.39	360.59	347.84	317.40	285.26	253.01	209.40	168.94	121.94	76.11	42.43
Error (%)		0.37	0.28	0.37	-0.00	-0.91	-0.01	1.51	5.64	8.24	10.30	11.23	11.15
ABS error (μm)		1.37	1.04	1.32	-0.01	-2.90	-0.03	3.76	11.18	12.87	11.39	7.69	4.26
RMSE (%)		0.62											
310 Measured Deflection		345.68	336.28	332.19	324.18	312.08	238.90	261.20	217.98	174.30	128.38	82.85	48.43
Predicted Deflection		345.56	341.77	335.68	326.75	304.21	277.60	249.22	207.89	168.46	122.13	76.49	42.92
Error (%)		-0.03	1.63	1.05	0.79	-2.58	-4.24	-4.59	-4.63	-3.35	-4.87	-7.68	-11.36
ABS error (μm)		-0.11	5.50	3.49	2.57	-8.05	-12.30	-11.98	-10.08	-5.84	-6.25	-6.36	-5.50
RMSE (%)		0.50											
460 Measured Deflection		276.19	274.11	271.09	265.94	254.46	237.39	217.01	183.76	151.09	112.11	72.34	43.14
Predicted Deflection		277.78	275.50	271.97	266.78	252.70	235.70	216.14	184.83	152.92	113.75	72.92	43.02
Error (%)		0.57	0.51	0.33	0.32	-0.69	-0.71	-0.40	0.58	1.21	1.46	0.81	-0.27
ABS error (μm)		1.59	1.39	0.88	0.85	-1.77	-1.68	-0.87	1.07	1.83	1.64	0.58	-0.12
RMSE (%)		0.07											
610 Measured Deflection		227.25	226.80	225.30	222.65	215.80	205.85	190.90	162.10	132.10	99.60	65.15	37.30
Predicted Deflection		228.66	227.18	224.82	221.30	211.42	199.14	184.79	161.28	136.12	104.20	70.37	41.38
Error (%)		0.62	0.17	-0.21	-0.61	-2.03	-3.26	-3.20	-0.50	3.05	4.62	8.03	10.95
ABS error (μm)		1.41	0.38	-0.48	-1.35	-4.38	-6.71	-6.10	-0.81	4.02	4.61	5.23	4.08
RMSE (%)		0.45											

NOTE: Load 40 kN; tire pressure 520 kPa.

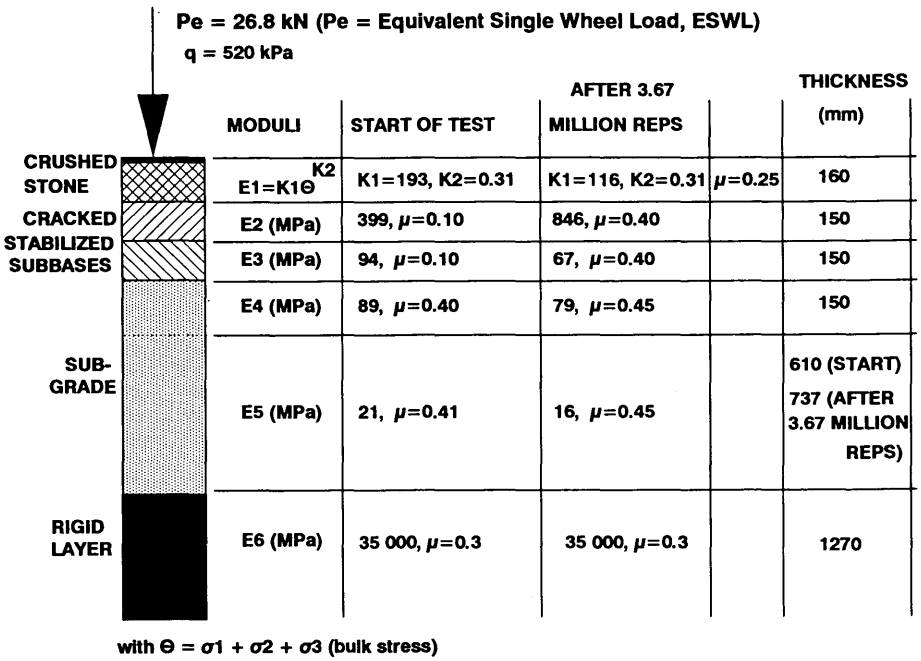

MODULI	START OF TEST	AFTER 3.67 MILLION REPS		THICKNESS (mm)
$E1=K1\Theta^{K2}$	K1=193, K2=0.31	K1=116, K2=0.31	μ=0.25	160
E2 (MPa)	399, μ=0.10	846, μ=0.40		150
E3 (MPa)	94, μ=0.10	67, μ=0.40		150
E4 (MPa)	89, μ=0.40	79, μ=0.45		150
E5 (MPa)	21, μ=0.41	16, μ=0.45		610 (START) 737 (AFTER 3.67 MILLION REPS)
E6 (MPa)	35 000, μ=0.3	35 000, μ=0.3		1270

FIGURE 8 Model parameters for crushed stone pavement structure (moduli in megapascals).

method (*16*). In the case discussed here, the flexible boundary with MICH-PAVE was placed at a depth of approximately 2.54 m. In this analysis, parameters $K1$ of the granular base and $E2$ to $E5$, including the Poisson's ratios for the various layers, were changed manually until measured and calculated deflections converged. In both sets of MDD basin measurements, the root-mean-square error (RMSE) percentage (*14*) varied between 0.01 and 0.70. Absolute errors were less than 33 μm, with maximum percentage errors less than 13. During the analysis of the measured deflection basins it was found that the surface deflection basin measured with the road surface deflectometer (RSD) (modified Benkelman beam) did not exactly coincide with those measured with the MDD module at the surface of the pavement. Although the maximum deflections were similar, the shape of the basin was different, the RSD basin measured relatively higher deflections, especially from a distance of 250 mm from the load toward the tail end of the basin. Because of these differences, which were believed to be related to the different reference systems (geometry) of the two deflection measurement systems—RSD referenced on surface, MDD referenced in depth—only the maximum RSD deflection together with the MDD depth deflection basin results were used in this study for backanalysis. See Figures 9 and 10.

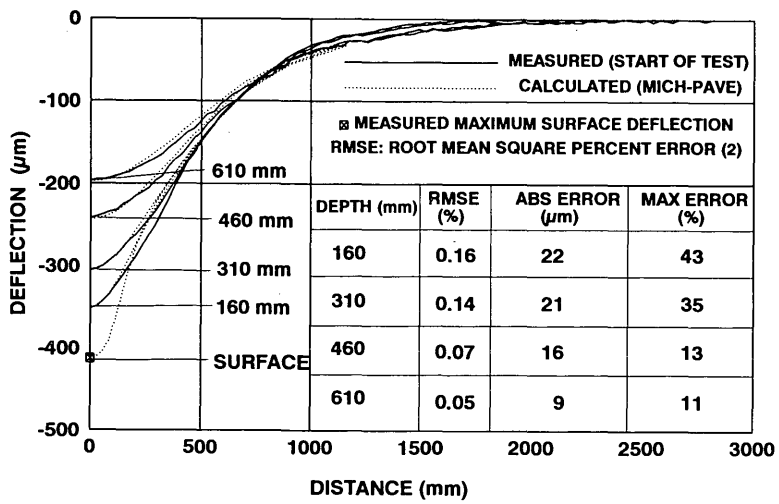

DEPTH (mm)	RMSE (%)	ABS ERROR (μm)	MAX ERROR (%)
160	0.16	22	43
310	0.14	21	35
460	0.07	16	13
610	0.05	9	11

FIGURE 9 Measured and calculated deflection basins at start of HVS testing on crushed stone section. (For actual deflections, see Tables 1 and 2.)

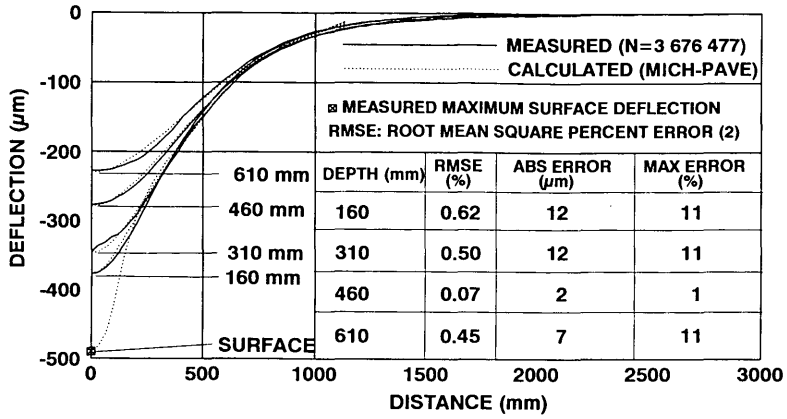

DEPTH (mm)	RMSE (%)	ABS ERROR (μm)	MAX ERROR (%)
160	0.62	12	11
310	0.50	12	11
460	0.07	2	1
610	0.45	7	11

FIGURE 10 Measured and calculated deflection basins after 3.67-million load repetitions on crushed stone section. (For actual deflections, see Tables 1 and 2.)

Discussion of Model Properties

It was found the $K1$ decreased from 193 to 116 MPa (−40 percent) as a result of HVS trafficking and a possible increase in moisture content of the granular material. The $K2$ appeared to be constant at a value of 0.31, as well as Poisson's ratio μ = 0.25 (see Figure 8). The $K2$ and μ compare favorably with tentative laboratory values determined with the K-mold rapid triaxial test proposed by Semmelink (*17,18*). It is believed that these constants may change slightly with improved surface basin measurements. At this stage, however, it is clear that the increase in surface deflection was primarily the result of a reduction in the $K1$ value of the crushed stone material. This reduction in $K1$ also effectively reduced the load-bearing capacity of the base layer, hence the higher deflections in the lower (subgrade) layers. Regarding the cracked-and-seated stabilized subbase layers (in the equivalent granular state), it was found that a two-layer linear elastic system with a modular ratio varying between 4.2 and 12.6 was needed to reproduce the best-fit basins in this case. That might be an indication of relatively strong stress dependency within these layers. Modeling these layers (or a single equivalent granular layer) using the crushed stone stress-dependent model could also produce acceptable basins. However, that approach was not pursued for this study because of uncertainty of acceptable $K2$ values for cracked stabilized material and also in order to limit the number of unknowns during the iteration process.

As a result of trafficking (traffic molding) it appeared that the modular ratio increased threefold, resulting in higher moduli for the upper stabilized layer and lower moduli for the lower layer (suggesting a possible reduction in $K1$ and an increase in $K2$ if the crushed stone stress-dependent model is assumed). In this case, a change in Poisson's ratio of both stabilized layers from 0.10 to 0.40 was also needed to reduce the RMSE of each basin. The reason for the increase in Poisson's ratio is not clear, but is believed to be related to a possible advanced state of cracking (more granular) of the already cracked stabilized layers, as well as possible "model dependency' of these values. Future research perhaps should aim to improve in situ methods for obtaining effective Poisson's ratios for backcalculation.

Finally, the authors found it was best to divide the subgrade into two layers (Layer 4 and Layer 5) on top of the relatively shallow rigid layer. If the subgrade is modeled as one layer with the rigid layer in place, the deflection at a depth of 610 mm is grossly underestimated. This finding is confirmed by Rohde (*14*). The modulus of Layer 4 was 89 MPa, and it was reduced to 79 MPa (−11 percent), probably as a result of increased deflection in the pavement structure. Poisson's ratio changed from 0.4 to 0.45. The second subgrade layer (Layer 5) modulus was 21 MPa at the start of test and changed to 16 MPa, with the Poisson's ratio changing from 0.41 to 0.45.

Although it is understood that these layer properties are model dependent, it is shown here that the layer properties can be used to reproduce deflections measured within the pavement system relatively accurately. Future research, however, should be directed at model-independent parameters and properties obtained through backcalculation.

SUMMARY AND CONCLUSIONS

In this paper, the structural behavior of a typical rehabilitated pavement structure with semirigid subbase layers is discussed. The structural behavior was quantified using HVS technology. The pavement structure involved a 150-mm crushed stone base on a cracked-and-seated lightly stabilized subbase layer. Detailed resilient modeling of the crushed stone base section was done with nonlinear finite element analysis. Measured resilient deflections at various depths in the pavement were used as input to model the behavior of the pavement.

The study indicated that results from full-scale accelerated testing (e.g., HVS) and MDD technology applied to pavement systems with varying materials (including semirigid layers) can assist with the input parameters for modeling pavement structure responses. Although some refinements in the model and measuring techniques are still needed, the methods adopted here strive to narrow the gap between theory and practice.

More emphasis should be given to the accurate measuring of surface deflection basins in association with multidepth deflection basin measurements. Further, nonlinear multilayer backcalculation techniques should be computerized to determine (backcalculate) in situ material and layer properties on a wider and more practical basis. However, full-scale research should be accompanied by de-

velopment of rapid laboratory testing methods for determining relevant material constitutive laws. The new rapid triaxial test is such a development (i.e., the so-called *K*-mold) (*17,18*), wherein the horizontal stress, σ_3, is mobilized automatically from application of the vertical stress, σ_1. From this test, stress-dependent moduli and Poisson's ratio can be determined, as well as Mohr-Coulomb parameters, in less than 1 min.

Implementation of the methods and findings summarized in this study will ensure more economical rehabilitation designs for semi-rigid pavement structures in southern Africa.

ACKNOWLEDGMENT

The authors thank both the Roads Branch of the Transvaal Provincial Administration (TPA) and the Director of the Division of Roads and Transport Technology for their support during this research and for permission to publish this paper.

REFERENCES

1. De Beer, M., E. G. Kleyn, H. Wolff, and J. R. Otte. Behaviour of Various Rehabilitation Options of a Cracked-and-Seated Semi-Rigid Pavement During Accelerated Testing in Transvaal. *Proc., 1991 Annual Transportation Convention*, Vol. 4B, Aug. 1991, 23 pp.
2. De Beer, M. *Aspects of the Design and Behavior of Road Structures Incorporating Lightly Cementitious Layers.* Ph.d dissertation. Department of Civil Engineering, University of Pretoria, Pretoria, South Africa, 1990.
3. Kleyn, E. G., C. R. Freeme, and L. J. Terblanche. The Impact of Heavy Vehicle Simulator Testing in Transvaal. *Proc., 1985 Annual Transportation Convention*, Pretoria, South Africa, 1985.
4. Yandell, W. O. *Mechano-Lattice Analysis.* Lecture Notes, LGI Short course, University of Pretoria, South Africa, 1990.
5. De Beer, M., E. G. Kleyn, and H. Wolff. *Field Behaviour and Modelling of a Cracked-and-Seated Semi-Rigid Pavement after Rehabilitation.* Research Report DPVT 221. Division of Roads and Transport Technology, CSIR, Pretoria, South Africa, March 1994.
6. De Beer, M., E. Horak, and A. T. Visser. The Multi-Depth Deflectometer (MDD) System for determining the Effective Elastic Moduli of Pavement Layers. In *1st Proc., International Symposium on Nondestructive Testing of Pavements and Backcalculation of Moduli*, Special Technical Publication 1026, ASTM, Philadelphia, Pa., 1988.
7. De Beer, M. Pavement Response Measuring System. *Proc., 2nd International Symposium*, West Lebanon, N.H. Sept. 1991.
8. De Beer, M. Developments in the South African Mechanistic Design Procedure for Asphalt Pavements. *Proc., 7th International Conference on Asphalt Pavements: Design Construction and Performance, Vol. 3*, University of Nottingham, England, Aug. 1992, pp. 54–76.
9. De Beer, M., E. G. Kleyn, and P. F. Savage. Towards a Classification System for the Strength-Balance of Thin Surfaced Flexible Pavements. *Proc., 1988 Annual Transportation Convention, Vol. 3D*, Pretoria, South Africa, July 1988.
10. De Beer, M. Use of the Dynamic Cone Penetrometer (DCP) in the Design of Road Structures. Presented at *10th African Regional Conference on Soil Mechanics and Foundation Engineering*, Maseru, Lesotho, South Africa, Sept. 1991.
11. Netterberg, F., and P. Paige-Green. *Carbonation of Lime and Cement Stabilised Layers in Road Construction.* Technical Report RS/3/84. NITRR, Council for Scientific and Industrial Research, Pretoria, South Africa, 1984.
12. *Guidelines for Road Construction Materials.* Technical Recommendations for Highways, TRH14, Committee of State Road Authorities, Department of Transport, Pretoria, South Africa, 1985.
13. Irick, P. E., and W. R. Hudson. *NCHRP Report 2A: Guidelines for Satellite Studies of Pavement Performance.* HRB, National Research Council, Washington, D.C., 1964.
14. Rohde, G. T. *The Mechanistic Analysis of Pavement Defections on Subgrades Varying in Stiffness with Depth.* Ph.d. dissertation. Texas A&M University, College Station, Dec. 1990.
15. Harichandran, R. S., and M. S. Yeh. Flexible Boundary in Finite-Element Analysis of Pavements. In *Transportation Research Record 1207*, TRB, National Research Council, Washington, D.C., 1988, pp. 50–60.
16. *ILLI-PAVE Users Manual.* Department of Civil Engineering, University of Illinois at Urbana-Champaign, 1986.
17. Semmelink, C. J. The Use of the DRTT K-Mould in Determining the Elastic Moduli of Untreated Roadbuilding Material. *Proc., 1991 Annual Transport Convention, Paper 6*, Pretoria, South Africa, 1991, 14 pp.
18. Semmelink, C. J., and M. De Beer. Development of a Dynamic DRTT K-Mould System. *Proc., 13th Annual Transportation Convention*, University of Pretoria, South Africa, June 28 to July 1, 1993.

Publication of this paper sponsored by Committee on Modelling Techniques in Geomechanics.

Three-Dimensional Dynamic Response Model for Rigid Pavements

JAGANNATH MALLELA AND K. P. GEORGE

Traditionally, elastic layer analysis has been employed in pavement design and evaluation. Three basic assumption of elastic layer analysis are that static loading, linear elastic materials, and infinite areal extents of layers are each inconsistent with real-world pavement structure. In an effort to resolve the issue, finite element techniques were used in this research. The three-dimensional finite element program ABAQUS (3D-DFEM) was employed to analyze pavements subjected to dynamic loading. Preliminary studies included a sensitivity analysis to formalize various aspects of the finite element model (e.g., mesh size and boundary conditions). Studies were conducted with 3D-DFEM to verify its static and dynamic analysis capabilities. Static results compared favorably with those in a previous study. The 3D-DFEM responses of an in-service flexible pavement were in agreement with measured falling-weight deflectometer (FWD) deflections and those predicted by an elastodynamic solution. Having verified both those capabilities, the model was employed for calculating deflection responses of factorially designed rigid pavement structures. Thicknesses and moduli of pavement layers varied over a wide range. A 9,670-lb FWD load with seven deflection sensors was configured. Statistical equations, one for each sensor position, were derived employing the deflection data base assembled from the factorial experiment. These equations, in turn, were validated by predicting the measured responses of in-service rigid pavements. An important practical application of the equations is to improve the mechanistic interpretation of FWD data in backcalculation routines. The 3D-DFEM with its numerous features simulating real-world conditions eventually could replace elastic layer analysis.

During the past two decades, the emphasis in pavement engineering has been to maintain existing infrastructure through efficient and cost-effective management practices. Nondestructive testing of pavements, in conjunction with backcalculation techniques, has become a popular tool for in situ material characterization of pavements. Backcalculation can be thought of as the inverse process of obtaining material parameters of pavement layers from surface deflections under a given test load. Backcalculation depends on how well surface deflections can be predicted from pavement structure and material characteristics. For surface deflection calculation, layered elastic theory is the preeminent choice. However, as currently used, elastostatic analysis assumes static loading conditions, infinite layers in the lateral direction, and linear elastic materials—all simplifications of the real-world problem. For example, loading mode has a tremendous effect on pavement response. Mamlouk (*1*) compares the effect of steady-state loading mode with that of static loading mode and reports an error of 24 percent predicted through static analysis. Sebaaly et al. (*2*) report that static analysis of pavement response to the FWD load always results in average surface deflections 20 to 40 percent larger than field measurement. The effect of loading mode on pavement response cannot be overemphasized.

Department of Civil Engineering, University of Mississippi, University, Miss. 38677.

To improve upon the backcalculation procedures, Sebaaly et al. (*2*) suggest an elastodynamic approach using multiple degrees of freedom to predict dynamic response of pavements under FWD loading. Ashton and Moavenzadeh (*3*) present an analysis procedure for the determination of stresses and displacement in a three-layered viscoelastic system. These studies are aimed at resolving the issues of what effect loading mode and material characterization have and the major drawbacks of the layered theory approach. Although promising, those techniques are not widely applicable and lack the speed and simplicity of layered elastic models. Finite element techniques that are used extensively in the aerospace industry now are being applied to other engineering fields for which analytical solutions have not been readily available. Finite element codes used for rigid pavement analysis, FIDIES (*4*), H51ES (*5*), ILLISLAB (*6*), GEOSYS (*7*), are each tailored to solve a specific problem. Whether dynamic load is more appropriate for simulating truck and FWD loading in the field is still debated. With the advent of supercomputers, large, general purpose finite-element codes have been developed that take advantage of their speed and memory capabilities. ABAQUS (*8*), referred to as 3D-DFEM, is one such finite element code; it was developed mainly for structural analysis. The program is capable of modeling any wheel-gear combination, or static, steady-state dynamic, impulse, or user-defined loading. Pavement discontinuities, loss of support conditions, and a variety of material behavior also can be implemented in the program code, providing a versatile tool for pavement analysis. Zaghloul et al. (*9,10*) used the code to conduct flexible pavement analysis.

The purpose of this study is to explore the use of a three-dimensional dynamic finite element program (3D-DFEM) in rigid pavement analysis. With the objective of validating the program for use in pavement analysis, static analyses were carried out and compared with analytical and other finite element solutions of some credibility. In addition, dynamic responses of 3D-DFEM were compared with FWD load response in the field and other numerical solutions.

Primary factors that affect pavement response are moduli and thickness of pavement layers. A factorial experiment was designed to investigate the effect of these factors on rigid pavement response, formalizing a comprehensive data base. Regression analysis was performed on this data base, developing statistical models for predicting dynamic pavement response. The models were validated by comparing the predicted responses with those measured under FWD load in two Strategic Highway Research Program (SHRP), General Pavement Studies (GPS) sections.

FINITE ELEMENT MODELING USING 3D-DFEM

An explicit integration scheme of the 3D-DFEM generally is more suitable for impact- or impulse-load analyses than an implicit

scheme. Accordingly, the former scheme was used for this study. The procedure is based on the implementation of an explicit integration rule together with diagonal or "lumped" element mass matrices. Equations of motion are integrated using the explicit central difference integration rule. Creating a finite element mesh with appropriate boundary features is a prerequisite to solving a boundary value problem. A preliminary study investigating the sensitivity of mesh size and boundary conditions, among other factors, was undertaken before attempting to solve a rigid pavement problem. The following features were thoroughly investigated leading to the final mesh configuration and attendant boundaries:

- Vertical and lateral subgrade extents,
- Pavement-shoulder interface,
- Material characterization,
- Mesh fineness and element aspect ratio, and
- FWD loading.

Vertical and Lateral Subgrade Extents

When applying numerical analysis procedures, it is important to eliminate the effect of boundaries on the responses. With this objective in mind, several finite element runs were performed to determine the depth and lateral extent to which the subgrade should be modeled. Consideration of a 12.2-m (40-ft) deep subgrade resulted in negligible (of the order 10^{-10} in. and less) deflections at the bottom boundary. Simulating this, the 12.2-m (40-ft) bottom boundary was assumed to permit no movement of the nodes lying on that boundary ($U_x = 0$, $U_y = 0$, $U_z = 0$). To determine the effect of lateral subgrade extent on pavement response, the subgrade was modeled to a distance of 3, 6, and 9.1 m (10, 20, and 30 ft) beyond the pavement edge. At each of these three distances, three different boundary conditions were tested: free, roller, and fixed. Vertical deflections at the center of the load from the nine runs were then compared (Figure 1). The finding that the response is virtually unaffected by a boundary beyond 9.1 m (30 ft) from the load has led to the adoption of a roller-type lateral boundary ($U_x = 0$, $U_y = 0$, $U_z \neq 0$) at 9.1 m (30 ft) from the pavement edge. Three undoweled concrete slabs, each 6.1 m (20 ft) long, were modeled in the direction of traffic. Introduction of dowel bars requires substantial meshing, adding to the complexity of the problem. In order to focus on the specific objective of the study, dowel bars were not modeled.

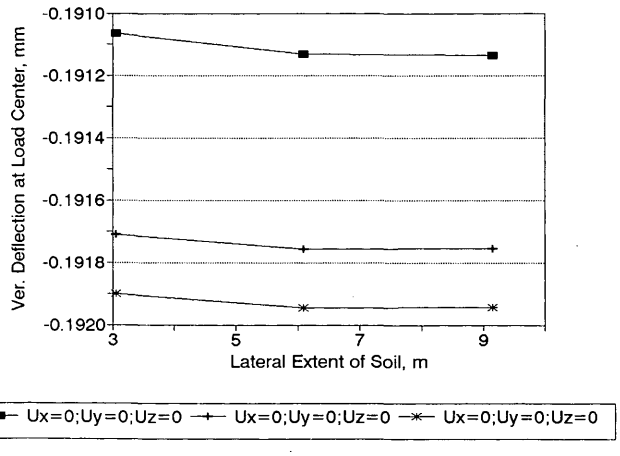

FIGURE 1 Effect of lateral soil extents and boundary conditions on deflection (1 mm = 39.37 mil; 1 m = 3.281 ft).

Pavement-Shoulder Interface

Because in the real world the proportion of concrete pavements having tied shoulders is relatively small, it was decided to model the pavement-shoulder interface as a discontinuity. That was accomplished by using special contact surface definitions provided in ABAQUS. In effect, the shoulder was not to provide any structural support to the pavement.

Material Characterization

Within the load range generally encountered in pavement design and analysis [standard 80-kN (18-kip) equivalent single axle load (ESAL)], stresses induced in each layer are not likely to exceed their respective elastic ranges. Elastic analysis is implemented accordingly.

Mesh Fineness and Element Aspect Ratio

One of the major precepts of finite element theory is to provide a finer mesh around areas of stress concentration than within the surrounding medium. Therefore, a fine uniform mesh with an element size of 75 mm (2.95 in.) was generated around the loaded area, and a nonuniform mesh with suitable "bias" factors was generated in the rest of the continuum. The biased mesh generation ensures a gradual change in the mesh size, with smaller elements in the vicinity and larger elements away from the load. Because three-dimensional linear elements were used, large elements away from the load helped to provide "quite" boundaries. The aspect ratio of the elements in the loaded area was kept below 2 for better precision. The surface layer was modeled as two sublayers (elements), the base and subbase were each modeled as a single element, and the subgrade was partitioned into five elements. By taking advantage of the symmetry afforded by the load placement, one-half or one-quarter of the problem was solved.

FWD Loading

Except for the static load comparison, for which an F-15 single wheel load was used, FWD loading was used for all other analyses. An FWD can simulate various load magnitudes; a peak load of 43 kN (9,670 lb) was adopted in this study. A finite element idealization of a typical load history (*11*) is presented in Figure 2, which indicates that the loading duration is about 25 msec. At 638 kPa (92.61 psi) contact pressure, the loaded area, assumed circular, is calculated to be 705 cm^2 (109.35 $in.^2$). The distributed circular loaded area is approximated using 12 square elements, each having a side length of 75 mm (2.95 in.). The 43-kN (9,670-lb) load is centered at the midsection of the slab, 3 ft from the edge of the pavement. Nodes are defined at various distances to match the location of the geophones measuring surface deflections for the FWD test. Figure 3 represents the final mesh configuration.

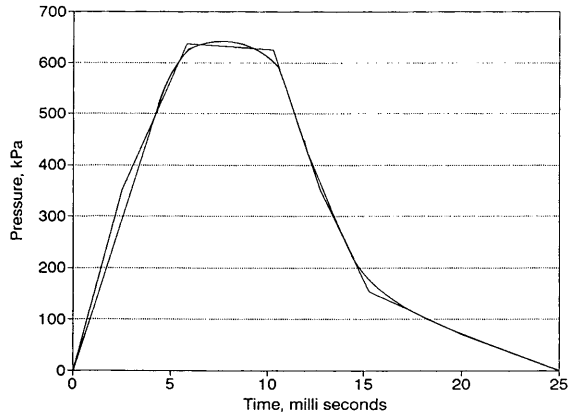

FIGURE 2 FWD load pulse simulated in the 3D-DFEM analysis (1 kPa = 0.145 psi).

As suggested by one of the reviewers, the authors have used the SHRP-FWD load pulse in the analysis (personal communication, Cheryl Richter, LTPP Division, FHWA; unpublished data). The average increase in deflection response with this pulse in weak pavements was 6.5 percent.

FEASIBILITY STUDIES OF ABAQUS

Validation of Static Analysis

In order to validate the analysis procedure of the 3D-DFEM, the authors configured and solved Ioannides and Donnelly's (*7*) slab-on-grade problem, which involves a slab on soft subgrade. Closed-form solutions are drawn from Losberg (*12*) with BISAR (*13*) and ILLISLAB (*5,6*) providing the layer elastic solutions. A finite element solution using the GEOSYS model (Table 1) with slightly different slab thickness is included for want of a better three-dimensional model. A single wheel load of an F-15 aircraft with a tire pressure of 2446 kPa (355 psi) and a total load of 133 kN (30 kips) was placed centrally on a slab-on-grade system. All of the materials were characterized as linear elastic. The continuum was modeled using eight noded, isoparametric, three-dimensional brick elements. Because of the symmetry of the model, only one-quarter of the slab was modeled. Table 1 presents a comparison of various solutions along with other pertinent details. The ABAQUS solution shows good agreement with BISAR, ILLISLAB, and closed-form solutions.

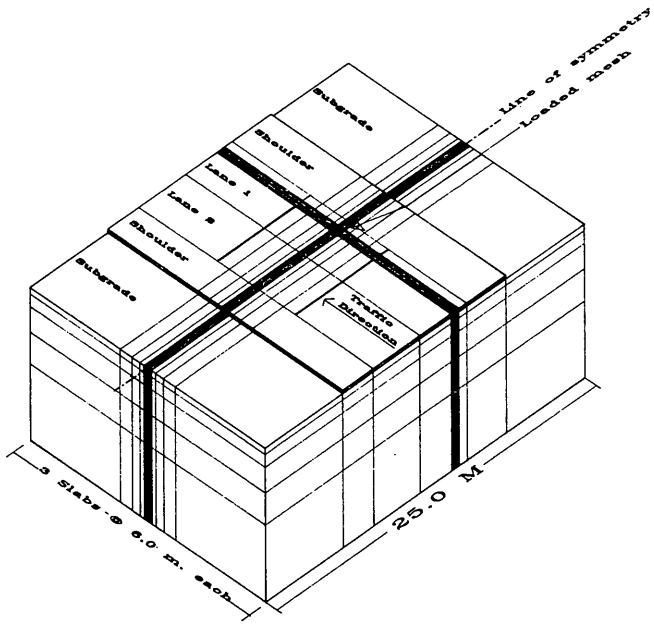

FIGURE 3 3D-DFEM problem showing partial mesh configuration (1 m = 3.281 ft).

Validation of Dynamic Load (FWD) Analysis

To verify the validity of the 3D-DFEM results, a theoretical analysis was performed on a typical in-service flexible pavement section. The pavement section originally was studied by Hoffman and Thompson (*14*) and later by Sebaaly et al. (*2*). Material properties were determined in the laboratory (*14*), except Poisson's ratios, which were assumed. Table 2 gives the material and geometric properties. The 3D-DFEM results are compared with the reported FWD measurements and the elastodynamic solution using the multilayer computer program DYNAMIC (*2*). Also included in this comparison is a static deflection basin using the DYNAMIC program with zero frequency load (or equivalent static solution).

The FWD used in field testing and simulated in the 3D-DFEM has a 30-cm (12-in.) diameter base plate; an impulse load of 36 kN (8 kips) was produced with a load duration of approximately 40 msec. The center of the load is at midsection, a distance of 910 mm (3 ft) from the edge of the pavement. The distributed loaded area is approximated using 12 square elements with 75-mm (2.95-in.) sides.

Measured and computed deflections at four geophone locations are compared in Figure 4. The 3D-DFEM deflections are reasonably close to the measured deflections; deviations are 5, 2, 9, and 34 percentage points at geophone locations 1, 2, 3, and 4, respectively (measured responses). Similar validation studies conducted by Zaghloul et al. (*10*) conclude that ABAQUS is indeed a feasible tool with which to perform nonlinear dynamic analysis of flexible pavements. The relatively large discrepancy at the fourth sensor may be attributable to the noise effect of reflected waves from the boundary. A new release of the 3D-DFEM (Version 5.2) provides an "infinite element" for modeling boundary by choosing suitable damping constants to minimize the reflection of dilatational and sheer-wave energy back into the model.

The fact that the 3D-DFEM results and nonlinear elastodynamic responses are in agreement is another indication that, for routine modeling, elastic characterization is adequate unless the pavement materials are extremely soft.

As pointed out in previously (*2*) and confirmed in this study, static analysis (as with BISAR) yields average deflection values approximately 25 to 30 percent higher than those obtained with 3D-DFEM on elastodynamic analysis.

TABLE 1 Comparison of Static Analysis Results (All Responses Measured at Center of Load)

RESPONSE	POSITION	ANALYSIS MODEL				
		Closed-form	ABAQUS-3D	BISAR	ILLISLAB-2D	GEOSYS*-3D
Vertical Deflection (mm)	Top of slab @ load center	1.07	1.04	1.02	1.04	0.82
Vertical stress (kPa)	Top of subgrade under the load	-45.6	-40.9	-44.9	-42.4	-34.7
Maximum bending Stress (kPa)	Bottom of slab under the load	5230	5121	5216	5483	4200

*The results from the GEOSYS model were based on a slab 203mm (8 inches) thick, whereas, the results from other models were based on a slab 183mm (7.2 inches), thick.

1mm = 0.039 inches; 1 kPa = 0.145 psi; 1 kip = 4.45 kN

Details:

E = 27.56 GPa Poisson's ratio = 0.15
E_S = 52.9 MPa Poisson's ratio = 0.45
Slab : 4.57m x 4.57m

TABLE 2 Material and Geometric Properties of Flexible Pavement at Sherrard Section (*2*)

Layer	Material	Layer Thickness, mm	Young's Modulus, MPa	Poisson's Ratio	Density, kN/m^3
Surface	Asphalt Concrete	102	3445	0.35	22.7
Base	Crushed stone	356	241	0.40	22.0
Subgrade	A-4(6)	18288	69	0.45	18.0

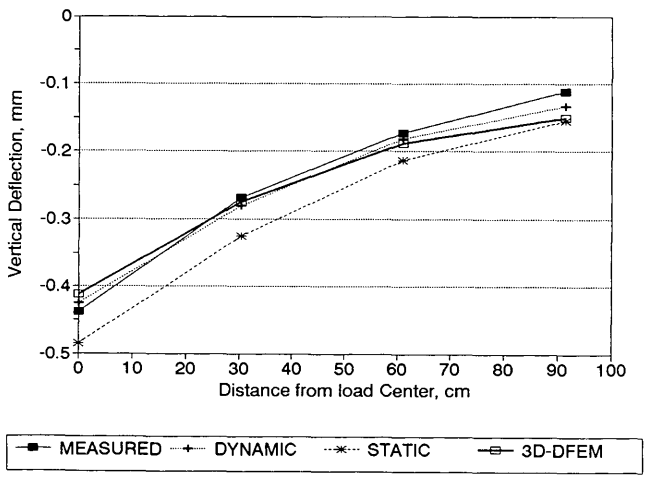

FIGURE 4 Measured, dynamic, static, and 3D-DFEM deflections at various distances for Sherrard section (1 mm = 39.37 mil; 1 cm = 0.393 in.).

STATISTICAL MODELS FOR DYNAMIC RESPONSE PREDICTION

Fractional Factorial Design

An experiment was designed to study the effect of layer thicknesses and moduli on pavement response. The following factors at various levels were considered in the factorial design:

- Surface layer (portland cement concrete) thickness (three levels),
- Base thickness (two levels),
- Subbase thickness (two levels),
- Concrete modulus (two levels),
- Base modulus (three levels),
- Subbase modulus (two levels),
- Subgrade modulus (three levels), and
- Pavement condition (three levels).

Table 3 gives the thickness and pavement moduli that were adopted for this study. The values are based on engineering judg-

TABLE 3 Attribute Values Used in Factorial Design

Factor	Number of levels		
	Level 1	Level 2	Level 3
Modulus of Surface layer, GPa (ksi)	20.7 (3000)	41.1 (6000)	-*
Modulus of base layer, GPa (ksi)	0.1 (15)	1.7 (250)	13.8 (2000)
Modulus of subbase layer, MPa (ksi)	69 (10)	170.0 (25)	-
Modulus of subgrade, MPa (ksi)	21 (3)	103 (15)	310 (45)
Thickness of surface layer, mm (in.)	203 (8)	254 (10)	330 (13)
Thickness of base layer, mm (in.)	102 (4)	203 (8)	-
Thickness of subbase layer, mm (in.)	0 (no subbase)	23 (8)	-

*Data not applicable

ment and experience. The number of levels attributed to each factor represents its full range of practical applications. To be of general use, different pavement condition scenarios need to be investigated, for example, both pavements in good condition with no discontinuity and, the other extreme, pavement in which the transverse joints have failed, resulting in voids at the joint. However, the present study concerns the first level only, that is, pavement in good condition.

Combinatorial design procedures were employed to assemble the experiment. A total of 1,296 combinations ($2^4 3^4$) were possible. Because it is prohibitively expensive to perform so many computational runs, a fractional factorial was adopted after Connor and Young (*15*). A one-eighth fraction replicate of the full factorial was selected for the study. For each combination, a response solution was obtained using 3D-DFEM, with the boundary conditions, material characterization, and FWD loading described earlier. The computations were performed on a Cray X-MP/16 supercomputer, and the desired responses (deflection, for instance) from each combination were stored in a data base for subsequent analysis.

Models for Deflection

Using the deflection data base, stepwise regression analyses were carried out developing statistical models for surface deflections at each geophone location of the FWD test setup. A SAS program was used for the analysis. For routine testing, many agencies, including SHRP, employ seven geophones, one at the center of the load and the remaining six at offset distances of 203, 305, 457, 610, 915, and 1,524 mm (8, 12, 18, 24, 36, and 60 in.), respectively. Two sets of seven model equations, one set for three-layer pavements and the other for four-layer pavements, are presented in Equations 1–14. The corresponding coefficients and R^2 values are listed in Table 4.

Equations for three-layer pavements:

$$D1 = A + B*\log_{10}E_4 + C*T_1 + D*T_2 + E*\log_{10}E_1*T_1 + F*\log_{10}E_2*T_2 \quad (1)$$

$$D2 = A + B*\log_{10}E_4 + C*T_1 + D*T_2 + E*\log_{10}E_1*T_1 + F*\log_{10}E_2*T_2 \quad (2)$$

$$D3 = A + B*\log_{10}E_4 + C*T_1 + E*\log_{10}E_1*T_1 + F*\log_{10}E_2*T_2 + G*\log_{10}E_1*\log_{10}E_2 + H*\log_{10}E_2*\log_{10}E_4 \quad (3)$$

$$D4 = A + B*\log_{10}E_4 + C*T_1 + E*\log_{10}E_1*T_1 + F*\log_{10}E_2*T_2 + G*\log_{10}E_1*\log_{10}E_2 + H*\log_{10}E_2*\log_{10}E_4 \quad (4)$$

$$D5 = A + B*\log_{10}E_4 + C*T_1 + E*\log_{10}E_1*T_1 + F*\log_{10}E_2*T_2 + G*\log_{10}E_1*\log_{10}E_2 + H*\log_{10}E_2*\log_{10}E_4 \quad (5)$$

$$D6 = A + B*\log_{10}E_4 + C*T_1 + E*\log_{10}E_1*T_1 + F*\log_{10}E_2*T_2 + G*\log_{10}E_1*\log_{10}E_2 + H*\log_{10}E_2*\log_{10}E_4 \quad (6)$$

$$D7 = A + B*\log_{10}E_4 + C*T_1 + D*T_2 + E*\log_{10}E_1*T_1 + F*\log_{10}E_2*T_2 + G*\log_{10}E_1*\log_{10}E_2 + H*\log_{10}E_2*\log_{10}E_4 \quad (7)$$

Equations for four-layer pavements:

$$D1 = A + B*\log_{10}E_1 + C*\log_{10}E_2 + D*\log_{10}E_4 + E*\log_{10}E_1*T_1 + F*\log_{10}E_2*T_2 + G*\log_{10}E_3*T_3 \quad (8)$$

$$D2 = A + B*\log_{10}E_1 + C*\log_{10}E_2 + D*\log_{10}E_4 + E*\log_{10}E_1*T_1 + F*\log_{10}E_2*T_2 + G*\log_{10}E_3*T_3 \quad (9)$$

TABLE 4 Summary of Regression Models for Three- and Four-Layer Pavements

Equation*	A	B	C	D	E	F	G	H	R^2-Value
1	8.6370	-2.1927	0.5499	0.1546	-0.2105	-0.0861	-**	-	0.9574
2	8.3554	-2.2848	0.4652	0.1433	-0.1824	-0.0785	-	-	0.9601
3	9.6629	-2.8505	0.3645	-	-0.1530	-0.0210	-0.1588	0.2175	0.9618
4	9.1665	-2.9167	0.3331	-	-0.1369	-0.0180	-0.1543	0.2401	0.9683
5	8.6785	-2.9514	0.3070	-	-0.1235	-0.0166	-0.1446	0.2546	0.9733
6	7.8922	-3.0162	0.2526	-	-0.1017	-0.0136	-0.1236	0.2477	0.9722
7	6.5106	-2.8653	0.1540	-0.0243	-0.0612	-	-0.1062	0.2072	0.9851
8	16.5614	-1.8386	-0.4273	-1.9043	-0.0563	-0.0321	-0.0769	-	0.9374
9	15.7317	-1.7182	-0.4303	-2.0004	-0.0452	-0.0279	-0.0944	-	0.9518
10	14.1212	-1.3992	-0.3976	-1.9930	-0.0424	-0.0244	-0.0859	-	0.9571
11	13.0566	-1.2514	-0.3704	-2.0168	-0.0351	-0.0197	-0.0893	-	0.9625
12	11.8815	-1.0759	-0.3394	-2.0295	-0.0284	-0.0151	-0.0920	-	0.9684
13	9.7651	-0.7922	-0.3242	-1.9254	-0.0180	-	-0.0944	-	0.9719
14	6.3211	-0.3994	-0.1686	-1.6979	-0.0054	-	-	-0.4973	0.9801

*Equations 1 through 7 are for three layered pavement systems and equations 8 through 14 are for four layered pavement systems.

**Data not applicable

$$D3 = A + B*\log_{10}E_1 + C*\log_{10}E_2 + D*\log_{10}E_4 + E*\log_{10}E_1*T_1 + F*\log_{10}E_2*T_2 + G*\log_{10}E_3*T_3 \quad (10)$$

$$D4 = A + B*\log_{10}E_1 + C*\log_{10}E_2 + D*\log_{10}E_4 + E*\log_{10}E_1*T_1 + F*\log_{10}E_2*T_2 + G*\log_{10}E_3*T_3 \quad (11)$$

$$D5 = A + B*\log_{10}E_1 + C*\log_{10}E_2 + D*\log_{10}E_4 + E*\log_{10}E_1*T_1 + F*\log_{10}E_2*T_2 + G*\log_{10}E_3*T_3 \quad (12)$$

$$D6 = A + B*\log_{10}E_1 + C*\log_{10}E_2 + D*\log_{10}E_4 + E*\log_{10}E_1*T_1 + G*\log_{10}E_3*T_3 \quad (13)$$

$$D7 = A + B*\log_{10}E_1 + C*\log_{10}E_2 + D*\log_{10}E_4 + E*\log_{10}E_1*T_1 + H*\log_{10}E_3 \quad (14)$$

where

$D_1, D_2, ..., D_7$ = sensor deflections 1, 2, ..., 7, respectively (mil);
E_i = modulus of ith layer (ksi), counting from surface to subgrade;
i = 1, 2, 3, 4;
T_i = thickness of ith layer (in.); and
$A, ..., H$ = regression coefficients (Table 4).

Note that the significance of the regression coefficients is evaluated using the respective t-ratios, a standard output of the SAS program. If the absolute value of the t-ratio is 2.0 or greater, the coefficient is considered reliable. On this basis, the coefficients of Equations 1–14 are highly significant. As can be noted from Table 4, the R^2 values range from 0.93 to 0.98 and are considered satisfactory.

In order to further confirm the robustness of the equations, standardized residuals are plotted against the predicted values to see whether they are distributed randomly. All 14 of the plots exhibited a random pattern, indicating the models' adequacy.

The sensitivity of the parameters was judged by the t-ratio, the premise being that the higher the t-ratio the greater the influence of that factor in the given relationship. As expected, the subgrade modulus influences the sixth and seventh sensor deflections significantly. For the other five sensor locations, again, subgrade modulus has the most influence on surface deflection.

Verification of Deflection Models

Models can be validated by comparing predicted and measured responses. Selected for comparison are three rigid pavement GPS sections of SHRP-LTPP from Mississippi. Table 5 indicates the layer thickness and elastic properties of two of these sections: one three-layer section and one four-layer section. The concrete moduli and the FWD deflection data were assembled from the SHRP data base, whereas the subgrade moduli were furnished by the SHRP regional contractor through the research division at the Mississippi DOT. For want of accurate information, the base and subbase moduli were estimated on the basis of laboratory results (*16*). Adopting these properties and inputting them into Equations 1–7 for three-layer sections and into Equations 7–14 for four-layer sections, the authors calculated seven sensor deflections for the two cases. In Figure 5, the predicted deflection basin is compared with the measured FWD basin for three-layer pavement. Also

TABLE 5 Layer Thicknesses and Properties of SHRP Sections Used for Comparisons of Deflection Bowls

Layer Properties	Three Layer Section (SHRP Sec. No 285803)	Four Layer Section (SHRP Sec. No. 285805)
Thickness of Surface Layer, mm (in.)	203 (8)	203 (8)
Thickness of Base Layer, mm (in.)	152 (6)	102 (4)
Thickness of Subbase Layer, mm (in.)	-*	178 (7)
Modulus of Surface Layer, GPa (ksi)	32.1 (4650)	39.0 (5650)
Modulus of Base Layer, GPa (ksi)	11.7 (1700)	3.5 (500)
Modulus of Subbase Layer, MPa (ksi)	-	137.6 (20)
Modulus of Subgrade, MPa (ksi)	81.7 (11.87)	75.6 (10.99)

*Data not applicable

plotted are deflection basins from direct solution of the 3D-DFEM and the multilayered elastic program BISAR. The predictions for the first five sensor locations are within ±5 percent of the field deflections, whereas the sixth and seventh sensors differ from the field deflections by 17 and 36 percentage points, respectively. Similar comparison of a four-layer system (Figure 6) indicates that predicted deflections consistently are larger than the measured ones, the average error being less than 15 percent. One factor contributing to this discrepancy may be the one-eighth factorial selected for the study; it may be insufficient to account for all interactive effects that arise in the model. Other reasons for the discrepancy may include the need for realistic (viscoelastic) characterization of subgrade and base layers, and the approximate moduli adopted for base and subbase. Static analysis, in both cases, overpredicts the field deflections by as much as 80 percent, however. Due in part to the discrepancy between dynamic and static deflections, the traditional backcalculation procedures, (in which the objective is to match the dynamic load basins with static deflections) would in all likelihood overpredict the layer moduli. This strongly suggests the need for employing dynamic load representation for pavement analysis or response equations—a much needed revision in backcalculation routines.

SUMMARY AND CONCLUSIONS

To improve on the current pavement analysis procedure, a 3D-DFEM was formalized. The 3D-DFEM can simulate moving or impulse loads and linear and nonlinear material properties. Response analysis with various boundary conditions and element aspect ratios helped to finalize an appropriate model geometry that was later used to model rigid pavements. An investigation was conducted with 3D-DFEM, establishing the model's validity in solving static and, more importantly, dynamic problems.

A one-eighth fractional factorial experiment was designed on the basis of pavement response to FWD loading (deflection, for instance) as a function of pavement geometry and material characteristics. Statistically significant equations were developed and the data base generated from computer models of 54 different combinations. The equations, in turn, were validated by predicting the measured deflections of two in-service rigid pavements. The average error resulting at each sensor location from the predictions was less than 15 percent. Significant to note, however, was that static deflections were larger than their dynamic counterparts. Larger apparent deflection response could result in overprediction

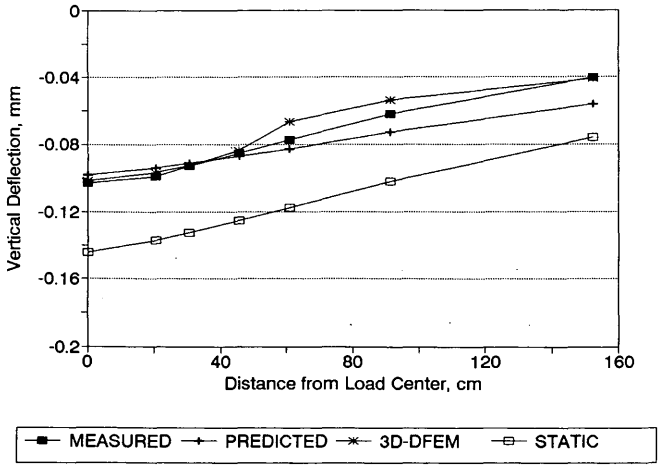

FIGURE 5 Measured, predicted, 3D-DFEM, and static deflections at various distances for SHRP Section 285803, SHRP FWD Test No. 300267 (1 mm = 39.37 mil; 1 cm = 0.393 in.).

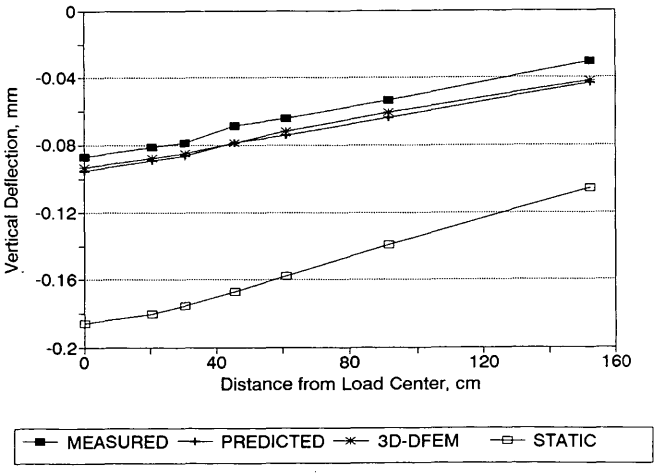

FIGURE 6 Measured, predicted, 3D-DFEM, and static deflections at various distances for SHRP Sec. 285805, SHRP FWD Test No. 300151 (1 mm = 39.37 mil; 1 cm = 0.393 in.).

of layer moduli in backcalculation algorithms. In short, static response analysis, traditionally employed in backcalculation algorithms, should be replaced with dynamic analysis routines. The 3D-DFEM program, with its numerous features simulating real-world pavement loading, is a needed tool for analyzing the response of flexible- and rigid-pavement structures.

ACKNOWLEDGMENTS

Alfred Crawley of the Mississippi DOT told the authors of a preliminary study to model a rigid pavement in Mississippi that had sustained premature cracking. Waheed Uddin and Robert Hackett of the Department of Civil Engineering, University of Mississippi, contributed immensely to adapting ABAQUS for rigid pavement analysis. The study was supported in part by the Department of Civil Engineering, in cooperation with the Office of Computing and Information Systems, of the university.

REFERENCES

1. Mamlouk, M. S. Use of Dynamic Analysis in Predicting Field Multilayer Pavement Moduli. In *Transportation Research Record 1043*, TRB, National Research Council, Washington, D.C., 1985, pp. 113–121.
2. Sebaaly, B. E., M. S. Mamlouk, and T. G. Davies. Dynamic Analysis of Falling Weight Deflectometer Data. In *Transportation Research Record 1070*, TRB, National Research Council, Washington, D.C., 1986, pp. 63–68.
3. Ashton, J. E., and F. Moavenzadeh. The Analysis of Stresses and Displacements in a Three-Layered Viscoelastic System. *Proc., International Conference, Structural Design of Asphalt Pavements*, 1967.
4. Ioannides, A. M. Finite Difference Solution for Plate on Elastic Solid. *Journal of Transportation Engineering*, Vol. 114, No. 1, ASCE, New York, Jan. 1988, pp. 57–75.
5. Ioannides, A. M. *Analysis of Slabs-on-Grade for a Variety of Loading and Support Conditions*. Report TR-85-0083. U.S. Air Force Office of Scientific Research, Air Force Systems Command, U.S. Air Force, Washington, D.C., Sept. 1984.
6. Ioannides, A. M., M. R. Thompson, and E. J. Barenberg. Finite Element Analysis of Slabs-on-Grade Using a Variety of Support Models. *Proc., Third International Conference on Concrete Pavement Design and Rehabilitation*, Purdue University, West Lafayette, Ind., April 1985, pp. 309–324.
7. Ioannides, A. M., and J. P. Donnelley. Three-Dimensional Analysis of Slab on Stress-Dependent Foundation. In *Transportation Research Record 1196*, TRB, National Research Council, Washington, D.C., 1988.
8. *ABAQUS, Finite Element Computer Program*. Hibbit, Karlsson, Sorenson, Inc., 1989.
9. Zaghlou, S., and T. D. White. Use of a Three-Dimensional-Dynamic Finite Element Program for Analysis of Flexible Pavement. In *Transportation Research Record No. 1388*, TRB, National Research Council, Washington, D.C., 1993, pp. 60–69.
10. Zaghloul, S., T. D. White, V. P. Drnevich, and B. Coree. Dynamic Analysis of FWD Loading and Pavement Response Using a Three-Dimensional Dynamic Finite Element Program. In *Nondestructive Testing of Pavements and Backcalculation of Moduli*, Vol. 2. STP 1198, ASTM, Philadelphia, Pa., 1994.
11. Bohn, A., P. Ullidtz, R. Stubstad, and A. Sorensen. Danish Experiments with the French Falling Weight Deflectometer. *Proc., 3rd International Conference on the Structural Design of Asphalt Pavements*, London, England, Sept. 11–15, 1972, pp. 1119–1128.
12. Losberg, A. *Structurally Reinforced Concrete Pavements*. Doktrsavhandlingar Vid Chalmers Tekniska Hogskola, Göteborg, Sweden, 1960.
13. *Bitumen Structures Analysis In Roads (BISAR) Computer Program*. Koninlilijke/Shell-Laboratorium, Amsterdam, Netherlands, July 1972.
14. Hoffman, M. S., and M. R. Thompson. *Nondestructive Testing of Flexible Pavements: Field Testing Program Summary*. Transportation Engineering Series 31, Illinois Cooperative Highway and Transportation Research Program, Series 188. University of Illinois at Urbana Champaign, Urbana, June 1981.
15. Connor, W. S., and S. Young. *Fractional Factorial Designs for Experiments with Factors at Two and Three Levels*. National Bureau of Standards, Applied Mathematics Series-58. Sept. 1961.
16. George, K. P. *Material Parameters for Pavement Design Using AASHTO Interim Guide*. Final Report. Department of Civil Engineering, University of Mississippi, University, 1981.

The opinions, findings, and conclusions expressed in this report are those of the authors and not necessarily those of the sponsoring organizations.

Publication of this paper sponsored by Committee on Modeling Techniques in Geomechanics.

Finite Element Simulation of Pavement Discontinuities and Dynamic Load Response

WAHEED UDDIN, DINGMING ZHANG, AND FRANCISCO FERNANDEZ

Assumption of a linear elastic system under static loading is questionable for structural response analysis of pavement-subgrade systems under dynamic nondestructive testing and moving wheel loads, especially if a deteriorated pavement is under study. Presented are the results of a parametric study using the three-dimensional finite element ABAQUS code; it investigates the effects of pavement discontinuities and dynamic analysis on the surface deflection response of a pavement-subgrade model under a standard falling-weight deflectometer (FWD) load. An optimum three-dimensional pavement subgrade model of a 18.3-m (60-ft) pavement length was established with a fixed boundary at the bottom and roller supports on the sides. ABAQUS static deflections are in good agreement with the static deflections calculated from the traditional elastic layer analysis for an uncracked pavement. The ABAQUS dynamic response using the backcalculated nonlinear moduli compares reasonably with the measured FWD deflections on an asphalt pavement site. The ABAQUS special-purpose gap elements are used to simulate longitudinal and transverse cracks in the surface layer. Dynamic deflections are 17 percent higher for a pavement with longitudinal cracks as compared with an uncracked pavement.

The current practice of using layered linear elastic theory for pavement-subgrade response analysis under static loading is a rational approach compared with older empirical pavement design methods, and the approach works reasonably well if a pavement-subgrade system behaves as a linear elastic system (*1*). However, the predicted linear elastic response can differ significantly from measured deflections under dynamic loading if the pavement-subgrade system has deteriorated, as is indicated by cracking and other pavement distresses, and if nonlinear behavior is expected from the unbound granular pavement layers and subgrade.

The results of finite element simulation of pavement discontinuities and dynamic loading are presented and selected results are compared with the measured deflection data.

BACKGROUND

Traditional Static Analysis of Pavement-Subgrade System

Pavement deflection response traditionally has been analyzed using the multilayered linear elastic model under static load (*1*) to calculate the in situ Young's modulus of elasticity for each layer in the pavement-subgrade system. In the layered linear elastic model of a pavement (Figure 1), each layer can be characterized by its Young's modulus of elasticity, E, and Poisson's ratio, μ.

Department of Civil Engineering, University of Mississippi, University, Miss. 38677.

Reasonable values of the Poisson's ratio can be assumed for typical pavement materials; these generally fall within a narrow range. Then assuming a semiinfinite subgrade, unique values of surface deflections can be predicted theoretically at specified distances from the load. Pavement nondestructive testing (NDT) and evaluation is performed by measuring surface deflections under a known NDT dynamic load. The backcalculation procedure involves an iterative application of the multilayered elastic theory to calculate the in situ modulus of each pavement layer. Surface deflections are predicted using assumed values of the modulus and Poisson's ratio of the pavement layers. Calculated surface deflections are matched with the measured deflections until the percentage of error is reduced to the lowest value (*1,2*). The test load is simulated by an equivalent static load, and the following assumptions are made:

- The existing pavement is considered to be a multilayered linear elastic system. Therefore, the principle of superposition is valid for calculating the response related to more than one load (e.g., for Dynaflect and design wheel loads).
- The peak dynamic force of the FWD is assumed to be equal to a pseudostatic load uniformly distributed on a circular area represented by the FWD loading plate.
- Gravity stresses are neglected.
- Effects of static trailer weight on the response of the pavement-subgrade system also are ignored. Considering the light

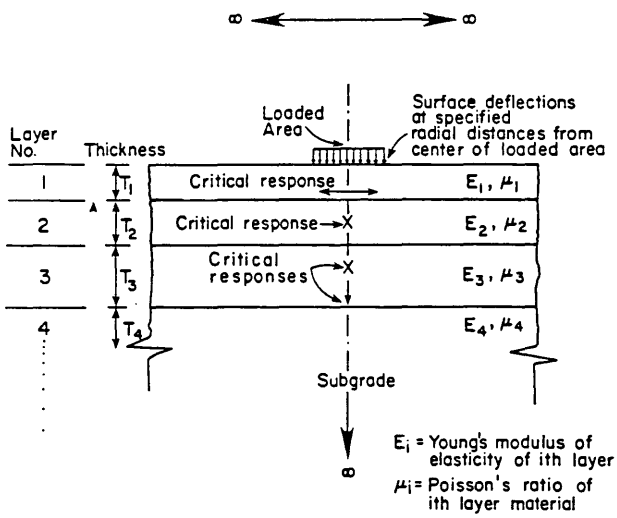

FIGURE 1 Linear elastic system.

static weights of these trailers and the measurement of only dynamic deflections, this is not an unreasonable assumption.

- The subgrade is characterized by an average modulus value. Whereas subgrade stiffness may vary with depth, below 20 to 30 ft, stresses and strains resulting from the test load are very small, and design procedures require only a single value for the Young's modulus of elasticity of the subgrade.
- Deflections are measured at locations away from the pavement edges and discontinuities such as cracks and joints.

If these assumptions are true, the linear elastic response of the pavement will be reasonable in the absence of pavement discontinuities and strongly nonlinear materials. However, the assumptions clearly are violated if a pavement has deteriorated or if granulary layers and subgrade exhibit nonlinear behavior; such conditions lead to adverse effects of dynamic loading.

Pavement Discontinuities

Typical discontinuities in asphalt and portland cement concrete pavements are presented in Figure 2. Discontinuities appear in asphalt pavements as longitudinal, transverse, and alligator cracks; potholes; and disintegration. Cracks are caused by fatigue or load repetitions, by environmental factors, or by the interaction of the two. Cracks, joints, and voids under concrete pavements caused by pumping and erosion of subbase and base materials are additional examples of pavement discontinuities that significantly affect pavement deflection response.

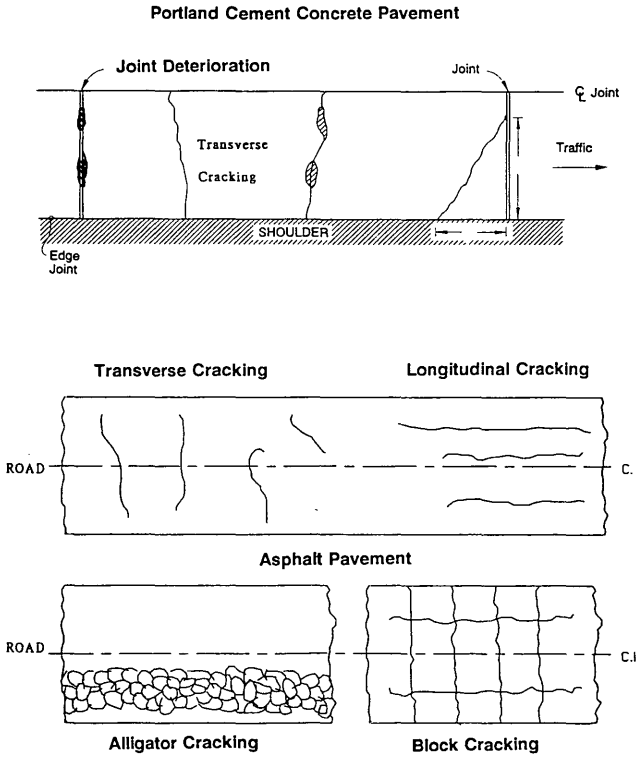

FIGURE 2 Typical pavement discontinuities.

Finite Element Analysis Approach

The traditional approach of pavement structural analysis is based on static linear elastic formulation with infinite dimensions in the horizontal plane and semiinfinite subgrade; however, it does not allow analysis of dynamic loads and discontinuities. In contrast, the finite element method analyzes pavements by considering finite dimensions of physical pavement structure. Concrete pavement joints and voids underneath the pavement have been modeled by the SLAB49 discrete element program (*3*). More recently, finite element models have been developed specially for pavement analysis, for example, ILLIPAVE for flexible pavements and ILLISLAB for rigid pavements (*4,5*). These models have been used for static load analysis.

Three-dimensional finite element codes (for example, ABAQUS) are available for comprehensive pavement structural response analysis that considers static and dynamic loads (impulse, steady-state vibratory force, and moving wheel load), linear elastic as well as nonlinear elastic and viscoelastic material constitutive models, and crack simulation models (*6,7*). Zaghloul and White (*8*) have successfully used ABAQUS for dynamic analysis of uncracked flexible pavements.

THREE-DIMENSIONAL FINITE ELEMENT SIMULATION

Basic Principles

The finite element method allows evaluation of the state of stresses and strains in a continuum medium by transforming the continuum medium into a number of finite elements. The three-dimensional finite elements must be interconnected at their common borders. Polynomial functions are used to interpolate the displacement field in order to obtain the stiffness matrix of each element. Using the stiffness matrix of each element, it is possible to assemble the global stiffness matrix as well as the global mass matrix for the complete model. Dynamic loads are considered, and displacements (dynamic deflections) are calculated using the appropriate routines and solving the dynamic governing equations. Finally, strains and stresses at each node of the elements are calculated.

ABAQUS Finite Element Code

ABAQUS software (*6*) is a comprehensive finite element program used to solve two- or three-dimensional problems under static, harmonic, transient dynamic loading, and thermal gradient conditions. Layer material can be modeled as linear elastic, nonlinear elastic, viscoelastic, and modified elastic (allowing no tension layers). The program can analyze cracks, voids, and the effects of water penetration in cracks. Simulation of the above parameters leads to a better understanding of pavement performance and estimation of loss of support over the pavement's life.

Optimization of Pavement-Subgrade Model Parameters

A three-dimensional finite element model was developed in order to optimize the size and boundary conditions of a pavement-

subgrade structure. The model was formed with different lengths, widths, and subgrade depths as well as different boundary conditions. After analysis of the above parameters, the optimum dimensions and boundary conditions were established by carrying out the following analyses:

- Optimum subgrade thickness was investigated by studying the effect of different depths on surface deflections, and it was found that 12.20 m (40 ft) of subgrade depth simulates a semiinfinite subgrade.
- Nodes at the bottom of the model were fixed and a study was made with free, fixed, and roller boundary conditions of nodes in the sides of the model. It was found that the best simulation response is obtained by using rollers in the lateral sides of the model.
- Optimum subgrade width was found by studying the lateral extent of the subgrade below the pavement. The optimum dimensions are 11 m (36 ft) from the right (outside) edge and 8.3 m (27.3 ft) from the left (inside) edge of the pavement. The total width of the subgrade is 26.6 m (87.3 ft).
- To determine the optimum pavement length, lengths varying from 12.2 m (40 ft) to 73.2 m (240 ft) were studied; it was found that the optimum length is 18.3 m (60 ft).
- Shoulders (with the same material properties as the granular base layer) were added in the model. Shoulders were considered discontinuous along the pavement edges and gap elements were used, as described later. The outside shoulder is 2.4 m (8 ft), and the inside shoulder is 1.2 m (4 ft). Maximum deflection under the FWD load for the pavement with shoulders decreased by 1 percent. Discontinuous shoulders were subjected to further analysis, as reported in this paper.

ABAQUS Finite Element Model for Uncracked Pavements

The optimized pavement-subgrade model's boundary conditions were as follows: fixed at the bottom with a roller supporting the lateral sides. The pavement was modeled as a three-layer elastic system. Material properties for each layer used in the analysis are provided in Table 1. The asphalt surface layer, base layer, and subgrade are modeled as linear elastic materials.

Falling-weight deflectometer (FWD) loading is considered in the analysis. The center of the load is located at a distance of 0.91 m (3 ft) from the edge of the outside shoulder and along the center line of the pavement length.

Static Analysis

For the static analysis, the FWD load is taken as 40 kN (9,000 lbf) distributed on an area of 705.5 cm^2 (109.4 $in.^2$). Table 1 shows thickness and material properties for a flexible pavement structure used in the study. The Young's modulus of elasticity for each pavement layer and the subgrade were backcalculated from measured deflection data using the FPEDD1 program (*1*). Deflections were calculated using BISAR layered elastic static analysis and ABAQUS. Comparisons indicate a difference of 1 percent between the results of the two programs. The ABAQUS maximum static deflection was 998 μm (39.3 mils), which is in good agreement with the 985 μm (38.8 mils) calculated by the multilayer linear elastic program for a semiinfinite subgrade. That benchmark comparison establishes the adequacy of the geometry, mesh, and boundary conditions of the finite element model.

Dynamic Analysis

Dynamic analysis was performed using the ABAQUS IMPLICIT and EXPLICIT (*6,7*) approaches. The basic differences between the two approaches is that the IMPLICIT method computes the deflections at any time t by solving a set of nonlinear equations to determine the deflections at time $t - 1$. The EXPLICIT method, however, computes the deflections at any time t by adding to the deflection at time $t - 1$ the increment in deflections between time t and $t - 1$ computed by double integration of the acceleration obtained from dynamic equations at that degree of freedom. A comparison of the results indicates that the deflections obtained using IMPLICIT are closer to the static deflections and higher than the deflections obtained using EXPLICIT. Moreover, IMPLICIT generally converges better than does EXPLICIT. Therefore, the IMPLICIT method has been used for further dynamic analyses. Using the 18.3-m (60-ft) pavement model with discontinuous shoulders, the maximum deflection computed by IMPLICIT dynamic analysis was 817 μm (32.2 mils), which is 18 percent less than the corresponding ABAQUS static analysis.

TABLE 1 Pavement Subgrade Material Properties Used in Finite Element Analyses

Layer	Thickness mm (inches)	Poisson's Ratio	Young's Modulus kPa (psi)
AC Surface	114 (4.5)	0.35	2,928,250 (425,000)
Granular Base	152 (6.0)	0.45	199,810 (29,000)
Subgrade	12,192 (480.0)	0.45	34,450 (5,000)

Nonlinear Elastic Analysis and Field Validation

ABAQUS can be used with a variety of nonlinear material models for any layer. The current research study focuses on optimization of a three-dimensional pavement-subgrade model under dynamic loading by restricting to linear elastic material behavior for all layers. However, a preliminary study was undertaken to compare the measured FWD deflection response with the ABAQUS response and the nonlinear material behavior of the granular base and subgrade. Table 2 shows the backcalculated pavement moduli from the FWD deflection data and the nonlinear backcalculated moduli from the Dynaflect deflection data taken from a previous FHWA study (*9*). A measured FWD maximum deflection of 518 μm (20.4 mils) is reported for the selected test location.

The ABAQUS maximum static deflection under a simulated FWD load is 459 μm (18.1 mils) for the pavement-subgrade model analyzed with the FWD linear backcalculated moduli as compared with the 510-μm (20.1-mil) maximum static deflection calculated from the multilayered elastic analysis for a semiinfinite subgrade. The ABAQUS maximum static deflection is 873 μm (34.35 mils) for the pavement-subgrade model analyzed with the Dynaflect nonlinear backcalculated moduli. It is expected that the ABAQUS maximum dynamic deflection under the standard FWD load will be less than the corresponding static deflection for the same pavement structure and material properties, as was discussed earlier.

The ABAQUS maximum deflection under the simulated FWD load and nonlinear backcalculated moduli is 585 μm (23.3 mils). For the FWD linear backcalculated moduli, the ABAQUS maximum dynamic deflection is 331 μm (13.2 mils). Figure 3 illustrates the ABAQUS dynamic deflection bowl under the simulated FWD load, linear, and nonlinear backcalculated moduli, as well as the measured FWD deflections. The measured deflections agree more closely with deflections calculated from the nonlinear moduli, which leads to the conclusion that nonlinear behavior of granular layers and subgrade also can contribute significantly to the pavement structural response analysis.

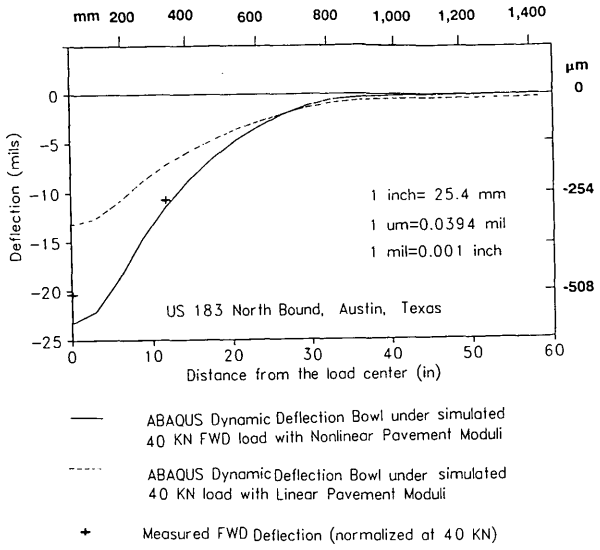

FIGURE 3 Comparison of ABAQUS dynamic deflection bowl with measured FWD deflections.

MODELING OF CRACKS

Longitudinal, transverse, alligator, and other types of cracks present critical pavement discontinuities in asphalt-surfaced pavements. Longitudinal and transverse cracks, joints, and voids beneath the concrete surface layer are the most critical discontinuities in portland cement concrete pavements. The structural response of a cracked pavement can be significantly different from that of an uncracked pavement. ABAQUS static and dynamic analyses were made to study the effect of cracks on pavement surface deflections.

Behavior of cracks in the pavement can be simulated using appropriate meshing and special-purpose elements. The present

TABLE 2 Pavement Structure and Backcalculated Young's Moduli from FHWA Study (*9*)

Layer	Thickness mm (inches)	Backcalculated Moduli, kPa (psi)	
		Texas FWD	Dynaflect
AC Surface	63.5 (2.5)	4388,930 (637,000)	1736,280 (252,000)
Granular Base	432 (17.0)	268,710 (39,000)	172,250 (25,000) *
Subgrade +	Semi-infinite	112,996 (16,400)	49,608 (7,200) *

* Moduli corrected for non-linear behavior.

\+ For the ABAQUS analysis, 12.2 meters (40 feet) subgrade was assumed.

study focuses on the simulation of longitudinal and transverse cracks. A crack is simulated in the model by having two independent nodes between continuous elements and being linked by special-purpose unidirectional gap elements known as GAPUNI. Gap elements allow two continuous surfaces to be either in or out of contact by simulating contact pressure and friction between the contacting surfaces.

The GAPUNI element is specified by two nodes separated by varying widths at the top and joined together at the bottom of two continuous elements. ABAQUS monitors the relative displacement of the two nodes of the element in the given direction. The arrangement results in two contact surfaces, A and B, which are separated by an initial selected gap width at the top. The GAPUNI element controls the interaction between Contact Surfaces A and B in such a way that these surfaces do not penetrate each other under any contact pressure. An appropriate value of the friction coefficient between Contact Surfaces A and B should be assumed in the analysis. A zero friction coefficient means that no shear force will develop and the contact surfaces are free to slide. A very large friction coefficient implies that the surfaces will lock and no sliding will occur. For this study, it is assumed that cracks are in the top asphalt layer under the loading plate.

STUDY OF CRACK GAP WIDTH

Figure 4(*a*) and (*b*) illustrate the finite element model configuration for 18.3-m (60-ft) pavement with shoulders and a longitudinal crack located 0.91 m (3 ft) from the outside pavement edge (under the central axis of the FWD load). The discontinuous shoulder was simulated by placing GAPUNI elements with a gap width of 0.51 mm (0.02 in.) and a zero friction coefficient.

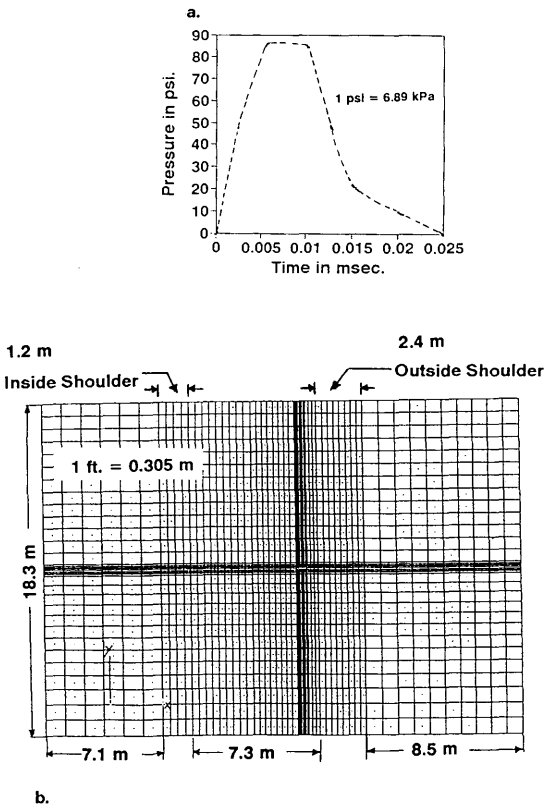

FIGURE 4 Finite element pavement subgrade model configuration for pavement crack study (*a*) FWD load pulse, (*b*) plan view of three-dimensional finite element model.

Longitudinal crack simulation in the asphalt layer initially was done by creating GAPUNI elements with a gap opening of 5.1 mm (0.2 in.) and assuming (*a*) a friction coefficient of 0.5 between the two contact surfaces of the GAPUNI element, and (*b*) a zero friction coefficient. Dynamic and static analyses were carried out, and it was observed that the effect of the friction coefficient on the calculated surface displacements is insignificant at the gap opening of 5.1 mm (0.2 in.), because the gap remained open throughout the analysis. When the gap opening was reduced to 2.5 mm (0.1 in.), 1.25 mm (0.05 in.), and 0.51 mm (0.02 in.), the effect of friction on the calculated surface displacements was still insignificant for the range of gap openings. When the gap was reduced to 0.25 mm (0.01 in.), the surface displacements were large enough to close the gap and therefore the effect of friction was significant. The study concluded that the critical gap opening is 0.25 mm (0.01 in.), at which point the friction coefficient is significant, as would be expected for a closely held crack on the pavement. A friction coefficient of 0.5 was assumed for crack simulation throughout the study.

CRACKED PAVEMENT RESPONSE

Longitudinal Cracked Pavement Response

Under Static Loads

In the cracked pavement model, a longitudinal crack in the asphalt layer in the outer wheel path was simulated using GAPUNI elements with a 0.25-mm (0.01-in.) gap opening and a friction coefficient of 0.5 between contact surfaces. Figure 5 shows a comparison of deflections in the pavement with cracking and without cracking; it is observed that the maximum static deflection in the cracked pavement is 1,162 μm (45.8 mils)—14 percent higher than that of the uncracked pavement. Figure 6 illustrates the deflection bowl caused by the FWD load in the 18.3-m (60-ft) pavement-subgrade model with shoulders using static analysis.

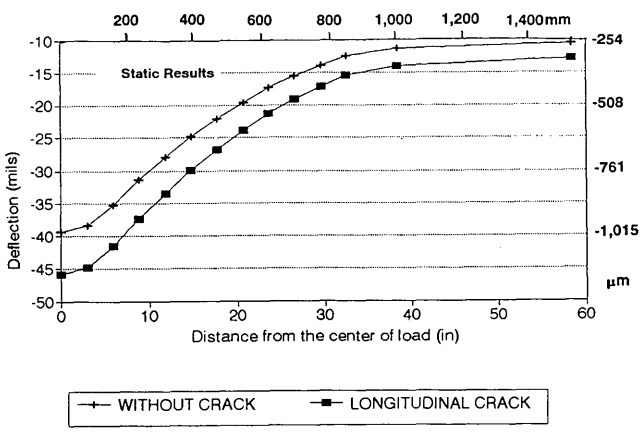

FIGURE 5 ABAQUS static load results of surface deflections for longitudinal cracked and uncracked pavements.

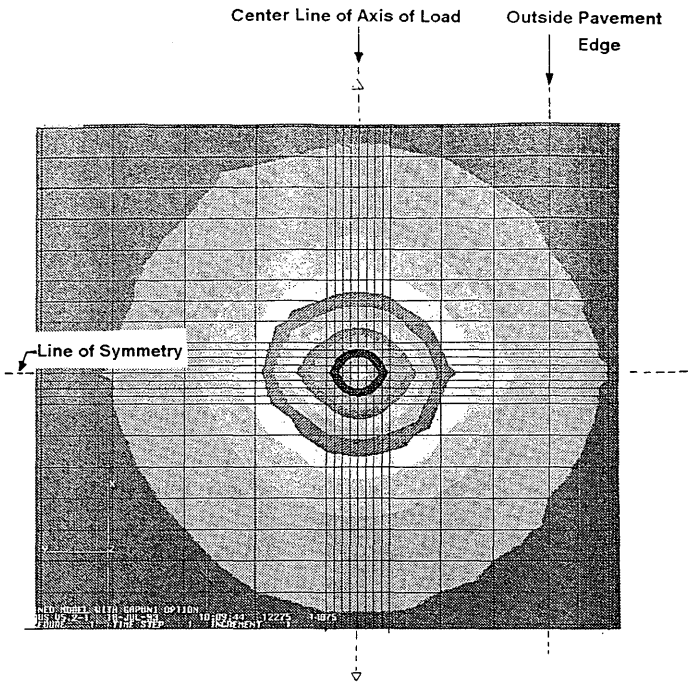

FIGURE 6 Area of concentration of surface deflections.

Under Dynamic Loads

Figure 7 indicates that dynamic loading causes a higher deflection response in the cracked pavement than the dynamic deflections calculated for the uncracked pavement. Maximum dynamic deflection under the NDT load, in the case of cracked pavement, is 985 μm (38.8 mils), which is 17 percent higher when compared with the dynamic deflection of the uncracked pavement. It is interesting to note that this difference becomes smaller farther away from the load.

Transverse Cracked Pavement Response Under Dynamic Loads

First, a transverse crack was simulated 75 mm (2.95 in.) from the load center; Figure 8 illustrates the results. Maximum dynamic deflection was 911 μm (35.9 mils), which is 10 percent higher than the corresponding deflection calculated for uncracked pavement. The transverse crack study was extended to investigate the effect of transverse crack spacing. Maximum dynamic deflection was 817 μm (32.2 mils) for a transverse crack simulated at 974

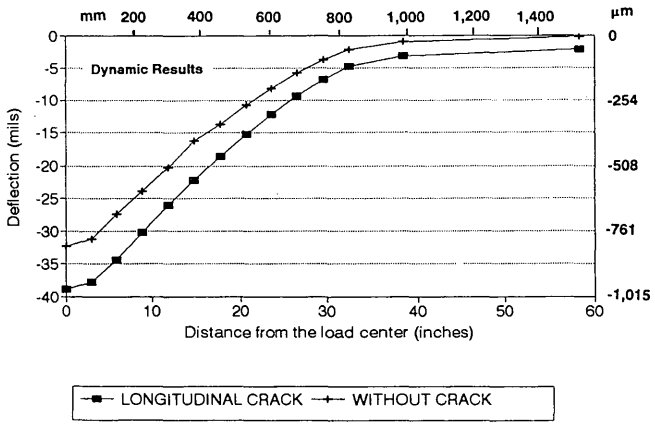

FIGURE 7 ABAQUS dynamic load results of surface deflections for longitudinal cracked and uncracked pavements.

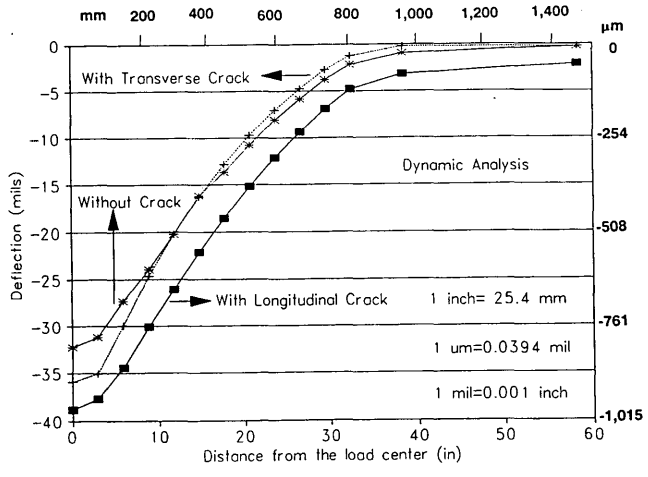

FIGURE 8 ABAQUS dynamic deflections for a pavement with transverse crack.

mm (38.35 in.) and again for a transverse crack simulated at 1 482 mm (58.35 in.) from the load center. Probably there is no significant effect on maximum dynmic deflection if a transverse crack is located beyond 1 m (3.3 ft) from the load center.

Dynamic Response of Pavement with Multiple Transverse Cracks

Multiple transverse cracks are often observed on a severely distressed pavement. In this study, multiple transverse cracks were simulated on either side of the symmetry at distances of 75, 300, 450, 974, and 1 482 mm (2.95, 11.8, 17.7, 38.35, and 58.35 in.) from the load center. Maximum dynamic deflection for the cracked pavement is 1,045 μm (41.2 mils), which is 22 percent higher than the corresponding deflection of the uncracked pavement.

SUMMARY AND CONCLUSIONS

Effects of pavement discontinuities and FWD dynamic NDT loads on the structural response of pavement-subgrade systems were analyzed using the three-dimensional ABAQUS finite element code. Principal findings are as follows:

- The optimum three-dimensional finite element model of a pavement-subgrade system used in this parametric study is 18.3 m (60 ft) long, with outside and inside shoulders measuring the lateral extent of the subgrade from the outside pavement edge of 11 m (36 ft) and a subgrade depth of 12.2 m (40 ft) with a fixed boundary at the bottom. Roller support is ideal along the sides of the model, and the ABAQUS static deflections compare very well with the static deflections computed from the traditional elastic layer analysis.
- For a linear elastic system, the ABAQUS IMPLICIT dynamic maximum deflection under a simulated FWD load is about 18 percent less than the corresponding ABAQUS static deflection.
- The ABAQUS dynamic deflection bowl computed from the backcalculated nonlinear moduli for an asphalt pavement section compares reasonably with the measured FWD deflection data taken from a previous FHWA study.
- Special gap elements are used to simulate pavement cracking and other discontinuities. An optimum crack gap width of 0.25 mm (0.01 in.) and a friction coefficient of 0.5 were established to simulate longitudinal and transverse cracks. A gap width of 0.51 mm (0.02 in.) and zero friction coefficient were used to simulate the discontinuous shoulders.
- ABAQUS dynamic maximum deflection for a longitudinally cracked pavement is about 17 percent higher than that for an uncracked pavement.
- For a severely distressed pavement with multiple transverse cracks, the ABAQUS maximum dynamic deflection is 22 percent higher than that for an uncracked pavement.

Higher dynamic deflections are expected for a cracked pavement as compared with the dynamic deflections calculated for uncracked pavements. However, the corresponding static deflection under the assumption of a linear elastic system remains higher than the dynamic deflections for a cracked pavement. This study demonstrates the usefulness of three-dimensional finite element simulation of pavement cracking and dynamic loads, simulation that is not possible using traditional layered elastic analysis and other finite element programs that do not allow crack simulation and dynamic analysis.

Further three-dimensional finite element simulations are under way to evaluate the effects of alligator cracking and crack severity on asphalt pavement responses. Studies are also being conducted to simulate pavement cracking, joint deterioration, and voids (loss of support under portland cement concrete surface layer) for concrete pavement-subgrade systems.

ACKNOWLEDGMENTS

Research reported in this paper was supported partially by a grant from the University of Mississippi. Allie Smith's support is gratefully acknowledged. The authors also thank Robert M. Hackett for his guidance in this study and the assistance of graduate students J. Mallela, V. S. Tagore, and Zhou Pan. The finite element simulations were conducted on a Cray supercomputer with the support of the staff of the Mississippi Center for Supercomputing Research.

REFERENCES

1. Uddin, W., A. H. Meyer, W. R. Hudson, and K. H. Stokoe II. Project-Level Structural Evaluation of Pavements Based on Dynamic Deflections. In *Transportation Research Record 1007*, TRB, National Research Council, Washington, D.C., 1985, pp. 37–45.
2. Uddin, W., A. H. Meyer, and W. R. Hudson. Rigid Bottom Considerations for Nondestructive Evaluation of Pavements. In *Transportation Research Record 1070*, TRB, National Research Council, Washington, D.C., 1986, pp. 21–29.
3. Hudson, W. R., and H. Matlock. Analysis of Discontinuous Orthotropic Pavement Slabs Subjected to Combined Loads. In *Highway Research Record 131*, HRB, National Research Council, Washington, D.C., 1966.
4. Elliott, R. P., and M. R. Thompson. *Mechanistic Design Concepts for Conventional Flexible Pavements.* Transportation Engineering Series No. 42. University of Illinois, Urbana, 1985.
5. Tabatabaie, A. M., and E. J. Barenberg. Finite-Element Analysis of Jointed or Cracked Concrete Pavements. In *Transportation Research Record 671*, TRB, National Research Council, Washington, D.C., 1978, pp. 11–19.
6. *ABAQUS, Finite Element Computer Program.* Hibbit, Karlsson, Sorenson, Inc. 1989.
7. *ABAQUS, Explicit User Manual.* Hibbit, Karlsson, Sorenson, Inc., 1989.
8. Zaghloul, S., and T. White. Use of a Three-Dimensional, Dynamic Finite Element Program for Analysis of Flexible Pavement. In *Transportation Research Record 1388*, TRB, National Research Council, Washington, D.C., 1993, pp. 60–69.
9. Hudson, W. R., G. E. Elkins, W. Uddin, and K. T. Reilley. *Evaluation of Pavement Deflection Measuring Equipment.* Report FHWA-TS-87-208. FHWA, U.S. Department of Transportation, March 1987.

Publication of this paper sponsored by Committee on Rigid Pavement Design.